

EFFECTS OF POST-TRANSLATIONAL MODIFICATIONS ON ALPHA-  
SYNUCLEIN BINDING TO MEMBRANES

A Dissertation

Presented to the Faculty of the Weill Cornell Graduate School  
of Medical Sciences  
in Partial Fulfillment of the Requirements for the Degree of  
Doctor of Philosophy

by

Igor Dikiy

January 2015

© 2015 Igor Dikiy

EFFECTS OF POST-TRANSLATIONAL MODIFICATIONS ON ALPHA-  
SYNUCLEIN BINDING TO MEMBRANES

Igor Dikiy, Ph.D.

Cornell University 2015

Parkinson's disease is a neurodegenerative disease that affects approximately 1% of people over the age of 60. In the rapidly aging population of the Western world, this represents an increasingly heavy social and economic burden. Along with related synucleinopathies, Parkinson's disease is genetically and pathologically linked to the presynaptic protein alpha-synuclein, which aggregates in intraneuronal Lewy bodies in patients. Aside from its interaction with synaptic vesicles, which implicates alpha-synuclein in regulation of synaptic vesicle exocytosis, the normal function of this protein is not well understood. In dilute aqueous solution, alpha-synuclein contains no stable secondary or tertiary structure, making it a member of the class of intrinsically disordered proteins; however, much of alpha-synuclein undergoes a disorder-to-helix transition when binding to lipid membranes. Alpha-synuclein is also post-translationally modified *in vivo*, in the form of ubiquitous and permanent N-terminal amine acetylation and transient phosphorylation on several serine and tyrosine residues. How these modifications play into the role of alpha-synuclein is also unclear. The effects of N-terminal acetylation and phosphorylation of tyrosines 39 and 125 on alpha-synuclein structure in the free state were assessed using NMR and CD spectroscopy, as were the effects on binding to synthetic lipid vesicles and membrane-

mimetic detergent micelles. N-terminal acetylation increases helicity at the very N-terminus of alpha-synuclein in the free state; this effect propagates into the membrane-bound state, with the acetylated protein displaying stabilized helicity at the N-terminus and tighter binding to more curved lipid vesicles with lower, more physiologically-relevant proportions of negatively-charged lipids, similar to synaptic vesicles. The modified protein binds to  $\beta$ -octyl-glucoside micelles in a previously unknown, partly helical conformation that may serve as a model for *in vitro* studies of pathogenic intermediates. In contrast, phosphorylation at tyrosine 39 has minor effects on the disordered state but greatly perturbs the lipid-bound protein, with the C-terminal half of the lipid-binding domain detaching from the membrane. This phosphorylation event may thus control rearrangements of alpha-synuclein molecules bound to membrane surfaces at the synapse, and play an important role in the native function of alpha-synuclein, knowing which is key to making progress in understanding Parkinson's disease.

## BIOGRAPHICAL SKETCH

Igor Dikiy was born in Moscow, Russia in 1987. At the age of 7, he moved with his family to New York in the USA in 1995. He attended NYC public schools from 2<sup>nd</sup> to 8<sup>th</sup> grade, then Collegiate School for Boys for high school. He matriculated at Princeton University, from where he graduated with honors with a B.S.E. degree in Chemical Engineering and a certificate in Engineering Biology in 2009. For his senior thesis work at Princeton, Igor worked in the lab of Dr. A. James Link, using peptide synthesis to study the folding of the antimicrobial peptide microcin J25. Immediately after Princeton, Igor entered the BCMB (Biochemistry and Structural Biology, Cell and Developmental Biology, and Molecular Biology) Allied Program at the Weill Cornell Graduate School of Medical Sciences. There, he joined the lab of Dr. David Eliezer in the Department of Biochemistry at Weill Cornell Medical College to study the conformational properties of intrinsically disordered proteins involved in neurodegenerative diseases.

## ACKNOWLEDGMENTS

First, I would like to acknowledge the many contributions of the members of the Eliezer lab, chief among them my mentor David Eliezer. It's often said that a PhD student takes on the characteristics of his or her PhD advisor, and I am very happy that this is true in my case (and not just the long hair). Since I came into graduate school with very little experience in biochemistry and biology, my approach to biological problems has been irrevocably shaped by David, whose helpful but hands-off approach to mentorship has been invaluable in teaching me how to not only do but think about science (and also to write really long sentences). The other lab members have been no less valuable, especially Trudy, who produced huge quantities of protein for my experiments and taught me many lab techniques, and David Snead, with whom I had many helpful and interesting discussions about science and life, some of which were carried out entirely in Futurama quotes. Thanks also to Shifeng, Guohua, Nick, Khurshida, and other past and present lab members for making it a great place to work.

Funding is also important. My research was funded through NIH grants R37AG019391 and R01AG025440 to David Eliezer, as well as the Irma T. Hirschl Foundation and a gift from Herbert and Ann Siegel. David Eliezer is a member of the New York Structural Biology Center. The data collected at NYSBC was made possible by a grant from NYSTAR and ORIP/NIH facility improvement grant CO6RR015495. The 900 MHz NMR spectrometers were purchased with funds from NIH

grant P41GM066354, the Keck Foundation, New York State Assembly, and U.S. Department of Defense.

Thanks also to the staff of the NYSBC, especially Dr. Shibani Bhattacharya, for making it as painless as possible to run many NMR experiments that I had no experience with. I'd also like to deeply thank Dr. Clay Bracken, who has forgotten more about NMR than I know, for teaching me some of it and putting up with a lot of annoyances to help me use the Weill Cornell NMR spectrometers. Almost all I know about NMR I learned from Clay and Shibani. I also greatly appreciate the contributions of my committee members, Scott and Jeremy, in helping to keep me focused. In addition, our lab's long-standing collaboration with the Lashuel lab was extremely fruitful during my dissertation research, and I'd like to thank everyone from EPFL, specifically Dr. Bruno Fauvet, who made a lot of protein for me as well and worked very closely with me on several of my projects.

Thanks to my BCMB classmates, other Tri-I graduate students, including the Lima lab crew, and other friends, especially Teck, for making these 5 years more fun. For some reason, it is customary to thank family last, so thanks; chiefly my wonderful in all ways wife Su whose support and organizational skills were very necessary for making it through my PhD studies, and who, despite my best efforts, actually kind of knows what I studied in grad school. Thanks to Stas for also kind of knowing what I studied and good luck carrying on the Dikiy name at Weill Cornell. And of course a bol'shoye spasibo to my parents and xixie to my in-laws for all the support in life and in my studies.

## TABLE OF CONTENTS

BIOGRAPHICAL SKETCH.....	iii
ACKNOWLEDGMENTS .....	iv
TABLE OF CONTENTS.....	vi
LIST OF FIGURES.....	x
LIST OF TABLES.....	xiv
LIST OF ABBREVIATIONS.....	xv
I. Introduction .....	1
I.a. Parkinson’s disease .....	2
I.b. Alpha-synuclein overview .....	3
I.c. Alpha-synuclein free-state properties .....	5
I.d. Alpha-synuclein binding to membranes .....	7
I.e. Alpha-synuclein aggregation and membranes.....	17
I.f. What is the functional state of alpha-synuclein? .....	22
I.g. Alpha-synuclein post-translational modifications .....	25
I.h. Motivations and goals .....	29
II. Methodology .....	32
II.a. Cloning, Protein Expression, and Purification .....	32
II.b. General NMR and CD Sample Preparation .....	38
II.c. HSQC Experiments .....	41
II.d. Lipid Vesicle Binding Studied by NMR .....	44
II.e. In-Cell NMR Experiments .....	49
II.f. Triple Resonance NMR Experiments .....	50

II.g. Relaxation NMR Experiments .....	55
II.h. PRE NMR Experiments .....	57
II.i. Amide Proton Exchange Experiments.....	60
II.j. Diffusion NMR Experiments .....	61
II.k. CD Spectroscopy.....	64
III. N-terminal acetylation increases alpha-synuclein helicity and binding to curved, low-negative-charge membranes .....	68
III.a. Introduction.....	68
III.b. Methods.....	72
III.c. Results Overview.....	80
III.d. Electrostatic and hydrophobic contributions to binding.....	120
III.e. Implications for curvature sensing <i>in vivo</i> .....	123
III.f. Fully-helical and partly helical states.....	127
III.g. Implications for tetrameric assembly.....	130
IV. Phosphorylation at Y39 regulates the lipid-binding mode of alpha-synuclein .....	131
IV.a. Introduction.....	131
IV.b. Methods.....	139
IV.c. Results Overview.....	143
IV.d. General structural effects of phosphotyrosine .....	167
IV.e. Functional implications for pY125 alpha-synuclein.....	169
IV.f. Does pY39 alpha-synuclein form an extended-helix? .....	170
IV.g. Functional implications for pY39 alpha-synuclein.....	173
V. PD-linked H50Q and G51D mutations have disparate effects on alpha-synuclein structure and interactions.....	177
V.a. Introduction.....	177

V.b. Methods.....	179
V.c. Results Overview.....	181
V.d. Potential role of H50Q mutation.....	192
V.e. Effect of G51D mutation on lipid vesicle binding.....	193
V.f. Comparison of G51D effects to other mutations and modifications ..	194
VI. Conclusions and future directions .....	197
VI.a. Effects of N-terminal acetylation and tyrosine phosphorylation .....	197
VI.b. Insights into the normal function of alpha-synuclein .....	199
VI.c. Future directions .....	201
APPENDICES.....	203
A1. Appendix 1: StARD4 .....	203
1a. Introduction .....	203
1b. Methods .....	206
1c. Results .....	210
1d. Conclusions .....	221
A2. Appendix 2: Alpha-synuclein and synaptobrevin.....	222
2a. Introduction .....	222
2b. Methods .....	222
2c. Results .....	227
2d. Conclusions .....	231
A3. Appendix 3: Alpha-synuclein and Hsc70.....	233
3a. Introduction .....	233
3b. Methods .....	234
3c. Results .....	235
3d. Conclusions .....	238

A4. Appendix 4: Alpha-synuclein and TAT fusions .....	239
4a. Introduction .....	239
4b. Methods .....	240
4c. Results .....	240
4d. Conclusions .....	245
BIBLIOGRAPHY .....	247

## LIST OF FIGURES

Figure 1.1: Primary sequence of human alpha-synuclein. ....	4
Figure 1.2: Structures of alpha-synuclein on membrane surfaces. ...	12
Figure 1.3: Proposed model of functional interconversion between alpha-synuclein states on membranes at the synapse. ....	16
Figure 2.1: Schematics of multidimensional NMR experiments used.	51
Figure 3.1: HSQC spectra of alpha-synuclein in intact cells and cell lysates. ....	81
Figure 3.2: Relative alpha-synuclein concentration in intact cell samples and in-cell NMR spectra. ....	82
Figure 3.3: HSQC spectra and amide chemical shift differences for acetylated and unmodified alpha-synuclein in aqueous buffer. ....	84
Figure 3.4: Alpha-carbon secondary shifts and intramolecular contacts for unmodified and acetylated alpha-synuclein in aqueous buffer. ...	86
Figure 3.5: HSQC spectra and amide chemical shift differences for acetylated and unmodified alpha-synuclein in the presence of SDS micelles. ....	88
Figure 3.6: Alpha-carbon secondary shifts and extent of amide proton exchange for unmodified and acetylated alpha-synuclein in the presence of SDS micelles. ....	89
Figure 3.7: Far-UV CD spectra of unmodified and acetylated alpha- synuclein with increasing BOG concentration. ....	91
Figure 3.8: HSQC spectra and amide chemical shift differences for acetylated alpha-synuclein with increasing BOG concentration. ....	93
Figure 3.9: Binding curves derived from CD and NMR data for acetylated alpha-synuclein with increasing BOG concentration. ....	95
Figure 3.10: HSQC spectra and amide chemical shift differences for acetylated alpha-synuclein in the presence and absence of BOG micelles. ....	97
Figure 3.11: Alpha-carbon secondary shifts, $R_2$ relaxation rates, and PRE effects from doped micelles for acetylated alpha-synuclein in the presence of BOG micelles. ....	99
Figure 3.12: Binding profiles of unmodified and acetylated alpha- synuclein to high and low negative charge SUVs and LUVs. ....	103
Figure 3.13: Titrations of unmodified and acetylated alpha synuclein to high and low negative charge SUVs and LUVs. ....	106
Figure 3.14: Titrations of unmodified alpha synuclein to low negative charge SUVs and LUVs. ....	113
Figure 3.15: Titrations of acetylated alpha synuclein to low negative charge SUVs. ....	115
Figure 3.16: On-rate for unmodified and acetylated alpha-synuclein binding to low negative charge SUVs. ....	116

Figure 3.17: Model of residues 1-7 as an ideal $\alpha$ -helix for unmodified and acetylated alpha-synuclein. ....	118
Figure 4.1: HSQC spectra and amide chemical shift differences for unphosphorylated and pY125 alpha-synuclein A107C in aqueous buffer. ....	144
Figure 4.2: Intramolecular contacts for unphosphorylated and pY125 alpha-synuclein A107C in aqueous buffer. ....	145
Figure 4.3: HSQC spectra and amide chemical shift differences for unphosphorylated and pY125 alpha-synuclein A107C in the presence of SDS micelles. ....	146
Figure 4.4: HSQC spectra and increasing intensity of phosphorylated peaks during phosphorylation reaction. ....	147
Figure 4.6: HSQC spectra and amide chemical shift differences for unphosphorylated and pY39 alpha-synuclein Y125F Y133F in the presence of SDS micelles. ....	150
Figure 4.7: Alpha-carbon and carbonyl secondary shifts for unphosphorylated and pY39 alpha-synuclein in the presence of SDS micelles. ....	152
Figure 4.8: Intramolecular PRE and partial sequential amide-amide NOE cross-peaks for pY39 alpha-synuclein in the presence of SDS micelles. ....	154
Figure 4.9: HSQC spectra and amide chemical shift differences for wild-type and Y39E alpha-synuclein in the presence of SDS micelles. ....	155
Figure 4.10: Alpha-carbon and carbonyl secondary shifts for wild-type and Y39E alpha-synuclein in the presence of SDS micelles. ....	156
Figure 4.11: Intramolecular PRE and partial sequential amide-amide NOE cross-peaks for wild-type and Y39E alpha-synuclein in the presence of SDS micelles. ....	158
Figure 4.12: Binding profiles of unphosphorylated and pY39 alpha-synuclein to low negative charge SUVs. ....	159
Figure 4.13: Binding profiles of wild-type and Y39E alpha-synuclein to low and high negative charge SUVs. ....	160
Figure 4.14: PFG LED diffusion fits for alpha-synuclein in low and high SDS. ....	162
Figure 4.15: Intramolecular PRE for alpha-synuclein at low and high SDS. ....	164
Figure 4.16: Model of phosphorylated and phosphomimic amino acids. ....	168
Figure 4.17: Model of pY39 alpha-synuclein modulating the interconversion between lipid-bound states. ....	175
Figure 5.1: Amide chemical shift difference, alpha-carbon secondary shifts, and intramolecular contacts for wild-type and H50Q alpha-synuclein in aqueous buffer. ....	182

Figure 5.2: Amide chemical shift difference and alpha-carbon secondary shifts in the presence of SDS micelles, and binding to low negative charge SUVs, for wild-type and H50Q alpha-synuclein. ....	183
Figure 5.3: Binding of wild-type and H50Q alpha-synuclein to copper(II), zinc(II), and iron(III). .....	185
Figure 5.4: Amide chemical shift difference and alpha-carbon secondary shifts for wild-type and G51D alpha-synuclein in aqueous buffer. ....	187
Figure 5.5: Amide chemical shift difference and alpha-carbon secondary shifts in the presence of SDS micelles, and binding to low negative charge SUVs, for wild-type and G51D alpha-synuclein. ....	189
Figure A1.1: Crystal structure of mouse StARD4.....	205
Figure A1.2: HSQC spectra and amide chemical shift differences for wild-type and L124D StARD4.....	211
Figure A1.3: Amide nitrogen $R_2$ relaxation rates for apo wild-type and L124D StARD4. ....	213
Figure A1.4: HSQC spectra for wild-type and L124D StARD4 in the absence and presence of lipid vesicles.....	214
Figure A1.5: PRE effect for wild-type StARD4 in the presence of increasing concentrations of doped lipid vesicles.....	215
Figure A1.6: HSQC spectra for wild-type StARD4 in the absence and presence of sterols presented by different means.....	216
Figure A1.7: PRE effect for wild-type StARD4 in the presence of lipid vesicles containing spin-labeled cholestane.....	218
Figure A1.8: Carbon HSQC spectra for wild-type StARD4 in the absence and presence of lipid vesicles containing spin-labeled cholestane. ....	219
Figure A1.9: HSQC spectra for wild-type StARD4 in the absence and presence of IP <sub>2</sub> (4,5). ....	220
Figure A2.1: HSQC spectra of alpha-synuclein and synaptobrevin-2 in the presence of SDS micelles.....	228
Figure A2.2: HSQC spectrum of synaptobrevin reconstituted in SUVs. ....	229
Figure A2.3: Binding profile of acetylated alpha-synuclein to SUVs with and without synaptobrevin.....	230
Figure A3.1: HSQC spectra of acetylated and unmodified alpha-synuclein in the presence of Hsc70 CTD. ....	235
Figure A3.2: Binding profiles of acetylated and unmodified alpha-synuclein to Hsc70 CTD.....	236
Figure A3.3: HSQC spectra of unmodified alpha-synuclein in the presence of Hsp104. ....	237
Figure A4.1: HSQC spectra of unmodified alpha-synuclein and TAT fusion proteins in aqueous buffer.....	241

Figure A4.2: Intramolecular PRE effect for alpha-synuclein TAT fusion proteins from a spin-labeled linker.....	243
Figure A4.3: Diagrams of likely intramolecular contacts for alpha-synuclein TAT fusion proteins.....	244

## LIST OF TABLES

Table 3.1: Bound fractions of different populations of unmodified and acetylated alpha-synuclein in the presence of high and low negative charge SUVs and LUVs. ....	105
Table 3.2: Computed apparent $K_D$ values and other parameters for unmodified and acetylated alpha-synuclein binding to high and low negative charge SUVs and LUVs.....	109
Table 3.3: Computed apparent $K_D$ and $B_{max}$ values for unmodified and acetylated alpha synuclein with low negative charge SUVs and LUVs. ....	114
Table 3.4: Computed on- and off-rates for unmodified and acetylated alpha-synuclein binding to low negative charge SUVs. ....	117
Table 4.1: Computed apparent $K_D$ values and other parameters for wild-type and Y39E alpha-synuclein with low and high negative charge SUVs. ....	161
Table 4.2: Hydrodynamic radii and diffusion coefficients for alpha-synuclein-micelle complex at low and high SDS. ....	163
Table 5.1: Summary of biophysical effects of alpha-synuclein mutations A30P, E46K, and A53T. ....	177
Table 5.2: Bound fractions of different populations of wild-type and PD-mutant alpha-synuclein in the presence of low negative charge SUVs. ....	184
Table 5.3: Hydrodynamic radii and diffusion coefficients for wild-type alpha-synuclein and PD-linked mutants in $D_2O$ . ....	192

## LIST OF ABBREVIATIONS

ATP – adenosine triphosphate  
BME –  $\beta$ -mercaptoethanol  
BOG –  $\beta$ -octyl-glucoside  
BSA – bovine serum albumin  
CBCA(CO)NH –  $\alpha/\beta$ -proton to  $\alpha/\beta$ -carbon (via carbonyl carbon) to nitrogen to amide proton correlation  
CD – circular dichroism  
cDNA – coding deoxyribonucleic acid  
CK – casein kinase  
CM – carboxymethyl  
CMC – critical micelle concentration  
CPMG – Carr-Purcell-Meiboom-Gill  
CTD – C-terminal domain  
DDC – dimethyldithiocarbamate  
DEAE – diethylaminoethanol  
DHE - dehydroergosterol  
DMSO – dimethyl sulfoxide  
DOPC – 1,2-dioleoyl-*sn*-glycero-3-phosphocholine  
DOPE – 1,2-dioleoyl-*sn*-glycero-3-phosphoethanolamine  
DOPS – 1,2-dioleoyl-*sn*-glycero-3-phospho-L-serine  
DPPC – 1,2-dipalmitoyl-*sn*-glycero-3-phosphocholine  
DTT – dithiothreitol  
EDTA – ethylenediaminetetraacetic acid  
ER – endoplasmic reticulum  
ESR – electron spin resonance  
FPLC – fast protein liquid chromatography  
GWAS – genome-wide association study  
HBHA(CO)NH –  $\alpha/\beta$ -proton (via carbonyl carbon) to nitrogen to amide proton correlation  
HN(CA)CO – amide proton to nitrogen (via  $\alpha$ -carbon ) to carbonyl carbon correlation  
HN(CO)CA – amide proton to nitrogen (via carbonyl carbon) to  $\alpha$ -carbon correlation  
HN(CO)CACB – amide proton to nitrogen (via carbonyl carbon) to  $\alpha/\beta$ -carbon correlation  
HNCA – amide proton to nitrogen to  $\alpha$ -carbon correlation  
HNCACB – amide proton to nitrogen to  $\alpha/\beta$ -carbon correlation  
HNCO – amide proton to nitrogen to carbonyl carbon correlation  
HPLC – high performance liquid chromatography  
HSQC – heteronuclear single-quantum coherence

HX – amide proton exchange  
IPTG – isopropyl  $\beta$ -D-1-thiogalactopyranoside  
LB – Luria-Bertani  
LED – longitudinal eddy current delay  
LUV – large unilamellar vesicle  
MAPK – mitogen-activated protein kinase  
mTOR – mechanistic target of rapamycin  
MTS – methanethiosulfonate  
MTSL - S-(1-oxyl-2,2,5,5-tetramethyl-2,5-dihydro-1H-pyrrol-3-yl)methyl methanesulfonylthioate  
NAC – non-amyloid component  
NMR – nuclear magnetic resonance  
NOE – nuclear Overhauser effect  
NOESY – nuclear Overhauser enhancement spectroscopy  
NYSBC – New York Structural Biology Center  
OD – optical density  
OSBP – oxysterol-binding protein  
PA – phosphatidic acid  
PCR – polymerase chain reaction  
PD – Parkinson’s disease  
PE – phosphatidylethanolamine  
PFG – pulsed field gradient  
PG – phosphatidylglycerol  
PIPES – piperazine-N,N'-bis(2-ethanesulfonic acid)  
PLK – polo-like kinase  
PMSF – phenylmethylsulfonyl fluoride  
POPC – 1-palmitoyl-2-oleoyl-*sn*-glycero-3-phosphocholine  
POPE – 1-palmitoyl-2-oleoyl-*sn*-glycero-3-phosphoethanolamine  
POPS – 1-palmitoyl-2-oleoyl-*sn*-glycero-3-phospho-L-serine  
PRE – paramagnetic relaxation enhancement  
SDS – sodium dodecyl sulfate  
SDS-PAGE – sodium dodecyl sulfate polyacrylamide gel electrophoresis  
SEC-MALS – size exclusion chromatography coupled to multi-angle static light scattering  
SH2-CD – Src-homology 2-catalytic domain  
SLAS – sodium lauroyl sarcosinate  
smFRET – single molecule Förster resonance energy transfer  
SNARE – soluble NSF attachment protein receptor  
SREBP – sterol regulatory element-binding protein  
StAR – steroidogenic acute regulatory protein  
START – StAR-related lipid-transfer  
SUMO – small ubiquitin-like modifier  
SUV – small unilamellar vesicle  
TFA – trifluoroacetic acid

TFE – trifluoroethanol  
TMV – tobacco mosaic virus  
Tris – tris(hydroxymethyl)aminomethane  
VAMP – vesicle-associated membrane protein  
WT – wild-type

## **I. Introduction**

In biological systems, proteins rarely act alone. On the contrary, they typically interact directly with other proteins, nucleic acids, lipids and/or small molecule ligands in order to carry out their biological functions. Usually, the physicochemical peptide properties combined with the native fold of a protein determine the type and strength of a protein's interactions with its binding partners. In an additional level of regulation, these interactions are frequently modulated by post-translational modifications, some static and others dynamically added and removed in a spatiotemporally-controlled manner. Thus, the specific cellular context of a protein can have a pivotal effect on its conformational state and can direct its interactions with binding partners. In addition to protein properties and modifications, the environment a protein inhabits can also play a role in modulating the interactions the protein undertakes. One very important and commonly encountered environment is the interface between the cell cytosol and a bounding lipid membrane. Many protein-protein interactions, enzymatic reactions, and signaling events occur in this environment and are profoundly affected by it in many ways yet to be fully elucidated. My thesis work addresses a small subset of these membrane-mediated interactions, specifically in the case of the Parkinson's disease-associated protein alpha-synuclein.

## **I.a. Parkinson's disease**

Parkinson's disease (PD) is a neurodegenerative disease, affecting most notably the dopaminergic neurons of the *substantia nigra pars compacta*, that affects approximately 1% of people over the age of 60 [1]. In the rapidly aging population of the Western world, this high incidence represents a heavy social and economic burden that will only get worse with time. The loss of dopaminergic neurons affects the neuronal connections between the *substantia nigra* and striatum, which eventually innervates the motor cortex, thus being responsible for the motor dysfunctions evident in PD [2]. The majority of PD cases are idiopathic, usually arising in an age-dependent manner, but also showing some correlation to environmental factors [3]. One of the pathological hallmarks of idiopathic PD is the appearance of Lewy bodies, intra-neuronal aggregates containing several proteins, the most abundant of which is alpha-synuclein, in the brain [4,5]. The majority of the alpha-synuclein protein in Lewy bodies exists in highly-structured, beta-sheet-rich aggregates known as amyloid fibrils [6–8]. Additionally, five point mutations (in order of discovery: A53T, A30P, E46K, H50Q, G51D) [9–13] in and duplications [14] or triplications [15] of the alpha-synuclein gene (SNCA) have been linked to familial, early-onset, autosomal dominant forms of Parkinson's disease and other neurological diseases termed “synucleinopathies.” These results, supported by recent GWAS studies [16,17], suggest a connection between alpha-synuclein and the etiology of PD.

Although the genetic link between alpha-synuclein and PD is quite strong, the precise nature of this link is unclear. Appearance of Lewy bodies seems to correlate with disease; however, there has been debate as to whether the mature amyloid fibrils found in Lewy bodies are toxic [7] or relatively benign endpoints for the actually toxic proto-fibrils or amorphous aggregates formed during the aggregation of monomers into mature fibrils [18,19]. Adding to the confusion, the primary biological function of alpha-synuclein is not well-established; therefore, it is as of yet impossible to determine whether a loss of native synuclein function or a toxic gain of function of the aggregates is the leading cause of PD.

### **I.b. Alpha-synuclein overview**

Alpha-synuclein has been studied in biochemical and cell-based assays for many years since its discovery and subsequent association with neurodegenerative disease. The first synuclein was discovered in the electric organ of the electric ray *Torpedo californica*, and soon rat homologues were isolated [20,21]. The name “synuclein” derived from its originally observed localization to synapses and the perinuclear region of neurons. In the next few years, synucleins in various organisms were “discovered” as either brain-expressed “phosphoneuroproteins” [22,23], precursors of amyloid fibril components [24,25], or, in one study, as a protein downregulated during song learning in the zebra finch [26]. Eventually, these early

data were synthesized to reveal a family of synuclein proteins: alpha-synuclein – mostly expressed in the brain and involved in PD; beta-synuclein – mainly expressed in the brain and reportedly protective against aggregation; and gamma-synuclein – mainly expressed in the peripheral nervous system and brain but present in many other tissues, with a later link to cancer [27–33].

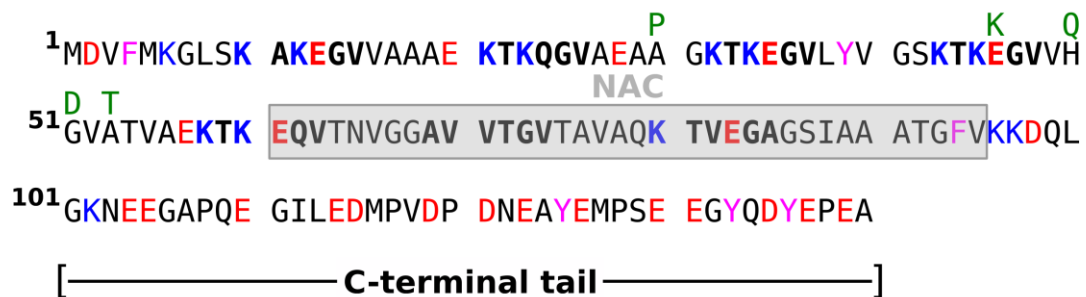


**Figure 1.1: Primary sequence of human alpha-synuclein.** The consensus KTKEGV repeats are bolded. Positively-charged and negatively-charged residues are in blue and red, respectively, while aromatic residues are in magenta. PD-linked point mutations are in green above the wild-type sequence. The C-terminal tail and hydrophobic non-amyloid component (NAC) region are marked.

One of the earliest observations about the alpha-synuclein primary amino-acid sequence was the existence of seven imperfect 11-residue repeats, containing the consensus sequence KTKEGV, in the N-terminal region (Figure 1.1). These repeats were noted to be similar to those of the exchangeable apolipoproteins, which form amphipathic helices and mediate reversible lipid interactions [34–36], leading to the hypothesis that alpha-synuclein binds membranes as part of its cellular function [26]. Indeed, early cell biological and biochemical studies revealed an association with synaptic terminals and

synaptosomes [21–23,26,37–39]. At around the same time, single point mutations in the alpha-synuclein gene were discovered in patients with genetic, early-onset forms of PD. The first mutation discovered was A53T, quickly followed by A30P. The A30P mutation was found to abrogate membrane binding of alpha-synuclein, suggesting a possible pathway of pathogenesis of the mutant; however, in the same study, the A53T mutant did not show any decrease in vesicle binding, indicating that the mutations either cause disease through different pathways, or that membrane binding perturbations are not on-pathway to the disease state [39].

Another interesting feature of alpha-synuclein discovered in the first decade of study was its apparent lack of stable secondary or tertiary structure when isolated in dilute aqueous solution, making it one of the first of a class of proteins originally termed “natively unfolded” and now referred to as “intrinsically disordered” [40,41]. Despite its deposition in an aggregated form in diseased brains, the isolated recombinant protein was determined to be monomeric, although it appeared as a larger species by SDS-PAGE gel (~19 kDa) and size exclusion chromatography (~70 kDa). This large apparent size was attributed to its disordered and dynamic nature [40,41].

### **I.c. Alpha-synuclein free-state properties**

Given the unexpected intrinsically disordered nature of alpha-synuclein, much of the next decade was dedicated to examining any

indications of transient or residual structure in the free monomer of alpha-synuclein. Given its ability to query structural and dynamical properties in a residue-specific manner, NMR spectroscopy emerged as a valuable tool in the study of alpha-synuclein as well as many other intrinsically disordered proteins. Using NMR approaches that had been developed for structured proteins, several research groups reported weak but detectable helical propensities near the N-terminus, most notably between residues 20 and 30, in the dynamic ensemble of conformations adopted by free alpha-synuclein [42,43]. The disease-associated A30P mutation was shown to decrease this helical propensity, but no clear link between local transient structure and aggregation propensity has emerged [43–46].

Additionally, transient intramolecular contacts between the positively-charged N- and negatively-charged C-terminal regions, likely mediated by electrostatics, were detected by paramagnetic relaxation enhancement (PRE) NMR experiments [28,47,48]. These transient contacts were originally hypothesized to be protective against aggregation and thought to be lost in the disease-linked mutants A30P and A53T [48,49]. However, a more careful comparison of these contacts in wild-type and mutant alpha-synuclein showed that the A30P and A53T mutations do not alter transient N- to C-terminal contacts in alpha-synuclein, and the E46K mutation actually slightly enhances them [44]. Moreover, the effect of the disease-linked mutations on fibrillization rate is not the same, with A53T and E46K increasing it and A30P decreasing it [50,51]. It has been postulated that the disease-linked mutations may have similar effects on oligomer

formation rather than mature fibril formation [51]; however, there is presently no unified theory of the etiology of Parkinson's disease that encompasses all known alpha-synuclein mutants.

NMR can be used to measure dynamical properties and two of the most informative measures of backbone motions on the picosecond-nanosecond timescale are the  $R_2$  relaxation rate and the steady-state heteronuclear NOE. Alpha-synuclein in aqueous solution displays  $R_2$  ( $\sim 4 \text{ sec}^{-1}$ ) and heteronuclear NOE ( $\sim 0.2$ ) values consistent with a highly disordered polypeptide exhibiting a high degree of motion [43]. A slight peak in the  $R_2$  rate, corresponding to slightly more rigidity, was seen around residue 20, and a decrease in both  $R_2$  and steady-state heteronuclear NOE values, corresponding to greater mobility, was seen in the C-terminal half of the N-terminal region, which forms the fibril-forming core, generally considered to consist of approximately residues 30-100 [52,53]. Most of the NMR-based structural studies contributing to the intrinsically disordered view of alpha-synuclein have been performed on purified recombinant protein at dilute concentrations in aqueous buffer; however, there is evidence that alpha-synuclein adopts a very similar disordered conformation in live intact *E. coli* cells [54].

#### **I.d. Alpha-synuclein binding to membranes**

Alpha-synuclein was shown to bind to synthetic phospholipid vesicles *in vitro* with a concomitant induction of helical structure [55–

57]. The increased affinity of alpha-synuclein for vesicles containing phospholipids with negatively-charged headgroups was demonstrated both qualitatively and quantitatively [55,58–62]. For example, one quantitative fluorescence correlation spectroscopy study found apparent  $K_D$  values of 1.7 mM and 100  $\mu$ M, for alpha-synuclein binding to synthetic vesicles composed of 100% POPC and a combination of 50% POPC and 50% POPS, respectively [61]. The size of phospholipid headgroup, proposed to correlate with existence of lipid packing defects, and level of saturation of the acyl chains were also found to influence alpha-synuclein binding, with alpha-synuclein binding more tightly to membranes containing phospholipids with smaller headgroups, such as PE and PA, and to those containing unsaturated fatty acyl chains [59,61]. Finally, vesicle curvature also plays a role, with alpha-synuclein having a strong preference for more highly curved (and therefore smaller) vesicles, similar to synaptic vesicles [55,61,63]. For instance, alpha-synuclein displays apparent  $K_D$  values of 170  $\mu$ M and 6  $\mu$ M for synthetic vesicles composed of 50% POPC and 50% POPS with diameters of 116 and 46 nm, respectively [61].

A tandem calorimetric and structural (CD) study revealed that binding of alpha-synuclein to vesicles containing lipids in a partially ordered gel state (DPPC) results in increased ordering of the lipids and a greater release of heat than can be explained by the disorder-to-helix transition that accompanies binding [59]. These results led to the hypothesis that alpha-synuclein can preferentially bind to defect structures that are present in the highly-curved, partially-ordered

membranes, resulting in “defect healing.” Lipid packing defects are structures arising from the exposure of hydrophobic regions of the lipid bilayer to the aqueous solution due to lipid molecules that do not conform to the canonical cylindrical shape [64]. Thus, defects are often associated with smaller lipid headgroups (such as PE and PA), “kinked” unsaturated acyl chains, and stress arising from high curvature. Membranes containing lipid packing defects are often found in the early secretory pathway, while “late membranes,” including the plasma membrane and secretory/synaptic vesicles, where alpha-synuclein is expected to act, tend to contain more charged lipids and fewer packing defects, partially due to the increased concentrations of sterols, which improve lipid packing [64].

Alpha-synuclein has also been shown to localize to various membrane structures in cultured cells and other cellular systems. When alpha-synuclein was originally isolated, it was found to localize to presynaptic nerve terminals, specifically clustered around (~70 nm diameter) vesicular structures, by immunogold staining and electron microscopy [21]. In an *in vitro* assay, alpha-synuclein (but not the A30P mutant) was shown to bind to isolated synaptic vesicles from rat brain [39]. Additionally, a significant proportion of alpha-synuclein (~15%) co-fractionated with membranes in a differential centrifugation scheme on rat brain homogenates [65]. In cultured cells pre-loaded with high concentrations of fatty acids, alpha-synuclein (but not the A30P mutant) localized to lipid droplets as well as the plasma membrane [66]. When heterologously expressed in yeast, alpha-synuclein localizes to the plasma membrane as well, although

increased copies of the alpha-synuclein plasmid result in punctate cytosolic staining [67]. These cytosolic puncta of alpha-synuclein also stain for yeast Ypt1, a Rab1 homolog that localizes to ER-to-Golgi transport vesicles in yeast, suggesting that these transport vesicles present a binding surface similar to that of synaptic vesicles for alpha-synuclein [68]. In hippocampal neurons cultured from rats overexpressing human alpha-synuclein, the protein co-localizes with a marker of synaptic vesicles (vGLUT-pHluorin) [69]. These data, when taken together, strongly implicate alpha-synuclein in binding to “late membranes,” such as the plasma membrane, late transport vesicles, and synaptic vesicles, in a host of cellular environments. In addition, the evidence suggests that this binding is involved in alpha-synuclein function.

At the same time, biochemical and spectroscopic studies elucidated the molecular details of alpha-synuclein binding to membranes. The binding was localized to the N-terminal region of the protein (approx. residues 1-100) by virtue of those peaks disappearing in a  $^1\text{H}$ - $^{15}\text{N}$  HSQC NMR spectrum due to the large effective size and slow tumbling rate of regions of the protein immobilized on the vesicle surface [42]. However, because the vesicle-bound protein is NMR-invisible, it is difficult to determine its structure at high resolution. Following strategies employed in early studies of apolipoprotein structure [70], micelles composed of the anionic detergent sodium dodecylsulfate (SDS) were used to mimic the membrane surface at a much smaller size (approximately 0.5 nm in diameter as opposed to 40 and 120 nm for small and large vesicles, respectively) [42,71,72]. In

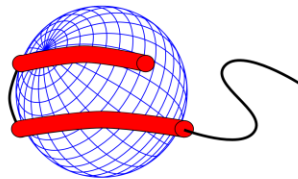
much the same way as with apolipoproteins, addition of SDS at micellar concentrations was found to induce a similar amount of helical structure in the N-terminal region as anionic phospholipid vesicles, as measured by CD spectroscopy, and to cause similar peaks to disappear from the HSQC spectrum. As a result, SDS micelles were deemed a suitable mimic for membrane surfaces in the case of alpha-synuclein.

In the presence of SDS micelles, alpha-synuclein adopts a “broken-helix” conformation, in which the N-terminal 90-100 residues form an amphipathic  $\alpha$ -helix, with a break around residue 42-44 [71–73] (Figure 1.2A). The helical structure (and break) was confirmed by measuring secondary shifts of the alpha-carbons and  $i, i+1$  amide-amide NOE cross-peaks. Interestingly, the helical region seems to be bounded by the aromatic side-chains present in phenylalanines 4 and 94 and tyrosine 39. The helical structure was found to exhibit an atypical 11/3 periodicity that aligns well with the 11-residue repeats of alpha-synuclein and thereby eliminates a super-helical twist of the hydrophobic moment, allowing the hydrophobic face of the helices to remain oriented towards the hydrophobic membrane or micelle interior, while the lysine residues lining the interface between the hydrophobic and hydrophilic faces ostensibly interact with the negatively-charged lipid headgroups.

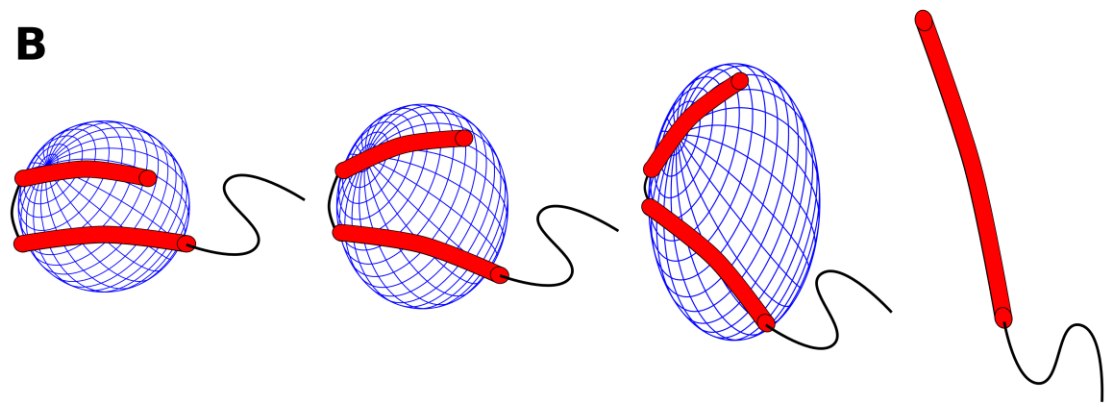
A high-resolution model of the SDS-bound state of alpha-synuclein was reported, integrating NMR-derived secondary structure information, NOEs, residual dipolar couplings, and PRE distance constraints in a molecular fragment replacement framework (PDB ID:

1XQ8) [74]. This structure illustrates the broken-helix conformation that alpha-synuclein adopts in the presence of spheroidal SDS

**A**



**B**



**C**

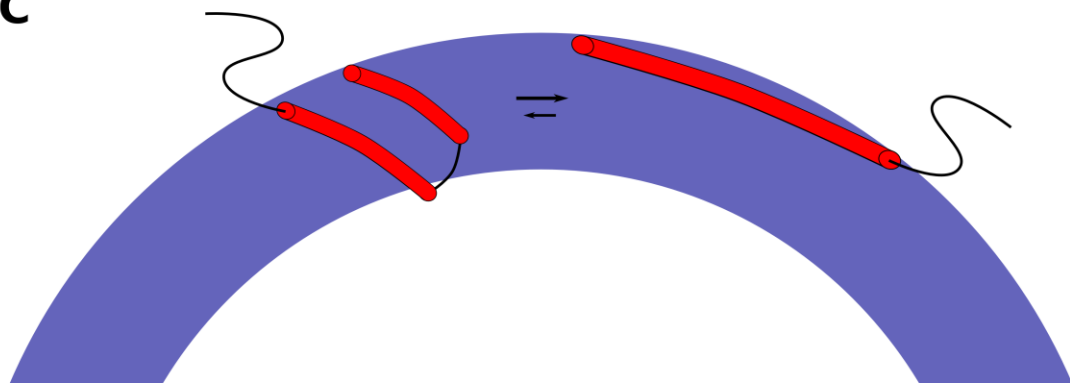


**Figure 1.2: Structures of alpha-synuclein on membrane surfaces.** (A) Broken-helix state on spheroidal SDS micelles. (B) Splaying apart of helices on micelles of increasing size, leading to extended-helix state. (C) Interconversion between broken- and extended-helix state on small vesicles.

micelles. In this structure, the N-terminal domain of alpha-synuclein consists of two curved, antiparallel  $\alpha$ -helices: helix-1, composed of residues 3-37, and helix-2, comprising residues 45-92. Connecting these two helices, which have no inter-helix contacts, is a non-helical but structured linker, which contains the tyrosine at position 39. The N-terminal 2 residues are disordered and the remaining C-terminal residues are in a slightly extended conformation. Dynamical and secondary structural parameters indicate that the regions around residues 30-35, 66-67, and 88 display “weaker” helical structure, indicative of some fraying, kinking, or flexibility in the helices at those positions [74,75].

The main advantage of using SDS micelles as a model for membrane binding is the small size of the resultant particles, which is amenable to high-resolution structural studies by NMR. However, the possibility exists that this small size and high curvature of SDS micelles is itself affecting the conformation of alpha-synuclein. In fact, the inter-helix distance in the broken-helix state was found to be very close to the expected size of a spheroidal SDS micelle. This match between the protein and micelle sizes led to the hypothesis that the broken-helix conformation is constrained by the topology of the SDS micelle. ESR (electron spin resonance) can be used to provide structural and dynamical information about sites labeled with paramagnetic spin-labels and is less limited by size than solution NMR; additionally, pulsed dipolar ESR can be used to measure distances between two spin-labeled sites. Therefore, this technique has been used extensively to characterize the conformational state of alpha-

synuclein on larger membrane surfaces. For example, continuous-wave ESR measurements at each site throughout the length of the N-terminal domain of alpha-synuclein in the presence of phospholipid vesicles suggested that the entire region may form a continuous, ordered  $11/3$  helix [76,77].

These results led to the hypothesis that a larger micelle might allow the two antiparallel helices to fuse into a single continuous helix. Supporting this, pulsed dipolar ESR studies using longer-chain lysophospholipid micelles, reported increased inter-helix distances compared to those observed using SDS micelles [78], indicating a splaying apart of the two helices of the broken-helix state on a larger surface (Figure 1.2B). Subsequently, pulsed ESR studies using binding partners of increasing sizes, including rod-like micelles, phospholipid bicelles, and lipid vesicles, yielded longer inter-helix distances that confirmed an “extended-helix” conformation in which the two helices are fully fused [79]. The application of other techniques, such as molecular dynamics simulations using ESR-derived distance restraints [77] and single molecule Förster resonance energy transfer (smFRET) spectroscopy [80,81] provided further evidence for the extended-helix conformation of alpha-synuclein in the presence of lipid vesicles. Interestingly, other contemporaneous ESR studies suggested that a broken-helix conformation persists in the presence of vesicles [82,83]. While the Bortolus et. al. study likely results from a misinterpretation of the data, the Drescher et. al. study, along with data in the original ESR distance measurements, suggests the possibility of interconversion between the extended-helix and broken-helix forms of

alpha-synuclein on the membrane surface (Figure 1.2C). Due to the substantial difference in surface curvature and hydrophobic chain packing between SDS micelles and lipid vesicles, this confirmation of similar helical structures of alpha-synuclein on lipid vesicles as on SDS micelles suggests strongly that these helical conformations are encoded in the alpha-synuclein sequence and can be induced by different lipid environments.

Further ESR studies of the conformation of alpha-synuclein in the presence of SDS showed a co-existence of the broken- and extended-helix states, and that the relative populations of the two conformations depend not only on absolute detergent concentration (which in the absence of protein determines micelle topology) but also protein:detergent ratio [84]. SDS concentrations were increased from those at which spheroidal micelles are expected to dominate to those at which rod-like micelles begin to form spontaneously with the expected switch from mostly broken-helix to mostly extended-helix alpha-synuclein. However, even at relatively low SDS concentrations, at which micelles are still expected to be spheroidal, extended-helix conformations of alpha-synuclein began to dominate when the detergent:protein concentration exceeded ~500. These data suggested that alpha-synuclein does not passively adapt its conformation to a presented lipid or detergent topology, but rather can remodel membrane-like surfaces to promote binding of a certain conformation. These findings were in agreement with sporadic previous and subsequent reports of alpha-synuclein remodeling membrane surfaces [57,63,85–89]. The remodeling of membranes into micelles or tubules

by alpha-synuclein seems to be a consequence of the amphipathic helix inserting to some extent into the membrane bilayer; in fact, similar tubulation has been observed for apolipoprotein A-1, which forms amphipathic helices very similar to those of alpha-synuclein [89]. Interconversion between the broken- and extended-helix states was suggested to contribute to the putative functions of alpha-synuclein at the presynaptic membrane, which presents a variety of membrane topologies to the protein. Specifically, broken-helix alpha-synuclein was envisioned to bridge two closely apposed membrane surfaces, such as a fusing or budding synaptic vesicle at the synaptic plasma membrane, while extended-helix alpha-synuclein, which is unable to form such a bridge, may exist as a reservoir for the active broken-helix form [84,90] (Figure 1.3).

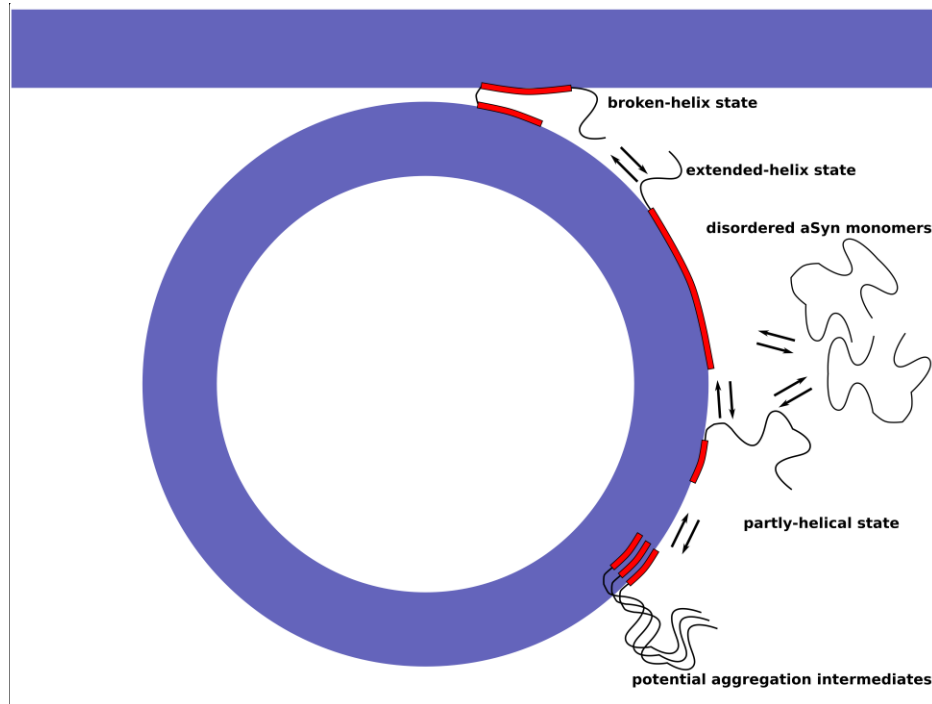


**Figure 1.3: Proposed model of functional interconversion between alpha-synuclein states on membranes at the synapse.**

As the above-referenced studies reveal, it has been difficult to obtain high-resolution structural information on the vesicle-bound form of alpha-synuclein, which, based on the association of alpha-synuclein with vesicles *in vivo*, is expected to be the functionally-relevant form. X-ray crystallography has not been productively applied to membrane surface associated proteins, solution-state NMR is hampered by the large size of the vesicles, and cryoelectron microscopy does not offer sufficient resolution for smaller, asymmetric assemblies. Structural information in the context of lipid vesicles has thus been largely limited to inferences from solution-state NMR methods [91,92], distance constraints measured by ESR and smFRET [80,81,83], and CD spectroscopy [93–95], although recently solid-state NMR was able to directly observe a small portion of the membrane-associated alpha-synuclein protein [96].

### **I.e. Alpha-synuclein aggregation and membranes**

Interestingly, several studies of membrane-associated alpha-synuclein have suggested that binding to membranes or lipid molecules may play a role in facilitating alpha-synuclein aggregation, implicating a transient partly-helical state in that process. Evidence for a partially-folded state of alpha-synuclein and its potential implication in fibrillogenesis cropped up in early spectroscopic studies of alpha-synuclein [97–100]. Several environmental factors, such as low pH (~3), heavy metal ions (e.g.  $\text{Cu}^{2+}$  and  $\text{Fe}^{3+}$ ), the pesticides DDC

and dieldrin, and high temperature, result in both a partly folded structure and a shorter lag phase for fibrillogenesis. A similar partly-folded CD signature was observed for alpha-synuclein in the presence of low concentrations of alcohols, in which fibril formation was enhanced [94]. Mixtures of water with alcohols, particularly fluorinated alcohols, have been used extensively as a membrane model for alpha-synuclein, building off previous protein folding studies that used such mixtures to recapitulate the low dielectric constant conditions expected to exist at the cytosol-membrane interface [101,102]. These results suggest that, in addition to other external factors, the membrane-water interface may induce partial folding of alpha-synuclein, which is correlated to fibril formation, and thus to dysfunction and disease.

At approximately the same time, early *in vitro* studies showed conflicting effects of the presence of lipid molecules on alpha-synuclein aggregation. Many studies found that the presence of various lipids and detergents increased the aggregation and fibrillization rates of alpha-synuclein [65,85,103,104], while a few found the opposite effect [105,106]. A synthesis of these disparate results suggests that high lipid:protein concentrations inhibit fibril formation and low lipid:protein ratios promote fibrillization [107]. As a result, it has been proposed that lipids promote alpha-synuclein aggregation by two possible mechanisms: by increasing the local concentration of protein as a result of confining alpha-synuclein molecules to a smaller area or by promoting a fibrillogenic folding intermediate [107,108]. In the first model, an increase in local alpha-synuclein concentration would not

be seen at higher lipid concentrations, since alpha-synuclein molecules would not be confined to a small area. In the second model, the concentration of the fibrillogenic intermediate would be more dilute at higher lipid concentrations. Thus, both models lead to the conclusion that lipid-mediated aggregation would only occur at low lipid:protein ratios.

Much of the early evidence for the fibrillogenic intermediate model was circumstantial, consisting of the observation that concentrations of membrane-mimetic detergent that promoted alpha-synuclein aggregation also induced partly helical conformations of alpha-synuclein [109–111]. One such correlative study used CD spectroscopy to infer the structure of alpha-synuclein in the presence of different concentrations of trifluoroethanol (TFE). At intermediate concentrations of the fluorinated alcohol, where, like in the presence of intermediate concentrations of lipids or detergents, alpha-synuclein formed fibrils more readily, the protein was found to populate a folding intermediate [95]. When the CD spectrum of this state was reconstructed, it revealed a partly helical conformation, with helical content of ~24 residues. These results suggested that at least some of the previously reported partially folded states correlating with enhanced fibril formation are a partly helical conformation in which part, but not all, of the N-terminal membrane binding domain forms an  $\alpha$ -helix. Other structural studies have detected N-terminal partly helical states of alpha-synuclein on membrane bilayer surfaces. For example, site-directed spin-labeling and continuous wave ESR detected a binding mode of alpha-synuclein in which (at least) the N-

terminal 18 residues were bound to a vesicle surface, while residues C-terminal to position 69 (at least) were detached [83]. This binding mode was especially prevalent on vesicles with low (below 40% PG headgroups) negative charge content.

Although solution-state NMR cannot directly observe the lipid vesicle-bound state of alpha-synuclein due to size constraints, NMR experiments can indirectly provide information about the extent of binding of different regions. This residue-specific resolution is one of the major advantages of NMR spectroscopy in the study of protein interactions. For instance, loss of signal due to immobilization on the vesicle surface has been used to quantify extent of binding in a residue-specific manner [58,91,92]. This method is especially useful for detecting partially bound states, in which the unbound regions of the protein retain their flexible and dynamic character while only the regions that are bound (or those nearby) are affected. Using this approach, it was shown that at low lipid:protein ratios, alpha-synuclein did not bind uniformly to the vesicles along the length of the polypeptide chain [91]. Specifically, while the N-terminal 90-100 residues all bound to some extent, the very N-terminus of the protein, consisting of approximately 20-30 residues, displayed relatively more binding than the remainder of the protein. Increased binding for that region was also indicated by stronger lipid-to-protein NOEs detected by NOE transfer experiments. These data suggest that a subset of the bound alpha-synuclein exists in a conformation in which only the N-terminal ~25 residues are bound to the vesicle, presumably in an  $\alpha$ -helical conformation.

The nonuniform binding profile of alpha-synuclein can provide quantitative estimates of the relative populations of different binding modes. Interestingly, the fractional population of the N-terminal partially bound state was found to be higher for the A30P, E46K, and A53T Parkinson's disease-associated mutants, despite their different effects on total binding [92]. This finding bolstered the hypothesis that a partially bound, partly helical conformation of alpha-synuclein, which prevails at low or limiting concentrations of membrane binding sites, enhances the aggregation of the protein, perhaps by bringing amyloidogenic regions closer together. Additionally, these studies localized the likely region of partial folding to the N-terminal ~25 residues, which closely matches the number of residues predicted to be helical in the partly helical folding intermediate indirectly observed in the presence of intermediate concentrations of TFE. A CD spectroscopy and ITC study looking at binding of overlapping alpha-synuclein peptides to lipid vesicles also concluded that the N-terminal ~25 residues trigger binding and folding of the entire N-terminal domain, also positing the existence of a partly helical state on vesicles [112]. Interestingly, this N-terminal section of the protein has also been implicated in protein-protein interactions, specifically calmodulin binding [113]. However, none of these studies were able to directly observe the hypothesized, aggregation-prone, partly helical state at high resolution.

### **I.f. What is the functional state of alpha-synuclein?**

The paradigm of alpha-synuclein existing mostly as a dynamic, disordered monomer in cells, with a small population of various lipid membrane bound states, has recently been challenged. Although alpha-synuclein was originally purified using standard methods used for natively folded proteins, its apparent disorder and heat-stability soon led to the proliferation of denaturing steps in the purification schemes. Currently, recombinant alpha-synuclein produced in *E. coli* (which is used for most structural studies) is usually purified using either a boiling step or a reverse-phase HPLC procedure. Both of these methods can be expected to break up any tertiary or quaternary structure that the native protein may adopt; in addition, the heterologous expression system and overexpression can also affect protein folding in the *E. coli* cells. In order to examine the effects of these relatively harsh expression and purification conditions on the native structure of alpha-synuclein, Selkoe and coworkers purified the protein using gentle, nondenaturing methods from an endogenous source [114]. An easily obtainable source with sufficient alpha-synuclein expression was found: human red blood cells, which have been shown to express significant amounts of the protein though the functional consequence of alpha-synuclein in this context is still unclear [115,116]. The protein purified from red blood cells (as well as neuroblastoma cell lines) using ammonium sulfate precipitation, hydrophobic interaction chromatography, and gel filtration exhibited a

size consistent with a tetramer (~60 kDa) by analytical ultracentrifugation and native-PAGE, and displayed helical character similar to vesicle-bound recombinant monomer by CD spectroscopy. In addition, the tetrameric species was shown to bind to synthetic lipid vesicles and to fibrillize more slowly than the monomer. This finding lent itself to an attractive dichotomous model: a native, functional helical tetramer and a fibrillogenic, unfolded monomer.

Further studies offered more evidence of a tetrameric form of alpha-synuclein. For instance, an alpha-synuclein construct containing a 10-residue N-terminal addition purified from *E. coli* under nondenaturing conditions was analyzed by NMR and other methods and showed some characteristics consistent with a helical tetramer [117]. Additional studies suggested that N-terminal acetylation (see section I.g) and purification in  $\beta$ -octyl glucoside was necessary to observe the tetrameric form of alpha-synuclein [118]. In contrast, several studies showing that alpha-synuclein exists primarily as a monomer when purified from multiple native and nonnative sources, and even in intact *E. coli* cells were published [119–121]. Currently, it is thought that alpha-synuclein exists in equilibrium between several forms *in vivo*: a majority of monomeric species, with some helical tetrameric and potentially amyloidogenic oligomeric forms as well [122].

Despite the controversy over the physiologically relevant, functional form of alpha-synuclein, the actual function of the protein is not well-established. Mice with alpha-synuclein knocked out have been generated and studied; however, the observed phenotypes were not consistent from study to study and depend on what the study was

designed to look at. For example, some studies specifically examined the effects on dopamine signaling in the brain and found a slight increase in dopamine release with a concomitant drop in overall dopamine levels upon loss of alpha-synuclein [123,124]; other studies looked at the effects on pools of synaptic vesicles in neurons in general and found a loss of undocked, or “reserve” synaptic vesicle pools [125]. Thus, alpha-synuclein plays a role at neuronal synapses in general and potentially a (different?) role in dopaminergic neurons. In cultured neurons, alpha-synuclein was shown to localize to presynaptic terminals fairly late, after they had become well-established [126], while alpha-synuclein knockdown neurons also displayed a decreased “reserve” pool of synaptic vesicles [127] and a loss of potentiation of glutamatergic synaptic transmission [128]. A double-knockout of alpha- and beta-synuclein showed no major deficiencies in synaptic function, aside from a decrease in complexin and 14-3-3 protein levels and decrease in brain dopamine levels [129]. While these findings implicate alpha-synuclein in regulation of synaptic vesicle exocytosis in general, they do not elucidate any coherent specific function for the protein.

One clue to a possible function of alpha-synuclein was discovered in mice lacking the synaptic chaperone CSP $\alpha$  [130]. These mice display loss of SNARE complex formation and rapid neurodegeneration that is ameliorated by the overexpression of alpha-synuclein. SNARE proteins are the machinery that drives vesicle fusion in cells, with a specific subset responsible for synaptic vesicle exocytosis in neurons [131]. The generation of alpha-, beta-, and

gamma-synuclein triple-knockout mice [132,133] implicated synucleins further in SNARE complex regulation. These mice displayed an age- and activity-dependent neurodegenerative phenotype. On a molecular level, the mice showed decreased neuronal SNARE complex assembly, which was remedied by expression of alpha-synuclein in cultured triple-knockout neurons and other cell lines [133]. These findings suggest that different synuclein proteins may have redundant functions in the brain, at least in terms of chaperoning the SNARE complex. A connection between alpha-synuclein and the neuronal SNARE complex is further supported by observed SNARE protein accumulation at synapses of mice expressing a truncated (1-120) form of alpha-synuclein, one of many animal models for PD [134]. However, this is only one putative function for alpha-synuclein, and a consensus on its *in vivo* function remains elusive.

### **I.g. Alpha-synuclein post-translational modifications**

N-terminal acetylation, a very common protein modification, was first discovered in 1958 [135]. As much as 80% of cytosolic mouse proteins were found to be N-terminally acetylated [136], while more recently, proteomics analyses have found that 84% of human and 57% of yeast proteins are N-terminally acetylated [137]. N-terminal acetylation, which consists of the transfer of an acetyl group to the protein primary amine by one of a group of N-acetyltransferase enzymes (NatA-NatF) [137,138], is thought to happen while the

nascent peptide is still on the ribosome [139,140], together with initiator methionine cleavage [141,142]. Each N-acetyltransferase acetylates a subset of proteins depending on the sequence of the N-terminal two or three residues [143,144]. Meanwhile, prokaryotes use an incompatible N-terminal acetylation system [145]; thus, eukaryotic proteins produced recombinantly in bacterial systems are not N-terminally acetylated.

Modification of the N-terminus of alpha-synuclein was originally observed when the protein purified from human brain was found to be N-terminally blocked [24]. However, the shift to recombinant protein for biophysical and biochemical studies prevented any further determination of the nature of the N-terminal modification until a study comparing modifications of cytosolic and Lewy body alpha-synuclein by mass spectrometry found ubiquitous N-terminal acetylation [146]. Subsequently, members of the yeast NatB complex appeared in a screen looking for mislocalization of alpha-synuclein expressed in yeast [147]. When the NatB complex was knocked out, the usual plasma membrane localization of alpha-synuclein was lost, resulting in a diffuse, cytosolic signal. NatB is known to acetylate proteins with N-terminal Met-Asp and Met-Glu sequences [143], which includes alpha-synuclein; therefore, while N-terminal acetylation of alpha-synuclein by NatB was not directly detected, it was suggested that this modification is important for plasma membrane localization. More evidence of a potential role of N-terminal acetylation in alpha-synuclein function was subsequently found, when several research groups reported the isolation of helical and tetrameric forms of alpha-

synuclein. In all of the reports, the isolated protein was N-terminally modified, either by endogenous N-terminal acetylation [114,118] or by a peptide scar left over from a purification tag [117]. One of the studies suggested that N-terminal acetylation, along with use of a buffer containing the detergent  $\beta$ -octyl glucoside (BOG) was necessary to observe the helical tetramer [118]. These findings sparked an outpouring of interest in the structural and functional roles of N-terminal acetylation of alpha-synuclein.

Although N-terminal acetylation is almost ubiquitous in eukaryotic proteomes, protein phosphorylation is the most extensively studied post-translational modification since the 1950s [148].

Phosphorylation, which in eukaryotes consists of the transfer of a phosphate group to either a serine (86%), threonine (12%), or tyrosine (2%) residue, is reversible, unlike N-terminal acetylation [149,150].

Phosphorylation by a kinase and dephosphorylation by a phosphatase form a dynamic signaling system that can regulate cellular processes in space and time. Phosphorylation increases the variety of protein surfaces for protein-protein interactions without increasing the gene number, as well as allowing the cell to respond to environmental changes faster than gene transcription and protein translation [151].

Different kinases have been shown to phosphorylate alpha-synuclein on a few serine and tyrosine residues [152–156]. The most common phosphorylated residue of alpha-synuclein is serine 129; this modification is found in cytosolic [157] and aggregated alpha-synuclein [146,158,159]. The effect of phosphorylation of Ser-129 on PD progression is unclear and is most likely context-dependent. There

is evidence that phosphorylation at Ser-129 can inhibit alpha-synuclein fibril formation *in vitro* [155] but also that it can increase fibril formation *in vitro* and aggregation in cells [158,160].

Phosphorylation of alpha-synuclein at another site, serine 87, was also detected in cell models [159]. Phosphorylation of alpha-synuclein at Ser-87 was demonstrated *in vitro* by the kinase Dyrk1A [161]. Also, alpha-synuclein phosphorylated at Ser-87 was found to be enriched in samples from PD patients and animal models of PD [154].

Eukaryotic proteins are also often phosphorylated on threonine and tyrosine residues. Despite containing 10 threonine residues due to the conserved KTKEGV repeat motif, alpha-synuclein does not seem to undergo phosphorylation on any of those residues. Tyrosine residues, on the other hand, have been shown to be phosphorylated. Studies in which alpha-synuclein was transfected into cell lines showed that tyrosine 125 could be phosphorylated [162,163]. Meanwhile, phosphorylation at tyrosines 133 and 136 was also detected, but at lower levels [162,164]. Alpha-synuclein phosphorylated at Tyr-125 was detected in human samples and animal models, decreasing in level with age [165]. However, the difficulty of producing pY125 alpha-synuclein *in vitro* and lack of widely accepted phospho-tyrosine mimicking mutations has prevented further biophysical characterization of alpha-synuclein phosphorylated at Tyr-125 or other tyrosine sites (such as tyrosine 39).

## **I.h. Motivations and goals**

Inspired by the nascent studies of the effect of N-terminal acetylation on alpha-synuclein structure and function, this thesis contains work aimed at determining these effects in greater detail. Specifically, the impact of N-terminal acetylation on the structure and intramolecular contacts of disordered monomeric alpha-synuclein, both in cells and in a purified form, is determined. In addition, the effects of these structural changes on alpha-synuclein interaction with membrane mimics, such as micelles of different detergents, and synthetic lipid vesicles of different composition and curvature are examined. The goal is to structurally characterize N-terminally acetylated alpha-synuclein in a similar way to the heretofore studied unmodified recombinant form of the protein, and to compare these structural and lipid-interaction characteristics. Studying the effects of N-terminal acetylation on alpha-synuclein binding to lipid vesicles similar to synaptic vesicles, its most well-validated *in vivo* binding partner, is expected to give insights into the still poorly-characterized native function of alpha-synuclein.

Analogously, the effects of another modification, tyrosine phosphorylation, are studied. Since a bevy of work has focused on serine phosphorylation in alpha-synuclein, this thesis focuses on the previously known phosphorylation site at Tyr-125 and the very recently discovered site at Tyr-39. The effects on free-state structure and membrane and detergent interactions are assessed. Due to the

location of Tyr-39 in the middle of the lipid-binding domain, specifically in the linker region, greater attention is paid to the effects of phosphorylation at that site on the membrane and micelle-bound structure of alpha-synuclein. The goal is to characterize the lipid membrane-bound state of phosphorylated alpha-synuclein in order to draw conclusions about the effect of phosphorylation on the function of the protein.

In addition to post-translational modifications, PD-associated point mutations can affect the structural properties and membrane interactions of alpha-synuclein. Recently, two newly-discovered mutations in alpha-synuclein have come to the forefront: H50Q, identified in patients with late-onset PD [12,166], and G51D, identified in patients with early-onset PD and multiple system atrophy [9,167]. The discovery of these two mutations allows previously proposed hypotheses of mutation roles in alpha-synuclein dysfunction to be tested. As with N-terminal acetylation and tyrosine phosphorylation, the impact of these point mutations on the structural characteristics of the free-state and micelle- and membrane-bound states of alpha-synuclein is assessed.

Before tackling what goes wrong with alpha-synuclein in PD, it would be helpful to have a better grasp of what the normal function of the protein is. Since the *in vivo* studies of alpha-synuclein function have yielded the inconsistent and confounding results described above, a greatly simplified *in vitro* system focusing on the structure of the protein and binding to synaptic-vesicle-like synthetic liposomes can be useful. This binding is expected to be central to the still poorly-defined

function of the protein and involves the N-terminal region, which contains all of the abovementioned modifications. Thus, it is hypothesized that these modifications affect the function of alpha-synuclein, and that studying their effects in this *in vitro* system will not only help determine their physiological effects, but also provide key information about the heretofore unclear function of alpha-synuclein.

## **II. Methodology**

In this work, the effects of various post-translational modifications on the structure of alpha-synuclein and on its interactions with membranes and membrane mimics were studied using NMR and CD spectroscopy. A wide variety of NMR experiments were applied to determine structural properties of different alpha-synuclein constructs and samples at residue-specific resolution, in isolation and in the presence of lipid vesicles and detergents. Additionally, CD spectroscopy was applied to measure binding, as detected by secondary structure changes, when appropriate. All such measurements required sample preparation, including molecular biology (mutagenesis and cloning), recombinant protein overexpression in bacterial culture (including isotopic labeling), protein purification, *in vitro* phosphorylation where relevant, site-directed spin-labeling when necessary, and lipid vesicle preparation. The methods used, including data analysis protocols, will be discussed in this section.

### **II.a. Cloning, Protein Expression, and Purification**

*Molecular Biology* – Human alpha-synuclein was expressed in *E. coli* under the control of a phage T7 promoter using a plasmid originally kindly provided by Dr. Peter T. Lansbury [40,42]. The plasmid also contained an ampicillin resistance marker. N-terminally

acetylated alpha-synuclein was produced in *E. coli* using a previously developed co-transformation method involving the yeast N-acetyltransferase complex NatB (plasmid pNatB), kindly provided by Dr. Daniel Mulvihill (University of Kent, UK) via Dr. Elizabeth Rhoades (Yale University). [168,169]. The pNatB plasmid contains a chloramphenicol resistance marker for co-selection with the T7 alpha-synuclein plasmid. Single-residue mutagenesis (PD mutants A30P, E46K, H50Q, G51D, and A53T; phosphomimic Y39E; cysteine mutants for spin-labeling S9C, E20C, E83C, and P120C; and C-terminal truncation [1-102] N103stop) were generated using an Agilent/Stratagene QuikChange site-directed mutagenesis kit with the appropriate forward and reverse primers manufactured by Life Technologies/Invitrogen. PCR-amplified plasmids were transformed into *E. coli* XL1-Blue cells for MiniPrep amplification and purification. Plasmids were stored at -20 °C and amplified in *E. coli* NovaBlue cells when necessary.

*Protein Expression and Purification* – All proteins were expressed in *E. coli* BL21 (DE3) cells. For production of N-terminally acetylated alpha-synuclein, the T7 alpha-synuclein plasmid and pNatB plasmid were simultaneously transformed into the bacterial cells, which were then plated on agar plates containing ampicillin (100 µg/mL) and chloramphenicol (34 µg/mL). Unmodified alpha-synuclein was produced by simply transforming the T7 alpha-synuclein plasmid into *E. coli* BL21 (DE3) cells followed by plating on ampicillin plates. For production of unlabeled (natural abundance of isotopes) protein for CD experiments, bacteria were grown in low volumes (100-400 mL) of LB

(Luria-Bertani) broth with appropriate antibiotics overnight, then transferred to larger volume cultures (1-4 L) for 2 hr at 37 °C. When the OD reached 0.6-1.0, protein expression was induced using ~1 mM IPTG and continued for 3-3.5 hr. A 1 mL sample was taken every 1 hr to check OD and saved to estimate protein expression using SDS-PAGE. Cells were harvested by centrifugation at 6,000 rpm (6,900 x g) for 15 minutes and the pellet stored at -20 °C. Typical preparations utilized 4 L of bacterial culture for producing unlabeled protein.

For production of isotopically-labeled protein for NMR studies (either  $^{15}\text{N}$ -labeled or  $^{15}\text{N},^{13}\text{C}$ -labeled), the “media swap” method was employed [170]. Transformed *E. coli* cells were grown in LB broth (usually 1 or 4 L) as for unlabeled proteins until an OD of 0.6-1.0 was reached, then centrifuged at 6,000 rpm (6,900 x g) for 15 minutes at 24 °C and the pellet resuspended in either 0.25 or 1 L “wash medium,” consisting of M9 minimal medium without carbon or nitrogen sources and containing appropriate antibiotics. This resuspension serves as a wash step to remove any natural abundance carbon and nitrogen sources remaining from the LB broth. The resuspended cells were then centrifuged again at 6,000 rpm (6,900 x g) for 15 minutes at 24 °C and the pellet resuspended in M9 minimal medium, supplemented with BME vitamins, the appropriate antibiotics, and either 1 g uniformly labeled  $^{15}\text{N}$  ammonium chloride and 4 g natural abundance dextrose or 1 g  $^{15}\text{N}$  ammonium chloride and 2 g  $^{13}\text{C}$  glucose for the production of  $^{15}\text{N}$ -labeled or  $^{15}\text{N},^{13}\text{C}$ -labeled protein, respectively. After recovery at 37 °C in minimal medium for 0.5-1 hr, protein expression was induced using ~1 mM IPTG and continued for 3-3.5 hr. A 1 mL sample was

taken every 1 hr to check OD and saved to estimate protein expression using SDS-PAGE. Cells were harvested by centrifugation at 6,000 rpm (6,900 x g) for 15 minutes and the pellet stored at -20 °C or used immediately for in-cell NMR experiments.

The purification scheme was the same for all recombinant alpha-synuclein proteins, regardless of mutation or acetylation, except that the scheme for purifying the N-terminal truncation alpha-synuclein 1-102 involved a different ion exchange chromatography step. Protein purification was performed on ice or at 4 °C whenever possible. Frozen bacterial pellets (from 1 L culture for isotopically labeled protein or 4 L culture for natural abundance protein) were thawed on ice and resuspended in 50 mL lysis buffer (10 mM tris pH 8.0, 1 mM EDTA, 1 mM DTT, 1 mM PMSF). The suspension was then homogenized using a Dounce homogenizer. The resultant homogenate was subjected to sonication by a tip sonifier (Branson) for 2 x 6 minutes at a power setting of 6 with a duty cycle of 50%. The sample was stirred between the two applications of the sonifier. The lysed cell suspension was then subjected to ultracentrifugation at 40,000 rpm (145,000 x g) for 1 hr at 4 °C. A sample for SDS-PAGE was taken after each step (resuspension, homogenization, sonication, and ultracentrifugation [pellet and supernatant]).

The ultracentrifugation pellet was saved at 4 °C while the supernatant (~45 mL), which contained the soluble fraction of lysed bacterial cells, was mixed with 1% w/v streptomycin sulfate (~0.45 g) and stirred at 4 °C for 30 min to precipitate nucleic acids. A white precipitate formed, and the resultant suspension was centrifuged at

15,000 rpm (18,000 x g) for 20 min at 4 °C. The pellet was saved at 4 °C and supernatant (~40 mL) used for the next step. The supernatant was subjected to two subsequent ammonium sulfate cuts. First, 0.116 g/mL of ammonium sulfate (~22% saturation) was added and stirred at 4 °C for 10 min. Usually, no precipitate formed, but if it did, the suspension was centrifuged at 15,000 rpm (18,000 x g) for 20 min at 4 °C and the supernatant used for the next cut. For the second cut, 0.129 g/mL of ammonium sulfate (~42% saturation) was added and the solution was stirred for 1 hr at 4 °C. A precipitate, containing the alpha-synuclein protein, formed due to a salting out effect, and the resultant suspension was centrifuged at 15,000 rpm (18,000 x g) for 20 min at 4 °C. The supernatant was saved at 4 °C and the pellet resuspended in 50 mL lysis buffer and set up to dialyze into 1 L of 25 mM tris pH 8, 20 mM NaCl, 1 mM EDTA overnight. After each step, samples of the resultant pellet and supernatant were saved for SDS-PAGE.

After dialysis, the protein was applied to an ion-exchange column using an AKTA FPLC system (GE Healthcare). An anion-exchange chromatography column (DEAE-cellulose, GE Healthcare) was used for full-length protein and a cation-exchange column (CM-cellulose, GE Healthcare) for the truncated alpha-synuclein 1-102 protein. The protein was eluted in buffer containing 25 mM tris pH 8, 1 mM EDTA, with a gradient from 20 mM to 1 M NaCl. Full-length alpha-synuclein usually eluted at 220-320 mM NaCl and alpha-synuclein 1-102 at 170-270 mM NaCl. Fractions of 0.5 mL were collected and protein was monitored by absorbance at 280 nm.

Samples from protein-containing fractions were taken for SDS-PAGE and the fractions pooled for dialysis into 5% acetic acid overnight. The dialyzed protein sample was applied to a reverse-phase preparative C4 column (Vydec) for HPLC purification using a Waters 2690 Separations Module. The column was eluted with buffer A (99.9% dH<sub>2</sub>O, 0.1% trifluoroacetic acid [TFA]) and a gradient from 20% to 100% buffer B (90% acetonitrile, 9.9% dH<sub>2</sub>O, 0.1% TFA). The eluant was monitored for protein absorbance at 229 nm; alpha-synuclein usually eluted at ~46% buffer B. Samples from HPLC peaks were taken for SDS-PAGE analysis, and protein-containing peaks were dried under vacuum to remove acetonitrile, then lyophilized for 2-3 days. For cysteine mutants of alpha-synuclein, the low pH during and after HPLC purification served to inhibit dimerization, and any covalent dimers are presumed to separate from monomeric protein on the column. The lyophilized powder was then stored at -20 °C. Purity was usually >90%.

*Phosphorylated Protein Samples* – Alpha-synuclein protein phosphorylated on tyrosine 39 was produced by Dr. Bruno Fauvet in Dr. Hilal Lashuel's lab (EPFL, Switzerland) for NMR experiments. Lyophilized alpha-synuclein protein was dissolved in buffer and incubated with the SH2-CD fragment of c-Abl and ATP. After the reaction was completed, the phosphorylated alpha-synuclein was purified by reverse-phase HPLC and lyophilized.

## II.b. General NMR and CD Sample Preparation

*Protein Sample Preparation* – For preparation of most protein samples for NMR and CD spectroscopy, lyophilized protein was dissolved in NMR buffer (10 mM Na<sub>2</sub>HPO<sub>4</sub>, 100 mM NaCl, pH 6.8). The pH was often low due to residual TFA from the HPLC step and was adjusted to around 6.8. The solution was then filtered through a 100 kDa centrifugal filter to remove large aggregates. Protein concentration was estimated from the mass of lyophilized protein dissolved or the absorbance at 280 nm (using an extinction coefficient of 5960 M<sup>-1</sup>\*cm<sup>-1</sup>). For more accurate protein concentration determination, samples of the protein stock were run on an SDS gel along with samples of BSA with a predetermined concentration. The gel was stained, destained overnight, imaged, and the band intensity quantified using ImageJ software [171]. The band intensity was then correlated with concentration for the BSA samples, and concentration of alpha-synuclein stock was calculated from the band intensity of those samples. This calculation usually resulted in a lower alpha-synuclein concentration than expected from mass of lyophilized protein.

Protein stocks were then mixed with stocks of detergents (SDS, BOG) or lipid vesicles or with buffer to obtain desired concentration. Protein-containing samples were kept either at room temperature or 4 °C, while those with lipid vesicles and BOG were kept exclusively at 4 °C and those with SDS were kept at room temperature or higher so as to be above the Krafft point of SDS, below which SDS solutions

form a crystalline phase. Finally, 10% D<sub>2</sub>O was added to NMR samples to provide a deuterium signal for locking the NMR signal. Titrations were generally performed using separate, matched samples for titration points, although occasionally the titrant was added stepwise to the same sample to conserve material.

*NMR Sample Considerations* – NMR experiments were usually run on samples dissolved in NMR buffer (10 mM Na<sub>2</sub>HPO<sub>4</sub>, 100 mM NaCl, pH 6.8, 10% D<sub>2</sub>O). This buffer composition has the advantage of having no extraneous NMR signals arising from the buffer components. However, the buffering strength of phosphate is not very robust around neutral pH, resulting in low pH (~3-4) after dissolving lyophilized protein, likely due to residual TFA from the HPLC buffers. While high pH is undesirable for NMR studies on disordered proteins due to increased amide proton exchange with the solvent, which leads to decreased NMR signal intensity for amide protons that are not protected (usually by hydrogen bonds), low pH induces a collapsed state in alpha-synuclein due to the neutralization of the many charged residues in the C-terminal tail [172]. As a result, pH was adjusted to slightly below neutral (pH 6.8) for most NMR experiments, to decrease the effects of amide proton exchange, or to slightly above neutral (pH 8.4) for those experiments in which increased amide proton exchange at high pH was harnessed to determine the extent of protection for amide protons. This pH adjustment could result in the addition of significant and unknown amounts of sodium and chloride ions to the sample.

High salt concentration increases the conductivity of the sample and requires input of higher power radio frequency pulses in NMR experiments, in addition to potentially modulating intermolecular interactions. To avoid the addition of extraneous salt and the formation of potentially insoluble salts with divalent metal cations, PIPES, which has a greater buffering capacity around pH 6, was used in certain samples. The “PIPES NMR buffer” consisted of 20 mM PIPES and 100 mM NaCl (salt concentration varied by experiment) at pH 6.8. Routine HSQC experiments with SDS or BOG detergents used natural abundance detergent; however, deuterated SDS was used for multidimensional NMR experiments and deuterated BOG was used when high concentrations of BOG were required. Deuterated detergents not only have decreased proton signal arising from the detergent, but also reduce the loss of magnetization through spin diffusion between the protein and detergent micelle protons.

Additionally, sample temperature can play a large role in the results of NMR experiments. High temperature, like high pH, is conducive to increased amide proton exchange with the solvent. On the other hand, high temperature decreases the viscosity of solvent and increases the tumbling rate of macromolecules, decreasing the loss of signal due to  $T_2$  relaxation (yup). This is especially advantageous for relatively large and slow-tumbling protein-micelle complexes. For this reason (as well as the tendency of SDS to transition to a crystalline phase below room temperature), all NMR spectra on samples containing SDS micelles were obtained at 40 °C. Spectra for which the observed signals originate from the free protein

were obtained at 10 °C, originally selected to minimize amide proton exchange, and subsequently used for consistency.

*NMR Equipment* – Most multidimensional NMR experiments were collected on either a Varian INOVA 600 MHz spectrometer, equipped with a cryogenically-cooled triple-resonance z-gradient probe at Weill Cornell Medical College, or Bruker AVANCE spectrometers with cryogenically-cooled triple-resonance gradient probes with proton frequency ranging from 600 to 900 MHz at the New York Structural Biology Center (NYSBC). The vast majority of pulse sequences were either standard ones from Varian BioPack or Bruker library pulse sequences modified and optimized by NYSBC staff. One-dimensional (mostly proton) spectra, as well as diffusion experiments, were usually collected on a Bruker AVANCE 500 MHz spectrometer with a room temperature broadband probe at Weill Cornell Medical College. All probes were 5 mm, and 5 mm NMR tubes, mostly thin wall precision NMR sample tubes from Wilmad-LabGlass, were used. On occasion, 5 mm solvent-matched Shigemi cells were used for low-volume or high-field applications.

### **II.c. HSQC Experiments**

HSQC (heteronuclear single quantum coherence) experiments use scalar couplings to correlate two different, chemically bonded, NMR-active nuclei, such as  $^1\text{H}$  and  $^{15}\text{N}$  or  $^1\text{H}$  and  $^{13}\text{C}$  [173]. This pulse sequence results in a two-dimensional spectrum with cross-peaks

corresponding to every H-N or H-C group in the sample, with the chemical shift of the proton on one axis and that of the heteronucleus on the other. The  $^1\text{H},^{15}\text{N}$ -HSQC is considered the “fingerprint” spectrum of a protein, since it contains a diagnostic peak for (the amide group of) each residue of the protein, except the proline residues, which lack an N-H. The peak position (i.e. amide proton and nitrogen chemical shifts) is very sensitive to the many factors that influence the electrochemical environment of the amide group, and thus can report on structural changes, binding interactions, nearby protonation states, phosphorylation, etc. Thus,  $^1\text{H},^{15}\text{N}$ -HSQC experiments are often used to monitor titrations of a binding partner, such as lipid vesicles, detergents, or metal ions, in the case of alpha-synuclein. Plots of chemical shift perturbations/differences *versus* protein primary sequence can help to localize interacting regions, especially for proteins with no well-defined tertiary structure. In this work, amide chemical shift differences were quantified as follows:

$$\Delta\delta_{avg} = \sqrt{(1/2) \cdot [\Delta\delta_{HN}^2 + (\Delta\delta_N / 5)^2]} \quad (1)$$

where  $\Delta\delta_{HN}$  and  $\Delta\delta_N$  are the amide proton and amide nitrogen chemical shift differences, respectively (the latter is scaled by 5 due to the larger chemical shift values of amide nitrogen nuclei). For HSQC experiments used for titrations, it is important to use samples that are as closely matched as possible (protein and salt concentration, pH, etc).

Lipid vesicle binding measurements are a special case, since the vesicle-bound protein tumbles too slowly and is invisible by NMR, so the proportion of the protein that is bound does not give rise to NMR

signals. This logic can also be applied to any sufficiently large particle, such as microtubules or LPS aggregates. In this case, signal intensity changes, rather than peak position changes, are used to monitor binding; therefore, protein concentration (which scales linearly with signal intensity) and receiver gain settings, must be the same between samples. Binding to paramagnetic metal ions, which decrease NMR signal intensity in a distance-dependent manner, can also be monitored by relative intensity ratios, rather than chemical shift changes.

Phosphorylation of alpha-synuclein by c-Abl was followed by incubating wild-type alpha-synuclein with and the catalytic truncation SH2-CD c-Abl and collecting successive 1 hr  $^1\text{H}$ ,  $^{15}\text{N}$ -HSQC experiments. A spectrum was also collected on a matched alpha-synuclein sample with no c-Abl to serve as a zero timepoint. The relative intensity of each phosphorylated peak was calculated and plotted *versus* time.

$^1\text{H}$ ,  $^{15}\text{N}$ -HSQC experiments were usually collected with 1024 points and an acquisition time < 100 msec (resulting in 14-20 ppm spectral width) in the direct dimension (proton) and at least 64 complex pairs (up to 512 complex pairs) in the indirect dimension (nitrogen), with a spectral window of around 104-128 ppm for SDS-containing samples and around 107-132 ppm for all others. Number of transients collected for each increment in the indirect dimension was optimized for each sample to obtain a sufficient signal to noise ratio. The spectra were processed with NMRPipe [174] using standard 2D processing scripts including a solvent filter in the direct dimension,

zero-filling and cosine-bell apodization in both dimensions, and polynomial baseline correction in the direct dimension, applied after Fourier transform of both dimensions. Linear prediction was generally not employed; thus number of complex points correlated directly with resolution in the indirect dimension. All NMR spectra were visualized and analyzed in NMRViewJ [175].

#### **II.d. Lipid Vesicle Binding Studied by NMR**

*Lipid Vesicle Preparation* – All lipids were purchased from Avanti Polar Lipids as solutions in chloroform and kept at -20 °C. A pre-made 5:3:2 mix of DOPE:DOPS:DOPC (“coagulation reagent I”) was used as a starting point for many lipid composition mixtures. Synthetic lipid vesicles of defined composition and different size distributions were made by sonication (SUVs) or extrusion (LUVs). In both cases, the appropriate volumes of each lipid type (coagulation reagent I, DOPC, DOPS, etc) were mixed in a glass tube. Frequently used lipid compositions were 15% DOPS 25% DOPE 60% DOPC (1:1 coagulation reagent I:DOPC) and 50% DOPS 15% DOPE 35% DOPC. The chloroform was removed by drying under nitrogen at 50 °C, followed by drying under vacuum. The dried lipid film was resuspended by pipetting up and down in the appropriate buffer (usually NMR buffer) and vortexing. SUVs were prepared by sonicating the multilamellar vesicle suspension in a bath sonicator 4 times for 3 min. The suspension became clearer as vesicles became smaller. The

suspension was then centrifuged at 60,000 rpm (160,000 x g) at 4 °C for 2 hr to remove larger vesicles. The supernatant was used as SUV stock. LUVs were prepared by freezing (in liquid nitrogen) and thawing (in room temperature water) the multilamellar vesicle suspension 10 times, then passing 21 times through a 400 nm membrane and 21 times through a 100 nm membrane using an Avanti mini-extruder. While lipid vesicles occupy wide size distributions, SUVs prepared by sonication have a distribution centered around a diameter of ~40 nm, while LUVs extruded through a 100 nm filter have distribution centered around a diameter of ~120 nm, based on dynamic light scattering data acquired for similarly prepared vesicles [176].

*Lipid Vesicle Titrations* – Lipid vesicle binding measurements were performed using concentration-matched samples with and without lipid vesicles. Since the vesicle-bound protein tumbles too slowly and is invisible by NMR, peak intensity is proportional to the fraction of protein in which that region is not bound to the vesicle. Thus, signal intensity changes were used to monitor binding. In a flexible and disordered protein like alpha-synuclein, regions of the protein that are not bound to the vesicle retain their disordered character, allowing for a nonuniform binding profile in which different regions of the protein that bind as a unit can be resolved. Peak intensity can be averaged over each such region to extract bound fractions of specific binding modes: “all bound states,” representing all states in which any (N-terminal) region is bound; “fully helical states,” representing the state in which the entire N-terminal domain (residues ~1-100) is bound and presumably helical; and “partly-helical states,”

the difference between the two, representing states in which only part of the N-terminal domain is bound, presumably in a helical conformation. As the C-terminal region is not expected to bind appreciably to lipid vesicles, the average intensity ratio of residues 129-137 was used as a control for protein concentration or nonspecific effects on signal intensity. The average intensity ratio of residues 3-9 and of residues 65-80 was divided by the average of residues 129-137 and subtracted from 1 to calculate the population of “all bound states” and “fully-helical states,” respectively.

Binding titrations were fit to equations derived from a simple bimolecular binding equilibrium using bulk lipid concentration [177]. This results in a quadratic equation with only one fitting parameter, an apparent  $K_D$  (e.g. equation 2, below). This one-parameter model equates bulk lipid concentration with binding site concentration, effectively assuming that each lipid molecule provides one binding site for alpha-synuclein. A more nuanced model can be set up by adding a parameter for the number of protein binding sites per lipid molecule ( $B_{max}$ ). This parameter can be used to calculate the number of lipids per binding site (by taking the inverse) and to estimate the number of binding sites per vesicle. Thus, the two-parameter model allows one to compare not only binding affinity but also quantity of protein “binding sites” (e.g. packing defects) on the vesicle. However, due to the sparseness of titration data, the one-parameter quadratic model was used for most analyses. This quadratic formulation is more rigorous than a commonly used hyperbolic model [61], although in the case of a

large excess of lipids, the derived apparent  $K_D$  values do not differ significantly.

As mentioned above, the use of bulk lipid concentration for lipid vesicle binding measurements is a necessary oversimplification. However, when comparing lipid vesicles of different size, using total lipid concentration ignores the difference in accessible outer membrane lipid concentration. In a sample with the same total lipid concentration, more curved lipid vesicles, such as SUVs, have a greater proportion of lipids on the outer surface able to form binding sites for protein. Thus, using total lipid concentration would underestimate accessible lipid concentration in SUVs relative to LUVs. To overcome this, the proportion of outer surface lipids for both SUVs (~40 nm in diameter) and LUVs (~120 nm in diameter) was estimated as follows: assuming a bilayer thickness of 5 nm, the outer and inner radii for SUVs (20, 15 nm) and LUVs (60, 55 nm) were calculated and used to determine the surface areas of the outer and inner monolayers of each vesicle. Given an estimated lipid headgroup cross-sectional area of 0.7 nm<sup>2</sup>, the number of lipids in each leaflet of each vesicle was calculated from the surface areas. As a result, SUVs were found to have 64% of total lipid concentration in the outer leaflet, while LUVs have 54%. These percentages agree well with those used to calculate effective outer lipid concentrations in other studies [61].

Fitting of NMR-derived bound fractions for different binding modes was performed using both total lipid concentration and outer lipid concentration using a simple equation derived from a bimolecular

binding equilibrium with or without a parameter for the number of binding sites per lipid molecule:

$$F_B = (1/2P_t) \left( L + P_t + K_{D,app} - \sqrt{(L + P_t + K_{D,app})^2 - 4P_t L} \right) \quad (2)$$

$$F_B = (1/2P_t) \left( L \bullet B_{max} + P_t + K_{D,app} - \sqrt{(L \bullet B_{max} + P_t + K_{D,app})^2 - 4P_t L \bullet B_{max}} \right) \quad (3)$$

where  $F_B$  is the bound fraction of the given bound state,  $P_t$  is protein concentration,  $L$  is the lipid concentration,  $B_{max}$  is the maximum number of binding sites per lipid molecule, and  $K_{D,app}$  is the apparent dissociation constant. Fitting was done with the nonlinear curve fitting module in XMGrace and the curve\_fit function in SciPy. Apparent dissociation constants were used to calculate selectivity for SUVs and “helix extension,” which is also the fraction of fully-helical bound protein, as follows:

$$SUVselectivity = K_{D,app,LUV} / K_{D,app,SUV} \quad (4)$$

$$extension = K_{D,app,total} / K_{D,app,full} = C_u C_v C_f / C_u C_v C_t = C_f / C_t \quad (5)$$

where  $K_D$ 's are apparent dissociation constants for the relevant binding modes and vesicles,  $C_u$  is unbound protein concentration,  $C_v$  is unbound vesicle concentration, and  $C_t$  and  $C_f$  are the concentrations of total bound protein and fully-helical bound protein, respectively.

## II.e. In-Cell NMR Experiments

NMR on intact *E. coli* cells has been applied to examine protein (mostly alpha-synuclein) structure in a biologically-relevant environment [120,178]. If the cells are grown in isotopically-labeled medium and the (overexpressed) protein is sufficiently mobile in the crowded intracellular milieu, many multidimensional protein NMR methods can be successfully applied to resuspended live cells, although cross-peak linewidths are significantly broader than for purified proteins in solution. The overexpressed protein signals usually dominate the spectra, although intense signals from bacterial metabolites and peptides are also present. An important control experiment is to examine the cell growth medium for evidence of protein leakage, to ensure that the signal in the in-cell NMR experiments actually arises from protein located within intact cells. It is also essential to quantify the protein concentration in the cell sample and compare to the apparent concentration observed in the NMR experiments to ascertain whether there is any significant NMR-invisible population. Large protein complexes tend to tumble very slowly in cells and thus become NMR-invisible at an even smaller size than in dilute aqueous solution. Finally, NMR experiments can also be performed on freshly lysed cells, in which case line broadening is not as severe as inside the crowded cells.

In this work, *E. coli* BL21 (DE3) cells were transformed with the T7 alpha-synuclein plasmid, the pNatB plasmid, or both. Cells

expressing solely the NatB complex served as a control, since the complex is over 100 kDa in size and should not give rise to detectable signals on an HSQC spectrum in either intact cells or cell lysates. Transformed *E. coli* cells were grown according to the media swap method in a lower culture volume and the pellet used immediately for in-cell NMR. The cell pellet was resuspended by adding NMR buffer and 500  $\mu$ L was taken to serve as the in-cell NMR sample. The remainder of the slurry was diluted by addition of 2 mL NMR buffer and subjected to sonication. The lysed cell suspension was then centrifuged and 500  $\mu$ L of the supernatant was used as the lysate NMR sample. The resuspended cell sample proved refractory to shimming, so shimming was performed on the volume- and length-matched lysate sample. Both samples were analyzed by Varian BioPack standard HSQC experiments at 10 °C, with parameters as described above. The high concentration of protein the resuspended cells and cell lysates allowed for high signal-to-noise with only a few transients.

## **II.f. Triple Resonance NMR Experiments**

*Experiments for Backbone Assignments* – While HSQC experiments provide a lot of data, they cannot be used to determine the connectivity between residues or reliably report on the local secondary structure. A suite of standard triple-resonance experiments on uniformly  $^{13}\text{C}$ ,  $^{15}\text{N}$ -labeled protein is usually used for these

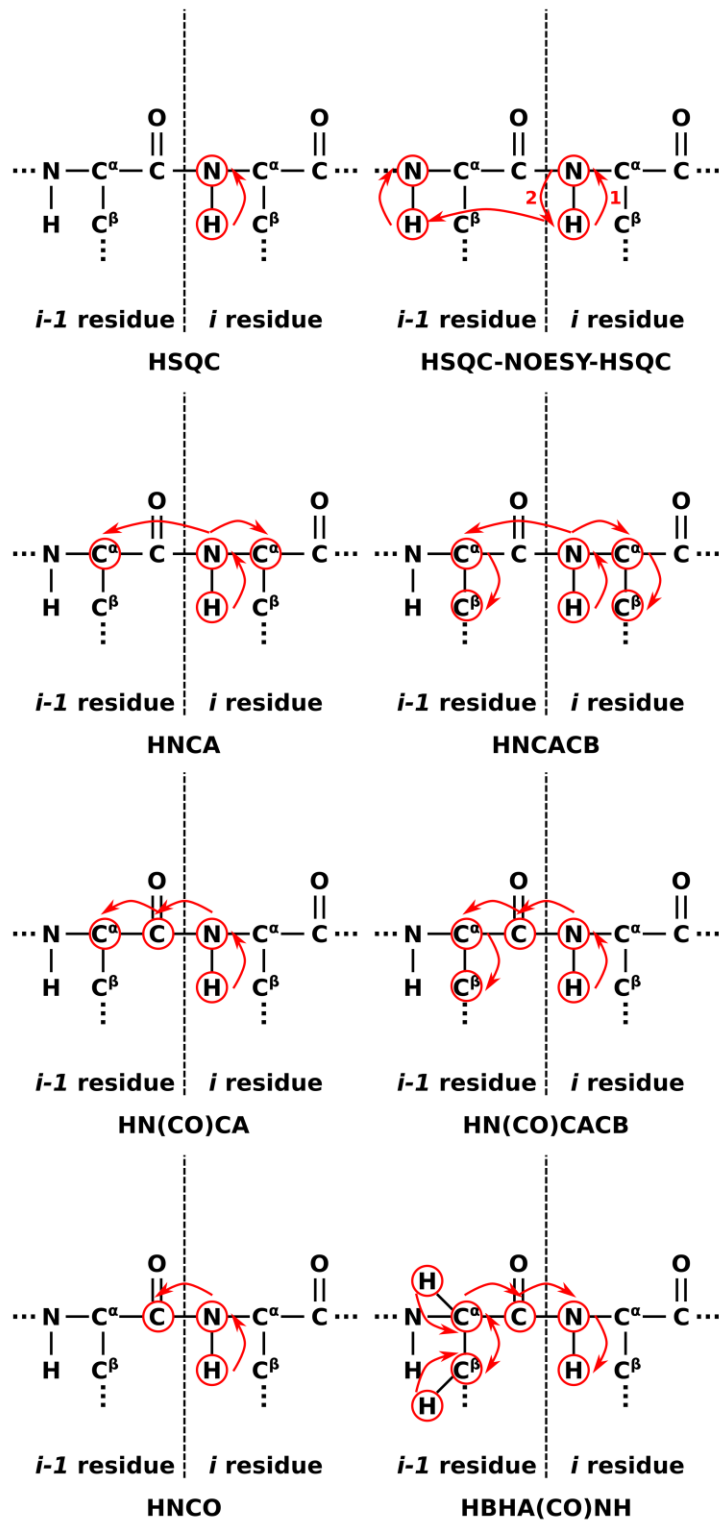


**Figure 2.1: Schematics of multidimensional NMR experiments used.** Red circles and arrows indicate magnetization transfer.

applications. Triple-resonance experiments such as HNCA, HN(CO)CA, HNCO, HN(CA)CO, HNCACB, and CBCA(CO)NH use scalar coupling to correlate the chemical shifts of covalently-bonded nuclei in three dimensions [179–182]. Experiments such as HNCA and HNCACB correlate carbon nuclei in the  $i-1$  and  $i$  residue to amide groups in the  $i$  residue, while HNCO and CBCA(CO)NH solely correlate  $i-1$  carbons to  $i$  amides (Figure 2.1). Alpha and beta carbon chemical shifts (and carbonyl chemical shifts to a lesser extent) are well-correlated to residue type; thus, high quality, complete, and non-overlapped spectra from the standard suite of six triple-resonance experiments listed above can be combined with knowledge of the amino acid sequence to identify sets of dipeptide chemical shifts. These sets of chemical shifts can be extended in a step-wise protocol to unambiguously assign chemical shifts for the majority of backbone atoms (amide proton, amide nitrogen, carbonyl carbon, and alpha [and beta] carbon) (e.g. [183]).

Amide chemical shifts obtained from this assignment protocol can be used to analyze HSQC spectra from binding titrations or other experiments. In addition, alpha, beta, and carbonyl carbon chemical shifts are highly sensitive to local secondary structure and are often analyzed in the form of secondary shifts, or differences between measured chemical shifts and sequence-calculated random-coil chemical shifts [184,185]. Positive (negative for beta carbon) secondary shifts reflect  $\alpha$ -helix structure, while negative (positive for beta carbon) secondary shifts reflect extended structure, chiefly  $\beta$ -sheet/strand or polyproline type II helix. Plots of secondary shifts *versus* protein

primary sequence can reveal regions of stable or nascent secondary structure. Contiguous secondary shifts greater than +/- 2 ppm are indicative of stable helix or sheet structure, respectively [186]. For slightly modified protein constructs, such as point mutants and phosphorylated or acetylated versions of alpha-synuclein, an HNCA experiment with very high resolution in the alpha-carbon dimension can suffice to determine amide (and alpha-carbon) assignments starting from previously known wild-type alpha-synuclein assignments [42,71].

*NOESY Experiments* – Connectivity can also be determined using isotope-filtered NOESY experiments, which take advantage of the nuclear Overhauser effect (NOE) to transfer magnetization through-space (as opposed to through-bond) using dipolar couplings between nuclei. Since the NOE is proportional to  $r^{-6}$ , where  $r$  is the distance between two nuclei, the transfer is only efficient for nuclei within a short distance (typically  $< 5 \text{ \AA}$ ) of each other. Different secondary structure elements are characterized by unique patterns of NOE connectivity between sequential residues. For example, an  $\alpha$ -helical region displays strong  $i,i+1$  amide proton-amide proton NOE cross-peaks and  $i,i+3$  and  $i,i+4$  amide proton-alpha proton NOE cross-peaks, while a  $\beta$ -sheet is characterized by stronger  $i,i+1$  amide proton-alpha-proton cross-peaks and weaker  $i,i+1$  amide proton-amide proton cross-peaks as well as the appearance of cross-strand amide proton-alpha proton cross-peaks [187]. Proton-proton NOESY experiments had been used extensively to determine sequential residue connectivity for short peptide assignments [187]; however, this use has been superseded by

heteronuclear 2D and 3D NMR for larger proteins due to spectral crowding in the presence of so many protons. Isotope-filtered ( $^{13}\text{C}$  or  $^{15}\text{N}$ ) NOESY experiments, coupled with known side-chain and backbone assignments, are now used to provide distance restraints for structure calculations.

Further filtering, such as in a  $^1\text{H},^{15}\text{N}$ -HSQC-NOESY-HSQC experiment, can decrease spectral crowding even more [188]. In this experiment, cross-peaks arising from  $i, i-1$  and  $i, i+1$  pairs of amide protons are visualized. Since the magnetization transfer is due to an NOE mixing period rather than scalar coupling (through-space *versus* through-bond), only cross-peaks arising from regions of relatively rigid and collapsed secondary structure, such as  $\alpha$ -helix,  $\beta$ -sheet, or turns, will be visible. This experiment can be used to confirm backbone amide assignments in structured regions or determine the existence of structured regions if assignments are known. This strategy has been used to delineate the break between the two antiparallel helices in the micelle-bound form of alpha-synuclein [71,72].

Multidimensional experiments were usually collected on spectrometers from 600 to 900 MHz. HNCA experiments had 50-72 complex pairs in the nitrogen indirect dimension and 130-160 complex pairs in the carbon indirect dimension. HNC0 experiments had 50-72 complex pairs in the nitrogen indirect dimension and about 64 complex pairs in the carbon indirect dimension.  $^1\text{H},^{15}\text{N}$ -HSQC-NOESY-HSQC experiments were run using a pulse sequence adapted from a four-dimensional proton-nitrogen-nitrogen-proton experiment [189] to yield proton-nitrogen-nitrogen chemical shifts and collected with 96

complex pairs in the first nitrogen dimension and at least 128 complex pairs in the second nitrogen dimension to provide sufficient resolution to overcome peak overlap. The spectral windows for nitrogen were as described above for HSQC spectra, while alpha-carbon and carbonyl spectral windows were usually 44-70 and 170-180 ppm, respectively. Number of transients collected for each increment in the indirect dimensions was optimized for each sample to obtain a sufficient signal to noise ratio in a reasonable amount of time (1-3 days for HNCA or HNCO, 3-4 days for  $^1\text{H},^{15}\text{N}$ -HSQC-NOESY-HSQC). The spectra were processed with NMRPipe [174] using standard 3D processing scripts including a solvent filter in the direct dimension, zero-filling and cosine-bell apodization in all dimensions, and polynomial baseline correction in the direct dimension, applied after Fourier transform of the second dimension. As for two-dimensional experiments, linear prediction was generally not employed. All NMR spectra were visualized and analyzed in NMRViewJ [175].

## **II.g. Relaxation NMR Experiments**

*Relaxation ( $R_1$  and  $R_2$ ) Experiments* – Longitudinal (“spin-lattice,” relaxation time  $T_1$ , relaxation rate  $R_1$ ) and transverse (“spin-spin,” relaxation time  $T_2$ , relaxation rate  $R_2$ ) relaxation are properties of NMR-active nuclei that generally reflect the mobility or flexibility of the molecule in that region.  $R_2$  relaxation rates of amide nitrogen nuclei (or side-chain methyl groups) are often used to estimate flexibility of a

protein arising from motions on the picosecond-nanosecond timescale or slower conformational or chemical exchange processes on the millisecond timescale [190]. Residue-specific  $R_2$  relaxation rates can be measured by collecting a series of HSQC-like experiments with variable time delays inserted when the magnetization resides on the amide nitrogen and is transverse (in the x-y plane), with CPMG (Carr-Purcell-Meiboom-Gill) refocusing pulses interspersed [191]. The signal intensity for each amide cross-peak is plotted as a function of the time delay and fit to a single exponential to extract the  $R_2$  relaxation rate. Relaxation time delays should be long enough to achieve at least a 70% reduction in signal intensity at the longest time point in order to get accurate fits. Peak intensities as a function of delay time were fit to a single exponential decay function using internal NMRViewJ [175] fitting module. The equation used was:

$$I = I_0 e^{-R_2 t} \quad (6)$$

where  $I$  is the signal intensity at time  $t$ ,  $I_0$  is the (fit parameter) intensity at time 0,  $R_2$  is the relaxation rate, and  $t$  is the relaxation time delay.

The measured  $R_2$  rates of a sample undergoing slow exchange to an invisible bound state can be decomposed into the  $R_2$  rate of the unbound state and a contribution from the binding process. When the forward binding rate is similar to the intrinsic  $R_2$  rate (which is very slow for free alpha-synuclein), the binding rate constant can be estimated from  $R_2$  measurements. Assuming that the exchange is between only two states, the bound and un-bound, and that only one

state can be observed, measurement and subtraction of  $R_2$  rates in the presence and absence of binding partner (e.g. lipid vesicles) can yield the on-rate contribution [92], and, when adjusted for protein and binding partner concentration, the second-order binding rate constant  $k_{on}$  in units of  $\text{sec}^{-1}\text{M}^{-2}$ .

## **II.h. PRE NMR Experiments**

*Spin-Labeling for PRE Experiments* – To achieve site-directed spin-labeling of proteins, single cysteine mutants of alpha-synuclein were labeled with paramagnetic moieties using two different approaches. In one, a methanethiosulfonate (MTS)-functionalized nitroxide spin label (S-(1-oxy-2,2,5,5-tetramethyl-2,5-dihydro-1H-pyrrol-3-yl)methyl methanesulfonothioate, MTSL, Toronto Research Chemicals) was covalently linked to the cysteine residue using MTS chemistry resulting in a disulfide bond. The lyophilized desired cysteine mutant of alpha-synuclein was dissolved in NMR buffer (usually 10 mM  $\text{Na}_2\text{HPO}_4$ , 100 mM NaCl, pH 6.8, see below) and 10 equivalents of MTSL (from a stock dissolved in DMSO and stored at  $-80\text{ }^\circ\text{C}$ ) was added. The pH was adjusted to above 5 to facilitate disulfide bond formation and the reaction mixture incubated with rocking for 30 min at room temperature. Excess unbound spin-label was removed using two sequential hand-poured size-exclusion columns (2 mL, Sephadex G25 beads) equilibrated 3 times with 2 mL NMR buffer. The conjugated protein sample was split into two, and 2

mM (final concentration) DTT added to one (equivalent volume of deionized H<sub>2</sub>O to the other) to reduce off the conjugated spin-label. After addition of 10% (final concentration) D<sub>2</sub>O and, optionally, detergent, the DTT-free and DTT-containing samples were used as the paramagnetic sample and diamagnetic control, respectively.

The second labeling method made use of a cysteine-linked EDTA (*N*-[*S*-(2-pyridylthio)cysteaminy]-EDTA, CysEDTA, Toronto Research Chemicals) chelated with either a paramagnetic (Mn<sup>2+</sup>) or a diamagnetic (Ca<sup>2+</sup>) divalent cation [74]. The lyophilized desired cysteine mutant of alpha-synuclein was dissolved in PRE buffer 1 (20 mM PIPES, 200 mM NaCl, 25 mM EDTA, pH 6.8) and 10 equivalents of CysEDTA (from a stock dissolved in methanol and DMSO and stored at -80 °C) was added. The reaction mixture was incubated with rocking for 30 min at room temperature. Excess unbound CysEDTA was removed using a PD-10 buffer-exchange column pre-equilibrated with PRE buffer 2 (20 mM PIPES, 20 mM NaCl, pH 6.8). The sample was split into two and 50 mM (final concentration) MnCl<sub>2</sub> or CaCl<sub>2</sub> added to the two samples. The samples were incubated with rocking at room temperature for 1 hr to facilitate metal chelation. Residual metal ions were removed from each sample using a PD-10 buffer-exchange column pre-equilibrated with PRE wash buffer (20 mM PIPES, 700 mM NaCl, pH 6.8). Each sample was then exchanged into PRE buffer 2 and concentrated to a volume suitable for NMR samples using centrifugal filters with a 3,000 MW cutoff. The advantage of the metal chelation approach is that the paramagnetic and diamagnetic samples are more similar, both containing alpha-synuclein covalently bonded to a metal-

chelated EDTA moiety, while the chemical difference between the MTSL-conjugated and unconjugated samples is greater and even manifests as chemical shift perturbations around the conjugation site. In addition,  $Mn^{2+}$  exerts a greater PRE effect due to having 3 unpaired electrons. The drawback of the metal chelation approach lies in the fact that alpha-synuclein is known to bind divalent metal cations; thus, extensive washing is needed.

Spin-labels were also incorporated into detergent micelles using 5-doxyI-stearate, a fatty acid with a nitroxide spin-label installed near the headgroup, to measure PRE between the micelle and bound protein. The position of the nitroxide near the headgroup of the fatty acid results in a notable PRE effect to protein bound to the surface of the micelle; the reagent 16-doxyI-stearate can be used to probe for PRE effects deeper in the micelle core, but was not utilized in these studies. A similar approach using incorporation of 5- or 16-doxyI-stearate into lipid vesicles can be used to examine protein-vesicle interactions, but was not used in this work [75].

*PRE Experiments* – Sample preparation for PRE experiments was described above. PRE experiments rely on the dipole-dipole interactions between introduced unpaired electrons, usually in the form of a spin-label radical, and NMR-active nuclei. Since the electron gyromagnetic ratio is about 1000 times greater than that of a proton, proton relaxation is greatly increased when compared to proton-proton dipole relaxation. The signal intensity is still lost as a function of  $r^{-6}$ , where  $r$  is the distance between the unpaired electron and the proton or other NMR-active nucleus, but the PRE effect is typically seen out to

distances as high as 25 Å away from the spin label. By controlling the location of the introduced paramagnetic moiety using site-directed spin-labeling, it becomes possible to identify nuclei on the same molecule (intramolecular PRE) or on contacting molecules (intermolecular PRE) that come within 25 Å of the labeling site, even transiently [192]. One advantage of PRE experiments is that even transient contacts leave a detectable signal; another is that rough distance restraints can be derived for structure calculation.

Complete PRE experiments involve measuring the amide proton  $R_2$  relaxation rate in the presence and absence of paramagnetic moiety using a suitable pulse sequence (e.g. [193]) and the analysis discussed above, then subtracting the two rates to derive the PRE contribution to  $R_2$ , termed  $\Gamma_2$ . A plot of  $\Gamma_2$  *versus* protein primary sequence reveals the regions that come in proximity of the paramagnetically-labeled site. Since amide cross-peak signal intensities are proportional to  $R_2$ , the ratio between signal intensities in matched paramagnetic and diamagnetic  $^1\text{H},^{15}\text{N}$ -HSQC experiments can approximate  $\Gamma_2$  [194]. The latter approach was used exclusively in this work.  $^1\text{H},^{15}\text{N}$ -HSQC experiments were collected on concentration-matched paramagnetic and diamagnetic samples and processed and described above.

### **II.i. Amide Proton Exchange Experiments**

Amide protons not protected by participating in hydrogen bonds or buried in the protein core are subject to exchange with the solvent.

This exchange happens on a similar timescale to other chemical exchange events and often leads to broadening of signals beyond detection. This process occurs to an even greater degree at high temperature and pH. While amide proton exchange is often undesirable, measurement of the rate of exchange through amide proton exchange (HX) experiments can provide important information about the structure of the protein.

HX experiments were performed on the SDS-bound state of alpha-synuclein at pH 8.4 to examine the extent of protection (by secondary structure or micelle-association) of different regions of the protein. The rate of proton exchange was measured using a modified Bruker HSQC sequence based on a previously published experiment by Ulmer et. al [74]. Ratios of peak intensity after application of a water inversion pulse to peak intensity without the pulse were calculated and plotted *versus* the protein primary sequence; peaks which were not observable at pH 8.4 without an inversion pulse were deemed to be exchanging very rapidly and assigned an intensity ratio of -1. Since the intensity ratio is proportional to the rate of exchange, it reports on the extent of protection from exchange for each residue. HSQC experiment parameters and processing were as described above.

## **II.j. Diffusion NMR Experiments**

NMR spectroscopy has long been applied to measure diffusion rates in solution using pulsed field gradient (PFG) methods (e.g. [195–

197]). The basic PFG LED (longitudinal-eddy-current delay) pulse sequence contains an “encoding” gradient pulse that imparts positional information to the nuclei in the sample, followed by a diffusion delay and a “decoding” gradient pulse that “reads” positional information from the nuclei. Since gradient pulses are by definition position dependent and the molecules are free to diffuse to different positions in between the encoding and decoding gradients, the full signal intensity will not be recovered after a diffusion delay. The rate of diffusion of each molecule/nucleus, as described by the diffusion constant, will determine how much signal intensity is recovered. In addition, the signal intensity depends on the diffusion delay length and gradient strength by the following relationship [195,196]:

$$I/I_0 = \exp\left(-(\gamma\delta G)^2(\Delta - \delta/3 - \tau/2)D\right) \quad (7)$$

where  $I/I_0$  is the relative signal intensity,  $\gamma$  is the gyromagnetic ratio (of proton in this case),  $\delta$  is the length of the gradient pulse,  $G$  is the strength of the gradient pulse,  $\Delta$  is the diffusion delay,  $\tau$  is the gradient spacer delay, and  $D$  is the diffusion coefficient. As can be seen from equation 7, the signal intensity depends on the diffusion delay or the square of the gradient strength; thus, either can be varied and the diffusion coefficient determined by fitting to equation 7.

The diffusion coefficient depends on solution viscosity and other variables, as per the Stokes-Einstein equation and can thus yield size information. Although molecular shapes differ from that of a perfect sphere, the Stokes-Einstein equation can be used to calculate the hydrodynamic radius ( $R_H$ , or “radius of hydration”), the radius of the

molecule if it were a sphere, a useful size parameter. Since  $D$  and  $R_H$  are inversely correlated, the other components of the Stokes-Einstein equation can be canceled out by including a standard of known  $R_H$  in the same sample and calculating the  $R_H$  of the unknown molecules from the inverse ratio of the diffusion coefficients. One commonly used standard is 1,4-dioxane, which has a hydrodynamic radius  $R_H$  of 2.12 Å [198].

Diffusion measurements were performed using a standard Bruker PFG LED pulse sequence [196] on proteins and  $^2\text{H}$  SDS (so as not to swamp the protein signal) dissolved in  $\text{D}_2\text{O}$  with 0.03% v/v (~4 mM) dioxane at 300 K using a Bruker AVANCE 500 MHz spectrometer with a room-temperature probe. Gradient strength was varied in a 32-step linear gradient between 2 and 95% of the maximum strength. The diffusion delay was optimized to achieve ~10% signal intensity with 95% gradient strength. The signal intensity for several protein and SDS aliphatic peaks, as well as the dioxane peak at ~3.6 ppm, was plotted as a function of gradient strength and fit to equation 7 using the Bruker TopSpin relaxation analysis module, which also provided the default value for maximum gradient strength. Maximum gradient strength can also be calculated by measuring the diffusion coefficient of residual HDO in  $\text{D}_2\text{O}$  and setting it equal to the published value of  $1.902 \pm 0.002 \times 10^{-9} \text{ m}^2\text{-sec}^{-1}$  [199].

## II.k. CD Spectroscopy

*CD Spectroscopy Experiments* – Far-UV CD spectroscopy can rapidly provide low-resolution information about protein secondary structure, requiring moderate sample concentration, by measuring the ellipticity of circularly polarized light passed through the sample [200,201]. While ellipticity spectra can be quantitatively decomposed into fractional contributions of helix, sheet, and coil structure [202,203], robust results require very high quality data that extends to short wavelengths (at least down to 190 nm). Reasonable estimates of secondary structure can be made more easily using specific spectral features in the far-UV region. Random coil or unstructured proteins have a relatively flat spectrum with a minimum at 195 nm [204], while  $\alpha$ -helical structure shows characteristic minima at 208 and 222 nm and a maximum at 193 nm [205]. The signature for  $\beta$ -sheets is a minimum at 218 nm and a maximum at 195 nm [206]. Folding or unfolding events can thus be tracked by a gain or loss of signal at one of these signature wavelengths; for example, CD spectroscopy (monitored at 220 or 222 nm) is often used to determine thermal denaturation curves for proteins (e.g. [207]). In the case of alpha-synuclein, where the transition is from predominantly disordered to  $\alpha$ -helix, ellipticity at 222 nm serves as a useful measure of helical folding and thus binding to detergent micelles or lipid vesicles [208].

Far-UV CD spectra from 200 to 250 nm were collected on an AVIV Biomedical Model 410 CD spectrometer with bundled software.

Due to scattering/absorption between 190 and 200 nm by sample components such as Cl<sup>-</sup> ions or lipid vesicles, spectral quality below 200 nm degraded rapidly. The wavelength step was 1 nm, with an averaging time of 1.5 sec per measurement. All spectra were collected at 25 °C on 50-100 μM alpha-synuclein dissolved in NMR buffer in a quartz cuvette (Starna) with a pathlength of 0.02 cm. Titrations were carried out with matched samples (70 μL) made from the same stocks of protein and lipid vesicles or detergent. Matched “blank” samples containing buffer and the same concentration of titrant without protein were collected for each titration point.

Each spectrum was collected 3 or 4 times, then averaged and the matching blank average subtracted. The measured signal was converted into mean residue ellipticity using the following equation:

$$[\Theta] = \theta / 10Cnl \quad (8)$$

where  $[\Theta]$  is mean residue ellipticity in deg-M<sup>-1</sup>-m<sup>-1</sup>,  $\theta$  is ellipticity in millidegrees, C is protein concentration in molar, n is the number of amino acids, and l is the pathlength in centimeters. The value of  $[\Theta]_{222}$  was then used for fitting binding equations (see below) or to calculate percent helicity:

$$f_h = ([\Theta]_{222} - [\Theta]_{coil}) / ([\Theta]_{helix} - [\Theta]_{coil}) \quad (9)$$

where  $f_h$  is the fraction of helical residues,  $[\Theta]_{222}$  is mean residue ellipticity at 222 nm, and  $[\Theta]_{coil}$  and  $[\Theta]_{helix}$  estimate minimum and maximum ellipticity, calculated from the equations below:

$$[\Theta]_{coil} = 2220 - 53T \quad (10)$$

$$[\Theta]_{helix} = (-44000 + 250T)(1 - 3/N_r) \quad (11)$$

where T is temperature in degrees Celsius and  $N_r$  is the number of residues [209,210].

*Fitting of Titrations* – Binding titrations were monitored by CD and spectroscopy and binding was quantified as increase in helical structure as measured by the mean residue ellipticity at 222 nm. Fitting of CD binding data was complicated by the inability to reach saturation at maximum attainable detergent concentrations (~600 mM), which were limited by low solubility and increased scattering at low wavelengths. To overcome this, bound fractions were not calculated before fitting; instead, the mean residue ellipticities at no binding and at full binding were estimated from inspection of the binding curves. These values were then used in the following equation:

$$[\Theta]_{222} = (1/2P_t) \left( B + P_t + K_{D,app} - \sqrt{(B + P_t + K_{D,app})^2 - 4P_t B} \right) ([\Theta]_{max} - [\Theta]_{min}) + [\Theta]_{min} \quad (12)$$

where  $[\Theta]_{222}$  is mean residue ellipticity at 222 nm,  $P_t$  is protein concentration, B is the bulk BOG concentration,  $K_{D,app}$  is the apparent dissociation constant,  $[\Theta]_{max}$  is mean residue ellipticity at full binding and  $[\Theta]_{min}$  is mean residue ellipticity at no binding. Fitting was done with the nonlinear curve fitting module in XMgrace and the `curve_fit` function in SciPy.

To compare binding data derived from CD and NMR measurements, the signal reporting on binding,  $[\Theta]_{222}$  in CD measurements and  $\Delta\delta_{avg}$  for well-resolved residues in the NMR

titrations, was normalized to between 0 and 1 at the minimum and maximum values obtained, respectively. The normalized CD and NMR binding data could thus be compared on a unitless axis. Since the data reported on the fraction bound, they were fit to equation 2.

### **III. N-terminal acetylation increases alpha-synuclein helicity and binding to curved, low-negative-charge membranes**

#### **III.a. Introduction**

N-terminal acetylation, first discovered in 1958 in the TMV coat protein [135], is one of the most common protein modifications in eukaryotic organisms. It has been known since the 1970s that as much as 80% of cytosolic mouse proteins (measured in Ehrlich ascites cells) may be N-terminally acetylated [136]. More recent proteomics analyses have determined that 84% of human and 57% of yeast proteins are N-terminally acetylated [137]. N-terminal acetylation is thought to occur on the ribosome [139,140], often in concert with initiator methionine cleavage [141,142], and involves the transfer of an acetyl group from acetyl coenzyme A to the primary N-terminal amine by one of a group of N-acetyltransferase complexes (NatA-NatF) conserved in eukaryotes [137,138]. Each of the different N-acetyltransferase complexes acetylates a subset of proteins depending on the sequence of the N-terminal two or three residues [143,144]. Prokaryotes, on the other hand, have a completely incompatible N-terminal acetylation system [145]; thus, eukaryotic proteins produced recombinantly in bacterial systems are not N-terminally acetylated.

Unlike phosphorylation and lysine acetylation, N-terminal acetylation is not a reversible modification and therefore unlikely to be involved in dynamic protein regulation [138]. Although the majority of

eukaryotic proteins are N-terminally acetylated, there is no consensus as to a general role or effect of this modification, although several suggestions have been put forth. One of the most well-established candidates for a global function of N-terminal acetylation is the Ac/N-end rule pathway, a subset of the N-end rule degradation pathway in which N-terminally acetylated proteins are recognized by a specific E3 ubiquitin ligase, polyubiquitylated, and subsequently degraded [211,212]. The Ac/N-end rule pathway is hypothesized to regulate, via degradation, the proper localization of N-terminally acetylated proteins via exposure or shielding of the acetylated N-terminus [212]. In this model, all N-terminally acetylated proteins are targeted for degradation unless the N-terminal degradation signal is shielded via intramolecular folding, oligomerization, or interaction with a binding partner. This system could be used to regulate protein levels to prevent the overabundance of nonfunctioning proteins. The process of shielding and exposure of a protein's N-terminal acetyl group can thus counteract the irreversibility of the N-terminal acetylation reaction itself and function as a dynamic signal similar to phosphorylation.

Accumulated evidence of acetylated N-termini playing important roles in protein-protein or protein-membrane interactions support this regulatory model. N-terminal acetylation has often been shown to increase avidity in specific protein-protein interactions, such as carboxypeptidase Y with its inhibitor Tfs1p [213]; tropomyosin with actin [214]; the Nedd8 E2 Ubc12 with the E3 Dcn1 [215]; and Sr3 with nucleosomes [216]. The crucial role that N-terminal acetylation plays in protein-protein recognition and binding in these biologically-varied

cases suggests that this modification can play a general role as an avidity enhancer. Additionally, the burial of the acetylated N-terminal in all of these cases supports the Varshavsky model of Ac/N-end rule degradation.

N-terminal acetylation does not only affect protein interactions with other proteins; it has also been shown to play a role in membrane localization. For instance, N-terminal acetylation of chaperonin 10 was shown to increase the helicity of its N-terminal, uncleaved mitochondrial import sequence and posited to promote mitochondrial import by increasing membrane binding [217]. This finding agrees with early work on synthetic model peptides, which found that acetylation of the N-terminal amine stabilizes helicity by acting as a helix N-cap [218,219]. More specifically, N-terminal acetylation (and C-terminal amidation) increased the helicity of a model peptide derived from an amphipathic helix from a plasma apolipoprotein both in buffer and in the presence of lipids [218]. These early data provide evidence that N-terminal acetylation can increase binding to membranes, and also propose a structural mechanism in the form of stabilized helicity in an amphipathic N-terminal region.

Further evidence implicates N-terminal acetylation of proteins in their localization to specific membranes. For instance, the loss of the N-acetyltransferase NatC activity in yeast resulted in failure of the nuclear protein Trm1-II to localize to the inner nuclear membrane [220]. N-terminal acetylation by NatC was found to be necessary but not sufficient for inner nuclear membrane localization. Similar situations were described for Arl3p targeting to the Golgi [221,222],

Grh1 localization to the cis-Golgi [223], and Gag coat protein (N-terminally acetylated by NatC) incorporation into viral particles [224]. While some of these systems have also been demonstrated to have an N-terminal amphipathic helix [221–223], the fact that other proteins are required to effect the correct localization means that either protein-protein interactions or direct protein-membrane interactions (or both) are affected by N-terminal acetylation in these cases.

Modification of the N-terminus of alpha-synuclein was noted as early as 1994 when alpha-synuclein purified from human brain was found to be N-terminally blocked and not amenable to Edman degradation [24]. Similar findings were made for “phosphoneuroprotein-14,” eventually named beta-synuclein [22,23]. However, the shift to recombinantly-produced proteins for biophysical and biochemical studies precluded further study of the nature of this N-terminal modification for over a decade.

Then, a study comparing modifications of cytosolic and Lewy body alpha-synuclein in human brains by mass spectrometry confirmed that N-terminal acetylation is ubiquitous in both pathogenic and nonpathogenic species of alpha-synuclein [146]. Additionally, members of the yeast NatB complex appeared in a screen targeting mislocalization of alpha-synuclein heterologously expressed in yeast [147]. When either of two subunits of the NatB complex was knocked out, the usual plasma membrane localization of alpha-synuclein in yeast was lost, resulting in a diffuse, cytosolic localization. NatB is known to acetylate proteins with N-terminal Met-Asp and Met-Glu sequences [143], which includes alpha-synuclein; therefore, it was

posited that NatB directly acetylates the N-terminal amine of alpha-synuclein, and this modification is important for its membrane localization. However, since N-terminal acetylation of alpha-synuclein was not measured directly in this study, it remained possible that the mislocalization was due to loss of N-terminal acetylation of any number of other proteins.

Further evidence for a potential role of N-terminal acetylation in alpha-synuclein function surfaced in 2011-12, when several research groups reported the isolation of a form of alpha-synuclein with characteristics of a helical tetramer. In each of these reports, the isolated protein was N-terminally modified, either by N-terminal acetylation [114,118] or by a decapeptide left over from a cleaved purification tag [117]. One of the studies suggested that N-terminal acetylation, along with purification in a buffer containing the detergent  $\beta$ -octyl glucoside was necessary for isolation of the helical tetramer [118]. These findings sparked intense interest in the structural and functional effects of N-terminal acetylation of alpha-synuclein.

### **III.b. Methods**

*Production of Acetylated Protein* – N-terminally acetylated alpha-synuclein was produced recombinantly in *E. coli* using a previously developed co-transformation method [168,169]. The bacterial cells are transformed with the T7 alpha-synuclein plasmid and with a pACYCduet plasmid containing the subunits (Naa20 and Naa25) of the

yeast N-acetyltransferase complex NatB (pNatB), kindly provided by Dr. Daniel Mulvihill (University of Kent, UK) via Dr. Elizabeth Rhoades (Yale University). Upon induction, the NatB components are produced and acetylate the alpha-synuclein protein co-translationally in the bacterial cells. The pNatB plasmid contains a chloramphenicol resistance marker for co-selection with the T7 alpha-synuclein plasmid. For production of N-terminally acetylated alpha-synuclein, the T7 alpha-synuclein plasmid and pNatB plasmid were simultaneously transformed into the bacterial cells, which were then plated on agar plates containing ampicillin (100 µg/mL) and chloramphenicol (34 µg/mL). The protein was then expressed and purified as detailed in section II.a.

*In-Cell NMR* – The effects on alpha-synuclein structure in the absence of potentially perturbing purification methods were determined using in-cell and cell lysate NMR. *E. coli* BL21 (DE3) cells were transformed with the T7 alpha-synuclein plasmid, the pNatB plasmid, or both. Cells expressing solely the NatB complex served as a control, since the complex is over 100 kDa in size and should not give rise to detectable signals on an HSQC spectrum in either intact cells or cell lysates. Transformed *E. coli* cells were grown according to the media swap method in a lower culture volume. Specifically, cells were grown in 1 L LB broth until an OD of 0.6-1.0 was reached, then centrifuged at 6,000 rpm (6,900 x g) for 15 minutes at 24 °C and the pellet resuspended in 0.25 L wash medium. The resuspended cells were then centrifuged again at 6,000 rpm (6,900 x g) for 15 minutes at 24 °C and the pellet resuspended in M9 minimal medium,

supplemented with BME vitamins, the appropriate antibiotics, and 1 g uniformly labeled  $^{15}\text{N}$  ammonium chloride and 4 g natural abundance dextrose. After recovery at 37 °C in minimal medium for 0.5-1 hr, protein expression was induced using ~1 mM IPTG and continued for 3 hr. A 1 mL sample was taken every 1 hr to check OD and saved to estimate protein expression using SDS-PAGE. Cells were harvested by centrifugation at 6,000 rpm (6,900 x g) for 15 minutes and the pellet used immediately for in-cell NMR.

The cell pellet was resuspended by adding 500  $\mu\text{L}$  NMR buffer to a total volume 2.5 mL, 500  $\mu\text{L}$  of which was taken to serve as the in-cell NMR sample after adding 55  $\mu\text{L}$   $\text{D}_2\text{O}$ . The remainder of the slurry was diluted by addition of 2 mL NMR buffer and (final concentrations) 1 mM EDTA and 1 mM PMSF. The suspension was subjected to sonication by a micro-tip sonifier (Branson) for 6 minutes at a power setting of 4 with a duty cycle of 50%, on ice. The lysed cell suspension was then centrifuged at 15,000 rpm (18,000 x g) for 20 min at 4 °C and 500  $\mu\text{L}$  of the supernatant were supplemented with 55  $\mu\text{L}$   $\text{D}_2\text{O}$  and used as the lysate NMR sample. The resuspended cell sample proved refractory to shimming, so shimming was performed on the volume- and length-matched lysate sample. Both samples were analyzed by Varian BioPack standard HSQC experiments at 10 °C, with parameters as described above. The high concentration of protein the resuspended cells and cell lysates allowed for high signal-to-noise with only a few transients.

Protein concentrations in the resuspended cell and lysate samples for both alpha-synuclein and alpha-synuclein + NatB were

quantified by SDS-PAGE with BSA standards. Samples of the resuspended cells or cell lysates (usually 2, 3, 4, 5, and 6  $\mu\text{L}$  in 16  $\mu\text{L}$  total sample) were run on an SDS gel along with samples of BSA with a predetermined concentration (by absorbance at 280 nm using an extinction coefficient of  $43824 \text{ M}^{-1}\cdot\text{cm}^{-1}$ ). The gel was stained, destained overnight, imaged, and the band intensity quantified using ImageJ software [171]. The band intensity was then correlated with concentration for the BSA samples, and concentration of alpha-synuclein was calculated from the band intensity, adjusted for number of amino acids, of resuspended cell and lysate samples. The relative concentrations of acetylated and unmodified alpha-synuclein observed by NMR were estimated using the intensities of several well-resolved amide cross-peaks arising from residues 31, 41, 54, 67, 86, 92, and 140 and compared to that measured by SDS-PAGE.

*NMR Experiments on Purified Protein* – Purified N-terminally acetylated protein was used to characterize the effects of the acetylation on the free and micelle- and vesicle-bound states of alpha-synuclein. Backbone assignments were transferred from previously determined ones using high-resolution HNCA experiments, which also provided alpha-carbon chemical shifts for secondary structure analysis (see section II.f). Amide chemical shift deviations derived from  $^1\text{H}, ^{15}\text{N}$ -HSQC experiments were used to monitor the effects of N-terminal acetylation (see section II.c). The effect of N-terminal acetylation on the broken-helix state of alpha-synuclein was assessed at 40 mM SDS, a concentration at which the detergent is expected to

form spheroidal micelles [225,226]. Again, secondary structure information was derived from HNCA experiments.

Most NMR experiments in the presence of BOG micelles were performed at 100 mM BOG to avoid the peak intensity loss seen at higher BOG concentrations. An HNCA experiment was performed at higher (300 mM) BOG concentration to determine the maximum helical structure in the BOG-bound state. Deuterated BOG was employed for this experiment to minimize magnetization loss from the protein nuclei via spin diffusion within the micelle.

*Amide Proton Exchange Experiments* – Amide protons participating in hydrogen bonds as part of stable secondary structure are protected from exchange with the solvent, even at high pH and temperature, and display decreased exchange rates. HX experiments were performed on the SDS-bound state of alpha-synuclein at pH 8.4 to examine the extent of protection (by secondary structure or micelle-association) of different regions of the protein. The rate of proton exchange was measured using a modified Bruker HSQC sequence based on a previously published experiment by Ulmer et. al [74]. A 5 msec Q3 inversion pulse [227] was applied to the water signal 10, 20, or 50 msec before the start of the HSQC experiment, resulting in greatly reduced or even inverted signal intensity for rapidly-exchanging amide protons, compared to the signal intensity in a spectrum collected without the inversion pulse. Intensity ratios were calculated and plotted *versus* the protein primary sequence; those peaks which were not observable at pH 8.4 even without an inversion pulse were deemed to be exchanging very rapidly and assigned an intensity ratio

of -1. Since the intensity ratio is proportional to the rate of exchange, it reports on the extent of protection from exchange for each residue (see section II.i).

*CD Spectroscopy* – Binding to BOG micelles was monitored by increasing helicity as measured by far-UV CD spectroscopy. Percent helicity was calculated using equation 9 from ellipticity at 222 nm and converted to number of fully helical residues using the number of residues in alpha-synuclein (140). Fitting of CD binding data was complicated by the inability to reach saturation at the concentrations of detergent used. To overcome this, bound fractions were not calculated before fitting; instead, the mean residue ellipticities at no binding and at full binding were estimated from inspection of the binding curves. The value of the mean residue ellipticity at 222 nm at 0 mM BOG for unmodified and acetylated alpha-synuclein was used as the value for no binding, while the value at 400 mM BOG for acetylated alpha-synuclein was used as the value for full binding for both proteins, assuming the fully-bound state has similar levels of helicity regardless of acetylation. Thus, BOG binding data from CD spectra was fit to equation 12, with  $[\Theta]_{\max}$  (mean residue ellipticity at full binding) set to  $-5060 \text{ deg-M}^{-1}\text{-m}^{-1}$  and  $[\Theta]_{\min}$  (mean residue ellipticity at no binding) set to  $-2343$  and  $-2811 \text{ deg-M}^{-1}\text{-m}^{-1}$  for unmodified and acetylated alpha-synuclein respectively.

A titration of unmodified and acetylated alpha-synuclein with similar concentrations of BOG (0 to ~300 mM) was performed and the interaction monitored by  $^1\text{H},^{15}\text{N}$ -HSQC spectra. In the NMR experiments, binding to detergent micelles was quantified as the amide

chemical shift difference from the free spectrum for several well-resolved residues, with residues 11 and 16 shown here. To compare BOG binding data derived from CD and NMR measurements, the signal reporting on binding,  $[\Theta]_{222}$  in CD measurements and  $\Delta\delta_{\text{avg}}$  for two residues in the NMR titrations, was normalized to between 0 and 1 at the minimum (at 0 mM BOG) and maximum (at 400 mM BOG in CD experiments and 321 mM BOG in NMR) values obtained, respectively. The two sets of normalized NMR binding data from residues 11 and 16 were averaged, although they were nearly identical. The normalized CD and NMR binding data could thus be compared on a unitless axis. Since the data reported on the fraction bound, they were fit to equation 2.

*Relaxation Experiments* – Amide proton  $R_2$  measurements in the presence of BOG micelles were carried out by running Varian BioPack HSQC-based  $T_2$  experiments with spectral windows and number of points as described in section II.c, using delays of 10, 10, 10, 30, 30, 50, 70, 90, and 110 msec. CPMG  $^{15}\text{N}$  refocusing pulses were at 625  $\mu\text{sec}$  intervals. The relaxation rates for each residue were calculated as detailed in section II.g. Spin-labels were also incorporated into detergent micelles using 5-doxyl-stearate, a fatty acid with a nitroxide spin-label installed near the headgroup, to measure PRE between the micelle and bound protein. The spin-label was dissolved in DMSO and mixed into stock solutions of BOG prior to mixing with alpha-synuclein stock solutions. The final concentration of spin-label was 4 mM in 100 mM BOG.

Amide proton  $R_2$  measurements in the presence of lipid vesicles were carried out by running Bruker HSQC-based  $T_2$  experiments with spectral windows and number of points as described above, using delays of 16.32, 16.32, 32.64, 130.56, 261.12, and 456.96 msec. CPMG  $^{15}\text{N}$  refocusing pulses were at 900  $\mu\text{sec}$  intervals. The relaxation rates for each residue were calculated as detailed in section II.g. The on-rate for each residue was calculated by taking the difference of  $R_2$  rates in the presence and absence of lipid vesicles, then dividing by the concentration of lipid vesicles (2.6 mM) and protein (80  $\mu\text{M}$  for acetylated and 215  $\mu\text{M}$  for unmodified alpha-synuclein). The on-rates for residues 3-9 and 65-80 were averaged to obtain the on-rates for N-terminal binding and fully-helical binding, respectively. The off-rate for each binding mode was then calculated by multiplying the off-rate by the apparent dissociation constant determined from an independent titration (Table 3.3).

*Lipid Vesicle Binding* – Binding to lipid vesicles was measured by decrease of amide cross-peak intensity in  $^1\text{H}, ^{15}\text{N}$ -HSQC spectra in the presence of lipid vesicles as detailed in section II.d. For the one-point measurements, protein concentration was  $\sim 140 \mu\text{M}$ , as determined by SDS-PAGE comparison with BSA stocks, and lipid concentration was 3 mM. For the one-point measurements, and the titrations presented in Table 3.2, samples for acetylated and unmodified protein were made in parallel with the same lipid stock, resulting in well-matched samples. Those titrations were performed by adding increasing volumes of lipid stock into the same NMR tube, while the titrations presented in Table 3.3 used independently made samples for each point.

### III.c. Results Overview

*In-cell conformation of alpha-synuclein is not affected by acetylation* – The conformation of alpha-synuclein with and without N-terminal acetylation in intact *E. coli* cells was queried by two-dimensional NMR, making use of isotopic labeling. The  $^1\text{H},^{15}\text{N}$ -HSQC spectrum of human alpha-synuclein overexpressed in *E. coli* (Figure 3.1A, black) is very similar to previously published in-cell spectra of alpha-synuclein [54,120] and shows the same disordered characteristics as the HSQC spectrum of the purified, monomeric protein (Figure 3.1B, blue). Peak linewidths in intact cells are significantly broader than in lysates or dilute aqueous solution, likely due to the effects of molecular crowding and nonspecific interactions within the cells. The majority of cross-peaks observed in the cells arise from alpha-synuclein, aside from several peaks likely corresponding to flexible small peptides and bacterial metabolites. These same background peaks appear in the spectrum of cells expressing only the NatB complex (Figure 3.1A, green), confirming that they do not arise from alpha-synuclein protein; since the NatB complex is too large to give rise to observable signal (~100 kDa), there are no peaks arising from any protein amide groups. While the alpha-synuclein spectrum is overall quite overlapped, several well-resolved N-terminal peaks (such as leucine 8 and serine 9) were not observed in intact cells. This selective N-terminal broadening has been previously observed [120],

and suggests that the N-terminus of alpha-synuclein may interact with large cellular components or undergo slow conformational exchange within *E. coli* cells.

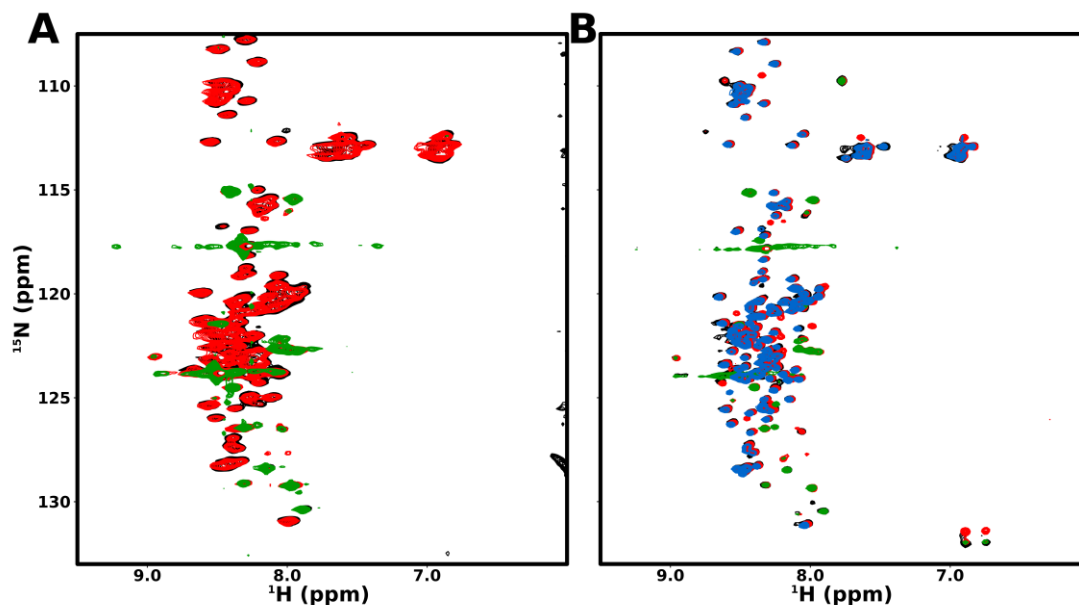


**Figure 3.1: HSQC spectra of alpha-synuclein in intact cells and cell lysates.** (A)  $^1\text{H}$ ,  $^{15}\text{N}$ -HSQC spectra of intact *E. coli* cells expressing alpha-synuclein (black), alpha-synuclein + NatB (red), and NatB alone (green). (B) Supernatant of sonicated cells expressing alpha-synuclein (black), alpha-synuclein + NatB (red), and NatB alone (green), overlaid with the spectrum of purified alpha-synuclein (blue).

The spectrum of alpha-synuclein co-expressed with the NatB complex in intact cells (Figure 3.1A, red) is nearly identical to that of alpha-synuclein alone. There are some peaks that display line broadening, such as that of serine 129, but the overall spectra are very similar, indicating that N-terminally acetylated and unmodified alpha-synuclein adopt the same disordered state inside intact *E. coli* cells, in the absence of any potentially structure-disrupting purification steps, as the purified unmodified protein does in dilute aqueous solution.

Additionally, there are no large conformational changes as a result of acetylation.

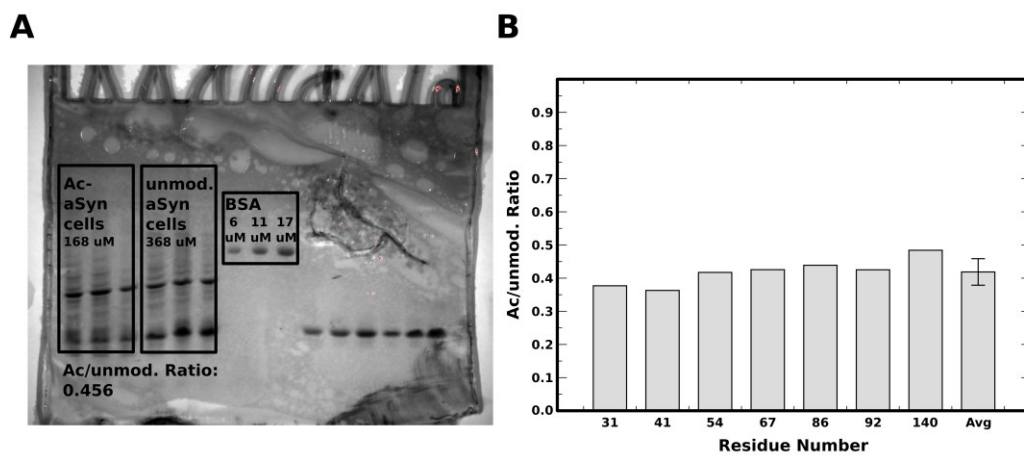


**Figure 3.2: Relative alpha-synuclein concentration in intact cell samples and in-cell NMR spectra.** (A) Alpha-synuclein concentration in intact cell samples run on SDS-PAGE with BSA standards of known concentration. (B) Relative intensity of acetylated to unmodified alpha-synuclein for each of 7 well-resolved cross-peaks and the average.

However, there remains a possibility that some fraction of acetylated alpha-synuclein protein in cells adopts a structured oligomeric assembly that would be invisible on an NMR-spectrum due to its size. In order to assess this possibility, the fraction of acetylation alpha-synuclein that was visible by NMR was estimated by comparing it with the signal observed for the unmodified protein, under the assumption that no alternate NMR-invisible state is formed by unmodified alpha-synuclein [120]. The total concentration of unmodified and acetylated alpha-synuclein in cells was quantified using SDS-PAGE with standards of BSA of known concentration (Figure 3.2A). In a representative experiment, the ratio of acetylated to unmodified alpha-synuclein concentration was 0.456. The relative

concentrations of acetylated and unmodified alpha-synuclein observed by NMR were then estimated using the integrated intensities of several well-resolved amide cross-peaks; the ratio of NMR-observable acetylated to unmodified alpha-synuclein concentration was 0.419 (Figure 3.2B), within 10% of that measured by SDS-PAGE, indicating that N-terminal acetylation does not result in the formation of any substantial NMR-invisible population of alpha-synuclein in intact bacterial cells.

A comparison of the HSQC spectra of unmodified alpha-synuclein in fresh cell lysate and in purified form (Figure 3.1B) shows that essentially all amide cross-peaks occupy the same positions, aside from the extra peaks arising from peptide contaminants in the lysate spectra. The HSQC spectrum of acetylated alpha-synuclein in cell lysates is also very similar to that of the unmodified protein; however, several cross-peaks arising from N-terminal residues, such as leucine 8 and serine 9, are noticeably shifted upon acetylation. The lack of peaks, down to the level of noise, in the peak positions corresponding to the unmodified protein demonstrates that, in this case, N-terminal acetylation is quantitative. This finding was supported by mass spectrometry analysis on the purified protein (data not shown); only one batch of coexpressed alpha-synuclein and NatB did not result in 100% N-terminal acetylation.

*Acetylation increases N-terminal helicity in the free state of alpha-synuclein* – In order to more accurately describe the structural difference between unmodified and acetylated alpha-synuclein, isotopically-labeled proteins were purified and subjected to

multidimensional NMR analysis. A comparison of the HSQC spectra of purified unmodified and acetylated alpha-synuclein (Figure 3.3A) shows the same N-terminal spectral differences as the lysate spectra. Backbone amide assignments for acetylated alpha-synuclein were transferred from those previously determined for unmodified alpha-synuclein [42]. With the assignments in hand, structural differences can be localized by plotting amide chemical shift changes ( $\Delta\delta_{\text{avg}}$ , section II.b, equation 1) *versus* residue number. A plot of chemical shift changes between acetylated and unmodified alpha-synuclein shows that peak shifts for the majority of the protein sequence are very small; only residues 3-13 show significant perturbations (Figure 3.3B). In addition, peaks for methionine 1 and aspartate 2 are visible

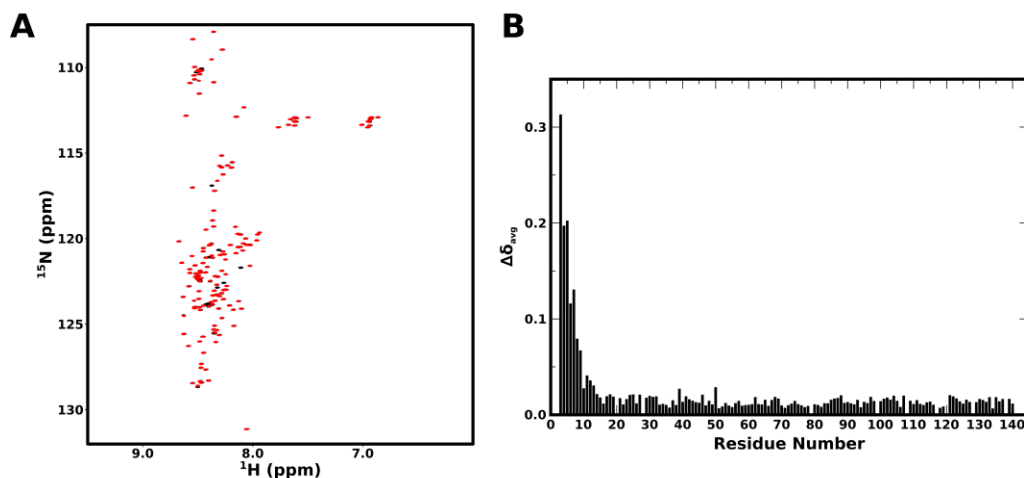


**Figure 3.3: HSQC spectra and amide chemical shift differences for acetylated and unmodified alpha-synuclein in aqueous buffer.** (A)  $^1\text{H}$ ,  $^{15}\text{N}$ -HSQC spectra of purified unmodified (black) and acetylated alpha-synuclein (red) in aqueous buffer. (B) Plot of amide chemical shift differences (equation 1) between unmodified and acetylated alpha-synuclein in aqueous buffer *versus* residue number.

in spectra of (purified and lysate) acetylated alpha-synuclein but not in the unmodified protein spectra, likely due to amide proton exchange with the solvent in the absence of acetylation. The extent of these effects is greater than would be expected from the addition of a small acetyl group to the very N-terminus of the protein, as a variety of point mutant have been shown to result in chemical shift perturbations in disordered alpha-synuclein that extend only +/- 3 residues around the site of modification (e.g. [228]).

Loss of one positive charge at the N-terminal amine could contribute to the unexpectedly long range of effect of N-terminal acetylation. However, examination of the secondary structure propensity using alpha-carbon secondary shifts, which are very sensitive to secondary structure, reveals that the N-terminal ~10 residues of acetylated alpha-synuclein display increased helicity *vis a vis* the unmodified protein (Figure 3.4A). While the unmodified protein residues have a secondary shift ranging from 0 to 0.2 in that region, the N-terminally acetylated protein secondary shifts reach 0.8. Although the amplitude of this deviation from random coil values does not indicate a stable, fully-formed helix in this region, it does suggest that the N-terminal 10 or so residues populate helical conformations a significant fraction of the time. Both proteins display the characteristic helical signature between residues 15 and 30, again indicative of significant populations of helical conformations, though acetylated alpha-synuclein does display slightly lower helicity in the region of residues 14-18. However, this is not reflected in significant changes in the amide chemical shifts. The rest of the protein sequence displays

highly similar alpha-carbon secondary shifts within the experimental error of the measurement.

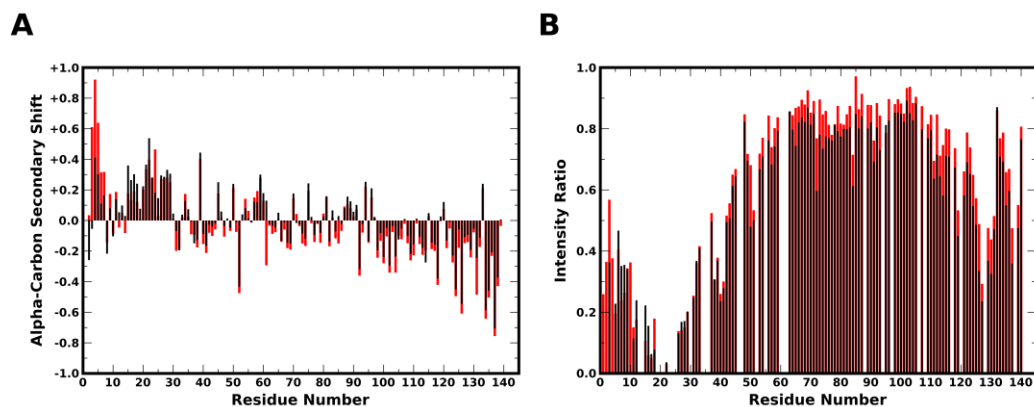


**Figure 3.4: Alpha-carbon secondary shifts and intramolecular contacts for unmodified and acetylated alpha-synuclein in aqueous buffer.** (A) Plot of alpha-carbon secondary shifts *versus* residue number for unmodified (black) and acetylated alpha-synuclein (red) in aqueous buffer. (B) Plot of the ratio of peak intensity for samples paramagnetically labeled at E20C to peak intensity in unlabeled samples *versus* residue number for unmodified (black) and acetylated alpha-synuclein (red) in aqueous buffer.

Despite being disordered, alpha-synuclein forms transient intramolecular contacts that can be measured by PRE experiments. The N- and C-terminal regions of alpha-synuclein contact each other, as evidenced by a PRE effect at the C-terminus when the N-terminus is spin-labeled and *vice versa* [28]. To examine the effects of N-terminal acetylation on these contacts, a spin-label was attached to a cysteine introduced at position 20 of the primary sequence in both unmodified and acetylated alpha-synuclein. The PRE effect plotted *versus* residue number shows a similar pattern in unmodified and acetylated alpha-synuclein (Figure 3.4B). The “well” of signal intensity around the

labeling site is almost identical irrespective of acetylation, and the intensity minimum indicating an intramolecular contact at around position 125 is present in both samples. However, all contacts of the spin-label with the polypeptide chain C-terminal to position 45 are weaker in acetylated alpha-synuclein. This can be attributed to the loss of the positive charge of the amino-terminus, since the intramolecular contacts between the net positive N-terminal region and net negative C-terminal region are mostly electrostatic in nature.

*Acetylation stabilizes helicity in SDS-bound state of alpha-synuclein* – Since N-terminal acetylation increase N-terminal helicity, which is intimately involved in alpha-synuclein binding to membranes and membrane mimics, this increase might be expected to affect this binding process. First, the effect of N-terminal acetylation on alpha-synuclein binding to SDS micelles was studied by NMR. In the presence of SDS micelles, alpha-synuclein adopts a broken-helix conformation that has been often used as an NMR-tractable model for the membrane-bound state of alpha-synuclein [71,72,74]. A comparison of the HSQC spectra of unmodified and acetylated alpha-synuclein in the presence of spheroidal SDS micelles shows two highly similar spectra with several notable spectral differences (Figure 3.5A). The overall similarity of the spectra suggests that acetylated alpha-synuclein adopts a very similar conformation to the unmodified protein on SDS micelles. Backbone amide assignments for acetylated alpha-synuclein were transferred from those previously determined for the unmodified protein [71] and the observed spectral differences were localized to the very N-terminus of the protein, with the N-terminal 13

residues showing significant peak shifts upon acetylation, much like in the free state (Figure 3.5B).

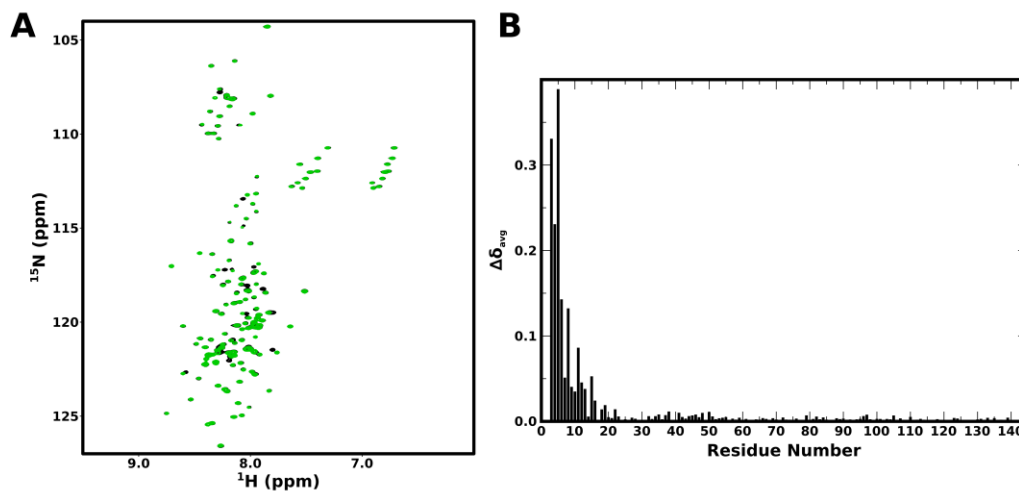


**Figure 3.5: HSQC spectra and amide chemical shift differences for acetylated and unmodified alpha-synuclein in the presence of SDS micelles.** (A)  $^1\text{H}$ ,  $^{15}\text{N}$ -HSQC spectra of purified unmodified (black) and acetylated alpha-synuclein (green) in 40 mM SDS. (B) Plot of amide chemical shift differences (equation 1) between unmodified and acetylated alpha-synuclein in 40 mM SDS *versus* residue number.

Since N-terminal acetylation was shown to increase N-terminal helicity of alpha-synuclein in aqueous solution and the SDS-bound protein already contains extensive stable helical structure throughout the N-terminal domain, N-terminal acetylation was not expected to greatly perturb the secondary structure of the SDS-bound state. However, the extent of the amide chemical shift changes upon acetylation (up to residue 13) suggested an effect on the local secondary structure, as in the free state. Thus, secondary structure propensity was determined by using alpha-carbon secondary shifts. Surprisingly, while the overall structure of two stable helical regions with a break around residue 40 is conserved, the N-terminal 10

residues of acetylated alpha-synuclein display increased helicity compared to the unmodified protein in the presence of SDS micelles (Figure 3.6A). These findings suggest that, in the absence of N-terminal acetylation, helix-1 of alpha-synuclein is frayed at the N-terminus, and acetylation reduces the extent of this fraying by stabilizing helical structure. In this way, studying the modified protein provided an insight into the structure of the unmodified protein.

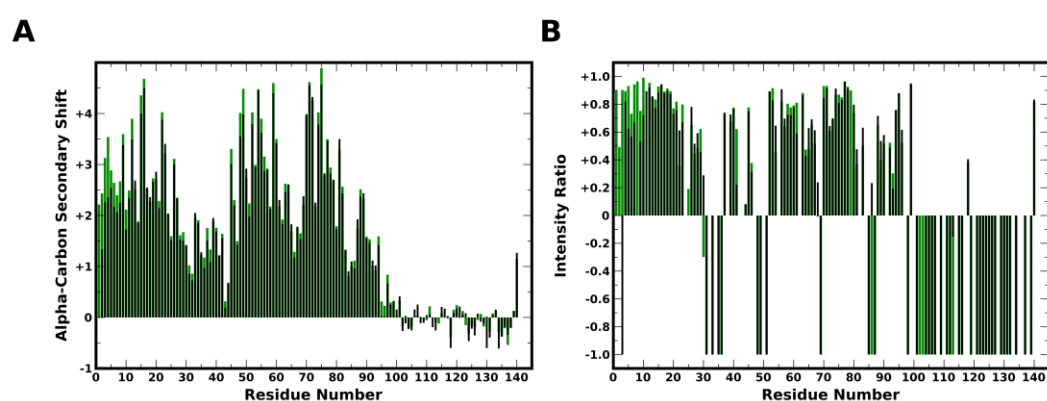


**Figure 3.6: Alpha-carbon secondary shifts and extent of amide proton exchange for unmodified and acetylated alpha-synuclein in the presence of SDS micelles.** (A) Plot of alpha-carbon secondary shifts *versus* residue number for unmodified (black) and acetylated alpha-synuclein (green) in 40 mM SDS. (B) Plot of the ratio of peak intensity with a water inversion pulse to peak intensity without water inversion *versus* residue number for unmodified (black) and acetylated alpha-synuclein (green) in 40 mM SDS at pH 8.4. The intensity ratio reports on level of protection of amide protons from solvent exchange.

In order to confirm increased helix stability at the N-terminus of alpha-synuclein, the extent of amide proton protection from exchange with the solvent was quantified. The N-terminal 10 residues were found to be more protected from exchange in the acetylated protein (Figure 3.6B), confirming the conclusions drawn from the secondary

shift analysis. These data show that the N-terminal acetyl group stabilizes helicity at the very N-terminus in the SDS micelle-bound state and, by inference, may be expected to do so in other lipid- and detergent-bound states.

*Acetylated alpha-synuclein binds to BOG micelles in a novel partly-helical conformation* – Several reports of a structured, helical form of alpha-synuclein purified from *E. coli* involved purification in a buffer containing low, sub-micellar concentrations of  $\beta$ -octyl-glucoside (BOG), a nonionic detergent commonly used to purify membrane proteins [117,118]. Since alpha-synuclein is known to bind to membranes and detergent micelles with a concomitant induction of helical structure, it is possible that N-terminally acetylated alpha-synuclein binds to BOG during purification, promoting helical structure in the protein. While the effects of a number of detergents on alpha-synuclein structure have been studied, the detergents employed tend to be negatively-charged and do not include BOG in their number [74,78,84,229].

In order to determine whether BOG induces helical conformations in unmodified and acetylated alpha-synuclein, the proteins were titrated with increasing concentrations of BOG and the secondary structure monitored using far-UV CD spectroscopy. CD spectra of unmodified and acetylated alpha-synuclein with increasing concentrations of BOG, far above the critical micellar concentration (CMC) of BOG, (~25 mM) are consistent with mostly disordered conformations, but with an increase of helicity, especially for the N-terminally acetylated protein (Figure 3.7A,B). In the absence of

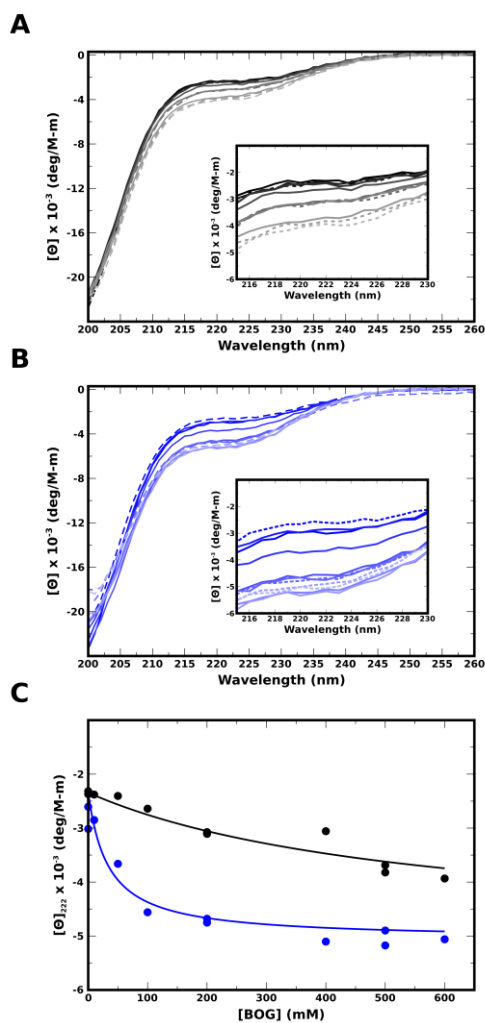


**Figure 3.7: Far-UV CD spectra of unmodified and acetylated alpha-synuclein with increasing BOG concentration.** Plot of mean residue ellipticity with increasing concentrations of BOG *versus* wavelength for (A) unmodified alpha-synuclein (black) and (B) acetylated alpha-synuclein (blue). BOG concentrations are 0, 10, 50, 100, 200, 400, 500, and 600 mM increasing with increasing lightness of line. Dashed lines indicate data from a second titration. The inset contains a zoom into the region containing the minimum associated with helical structure at 222 nm. (C) Plot of the mean residue ellipticity at 222 nm with increasing BOG concentration for unmodified (black) and acetylated alpha-synuclein (blue). The points are fit to equation 12 with a  $K_{D,app}$  of 613 and 51 mM for unmodified and acetylated alpha-synuclein, respectively.

detergent, acetylated alpha-synuclein already displays a higher fraction of helical residues (10%, corresponding to 14 fully-helical residues) than the unmodified protein (9%, 12 residues). At the end point of the titration (600 mM BOG), the maximum concentration practically attainable given the solubility of BOG, acetylated alpha-synuclein had a fractional helicity of 16%, corresponding to 22 fully-helical residues, while the unmodified protein only reached 13%, corresponding to 18 helical residues. These data strongly suggest a direct interaction between alpha-synuclein and BOG that results in induction of helical structure, most likely as a result of alpha-synuclein binding to the detergent micelles, similar to its interactions with SDS and other detergents [42,74]. This is a novel, heretofore uncharacterized interaction.

The mean residue ellipticity at 222 nm, proportional to fractional helicity, is plotted as a function of BOG concentration in Figure 3.7C. From the plot, it appears that the binding of acetylated alpha-synuclein to BOG reaches saturation in the concentration range studied, while the situation for unmodified alpha-synuclein is less clear. The binding could be reaching saturation around 600 mM BOG, but at an endpoint corresponding to lower fractional helicity than the acetylated protein, or it could be far from reaching saturation. Since higher concentrations of BOG were not reachable for this measurement, it was reasoned that the N-terminal modification should not have a large effect on the final conformation of the BOG-bound alpha-synuclein, which should therefore have similar levels of helical structure in unmodified and acetylated protein. As a result, when the

binding curves were fit to equation 12, final values of mean residue ellipticity at 222 nm were constrained to be the same for unmodified and acetylated alpha-synuclein. The fitting allowed apparent  $K_D$  values to be extracted; acetylated alpha-synuclein bound with a  $K_{D,app}$  of 51 mM and unmodified alpha-synuclein with an order of magnitude higher  $K_{D,app}$  of 613 mM. Thus, while unmodified alpha-synuclein binds BOG weakly, with an induction of some helical structure, N-terminal acetylation greatly increases the affinity of the binding interaction.

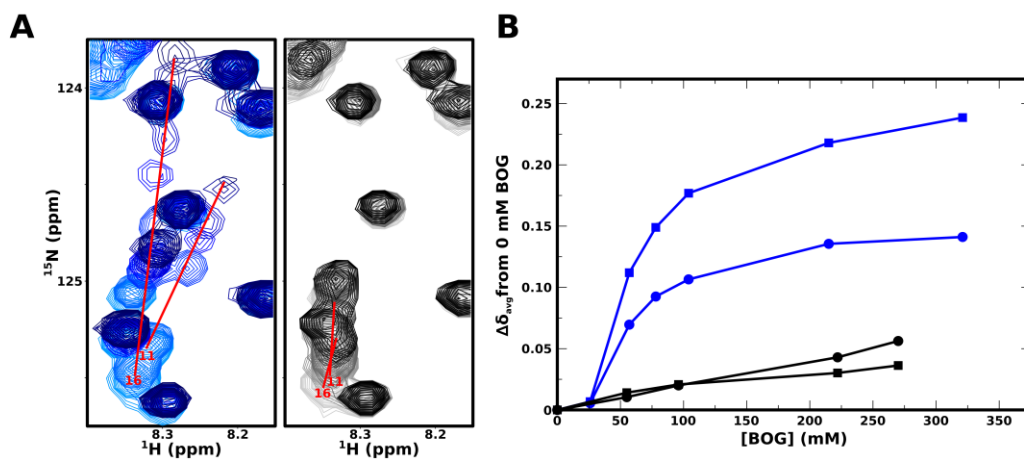


**Figure 3.8: HSQC spectra and amide chemical shift differences for acetylated alpha-synuclein with increasing BOG concentration.** (A) Zoomed regions of  $^1\text{H}$ ,  $^{15}\text{N}$ -HSQC spectra of unmodified (black, right) and acetylated alpha-synuclein (blue, left) with increasing concentrations of BOG. The red arrows illustrate linear paths of peak shifts for two peaks (A11 and A16). BOG concentrations are 0, 25, 50, 75 (acetylated), 100, ~200, and ~300 mM increasing with increasing darkness of contour. (B) Plot of the amide chemical shift difference from 0 mM BOG (equation 1) with increasing BOG concentration for the peaks of A11 (circles) and A16 (squares) for unmodified (black) and acetylated alpha-synuclein (blue).

In order to describe this interaction at single-residue resolution, NMR spectroscopy was employed. Increasing concentrations of BOG resulted in dose-dependent position shifts in several N-terminal peaks; two well-resolved peaks (A11 and A16) are shown in Figure 3.8A. The observed peak shifts are linear and do not show any peak doubling, consistent with a two-state equilibrium with exchange occurring faster than the NMR timescale in the experiment. The original peak position corresponds to fully free alpha-synuclein, the theoretical “final” peak position (not reached at these concentrations) corresponds to fully bound alpha-synuclein, and each intermediate peak corresponds to an average of the initial and final positions weighted by the relative populations of free and bound protein at that concentration. With only two states (free and bound), each intermediate peak falls on a straight line between the initial and final positions. Since the peaks broaden and decrease in intensity with increasing BOG concentrations, the exchange rate between the two states may be close to the relevant experiment timescale (i.e. approaching the “intermediate exchange regime,” in which signals are highly broadened), or, alternatively, the bound state may give rise to broad peaks due to increased relaxation, reflecting its larger size or dynamics in the bound state.

The change in chemical shift from the initial position can be plotted *versus* BOG concentration, giving titration curves similar to those obtained from CD data, which measure induction of helicity. The titration curves obtained from chemical shift perturbation for two N-terminal residues (A11 and A16) are shown in Figure 3.8B. The interaction between acetylated alpha-synuclein and BOG approaches

saturation by the end of the titration (~300 mM BOG), while unmodified alpha-synuclein shows small peak shifts even at the high end of the titration. Interestingly, amide cross-peaks of acetylated alpha-synuclein do not shift appreciably from the initial position at the lowest concentration of BOG added (~25 mM), which is very close to the CMC of BOG (20-25 mM), and only begin to shift above that concentration. The CD-monitored titration had only one measurement at a lower concentration (10 mM), and the ellipticity measured at that point was very similar to that for the free protein as well (Figure 3.7).

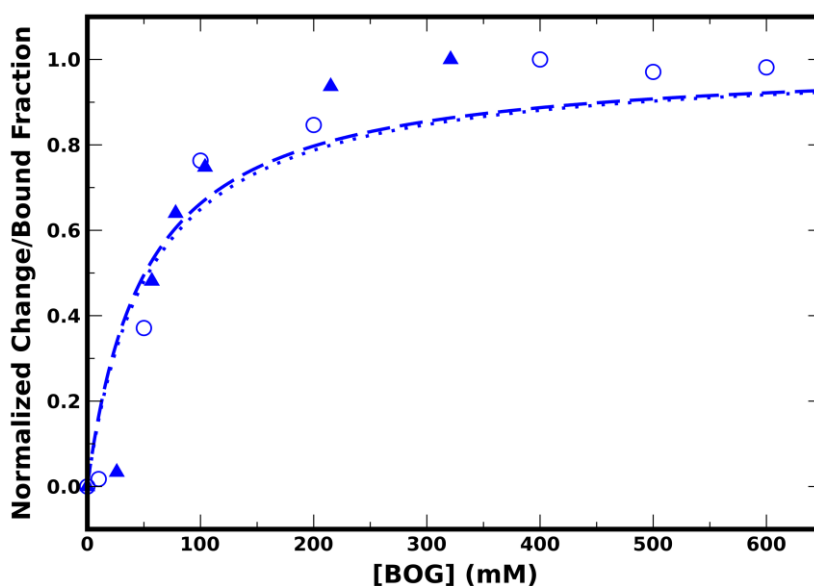


**Figure 3.9: Binding curves derived from CD and NMR data for acetylated alpha-synuclein with increasing BOG concentration.**

Plot of the binding curves derived from mean residue ellipticity (circles) and amide chemical shift difference from 0 mM BOG averaged for residues 11 and 16 (triangles) with increasing BOG concentration for acetylated alpha-synuclein (blue). The points are fit to equation 2 with a  $K_{D,app}$  of 51 and 54 mM for CD and NMR data, respectively.

The NMR and CD titration data ostensibly report on the same binding event of acetylated alpha-synuclein to BOG; the titrations were thus compared to see if they match. In order to compare the extent of the binding reaction, the signal reporting on binding in each experiment was normalized (see Methods, section III.b). A plot of this normalized signal change from both experiments is shown in Figure 3.9. The extents of binding at similar BOG concentrations from the two experiments are very similar. When fitted to equation 2, the CD data yield a  $K_{D,app}$  of 51 mM (as seen in Figure 3.7C) while the NMR data result in a  $K_{D,app}$  of 54 mM. The two methods are thus in very close agreement in measuring this novel binding interaction.

Since the binding of any form of alpha-synuclein to BOG micelles has not been reported before, the structural basis of this interaction is unknown and warrants further description. While the binding of acetylated alpha-synuclein to BOG micelles appears to saturate at ~300 mM BOG, the NMR signals for the affected residues are extremely weak at this high concentration (Figure 3.8A). Thus, an intermediate BOG concentration (100 mM) was chosen for further NMR analysis. From the titration curves (Figure 3.8B), approximately 70% of acetylated alpha-synuclein is bound at this concentration, and the peaks have sufficient intensity to be analyzed by NMR experiments. Comparison of the  $^1\text{H},^{15}\text{N}$ -HSQC spectra of acetylated alpha-synuclein in the presence and absence of 100 mM BOG shows several spectral changes that appear to be localized to a small region of the protein (Figure 3.10A). While backbone amide assignments had been provisionally transferred from the free state of acetylated alpha-

synuclein during the titration, they were confirmed by means of an HNCA experiment. A plot of peak position shifts *versus* protein primary sequence localizes the affected region to the N-terminal ~25 peaks (Figure 3.10B). This interacting region differs from the previously described SDS- and lipid vesicle-interacting region, which encompasses the entire N-terminal domain of ~100 amino acids [42,71]. However, it is similar to a region that forms a partially vesicle-bound state proposed based on NMR experiments at low vesicle:protein ratios [91,92] and is also similar to the region of alpha-synuclein that interacts with calmodulin [113].

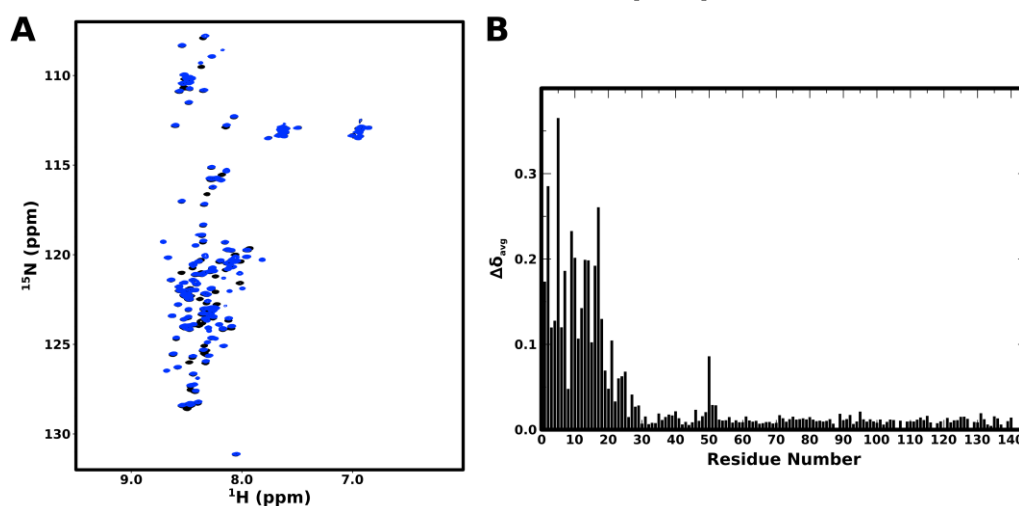


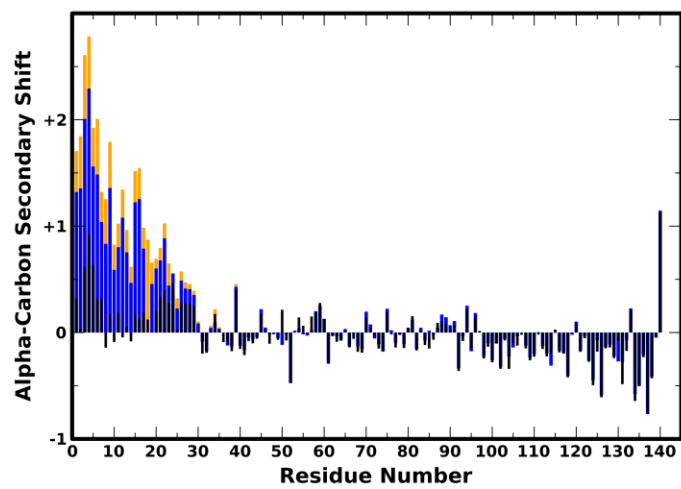
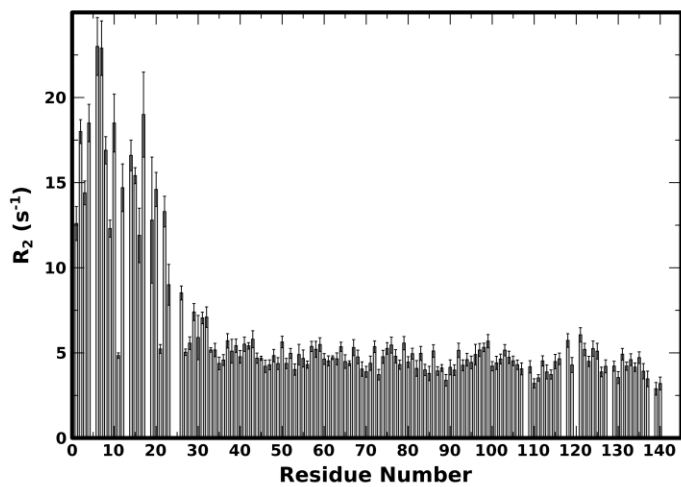
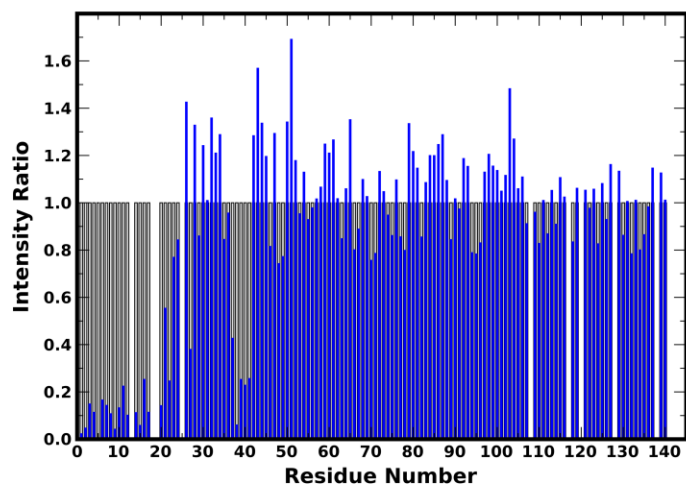
**Figure 3.10: HSQC spectra and amide chemical shift differences for acetylated alpha-synuclein in the presence and absence of BOG micelles.** (A)  $^1\text{H}$ ,  $^{15}\text{N}$ -HSQC spectra of acetylated alpha-synuclein in aqueous buffer (black) and 100 mM BOG (blue). (B) Plot of amide chemical shift differences (equation 1) for acetylated alpha-synuclein between aqueous buffer and 100 mM BOG *versus* residue number.

The chemical shift perturbations delineate the region interacting with BOG but, by themselves, do not provide any structural information about the nature of the interaction. Secondary shifts for

the alpha-carbons, derived from the abovementioned HNCA experiment, provide secondary structure information (Figure 3.11A, blue). The N-terminal 25-30 residues display increased positive deviations from random coil values, compared to the free protein, demonstrating that this region populates significant helical conformations. The values of the secondary shifts range from 0.5 to 2 ppm, indicating some regions (residues 1-10) of stable  $\alpha$ -helical structure and other regions of labile, frayed, or partially occupied helices. Since only ~70% of the protein is bound at this BOG concentration, it is possible that at full binding, the entire interacting region becomes stably helical. To examine this hypothesis, an HNCA experiment was performed on acetylated alpha-synuclein in the presence of 300 mM BOG. The secondary shifts at this concentration when almost all of the protein is micelle-bound show the same pattern in the N-terminal 25-30 residues as at 100 mM BOG, although the magnitude of the shift is 0.3-0.4 ppm higher (Figure 3.11A, orange). However, the pattern of secondary shifts suggests that even at full binding, only the N-terminal half of this region forms a stable helix, while the C-terminal half remains labile.

To confirm whether this helical interacting region directly binds the BOG micelle, two approaches were employed: amide nitrogen  $R_2$  relaxation rates, which report on flexibility or dynamics of the protein backbone on a picosecond-nanosecond timescale, and PRE NMR with spin-label-doped BOG micelles, which delineates the regions that come within ~25 Å of the micelle. Amide nitrogen  $R_2$  rates were similarly low between residues 30 and 140 (Figure 3.11B). The values of the  $R_2$

**Figure 3.11: Alpha-carbon secondary shifts,  $R_2$  relaxation rates, and PRE effects from doped micelles for acetylated alpha-synuclein in the presence of BOG micelles.** (A) Plot of alpha-carbon secondary shifts *versus* residue number for acetylated alpha-synuclein in aqueous buffer (black), 100 mM BOG (blue), and 300 mM  $^2\text{H}$  BOG (orange, only the first 40 residues are plotted). (B) Plot of transverse relaxation rate  $R_2$  for acetylated alpha-synuclein in 100 mM BOG *versus* residue number. Error bars show the error of fitting provided by NMRViewJ. (C) Plot of the ratio of peak intensity in the presence of paramagnetically doped BOG micelles (100 mM) to peak intensity in the presence of undoped micelles (100 mM) for acetylated alpha-synuclein *versus* residue number. The gray bars indicate which peaks were included in the analysis.

**A****B****C**

rates in this region (4-5 sec<sup>-1</sup>) are very similar to those obtained throughout the polypeptide chain for free alpha-synuclein [43] and (accounting for temperature difference) for the disordered C-terminal tail of SDS micelle-bound alpha-synuclein [75], suggesting that this region remains free and disordered in solution in the presence of BOG. The R<sub>2</sub> rates of the N-terminal ~30 residues, however, are much higher (10-20 sec<sup>-1</sup>), indicative of increased relaxation due to slower backbone motions or slow overall tumbling upon the formation of a protein-micelle complex. The magnitude of the R<sub>2</sub> rates in this N-terminal region is similar, accounting for temperature difference, to that seen in the SDS micelle-bound region of alpha-synuclein [75], suggesting that a similar protein-micelle complex is formed between the N-terminal ~25 residues of acetylated alpha-synuclein and BOG micelles.

The PRE results also implicate the same N-terminal region in binding to the micelle. In the presence of spin-label-containing BOG micelles, the cross-peaks for the N-terminal ~25 residues show greatly decreased signal intensity, indicating that that region is in close contact with the micelle (Figure 3.11C). The C-terminal portion of the protein does not show decreased signal intensity in the presence of spin-label, aside from a minimum near the aromatic tyrosine 39 residue, which may bind the spin-label directly [75]. The secondary shift, PRE and R<sub>2</sub> data are very consistent, strongly supporting a binding mode in which the N-terminal 25-30 residues bind to the detergent micelle in a mostly-helical conformation while the rest of the protein remains disordered. Intriguingly, there may be a slight decrease near residue 10 in both PRE effect and R<sub>2</sub> rate. This dip

suggests that binding to the micelle is not uniform throughout the N-terminal 25-30 residues and some detachment from the micelle may occur roughly in the middle of this region. This minimum may also signify a break in the helical structure of this region, as there is also a small dip in helicity around residue 10 in the alpha-carbon secondary shift data (Figure 3.11A). Clearly, while the binding region is more structured compared to the rest of the protein, it does not form a stable, well-formed helix. Additionally, the size and shape of the BOG micelle is not known, nor the extent of protein insertion into the micelle.

*Acetylation increases alpha-synuclein binding to curved lipid vesicles of lower charge* – Unmodified alpha-synuclein has been shown conclusively to bind to synthetic lipid vesicles, specifically those with significant proportions of negatively-charged lipids, with a concomitant adoption of helical structure in the N-terminal region [42,55,61,62]. A modification that affects the level of helicity at the very N-terminus may thus be expected to have an effect on alpha-synuclein binding to lipid vesicles. Early studies obtained contrasting results, with acetylated alpha-synuclein showing no difference from the unmodified protein in binding to large (~120 nm diameter) vesicles of 100% negatively-charged POPG [230] but binding about two times more tightly to more curved (~40 nm diameter) vesicles containing 30% negatively-charged DOPS (and more kinked DO lipids) [231]. In order to harmonize these results, a systematic study of acetylated and unmodified alpha-synuclein binding to lipid vesicles of different curvature and charge was undertaken. Both unmodified and

acetylated alpha-synuclein were incubated with synthetic lipid vesicles of two sizes and two lipid compositions: SUVs made by sonication (~40 nm diameter) and LUVs made by extrusion (~120 nm diameter) composed of either 50% DOPS, 35% DOPC, 15% DOPE (high negative charge) or 15% DOPS, 60% DOPC, 25% DOPE (low/medium negative charge).

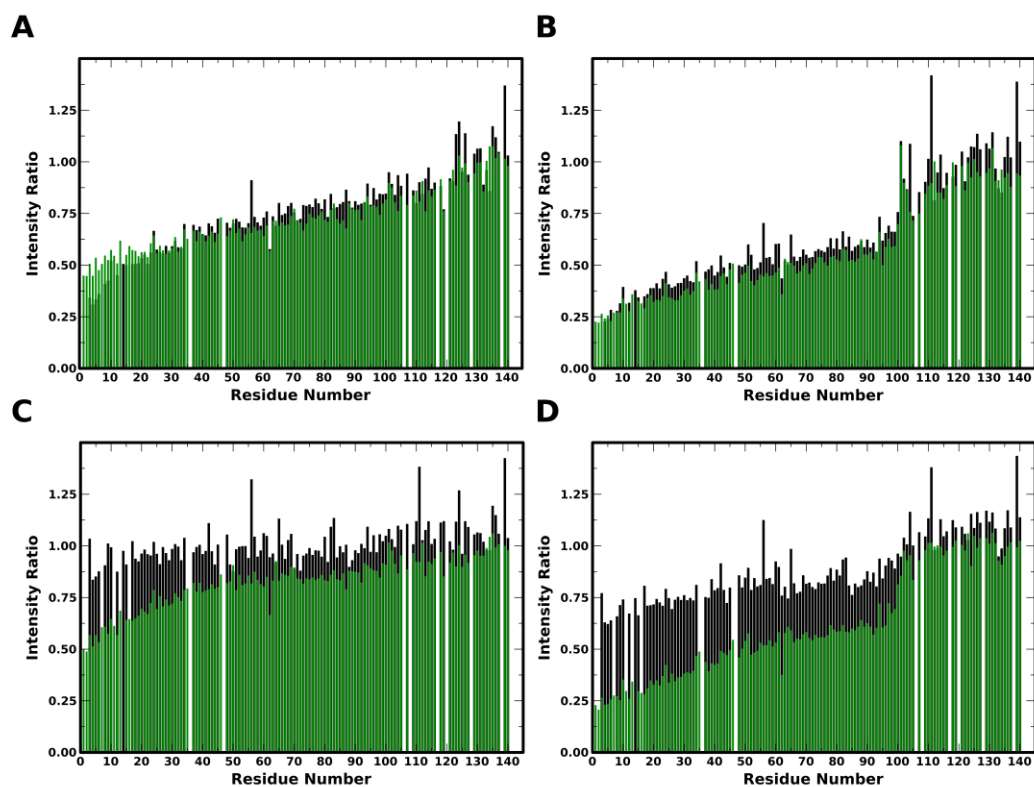


**Figure 3.12: Binding profiles of unmodified and acetylated alpha-synuclein to high and low negative charge SUVs and LUVs.** Plot of the ratio of peak intensity in the presence of 3 mM 50% PS LUVs (A) and SUVs (B) and 15% PS LUVs (C) and SUVs (D) to peak intensity in the absence of vesicles *versus* residue number for unmodified (black) and acetylated alpha-synuclein (green). Bound fractions of total binding and fully-helical binding are shown in Table 3.1.

At first, the level of binding in the presence of 3 mM lipid vesicles, a concentration at which only partial binding is expected [91], was assessed. In a partial-binding regime, the level of free protein can be monitored by the remaining cross-peak signal intensity in an HSQC spectrum, thus providing residue- or region-specific extents of binding. In the presence of high negative charge (50% PS) LUVs and SUVs, unmodified alpha-synuclein bound very tightly (Figure 3.12A,B), with 65% (LUVs) and 73% (SUVs) of the protein bound to some extent (Table 3.1). The N-terminally acetylated alpha-synuclein showed very similar extent of binding, with 49% and 73% binding to LUVs and SUVs, respectively (Figure 3.12A,B and Table 3.1). While the pattern of binding throughout the protein sequence was very similar for unmodified and acetylated alpha-synuclein, there was noticeably less binding of the acetylated protein in the N-terminal ~20 residues to 50% PS LUVs (Figure 3.12A). This difference was not seen for SUVs. This loss of binding suggests that electrostatic attraction plays a large role in alpha-synuclein binding to high negative charge, less curved vesicles, since the loss of the primary amine positive charge has such a noticeable effect.

In the presence of lower negative charge lipid vesicles (15% PS), much less unmodified alpha-synuclein was bound, approximately 14% for LUVs and 38% for SUVs (Table 3.1). Acetylated alpha-synuclein, however, displayed significantly more binding than the unmodified protein (Figure 3.12C,D), with 43% and 74% binding to LUVs and SUVs, respectively. The extent of acetylated alpha-synuclein binding to 15% PS lipid vesicles is comparable to the extent of binding to 50% PS

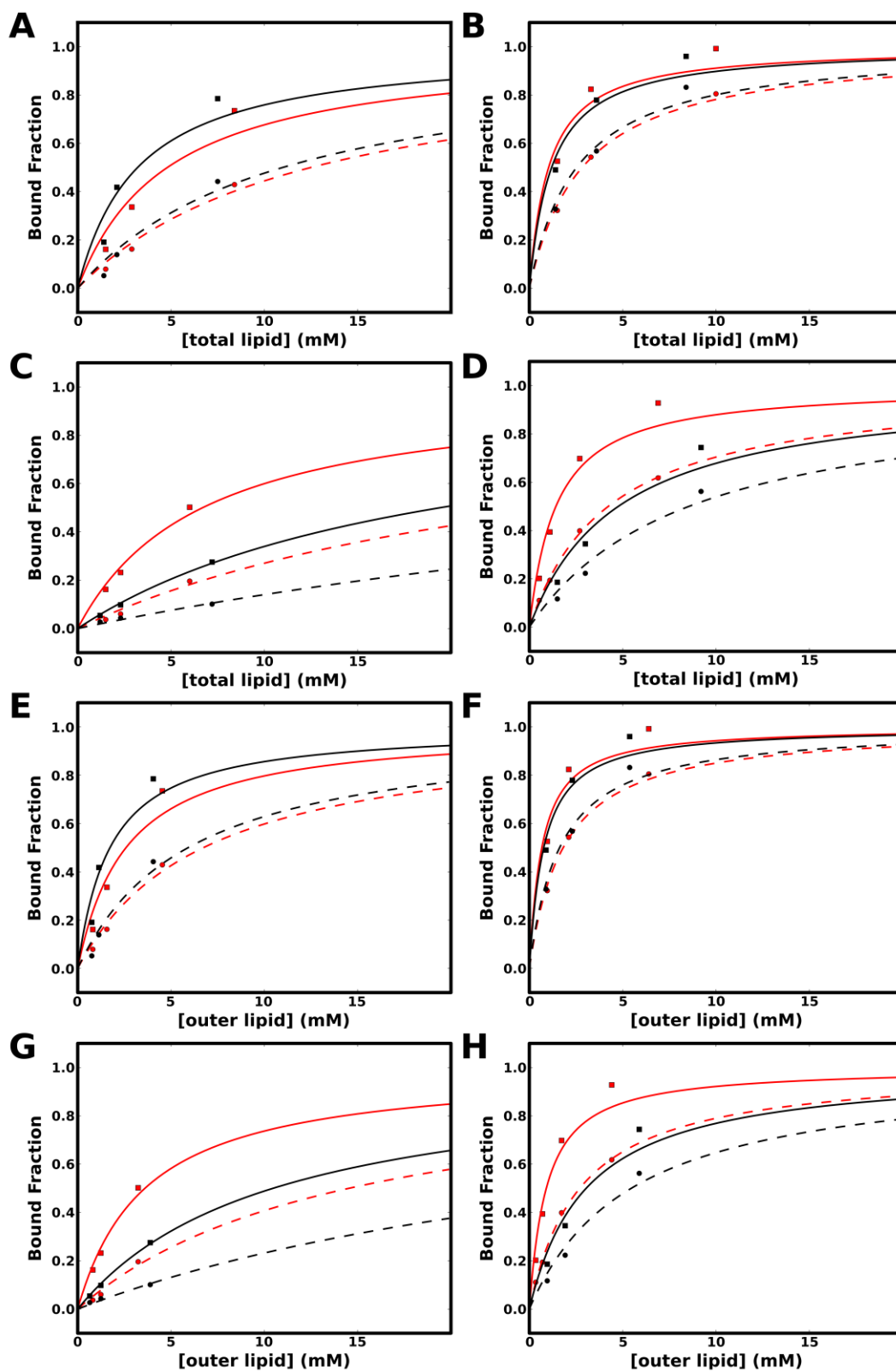
vesicles, suggesting that N-terminal acetylation of the protein selectively enhances binding to lower negative charge vesicles.

**Table 3.1: Bound fractions of different populations of unmodified and acetylated alpha-synuclein in the presence of high and low negative charge SUVs and LUVs.** Bound fractions were calculated as described in section III.b.

Lipid and Protein	Total Bound Fraction	Fully-Helical Bound Fraction
50% DOPS		
LUVs		
unmodified	0.645	0.241
acetylated	0.494	0.281
SUVs		
unmodified	0.733	0.437
acetylated	0.727	0.464
15% DOPS		
LUVs		
unmodified	0.135	0.077
acetylated	0.428	0.143
SUVs		
unmodified	0.383	0.234
acetylated	0.742	0.428

In order to assess the effects of acetylation on selectivity for membrane curvature or charge more quantitatively, unmodified and acetylated alpha-synuclein were titrated with increasing concentrations of the four previously studied synthetic lipid vesicles. Due to material limits, only 3 or 4 concentrations of each lipid vesicle stock were employed; the binding curves were fitted to equation 2, and apparent  $K_D$  values extracted for different binding modes (see Methods,

**Figure 3.13: Titrations of unmodified and acetylated alpha synuclein to high and low negative charge SUVs and LUVs.** Plots of the bound fractions of total binding (squares) and fully-helical binding (circles) with increasing concentrations of 50% PS LUVs (A,E) and SUVs (B,F) and 15% PS LUVs (C,G) and SUVs (D,H) for unmodified (black) and acetylated alpha-synuclein (red). Panels A-D use total lipid concentration, while E-H use only accessible outer lipid concentrations. The points are fit to equation 2 and extracted  $K_{D,app}$  values shown in Table 3.2.



section III.b) (Figure 3.13). The “total binding” apparent dissociation constants computed using total lipid concentrations agree with the single concentration results (Table 3.2). The affinity of unmodified alpha-synuclein for 50% PS lipid vesicles, both LUVs and SUVs, is very similar to that of the acetylated protein for the same curvature vesicles. In the case of 15% PS vesicles, the apparent  $K_D$  values for acetylated alpha-synuclein are 2.9 and 3.4 times smaller than those of the unmodified protein for LUVs and SUVs, respectively, indicating significantly tighter binding of the modified protein. Both forms of alpha-synuclein have lower dissociation constants with SUVs than with LUVs, quantitatively demonstrating the previously observed selectivity of alpha-synuclein for more curved vesicles (Table 3.2). The acetylated protein displays slightly greater selectivity for SUVs, regardless of negative charge content.

However, binding to SUVs and LUVs cannot be accurately compared using bulk lipid concentration, since vesicles of different curvature have different proportions of lipids available for binding on the outer leaflet. In order to facilitate these comparisons, the percentage of lipids on the outer leaflet was calculated for SUVs (64%) and LUVs (54%) (see Methods, section II.b) and the lipid concentrations normalized by those percentages for a second round of fitting (Figure 3.13E-H). The apparent dissociation constants thus obtained can be directly compared between SUVs and LUVs. When compared in this manner, acetylated alpha-synuclein shows significantly greater selectivity for SUVs than unmodified alpha-synuclein (4.2 *versus* 2.4 for 50% PS, 4.4 *versus* 3.5 for 15% PS),

**Table 3.2: Computed apparent  $K_D$  values and other parameters for unmodified and acetylated alpha-synuclein binding to high and low negative charge SUVs and LUVs.** Apparent  $K_D$  values were calculated from fitting titrations to equation 2 (see Figure 3.13) using total lipid concentration and only accessible outer lipid concentration (see Chapter II). “Effect of N-ac” was calculated as the ratio of  $K_{D,app}$  for acetylated alpha-synuclein over  $K_{D,app}$  for unmodified alpha-synuclein. “SUV Selectivity” was calculated using equation 4 and “Full Helix Fraction” was calculated using equation 5 (see section II.d).

Protein and Lipid	Total Lipid						Outer Lipid					
	Total Binding			Fully-Helical Binding			Total Binding			Fully-Helical Binding		
	K <sub>D,app</sub> (mM)	Effect of N-ac	SUV Selectivity	K <sub>D,app</sub> (mM)	Effect of N-ac	SUV Selectivity	Full Helix Fraction	K <sub>D,app</sub> (mM)	SUV Selectivity	K <sub>D,app</sub> (mM)	SUV Selectivity	SUV Selectivity
50% DOPS LUVs												
Unmod aSyn	3.1 ± 0.8			10.9 ± 2.0			0.28	1.7 ± 0.4		5.8 ± 1.0		
Ac-aSyn SUVs	4.7 ± 1.2	0.7		12.4 ± 1.4	0.9		0.38	2.5 ± 0.6		6.7 ± 0.7		
Unmod aSyn	1.1 ± 0.2		2.8	2.5 ± 0.3		4.4	0.44	0.7 ± 0.1	2.4	1.6 ± 0.2	3.6	
Ac-aSyn	1.0 ± 0.3	1.1	4.7	2.8 ± 0.2	0.9	4.4	0.36	0.6 ± 0.2	4.2	1.7 ± 0.1	3.9	
15% DOPS LUVs												
Unmod aSyn	19.3 ± 0.6			61.2 ± 4.7			0.32	10.4 ± 0.3		33.0 ± 2.6		
Ac-aSyn SUVs	6.6 ± 0.6	2.9		26.9 ± 3.1	2.3		0.25	3.5 ± 0.3		14.5 ± 1.7		
Unmod aSyn	4.7 ± 1.0		4.1	8.5 ± 1.2		7.2	0.55	3.0 ± 0.6	3.5	5.4 ± 0.7	6.1	
Ac-aSyn	1.4 ± 0.2	3.4	4.7	4.2 ± 0.1	2.0	6.4	0.33	0.8 ± 0.2	4.4	2.6 ± 0.1	5.6	

although both forms of the protein show a significant preference for binding the more highly curved SUVs (Table 3.2).

The binding discussed so far and measured by the “total binding”  $K_D$  potentially includes many different modes of alpha-synuclein binding to vesicles, such as the “fully helical” mode in which the entire N-terminal ~100 residues become helical and bind the vesicle surface and an unknown number of partly-helical binding modes in which shorter N-terminal regions bind the vesicle surface (presumably as an  $\alpha$ -helix). These partly-helical modes may include the proposed “SL1” binding mode comprising residues 1-25 [92] and a mode in which only helix-1 (residues 1-37) is bound. The “total binding” does not differentiate between these partly-helical modes, nor between them and fully-helical binding. Fully helical binding can be assessed on its own by measuring binding of a more C-terminal region of the lipid-binding ~100 residues. Apparent dissociation constants were also determined for this fully helical binding mode. In general, the relative affinities follow the same trend as those for total binding, with no effect of acetylation with 50% PS vesicles, and with increased binding to 15% PS vesicles, regardless of curvature (Table 3.2).

When outer membrane lipid concentration was used to compare binding to vesicles of different curvature, unmodified and acetylated alpha-synuclein showed similar levels of preference for binding to SUVs in the fully-helical conformation (3.6 and 3.9 for 50% PS, 6.1 and 5.6 for 15% PS) (Table 3.2). As for total binding, fully-helical

binding has greater selectivity for SUVs when binding to 15% PS vesicles. Contrary to the situation for total binding, however, acetylation does not increase selectivity for SUVs. This difference suggests that the curvature selectivity of the full helix is not greatly affected by N-terminal acetylation, and that most of the effect of N-terminal acetylation on curvature selectivity is mediated through increased partly-helical binding.

One other interesting finding is that higher curvature generally promotes “helix extension,” here estimated as the ratio of total binding  $K_D$  to fully helical  $K_D$ , which also corresponds to the fraction of fully-helical bound protein (see Methods, section III.b) (Table 3.2). In addition, N-terminal acetylation generally disfavors helix extension, indicating that it stabilizes partly-helical states. The one exception to both is due to the low N-terminal binding of acetylated alpha-synuclein to high negative charge LUVs, likely a result of the decreased electrostatic attraction at the very N-terminus due to loss of the positive charge at the amino-terminus.

Treating alpha-synuclein binding to lipids as a one-binding-site system characterized only by affinity ignores one important factor: potentially different binding sites offered by lipid membranes of different curvature or lipid composition. In order to gain insight into the effect of vesicle type on alpha-synuclein binding sites, titrations were fit using equation 3, which allows a parameter  $B_{max}$ , or maximum number of protein binding sites per lipid molecule, to be extracted. This parameter can yield how many lipid molecules are required to bind one protein molecule and an estimate of the number of

productive binding sites offered by different membrane configurations (see Methods, section III.b). In order to perform fits with this equation, titrations with measurements at more concentrations were required. Unmodified alpha-synuclein was titrated with LUVs and SUVs of the low negative charge composition (15% DOPS, 60% DOPC, 25% DOPE) and the bound fractions plotted as a function of outer membrane lipid concentration and fit to equations 2 and 3. Interestingly, the curves derived from equation 3 fit the points much more closely, (Figure 3.14). On the other hand, equation 3 could not be fit to fully helical bound fractions while giving reasonable values for  $K_D$  and  $B_{max}$ . This suggests that fully-helical binding of alpha-synuclein to lipid vesicles cannot be described as a bimolecular binding equilibrium with independent binding sites.

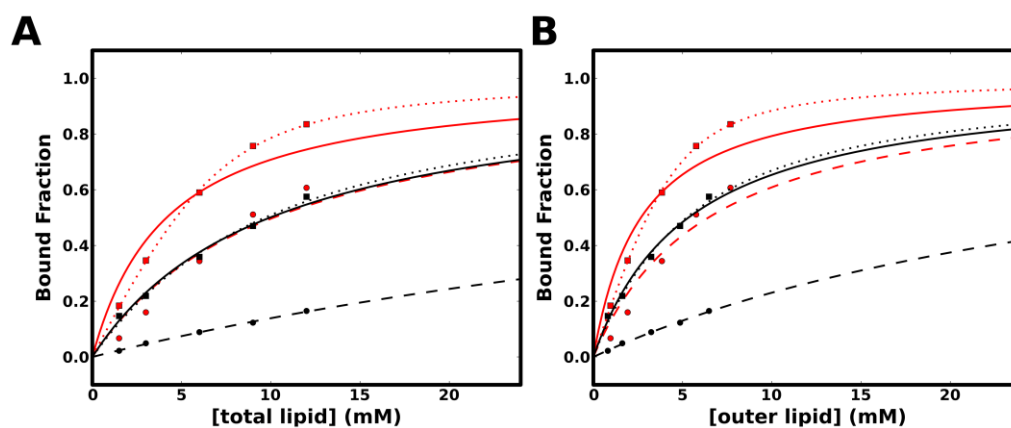


**Figure 3.14: Titrations of unmodified alpha synuclein to low negative charge SUVs and LUVs.** Plot of the bound fractions of total binding (squares) and fully-helical binding (circles) with increasing concentrations of 15% PS LUVs (black) and SUVs (red) for unmodified alpha-synuclein. Panel A uses total lipid concentration, while B uses only accessible outer lipid concentrations. The points are fit to equation 2 (solid, dashed lines) and equation 3 (dotted line, only total binding) and extracted  $K_{D,app}$  and  $B_{max}$  values shown in Table 3.3.

The apparent dissociation constants extracted from fitting to equation 2 showed increased affinity for curved SUVs, as before (Table 3.3). The values were comparable to those derived from the independent titration in Table 3.2, despite the use of different protein and lipid stocks, showing the reproducibility of this method. The fit to the equation 3 was very good (Figure 3.14). However, the dissociation constant and number of binding sites extracted for LUV binding had very high error, precluding a comparison with SUV binding.

**Table 3.3: Computed apparent  $K_D$  and  $B_{max}$  values for unmodified and acetylated alpha synuclein with low negative charge SUVs and LUVs.** Apparent  $K_D$  and  $B_{max}$  values were calculated from fitting titrations to equations 2 and 3 (see Figure 3.14 and 3.15) using total lipid concentration and only accessible outer lipid concentration (see section III.b).

	Total Lipid				Outer Lipid			
	Equation 2 Fit		Equation 3 Fit		Equation 2 Fit		Equation 3 Fit	
Protein and Lipid	$K_{D,app}$ (mM) – Total	$K_{D,app}$ (mM) – Fully-Helical	$K_{D,app}$	$B_{max}$	$K_{D,app}$ (mM) – Total	$K_{D,app}$ (mM) – Fully-Helical	$K_{D,app}$	$B_{max}$
Unmodified								
LUVs	$9.8 \pm 0.4$	$61.7 \pm 0.9$	$0.469 \pm 0.617$	$0.057 \pm 0.063$	$5.2 \pm 0.2$	$33.2 \pm 0.5$	$0.467 \pm 0.617$	$0.106 \pm 0.116$
SUVs	$4.1 \pm 0.7$	$10.0 \pm 1.3$	$0.031 \pm 0.003$	$0.025 \pm 0.001$	$2.6 \pm 0.4$	$6.4 \pm 0.8$	$0.031 \pm 0.003$	$0.039 \pm 0.001$
Acetylated								
SUVs	$1.0 \pm 0.1$	$3.7 \pm 0.1$	$0.015 \pm 0.002$	$0.035 \pm 0.002$	$0.6 \pm 0.1$	$2.4 \pm 0.1$	$0.015 \pm 0.002$	$0.055 \pm 0.003$

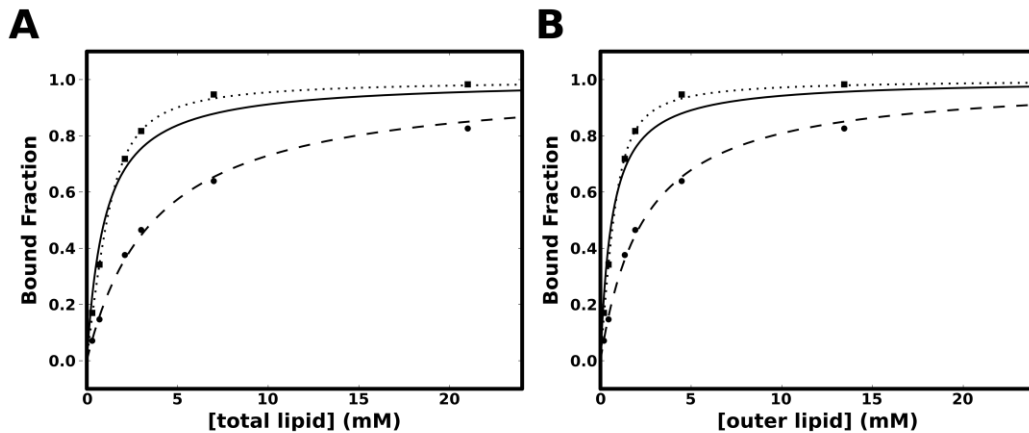


**Figure 3.15: Titrations of acetylated alpha synuclein to low negative charge SUVs.** Plot of the bound fractions of total binding (squares) and fully-helical binding (circles) with increasing concentrations of 15% PS SUVs for acetylated alpha-synuclein. Panel A uses total lipid concentration, while B uses only accessible outer lipid concentrations. The points are fit to equation 2 (solid, dashed lines) and equation 3 (dotted line, only total binding) and extracted  $K_{D,app}$  and  $B_{max}$  values shown in Table 3.3.

An independent titration was carried out with acetylated alpha-synuclein using different lipid stocks and protein concentration (Figure 3.15). The apparent  $K_D$  values extracted from fitting to equation 2 were again comparable to those shown in Table 3.2. Fitting to equation 3 yielded the number of binding sites per lipid molecule  $B_{max}$ , which was slightly larger than that obtained for unmodified protein (0.035 *versus* 0.025, 29 *versus* 40 lipids per binding site, ~250 *versus* ~180 binding sites per SUV). Additionally, the dissociation constant for each binding site was smaller than that obtained for unmodified protein (0.015 *versus* 0.031), suggesting that the increased binding of acetylated alpha-synuclein derives from both increased affinity and more “available” binding sites. Although the lipid configuration is the same,

acetylated alpha-synuclein can somehow “sense” more favorable binding sites than the unmodified protein.

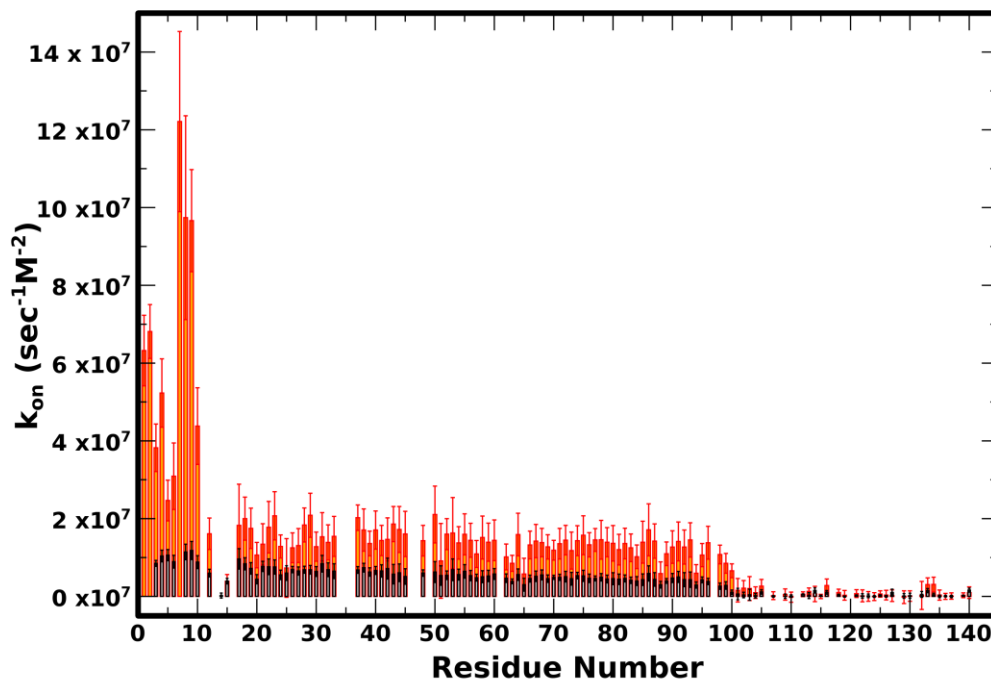


**Figure 3.16: On-rate for unmodified and acetylated alpha-synuclein binding to low negative charge SUVs.** Plot of on-rate  $k_{on}$  for unmodified (grey) and acetylated alpha-synuclein (orange) in the presence of 2.6 mM 15% PS SUVs *versus* residue number. The rate was calculated from  $R_2$  relaxation rates as described in sections II.g and III.b.

The effect of N-terminal acetylation on alpha-synuclein binding to lipid vesicles can manifest itself as an effect on the on-rate and/or on the off-rate. In order to address this distinction, the on-rate for unmodified and acetylated alpha-synuclein binding to 15% PS SUVs was estimated by measuring  $R_2$  transverse relaxation rates in the

presence and absence of lipid vesicles (see sections II.g and III.b). The off-rate was then calculated using the equilibrium dissociation constant from the vesicle titrations (Table 3.3). The plot of  $k_{on}$  versus residue number reveals three distinct regions of binding (Figure 3.16). The C-terminal tail, as seen before, shows no binding, while the N-terminal ~10 residues display an increased on-rate of binding compared to the remainder of the N-terminal lipid-binding region, which has a relatively flat profile. The difference between the on-rates of these two regions is much more pronounced for acetylated alpha-synuclein. Overall, acetylation increases the on-rate for the N-terminal region by a factor of ~6 ( $6.6 \times 10^7 \text{ sec}^{-1}\text{M}^{-2}$  versus  $1.0 \times 10^7 \text{ sec}^{-1}\text{M}^{-2}$ ) and for the rest of the helical binding region by a factor of ~3 ( $1.3 \times 10^7 \text{ sec}^{-1}\text{M}^{-2}$  versus  $4.8 \times 10^6 \text{ sec}^{-1}\text{M}^{-2}$ ). The calculated off-rates are more comparable between acetylated and unmodified protein (Table 3.4), suggesting that N-terminal acetylation mostly increases the on-rate of alpha-synuclein binding to SUVs.

**Table 3.4: Computed on- and off-rates for unmodified and acetylated alpha-synuclein binding to low negative charge SUVs.**

On-rates were calculated from measured  $R_2$  relaxation rates in the presence and absence of SUVs (see sections II.g and III.b) and off-rates were calculated using the apparent  $K_D$  values from Table 3.3.

Protein	N-terminal Binding		Fully-Helical Binding	
	$k_{on}$ ( $\text{sec}^{-1}\text{M}^{-2}$ )	$k_{off}$ ( $\text{sec}^{-1}\text{M}^{-1}$ )	$k_{on}$ ( $\text{sec}^{-1}\text{M}^{-2}$ )	$k_{off}$ ( $\text{sec}^{-1}\text{M}^{-1}$ )
unmodified	$1.0 \times 10^7$	$4.1 \times 10^4$	$4.8 \times 10^6$	$4.8 \times 10^4$
acetylated	$6.6 \times 10^7$	$6.6 \times 10^4$	$1.3 \times 10^7$	$4.8 \times 10^4$

Overall, N-terminal acetylation stabilizes helical states at the very N-terminus of alpha-synuclein, both in the disordered state

prevalent in dilute aqueous solution and in lipid- and detergent-stabilized fully-formed helical conformations. The N-terminally appended acetyl group has long been known, from previous research on peptides, to act as an N-terminal cap for  $\alpha$ -helices [218,219]. Helical structure is stabilized by intraresidue  $i,i+4$  hydrogen bonds between backbone amide protons and carbonyl oxygens; however, this pattern is broken at N- and C-terminal ends, leaving the first four amide protons and last four carbonyl oxygen atoms without hydrogen bond partners [232]. Introduction of another amino acid into the helical structure would add one hydrogen bond partner, but would also add one partner-less hydrogen bond donor, leading to no net stabilization.

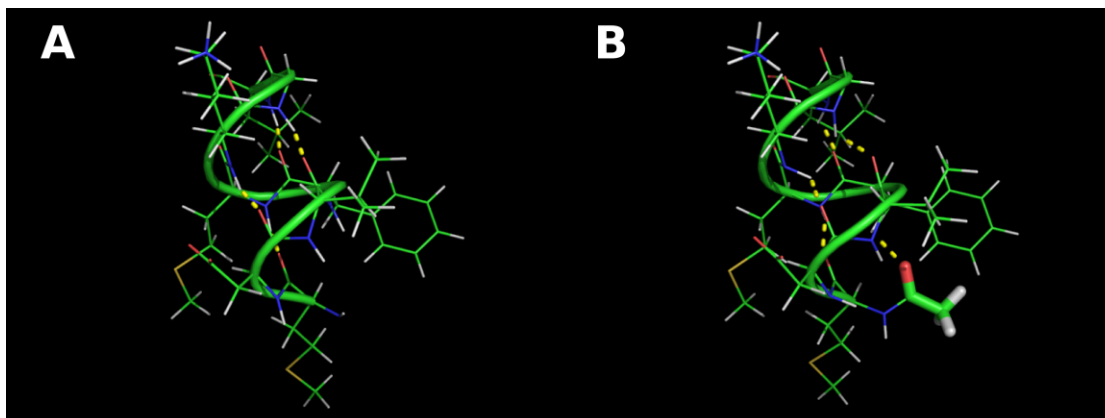


**Figure 3.17: Model of residues 1-7 as an ideal  $\alpha$ -helix for unmodified and acetylated alpha-synuclein.** (A) Unmodified alpha-synuclein. (B) Acetylated alpha-synuclein. The acetyl group in (B) is shown as sticks. Hydrogen bonds between residues 1-4, 2-5, 3-6, and 4-7, as well as acetyl-3, are shown as dashed yellow lines.

Several amino acids, known as N-caps, can stabilize both N- and C-terminal ends of helices by forming side-chain-to-backbone hydrogen bonds without introducing another unsatisfied backbone

hydrogen bond donor [232,233]. Acetylation of the N-terminal amine can act in a parallel manner, allowing a hydrogen bond between its carbonyl oxygen atom and the amide proton of the fourth amino acid (phenylalanine 4 in alpha-synuclein) (Figure 3.17). This capping can lead to the observed stabilization of helicity in the N-terminal ~10 residues of alpha-synuclein in the free and membrane-bound states. However, it is interesting that the addition of one hydrogen bond (~1 kcal/mol stabilization) can stabilize up to 3 helical turns at the N-terminus of alpha-synuclein; this likely points to very strong cooperativity in helix formation/propagation in the amphipathic helix region of alpha-synuclein.

The straightforward stabilization of N-terminal helicity in the free and SDS-bound states of alpha-synuclein leads to more significant consequences in binding to lipid vesicles. N-terminal acetylation increases alpha-synuclein overall binding to lipid vesicles with lower proportions of negatively-charged lipids. This likely occurs through an increased on-rate in alpha-synuclein binding to the vesicles. The presence of negatively-charged phospholipids such as PS is often thought to be necessary for efficient alpha-synuclein binding to lipid membranes (e.g. [234]). This is at odds with the moderate negative charge content of synaptic vesicles, the putative binding partner for alpha-synuclein *in vivo*, which is thought to be ~10%, although the distribution between the outer and inner leaflet is not known [235]. However, the addition of an N-terminal acetyl group increases alpha-synuclein affinity for lipid vesicles with 15% PS by a factor of 3. In a similar manner, acetylated alpha-synuclein binds to

micelles of the nonionic detergent BOG, while the unmodified protein has practically no interaction with the detergent at similar concentrations. The conformation acetylated alpha-synuclein adopts upon binding to BOG micelles is a never-before-seen partly-helical state in which the N-terminal ~25 residues adopt helical structure while the rest of the protein remains disordered.

### **III.d. Electrostatic and hydrophobic contributions to binding**

In two different systems (BOG and 15% PS vesicles), N-terminal acetylation increases alpha-synuclein interactions with relatively less charged binding surfaces. The N-terminal lipid binding region (residues 1-96) of unmodified alpha-synuclein has a net charge of +5 at neutral pH, arising from 9 ionized negatively-charged side-chains, 13 ionized positively-charged side-chains, 1 unprotonated histidine side-chain, and the protonated amino terminus. Thus, the binding interaction between this region of the protein and negatively-charged lipid membranes has a significant contribution from electrostatic attraction. In contrast, the C-terminal tail (residues 97-140) has a net charge of -14, explaining its strong reluctance to bind membranes. Another contributing driving force for alpha-synuclein binding to membranes is the favorable hydrophobic interaction between the apolar face of the amphipathic helix that forms on and partially inserts into membranes and the hydrophobic lipid acyl chains. Additionally,

there are contributions from the folding of the amphipathic helix and lipid defect healing in the membrane [59,63]. These contributions, summed together, result in the observed affinity of unmodified alpha-synuclein for lipid membranes.

One calorimetric study estimated the relative contributions to the enthalpy of alpha-synuclein binding to vesicles [59]. The helix folding was estimated to contribute ~75% of the binding enthalpy, leaving ~25% for the electrostatic attraction. When gel state vesicles (100% DPPC) were used, the binding enthalpy was found to be much greater, while final percent helicity remained comparable, suggesting that a large (~70%) contribution to binding to these SUVs comes from alpha-synuclein “healing” lipid membrane defects in the gel state membranes. In addition, there is some entropic contribution of helix folding and membrane defect healing. How does N-terminal acetylation change this balance of driving forces?

The addition of an acetyl group at the N-terminus removes one positive charge, so it decreases the electrostatic attraction to negatively-charged membranes. However, the electrostatic contribution to binding is not very great, especially if the target membranes have a large number of defects and relatively low negative charge. The other effect of N-terminal acetylation is to stabilize helical states in both the free protein and, presumably, in the lipid-bound protein. In the case of high negative charge (50% PS) vesicles, both SUVs and LUVs, used in this study, the effect of the loss of one positive charge and increased helicity appear to be roughly equal and opposite, as seen in the similar levels of binding of N-terminally acetylated and unmodified alpha-

synuclein. In the case of lower negative charge (15% PS) vesicles, the effect of losing one positive charge can be expected to be less than in the case of 50% PS due to the decrease in negative charge, while the effect of gaining helicity can be expected to remain the same as it was for highly charged vesicles. This differential effect is reflected in the increased (~3-times) binding affinity observed for acetylated alpha-synuclein for lower negative charge vesicles. In the case of high negative charge, the electrostatic attraction dominates and N-terminal acetylation has very little effect. In the lower negative charge regime, the hydrophobic effects dominate and stabilization of the helix by N-terminal acetylation increases binding.

These findings can have interesting implications for alpha-synuclein binding to membranes in the cell. While unmodified alpha-synuclein exhibits a substantial preference for 50% PS vesicles over 15% PS vesicles (4-6 times stronger binding), the difference is much smaller for the N-terminally acetylated protein (1.4 times stronger binding). All previous studies in reconstituted *in vitro* systems made use of the unmodified recombinant protein, and may have given a false impression of the necessity of high negative charge density for alpha-synuclein binding. Many *in vitro* studies use lipid vesicles with unnaturally high PS (or PG) concentrations (50-100%) [62,230], while it is unlikely that the protein ever comes into contact with such membranes in its native environment. Even the plasma membrane or late secretory/synaptic vesicles probably do not contain more than 15% PS in mammalian cells, although yeast cells may have significantly higher proportions of PS in the plasma membrane [236].

Thus, it seems that *in vivo*, alpha-synuclein (which is N-terminally acetylated) interacts with membranes similar to the “low negative charge content” vesicles examined in this work, to which the acetylated protein binds nearly as tightly as to much more negatively charged membranes.

### **III.e. Implications for curvature sensing *in vivo***

N-terminal acetylation also affects alpha-synuclein selectivity for vesicle curvature. Unmodified alpha-synuclein has been shown to have a preference for more curved membrane surfaces, such as SUVs. This curvature preference is confirmed by the results obtained here, with unmodified alpha-synuclein displaying 2.5-3.5 times stronger binding to SUVs than LUVs (after accounting for different proportions of accessible outer leaflet lipids in SUVs and LUVs); however, the acetylated protein was found to have ~4 times greater affinity for the more curved SUVs than the LUVs. For both N-terminally acetylated and unmodified alpha-synuclein, preference for SUVs was more noticeable at lower negative charge compositions, suggesting that strong electrostatic attraction can mask curvature sensing. One can compare the effects of curvature (LUV to SUV) and of charge (15% to 50% PS) for unmodified and acetylated alpha-synuclein. For unmodified protein, increasing negative charge and increasing curvature results in an increase in affinity by a factor of 6 and 3.5, respectively. For N-terminally acetylated alpha-synuclein, the same

increases are 1.4 and 4.4. Thus, unmodified alpha-synuclein binding affinity is increased more by the addition of negative charges to the membrane than by increasing the curvature, while for acetylated alpha-synuclein, the situation is reversed.

How does one small modification change the effects of curvature and charge so much? The answer depends on the mechanism of alpha-synuclein curvature sensing, which is still unclear. One theory implicates the mismatch between the two faces of the amphipathic helix – the hydrophilic face is well-developed compared to other amphipathic helices, with many charged residues, while the hydrophobic face is quite small and composed of not very hydrophobic residues [62]. A balanced amphipathic helix would bind strongly to any hydrophobic surface, such as a flat membrane, while the mismatched alpha-synuclein amphipathic helix must derive more stabilization from membrane properties. In the case of highly curved membranes, this arises from the increased population of lipid packing defects, which allow the nonpolar face of alpha-synuclein to insert into the hydrophobic chain region of the bilayer. By increasing N-terminal helicity and removing the primary amino charge, N-terminal acetylation decreases non-curvature-specific electrostatic attraction that promotes alpha-synuclein binding to any negatively-charged surface, while increasing the contribution of forming the amphipathic helix, which relies on the membrane defects present in highly curved membranes for tight binding.

One interesting observation in the binding profiles of unmodified and acetylated alpha-synuclein can be seen in the case of high

negative charge LUVs. While low negative charge LUVs lack both the high membrane curvature and high negative charge that drive alpha-synuclein binding, and thus display the weakest binding, the higher negative charge LUVs at least have increased electrostatic attraction towards alpha-synuclein molecules. Here, the effect of the loss of the primary amino charge upon N-terminal acetylation is most evident, as the N-terminal 20 residues of the acetylated protein display less binding than those of the unmodified protein in the presence of the same concentration of lipid vesicles (Figure 3.12A). This observation suggests that the primary amino positive charge anchors the unmodified protein on very negatively charged vesicles, in the absence of other possible anchoring characteristics, such as high curvature. Therefore, in the absence of N-terminal acetylation, high negative charge in the binding partner can make up for non-ideal low curvature in terms of N-terminal binding initiation, but this effect is abrogated upon acetylation, and is not relevant *in vivo*.

As mentioned above, one likely mechanism by which high membrane curvature promotes alpha-synuclein binding is by increasing the concentration of lipid packing defects to which the protein can preferentially bind. Membrane curvature is not the only property that affects the amount of membrane defects – the composition of fatty acid phospholipid chains also plays a role. Many cellular membranes contain phospholipids with unsaturated acyl chains, which are kinked and introduce disorder in the membrane. The presence of these kinked unsaturated acyl chains, as well as small lipid headgroups such as PE and PA, also increases the amount of

lipid packing defects, which expose the acyl chains and can promote binding of alpha-synuclein. In fact, alpha-synuclein has a strong preference for binding to lipid membranes containing unsaturated acyl chains, leading to increased recent use of DO (di-oleoyl) lipids in alpha-synuclein studies, which contain two monounsaturated acyl chains, (this work; [92,96,231]. Since it appears that alpha-synuclein has a strong preference for lipid packing defects [59,62], whether caused by high curvature or lipid composition, it can be posited that alpha-synuclein uses this preference to localize to a specific target membrane in cells.

A simplified treatment of subcellular localization of different lipid membranes identifies three physicochemical properties of membranes: charge (mostly PS content), packing defects, and curvature (which also influences packing defects) [64]. These three properties define two broad regions of membranes in the cell – a region dominated by high curvature and high incidence of packing defects (ER and cis-Golgi) and a region dominated by electrostatics (secretory vesicles, endosomes, and plasma membrane). While this general treatment is useful, it is not very applicable to the situation of alpha-synuclein, which has preference for both lipid packing defects and negatively-charged lipids. However, synaptic vesicles offer a unique lipid environment which contains the relatively high negative charge of the plasma membrane while providing high curvature and a large proportion of lipids with unsaturated acyl chains, likely resulting in a significant amount of lipid packing defects [235]. This lipid composition thus seems ideally suited to promote alpha-synuclein binding, especially if the protein is

N-terminally acetylated. In addition, the large proportion of negatively-charged lipids in the plasma membrane leaves open the possibility of significant alpha-synuclein binding there as well.

### **III.f. Fully-helical and partly helical states**

Most of the discussion of binding to lipid vesicles has focused on total binding, which includes both fully- and partly-helical states. The effect of N-terminal acetylation on fully-helical binding generally mirrors that on total binding. Selectivity for highly curved vesicles, however, is not increased by N-terminal acetylation in the fully-helical bound state. This suggests that most of the increased binding to highly curved membrane surfaces engendered by N-terminal acetylation is in the form of partly-helical, N-terminally bound states.

One interesting consequence of having measured separate affinities for total binding and fully-helical binding is the ability to calculate the full helix fraction (section II.d, Table 3.2). A pattern emerges in which the full helix fraction is higher for more curved SUVs than LUVs for each protein and lipid composition combination. The only exception is the higher full helix fraction for acetylated alpha-synuclein on high negative charge LUVs, arising from decreased partly-helical binding due to the loss of the primary amino positive charge. In all other cases, increased curvature results in increased binding in the fully-helical mode. This finding can be interpreted as increased curvature promoting the folding of helix-2 and/or the

extended-helix state. This is possible since helix-2 displays a higher curvature than helix-1 on SDS micelles [74], while the extended helix is expected to have an overall curvature that matches an SUV/synaptic vesicle sized vesicle [77]. Alternatively, greater number of lipid packing defects, an indirect result of higher membrane curvature, can be responsible for increased helix-2 and/or extended-helix binding due to the presence of more hydrophobic binding sites for a longer amphipathic helix. Whatever the mechanism, less curved membrane surfaces have a greater proportion of partly-bound states of alpha-synuclein, while more curved surfaces have more binding sites for the longer fully-bound state.

What are these mysterious partly-bound states? The BOG-bound conformation may offer some structural clues. There is significant evidence for a partly-helical state of alpha-synuclein that may be correlated with aggregation [92,95]. This partly-helical state is expected to have 20-25 helical residues, likely at the N-terminus. This description matches what is observed for N-terminally acetylated alpha-synuclein in the presence of BOG micelles. The unmodified protein does not appreciably bind to this nonionic detergent, but upon elimination of the primary amino positive charge and increase of helicity at the N-terminus, binding in a partly-helical state is favored. This binding interaction was measured by two complementary approaches, NMR chemical shifts, which report on extent of binding, and CD ellipticity, which reports on extent of helical structure. The two measurements of binding overlay very closely, showing that helix formation is concomitant with binding to the micelle, a situation that

is different from that seen for other membrane-binding proteins, such as complexin [176]. There is evidence for the partly-helical state existing on lipid vesicles [92], and it may be an early intermediate in binding to the membrane, with binding nucleated at the N-terminus, then propagating through the formation of more helical structure.

The end point of this helical intermediate, around residue 25-30, may be meaningful given the existence of the PD-linked mutant A30P, a helix-breaking mutation. This mutation greatly decreases lipid-binding overall and increases the proportion of the partly-helical state [39,92]. Interestingly, other PD-linked mutations such as E46K and A53T, while not having such a stark effect on total lipid binding, increase the proportion of alpha-synuclein that is bound in a partly-helical state, suggesting that this partly-helical state may be the common denominator among PD mutants of alpha-synuclein [92]. This potential link to pathology indicates that the partly-helical state is either itself pathogenic or interferes with alpha-synuclein carrying out its function *in vivo*. Previously, in order to glean information about the partly-helical state in the presence of lipid vesicles, very dilute concentrations of SUVs had to be used, as binding to SUVs causes the formation of a large immobile complex and the corresponding disappearance of amide cross-peaks. In the presence of BOG, the amide cross-peaks of bound residues remain visible (although decreased in intensity) even when fully bound, presumably due to the smaller size of BOG micelles. This allows for further high-resolution study of this state, and more specifically the effects of PD-linked mutations on its structure and folding pathways.

### **III.g. Implications for tetrameric assembly**

Increased N-terminal helicity in alpha-synuclein upon N-terminal acetylation could be responsible for a helical, tetrameric assembly that was purified from various sources, all involving N-terminally modified protein [114,117,118]. The NMR results (both in intact cells and on purified protein) presented here rule out the presence of significant amounts of such a conformation of acetylated alpha-synuclein both in *E. coli* cells and in the test tube. However, the glycerol and BOG used in the purification buffers in two of these studies [117,118] may interact with acetylated alpha-synuclein and contribute to detected helical structure and large molecule size. The conformation of acetylated alpha-synuclein in the presence of BOG micelles described here displays much less helical character than in those studies (~25 residues *versus* ~90 residues), so it is unlikely to be the culprit. However, the potential effect of glycerol or *E. coli* contaminants maintained through the purification scheme was not evaluated, and may be responsible.

## **IV. Phosphorylation at Y39 regulates the lipid-binding mode of alpha-synuclein**

### **IV.a. Introduction**

Although N-terminal acetylation is almost ubiquitous in eukaryotic proteins, protein phosphorylation is the most extensively studied post-translational modification since its discovery in the 1950s [148]. Unlike N-terminal acetylation, phosphorylation, which in eukaryotes consists of the transfer of a phosphate group, usually from ATP, to either a serine (86%), threonine (12%), or tyrosine (2%) residue by an enzyme called a kinase, is reversible [149,150]. Protein phosphorylation by a kinase and dephosphorylation by a phosphatase combine to form a dynamic signaling system that can regulate myriad cellular and organismal processes in space and time. Systems as varied as signal transduction through receptor tyrosine kinases [237], growth signal regulation through the mTOR pathway [238], and stress and inflammation response via MAPK pathways [239] all make use of networks of phosphorylation and dephosphorylation. When combined with other dynamic post-translational modifications, phosphorylation acts to increase the variety of protein surfaces for protein-protein interactions without increasing the gene number, as well as allowing the cell to respond to environmental changes faster than simple protein translation [151].

One advantage of a phospho-residue is the unique chemical surface formed by the addition of a highly negatively-charged phosphate group [150]. Thus, phosphorylated residues can be easily recognized by specific domains through hydrogen bonds or ionic interactions, either intra- or inter-molecularly. Addition of a phosphate group can lead to specific protein-protein recognition or to dissociation of protein complexes [240]. In a simple example, increasing phosphorylation of the N-terminal region of the circadian clock protein FRQ induces its dissociation from the C-terminus, allowing the protein to be degraded in a time-dependent manner [241]. In addition to modulating protein-protein recognition directly, phosphorylated residues can elicit conformational changes and thus indirectly affect protein-protein interactions [150,240]. Regulation of these interactions can also modulate protein localization as a result of phosphorylation or dephosphorylation. The creation and abolition of protein-recognition sites, dynamically and spatiotemporally regulated by kinases and phosphatases, is what allows protein phosphorylation to be such an effective signal integrator and regulator in the cell.

While phosphorylation is known to affect protein conformations, there is no general model of the direct structural effects of the addition of a phosphate group to a serine, threonine, or tyrosine residue. Complicating matters is the fact that phosphorylation occurs disproportionately in areas of intrinsic disorder on proteins [242,243]. A review of 17 pairs of phosphorylated and unphosphorylated structures found that the changes effected by phosphorylation varied widely, but most were driven by the need to accommodate the large negative

charge introduced by the phosphate group [244]. The conformational changes included small and large effects, local and long-range changes, and order-to-disorder and disorder-to-order transitions. A later bioinformatics study of the structural effects of phosphorylation and other modifications found that, while local and global conformational changes due to phosphorylation are significant, most (>80%) are small [245]. In addition, phosphorylation was found to alter the global energy landscape of proteins, specifically by stabilizing the overall protein structure, likely through new hydrogen bonds and ionic interactions. These results suggest that phosphorylation acts to restrict conformational flexibility in a protein. Examples of phosphorylation suppressing intrinsic disorder have been seen in molecular dynamics simulation as well [246].

NMR studies on short, disordered model peptides showed that phosphorylation of serine and threonine residues directly affects the preferred dihedral angles of the polypeptides, while phosphorylation of tyrosine residues does not [247]. However, in the presence of charges in the vicinity of the phosphotyrosine, the addition of the phosphate group did affect the dihedral angles adopted by the peptide. These results suggest that phosphorylation of serine and threonine residues can directly affect peptide backbone conformations through hydrogen bonds between the amide proton and phosphate group of the phosphorylated residue. For tyrosine, on the other hand, the larger size and rotational range of the side-chain precludes a similar interaction between the phosphate and amide groups, and the effect of phosphorylation is mediated by interactions with nearby charges,

whether on the polypeptide chain or in an interacting partner. Another example of the specific structural effects of tyrosine phosphorylation occurs in the  $\beta_3$  integrin cytoplasmic tail [248]. Phosphorylation of one or two tyrosine residues in the tail region changes the conformation to one that does not interact with the  $\alpha$  integrin tail, since the intramolecular interactions with the added phosphate group are stronger than intermolecular interactions between the two tails. Tyrosine phosphorylation also introduces repulsion from the membrane, which may free the tail for other interactions.

Many kinases have been shown to phosphorylate alpha-synuclein on several serine and tyrosine residues, mostly in the acidic C-terminal tail [152–156]. The most commonly detected phosphorylation of alpha-synuclein *in vivo* is at serine 129; this modification is seen in cytosolic alpha-synuclein [157] but to a greater extent in alpha-synuclein found aggregated in Lewy bodies [146,158,159]. While Ser-129 phosphorylation of alpha-synuclein has been extensively studied, its effect on alpha-synuclein fibril formation and PD progression is not clear and is most likely context-dependent. There is evidence that phosphorylation of alpha-synuclein at Ser-129 (pS129) inhibits alpha-synuclein fibril formation *in vitro* [155] but also contradicting evidence that pS129 increases alpha-synuclein fibril formation *in vitro* and aggregation in cells [158,160]. Studies in several animal models of PD also produced conflicting results on the effect of Ser-129 phosphorylation on alpha-synuclein aggregation and toxicity (summarized in [156]). The major kinase families that have been shown to phosphorylate alpha-synuclein at Ser-129 are the Polo-like kinase

(PLK) family, specifically PLK2 and PLK3 [153] and the casein kinase (CK) family, specifically CK1 and CK2 [159]. Robust phosphorylation of alpha-synuclein at Ser-129 by PLK2 especially has been demonstrated in both mice and yeast models [156,249]. Complicating matters further, PLK2 has been shown to be upregulated in and to decrease alpha-synuclein toxicity when introduced into animal models of PD [153,250]. Additionally, loss of pS129 (whether through dephosphorylation or truncation) may occur preferentially on synaptic membranes [251].

Phosphorylation of alpha-synuclein at a secondary site, serine 87, was also detected in cell models and ascribed to CK1 [159]. In addition, phosphorylation of alpha-synuclein at Ser-87 was demonstrated *in vitro* by the tyrosine-regulated kinase Dyrk1A [161]. alpha-Synuclein phosphorylated at Ser-87 was found to be enriched in samples from PD patients or animal models of PD, especially in the membrane fraction [154]. Somewhat paradoxically, the pS87 alpha-synuclein was shown to bind less tightly to acidic lipid vesicles composed of POPG. The same study also showed that phosphorylation at Ser-87 decreased alpha-synuclein fibril formation. While phosphorylation on the flexible C-terminal tail (such as pS129) may be more tolerated in the course of fibril formation, the addition of a highly negative chemical group in the fibril core region would be expected to inhibit the self-association required for fibril formation due to electrostatic repulsion.

Phosphorylation of alpha-synuclein at these two serines has not been shown to result in major structural rearrangements in either the free, disordered or SDS-bound states of the protein [154,155]. The CD

spectrum of free alpha-synuclein reveals generally disordered structure regardless of phosphorylation at Ser-87 and Ser-129 and NMR chemical shifts are only perturbed for a few residues in the vicinity of the phosphorylation site, with no local induction of secondary structure. However, addition of the phosphate group at either site results in alpha-synuclein populating more expanded conformations in aqueous buffer, with a greater effect seen for pS129 [154]. Interestingly, mutation to aspartate or glutamate at these sites, which is commonly used to mimic phosphorylation, does not result in the same expansion. This finding supports an important role for electrostatics in the expanded state of alpha-synuclein, since phosphoserine adds two negative charges while aspartate or glutamate only add one at physiological pH.

Phosphorylation at Ser-129, as expected, has no effect on the membrane- and detergent-bound structure of alpha-synuclein [155]. Seeing as Ser-87 is within the membrane-binding region, addition of a phosphate group there decreases alpha-synuclein helicity upon binding to acidic lipid vesicles and local helicity at the C-terminal end of helix-2 in the SDS-bound state [154]. These results suggest that the very C-terminal end of the lipid-binding region dissociates from the membrane or micelle surface when Ser-87 is phosphorylated. Thus, phosphorylation at either of these serine residues only has a local, electrostatics-mediated effect on the membrane bound state, while adding the negatively-charged phosphate group, particularly at Ser-129, biases the disordered ensemble toward more expanded conformations, possibly by disrupting the transient intramolecular

contacts within alpha-synuclein, although adding a negatively-charged phosphate group would be expected to strengthen these contacts.

In addition to serine residues, eukaryotic proteins are often phosphorylated on threonine and tyrosine residues. Despite alpha-synuclein containing 10 threonine residues due to the conserved KTKEGV repeat motif, there has been no evidence of any threonine phosphorylation. Tyrosine residues, however, have been shown to be phosphorylated (and nitrated). Early studies on alpha-synuclein transfected into cell lines showed that tyrosine 125 could be phosphorylated, and likely by members of the Src family of kinases, especially Fyn [162,163]. Phosphorylation at tyrosines 133 and 136 was also detected, but at lower levels [162,164]. alpha-Synuclein phosphorylated at Tyr-125 was shown in human samples and animal models, and its levels were found to decrease with age [165]. However, the difficulty of producing pY125 alpha-synuclein *in vitro* and lack of widely accepted mutations that mimic the physicochemical properties of a phosphotyrosine side-chain had previously prevented biophysical characterization of the phosphoprotein. In this work, such an analysis, using a chemically synthesized pY125 form of the protein is presented.

Nitration of the C-terminal tyrosine residues of alpha-synuclein as a result of oxidative stress has also been observed in PD brain samples [252]. Damage from reactive oxygen species or oxidative stress has been implicated in PD for decades [253,254]. Peroxynitrite, generated by superoxide and nitric oxide, can react with tyrosine residues on proteins to generate 3-nitrotyrosine. Proteins containing 3-nitrotyrosines were detected in Lewy bodies [255], and specifically

shown to be nitrated alpha-synuclein [252]. These alpha-synuclein species contained 3-nitrotyrosine residues at positions 39, 125, 133, and/or 136 [252,256].

Nitrated alpha-synuclein was shown to accelerate fibril formation of unmodified alpha-synuclein to which it had been added, while itself being resistant to fibrillization, and alpha-synuclein specifically nitrated at Tyr-39 exhibited decreased binding to acidic lipid vesicles [257]. A study that dissected the effects of Tyr-39 and C-terminal tyrosine nitration in alpha-synuclein demonstrated that nitration of C-terminal tyrosine residues also decreased alpha-synuclein binding to lipid vesicles [258]. This somewhat surprising result suggests that intramolecular interactions between the C-terminal tail and N-terminal regions of alpha-synuclein [259] may affect membrane binding. Nitration of alpha-synuclein was also shown to result in high molecular weight aggregates covalently cross-linked via di-tyrosine linkages [260]. Within the framework of the toxic pre-fibrillar oligomer hypothesis, such effects of nitration would suggest a pathogenic result of this modification. In fact, nitrated alpha-synuclein does exhibit cellular toxicity in various cell culture and animal models [261–263]. However, nitrated alpha-synuclein was not examined further here. Instead, attention was focused on examining the effects of phosphorylation at the only known site located well within the membrane-binding domain of alpha-synuclein, Y39.

## IV.b. Methods

*Phosphorylated Protein Samples* – The effects of phosphorylation of tyrosine residues 39 and 125 on alpha-synuclein structure and binding to membranes and membrane mimics were assessed using a number of different NMR experiments. Authentically phosphorylated alpha-synuclein was produced by a semisynthetic method for pY125 alpha-synuclein and by incubating recombinant alpha-synuclein with the kinase c-Abl for pY39 alpha-synuclein. Partially isotopically labeled and unlabeled pY125 alpha-synuclein was produced by expressing A107C alpha-synuclein in *E. coli* and synthesizing the (unlabeled) 108-140 peptide with a phosphotyrosine residue incorporated at position 125, then ligating the peptides using intein chemistry [152]. While this method allows for the production of sufficient quantities of authentically phosphorylated protein for NMR studies, as a result the C-terminal region is not isotopically-labeled and thus invisible to heteronuclear NMR methods. Notably, this synthesis was carried out in the laboratory of Dr. Hilal Lashuel (EPFL, Switzerland) by his at the time student, Dr. Bruno Fauvet.

Alpha-synuclein protein phosphorylated on tyrosine 39 was also produced by Dr. Fauvet in Dr. Lashuel's lab. In order to avoid phosphorylation on sites other than Tyr-39, full-length Y125F Y133F alpha-synuclein or truncated alpha-synuclein 1-102 were used as the substrate. Isotopically-labeled protein was produced as described in section II.a. Lyophilized alpha-synuclein protein was dissolved in pH

7.5 buffer, filtered using a 100 kDa cutoff filter, and incubated with the SH2-CD fragment of c-Abl and ATP. After the reaction was completed, the phosphorylated alpha-synuclein was purified by reverse-phase HPLC and lyophilized. Phosphorylation was assessed by mass spectrometry. Due to the difficulty of producing large quantities of authentic pY39 alpha-synuclein, the phosphomimic mutant Y39E was also used. The Y39E alpha-synuclein protein was produced as described in section II.a.

*Basic NMR Experiments* – Phosphorylation of alpha-synuclein by c-Abl was followed by NMR. Wild-type alpha-synuclein (~100  $\mu$ M) dissolved in 20 mM tris, 10 mM MgCl<sub>2</sub>, 1 mM DTT, pH 6.8 buffer (400  $\mu$ L total volume) was incubated with 1 mM ATP and 10  $\mu$ g of the catalytic truncation SH2-CD c-Abl and successive 1 hr <sup>1</sup>H,<sup>15</sup>N-HSQC experiments were collected overnight at 15 °C. A spectrum was also collected on a matched alpha-synuclein sample with no c-Abl to serve as a zero timepoint. The relative intensity of each phosphorylated peak was calculated as the signal intensity of the peak arising from phosphorylated protein divided by the sum of intensities of the peaks arising from unphosphorylated and phosphorylated protein. This relative intensity was then plotted *versus* time, here taken as the midpoint of each HSQC experiment (i.e. 0.5 hr, 1.5 hr, etc).

Authentically phosphorylated and phosphomimic protein was used to characterize the effects of the phosphorylation on the free and micelle- and vesicle-bound states of alpha-synuclein. Backbone assignments were transferred from previously determined ones by transferring peaks to the closest unassigned peak in HSQC

experiments (pY125) or by using high-resolution HNCA experiments (pY39), which also provided alpha-carbon chemical shifts for secondary structure analysis (see section II.f). Amide chemical shift deviations derived from  $^1\text{H},^{15}\text{N}$ -HSQC experiments were used to monitor the effects of phosphorylation (see section II.c).

The effect of pY125 and pY39 on the broken-helix state of alpha-synuclein was assessed at 40 mM SDS, a concentration at which the detergent is expected to form spheroidal micelles [225,226]. Again, secondary structure information was derived from HNCA experiments. Deuterated SDS was employed for the triple resonance NMR experiments to minimize magnetization loss from the protein nuclei via spin diffusion within the micelle. The HNCA experiments provided alpha-carbon chemical shifts which were used to analyze the secondary structure of pY39 and Y39E alpha-synuclein in the presence of SDS micelles using secondary shifts. In addition, carbonyl carbon chemical shifts were obtained from HNCO experiments and used to assess secondary structure as well. A  $^1\text{H},^{15}\text{N}$ -HSQC-NOESY-HSQC experiment was used to determine whether helical structure is continuous in the SDS-bound pY39 and Y39E alpha-synuclein [71] (see section II.f).  $^1\text{H},^{15}\text{N}$ -HSQC-NOESY-HSQC experiments were run using a pulse sequence adapted from a four-dimensional proton-nitrogen-nitrogen-proton experiment [189] to yield proton-nitrogen-nitrogen chemical shifts and collected with 96 complex pairs in the first nitrogen dimension and at least 128 complex pairs in the second nitrogen dimension to provide sufficient resolution to overcome peak

overlap. The NOE mixing time was 300 msec and deuterated SDS was used to prevent transfer of NOE through detergent protons.

*PRE Experiments* – Intramolecular contacts in the free state of pY125 and Y39E alpha-synuclein were assessed using PRE experiments. Paramagnetic spin-labels were covalently linked to cysteine residues introduced by mutagenesis at position 9 for Y39E and 107 for pY125, which was left over from the semisynthesis scheme. PRE experiments were also used to determine whether pY39 and Y39E alpha-synuclein adopts an antiparallel helical conformation in the presence of SDS micelles. The paramagnetic labels were linked to cysteines introduced at the ends of helix-1 and helix-2, namely position 9 or 83. An observed PRE effect on the opposite helix suggests that the helices are in an antiparallel, broken-helix-like conformation. For more details on the preparation of samples and execution of PRE experiments, see section II.h.

*Lipid Vesicle Binding* – Binding to lipid vesicles was measured by decrease of amide cross-peak intensity in  $^1\text{H}, ^{15}\text{N}$ -HSQC spectra in the presence of lipid vesicles as detailed in section II.d. Samples for unphosphorylated and pY39 or wild-type and Y39E proteins were made in parallel with the same lipid stock, resulting in well-matched samples. Those titrations were performed on independently made samples for each point.

*Diffusion Experiments* – Diffusion measurements were performed using the Bruker “ledbpgp2s192d” PFG LED pulse sequence [196] on proteins and  $^2\text{H}$  SDS (so as not to swamp the protein signal) dissolved in  $\text{D}_2\text{O}$  with 0.03% v/v (~4 mM) dioxane at 300 K using a Bruker

AVANCE 500 MHz spectrometer with a room-temperature probe. Gradient strength was varied in a 32-step linear gradient between 2 and 95% of the maximum strength. The diffusion delay was optimized to achieve ~10% signal intensity with 95% gradient strength. The diffusion delay was 100 msec, the tau was 0.2 msec, the gyromagnetic ratio was 4,257.7 Hz/G for proton, the shape factor was 0.630 for a sine-shaped gradient, the gradient duration was 7 msec, and the maximum gradient strength was 85 G/cm. The signal intensity for several protein and SDS aliphatic peaks, as well as the dioxane peak at ~3.6 ppm, was plotted as a function of gradient strength and fit to equation 7 (see section II.j) using the Bruker TopSpin relaxation analysis module, which also provided the default value for maximum gradient strength. Maximum gradient strength can also be calculated by measuring the diffusion coefficient of residual HDO in D<sub>2</sub>O and setting it equal to the published value of  $1.902 \pm 0.002 \times 10^{-9} \text{ m}^2\text{-sec}^{-1}$  [199].

#### **IV.c. Results Overview**

*Structure of alpha-synuclein is not greatly perturbed by pY125 –*  
The <sup>1</sup>H,<sup>15</sup>N-HSQC spectra of full-length unphosphorylated alpha-synuclein A107C was compared to that of pY125 alpha-synuclein A107C thus produced, in aqueous buffer (Figure 4.1A). Since the region containing the phosphorylation site was NMR-invisible, no

spectral changes were seen, suggesting that phosphorylation may have only local effects on the structure of the free state of alpha-synuclein (Figure 4.1B).

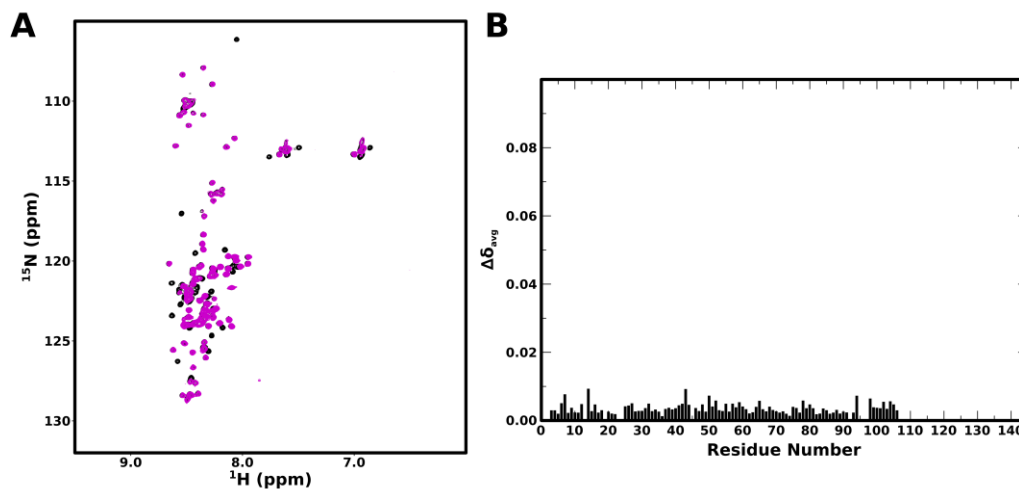


**Figure 4.1: HSQC spectra and amide chemical shift differences for unphosphorylated and pY125 alpha-synuclein A107C in aqueous buffer.** (A)  $^1\text{H}$ ,  $^{15}\text{N}$ -HSQC spectra of unphosphorylated (black) and pY125 (purple) alpha-synuclein A107C in aqueous buffer. (B) Plot of amide chemical shift differences (equation 1) between unphosphorylated and pY125 alpha-synuclein A107C *versus* residue number.

In addition, the effect of phosphorylation of tyrosine 125 on the intramolecular contacts of alpha-synuclein was assessed by PRE experiments with MTSL spin-labels attached at position A107C and by PFG diffusion measurements. The PRE effect, when plotted against protein primary sequence, was not significantly different for the phosphorylated and unphosphorylated protein (Figure 4.2). Interestingly, spin-labeling at position 107 does not seem to report on the known C- to N-terminal contacts in alpha-synuclein, so this technique was not able to determine whether those contacts are

preserved upon phosphorylation. However, the well near the label site appears to be narrower in the pY125 sample, with the intensity ratio reaching 1 by residue 85, while it remains below that value until residue ~70 in the unphosphorylated sample. This discrepancy suggests that the C-terminal region occupies more extended conformations when tyrosine 125 is phosphorylated, thus experiencing less PRE due to the spin-label at 107. Intramolecular contacts were also assessed by measuring the diffusion coefficient, and thus the hydrodynamic radius, of the phosphorylated protein molecule.

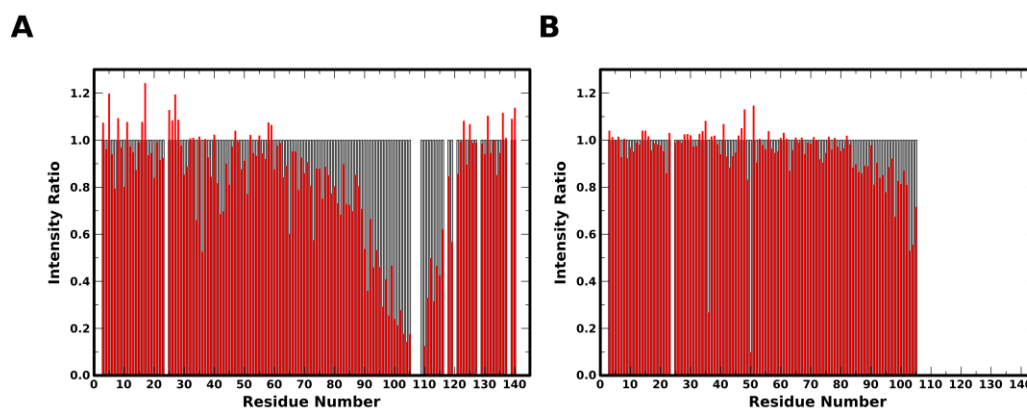


**Figure 4.2: Intramolecular contacts for unphosphorylated and pY125 alpha-synuclein A107C in aqueous buffer.** Plot of the ratio of peak intensity for samples paramagnetically labeled at A107C to peak intensity in unlabeled samples *versus* residue number for unphosphorylated (A) and pY125 alpha-synuclein (B) in aqueous buffer. The gray bars indicate which peaks were included in the analysis.

Previous studies on phosphorylated alpha-synuclein (pS129) [155] had shown that phosphorylation results in drastic expansion of the protein molecules, reflected in ~25% increase in hydrodynamic radius. The

pY125 alpha-synuclein displayed a hydrodynamic radius virtually identical (102%) to that of the unphosphorylated protein, thus precluding any expanded protein conformations such as those seen for pS129.

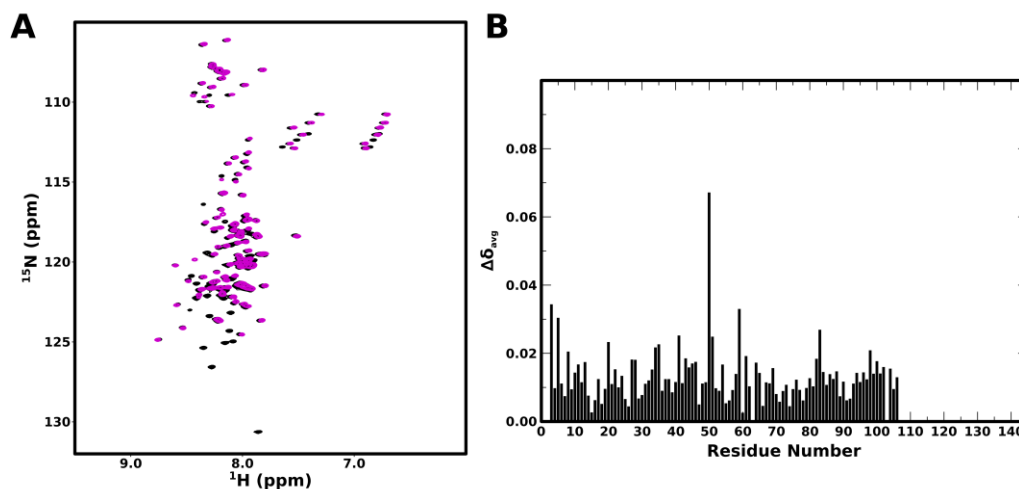


**Figure 4.3: HSQC spectra and amide chemical shift differences for unphosphorylated and pY125 alpha-synuclein A107C in the presence of SDS micelles.** (A)  $^1\text{H},^{15}\text{N}$ -HSQC spectra of unphosphorylated wild-type (black) and pY125 alpha-synuclein A107C (purple) in 40 mM SDS. (B) Plot of amide chemical shift differences (equation 1) between unphosphorylated wild-type and pY125 alpha-synuclein A107C in 40 mM SDS *versus* residue number.

The effect of phosphorylation at tyrosine 125 on the micelle-bound form of alpha-synuclein was also assessed. Comparison of  $^1\text{H},^{15}\text{N}$ -HSQC spectra of unphosphorylated and pY125 alpha-synuclein in the presence of 40 mM SDS reveals overall similarity between the spectra, reflecting a lack of large-scale structural changes due to phosphorylation (Figure 4.3A). Assignments from the wild-type protein were transferred to the closest unassigned peak in the pY125 spectrum and the transferred assignments were then used to analyze

the locations of the spectral changes along the peptide chain (Figure 4.3B). The magnitude of most of the peak shifts was very low, except for that of histidine 50, which is very sensitive to even small changes in pH. These shifts suggest that the phosphorylation does not affect the overall fold of the protein.

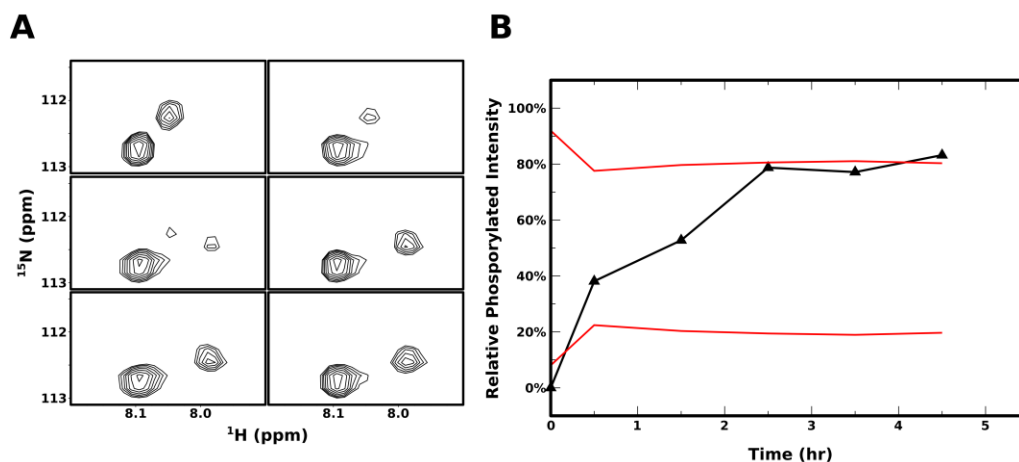


**Figure 4.4: HSQC spectra and increasing intensity of phosphorylated peaks during phosphorylation reaction.** (A) Zooms of consecutive 1-hour  $^1\text{H},^{15}\text{N}$ -HSQC spectra of alpha-synuclein incubated with SH2-CD c-Abl. The regions focus on the peak for G41 and show the disappearance of the unphosphorylated peak and appearance of the phosphorylated peak. (B) Plot of relative intensity of the phosphorylated peak for G41 with increasing time. Red lines show the approximate level of noise.

*Free state structure of alpha-synuclein is not greatly perturbed by pY39* – alpha-Synuclein can also be phosphorylated on tyrosine 39, which is located within the membrane-binding domain, albeit in a region that forms the somewhat flexible linker region in the broken helix state. The tyrosine kinase c-Abl specifically phosphorylates this site [264]. The phosphorylation reaction can be followed in real time by

multidimensional NMR; wild-type alpha-synuclein was incubated with SH2-CD c-Abl and consecutive 1 hr  $^1\text{H}$ ,  $^{15}\text{N}$ -HSQC spectra were collected. The spectral changes were characterized by disappearance of cross-peaks arising from residues near position 39 (such as glycine 41) in the unphosphorylated protein and appearance of new peaks nearby, ostensibly arising from the phosphorylated protein (Figure 4.4A).

The fact that peaks arising from phosphorylated and unphosphorylated alpha-synuclein are both visible demonstrates that the phosphorylation reaction is slower than the NMR timescale in the experiment. The intensities of the phosphorylated and unphosphorylated peaks are anti-correlated with increasing time, suggesting that the progress of the reaction can be monitored by the increasing intensity of the phosphorylated peaks. When plotted against time (the midpoint of each hour-long HSQC experiment), the intensity of the phosphorylated peak relative to the total intensity for both peaks increases and reaches a maximum by ~3 hr (Figure 4.4B). Interestingly, the unphosphorylated peaks remain at ~20% of the total intensity after this time, consistent with the noise threshold of this experiment, as estimated by the NMRViewJ peak picking module (Figure 4.4B, red). While secondary phosphorylation at tyrosine 125 was detected by mass spectrometry [264], the peak for that residue is in a very crowded region and no spectral changes could be resolved.

To determine the effects of phosphorylation at tyrosine 39 on the conformation of alpha-synuclein in aqueous buffer, isotopically-labeled pY39 alpha-synuclein was produced by incubating alpha-synuclein Y125F Y133F (to increase the efficiency of phosphorylation) with c-Abl.

A comparison of  $^1\text{H},^{15}\text{N}$ -HSQC spectra of unphosphorylated and pY39 alpha-synuclein Y125F Y133F reveals small spectral changes, although the overall spectrum is very similar (Figure 4.5A).

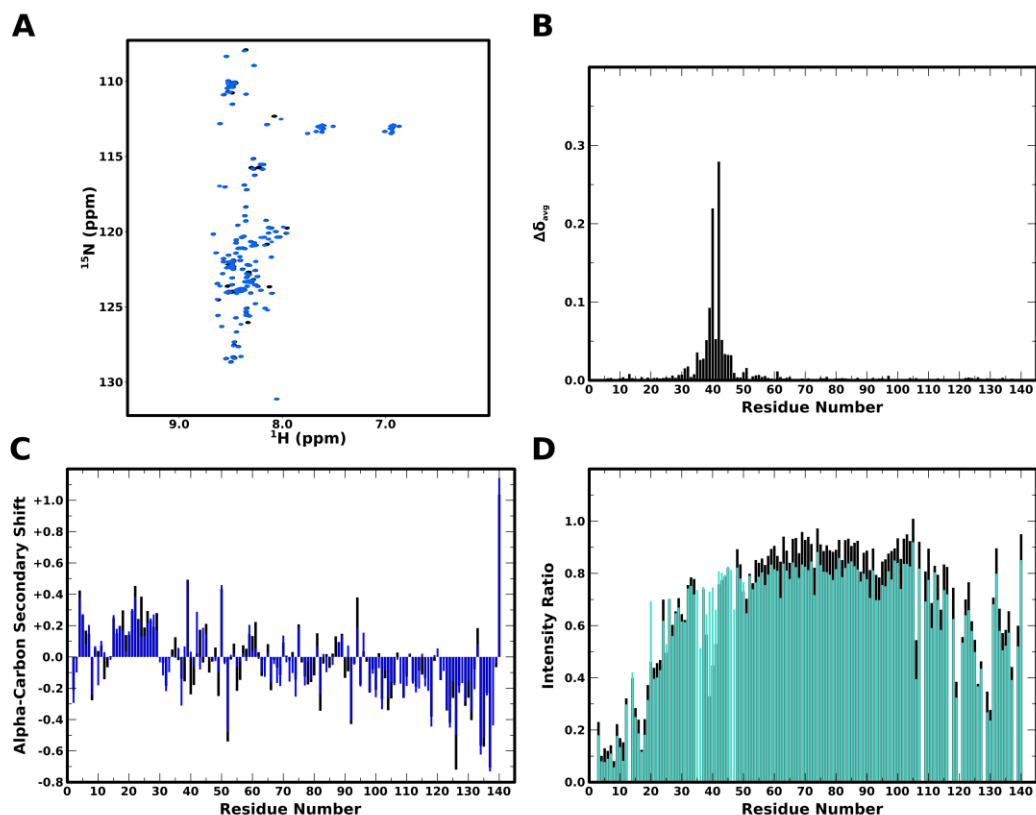


**Figure 4.5: HSQC spectra, amide chemical shift differences, and alpha-carbon secondary shifts for unphosphorylated and pY39 alpha-synuclein Y125F Y133F in aqueous buffer.** (A)  $^1\text{H},^{15}\text{N}$ -HSQC spectra of unphosphorylated (black) and pY39 (blue) alpha-synuclein Y125F Y133F in aqueous buffer. (B) Plot of amide chemical shift differences (equation 1) between unphosphorylated and pY39 alpha-synuclein Y125F Y133F *versus* residue number. (C) Plot of alpha-carbon secondary shifts *versus* residue number for unphosphorylated (black) and pY39 alpha-synuclein Y125F Y133F (blue) in aqueous buffer. (D) Plot of the ratio of peak intensity for samples paramagnetically labeled at S7C to peak intensity in unlabeled samples *versus* residue number for wild-type (black) and Y39E alpha-synuclein (cyan) in aqueous buffer.

Assignments for backbone amide resonances were transferred from those for wild-type alpha-synuclein using an HNCA experiment. When the amide cross-peak chemical shift deviations upon phosphorylation were plotted as a function of primary sequence, the major changes localized to the region immediately surrounding the phosphorylation site ( $\pm 5$  residues) (Figure 4.5B). The extent of these perturbations was similar to that seen for phosphorylation of alpha-synuclein at other disordered sites [154,155]. In addition, alpha-carbon secondary shifts were very similar for phosphorylated and unphosphorylated protein (Figure 4.5C), and the N-terminal to C-terminal transient intramolecular contacts were not affected by a phosphomimic Y39E mutation (Figure 4.5D), suggesting that pY39 does not induce any secondary structural changes in the protein in aqueous buffer.

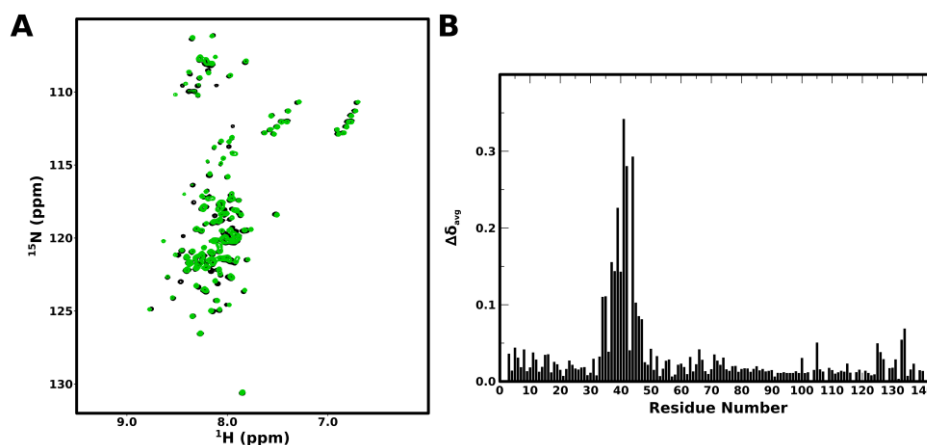


**Figure 4.6: HSQC spectra and amide chemical shift differences for unphosphorylated and pY39 alpha-synuclein Y125F Y133F in the presence of SDS micelles.** (A)  $^1\text{H},^{15}\text{N}$ -HSQC spectra of unphosphorylated wild-type alpha-synuclein (black) and pY39 alpha-synuclein Y125F Y133F (green) in 40 mM SDS. (B) Plot of amide chemical shift differences (equation 1) between unphosphorylated wild-type alpha-synuclein and pY39 alpha-synuclein Y125F Y133F in 40 mM SDS *versus* residue number.

*Linker region structure in micelle-bound state is altered by pY39 but broken-helix state remains* – While the phosphorylation of Tyr-39 does not have a large effect on the structure of alpha-synuclein in aqueous solution, the position of the phosphorylation site in the linker region between the two helices in the SDS-bound state suggests that phosphorylation may have some structural effects on the broken-helix conformation. Figure 4.6A shows a comparison of  $^1\text{H}, ^{15}\text{N}$ -HSQC spectra of unphosphorylated and pY39 alpha-synuclein Y125F Y133F in the presence of SDS. Significantly more spectral changes can be seen than in the absence of SDS. The backbone resonance assignments were transferred from those of wild-type unphosphorylated protein in SDS [71]. The major chemical shift changes localize to approximately residues 30-50, or ~10 residues in each direction from the phosphorylation site (Figure 4.6B). The greater extent of significant chemical shift perturbations along the peptide chain in the presence of SDS suggests that phosphorylation has some structural effects. Alternatively, the change in the electrochemical environment upon addition of a phosphate group may be sensed by residues farther away in primary sequence due to the compact, helical structure in the presence of SDS micelles.

In order to elucidate the potential changes in secondary structure due to phosphorylation at Y39, alpha- and carbonyl carbon secondary shifts were calculated from chemical shifts measured via HNCO and HNCA experiments and plotted *versus* residue number (Figure 4.7). The secondary shifts were quite similar to that of the unphosphorylated protein throughout the peptide chain, except for the

linker region (res. 37-45), which showed increased average alpha-carbon (from 1.43 to 2.42 ppm) and carbonyl (from 0.92 to 1.34 ppm) secondary shifts. This increase is suggestive of increased helicity in the linker region, although the level of secondary shift (and thus helicity) does not reach the maximum seen for helix-1 and helix-2. The increase in secondary shifts in two different carbon nuclei strongly suggests that phosphorylation at Y39 increases helicity in the linker region and potentially eliminates the break between helix-1 and helix-2, thus promoting the extended-helix state, in which the two antiparallel helices fuse into one long helix.

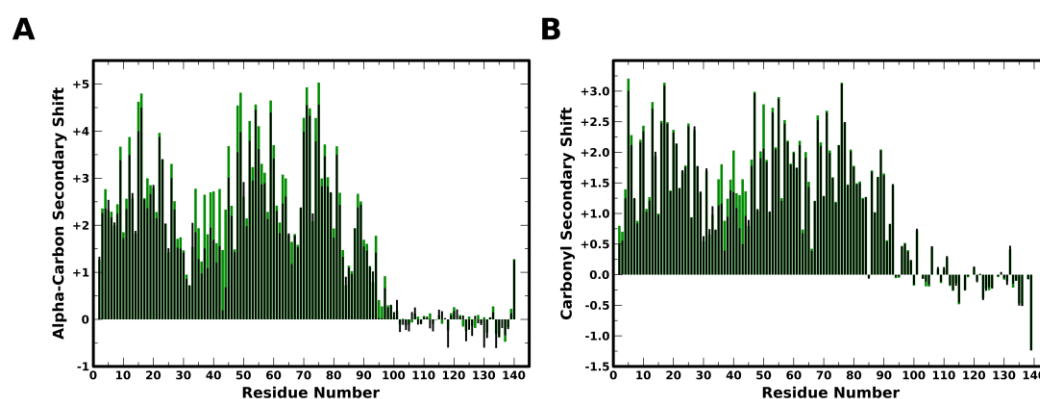


**Figure 4.7: Alpha-carbon and carbonyl secondary shifts for unphosphorylated and pY39 alpha-synuclein in the presence of SDS micelles.** Plot of alpha-carbon (A) and carbonyl (B) secondary shifts *versus* residue number for unphosphorylated wild-type (black) and pY39 alpha-synuclein Y125F Y133F (green) in 40 mM SDS.

The broken-helix state is characterized by a break in the  $i, i+1$  amide-amide NOE peaks between residue 41, 42, and 43 [71]. These NOE peaks are usually indicative of helical structure, so a break in them argues against an extended helix. Additionally, in the broken-

helix state, there are PRE effects on one helix from a spin-label on the opposing helix [75]; these effects would not be seen in the extended-helix state. These two methods were used to ascertain whether the broken-helix conformation is lost upon Y39 phosphorylation. For PRE experiments, truncated alpha-synuclein (1-102) was used. This fragment of alpha-synuclein contains the entire lipid-interacting domain and lacks the other tyrosine residues that can be phosphorylated by c-Abl.

Since cross-peaks arising from residues distant from pY39 in both phosphorylated and unphosphorylated protein have the same chemical shift, it is impossible to separate the PRE effect measured on a mixture of phosphorylated and unphosphorylated material. Such a mixture is to some extent unavoidable due to the incompleteness of the phosphorylation reaction and inability to fully separate the modified and unmodified protein by HPLC, thus complicating analysis of PRE data. Unphosphorylated protein, labeled at position E83C, shows an unmistakable PRE effect at the N-terminal end of helix-1, around residues 3-8, confirming the presence of the broken-helix state (Figure 4.8A). However, the phosphorylated sample, which contains ~25% unphosphorylated material (as estimated by peak intensities), shows a PRE effect on the N-terminal residues comparable to that seen in the wholly unphosphorylated sample (Figure 4.8B). The extent of the PRE effect seen across helices is too great to arise from only 25% of the alpha-synuclein molecules, arguing strongly for the presence of the broken-helix state even in pY39 alpha-synuclein.

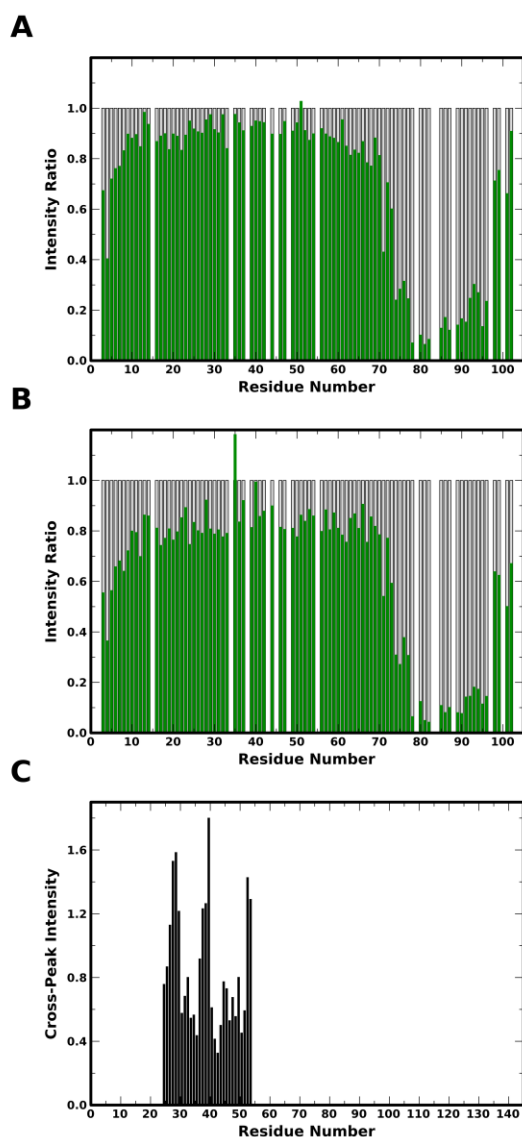


**Figure 4.8: Intramolecular PRE and partial sequential amide-amide NOE cross-peaks for pY39 alpha-synuclein in the presence of SDS micelles.** Plot of the ratio of peak intensity for samples paramagnetically labeled at E83C to peak intensity in unlabeled samples *versus* residue number for unphosphorylated (A) and pY39 (B) alpha-synuclein 1-102 in 40 mM SDS. The gray bars indicate which peaks were included in the analysis. (C) Plot of average intensity of the sequential amide NOE cross-peaks between each pair of residues between 24 and 53 for pY39 alpha-synuclein Y125F Y133F in 40 mM SDS *versus* residue number.

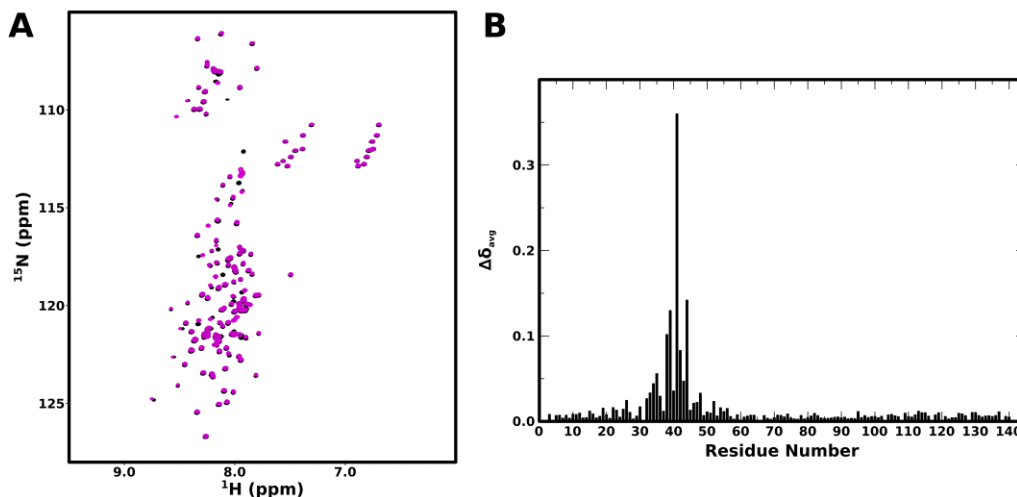


**Figure 4.9: HSQC spectra and amide chemical shift differences for wild-type and Y39E alpha-synuclein in the presence of SDS micelles.** (A)  $^1\text{H}$ ,  $^{15}\text{N}$ -HSQC spectra of wild-type (black) and Y39E (purple) alpha-synuclein in 40 mM SDS. (B) Plot of amide chemical shift differences (equation 1) between wild-type and Y39E alpha-synuclein in 40 mM SDS *versus* residue number.

Sequential ( $i, i+1$ ) NOE cross-peak intensities from an H-N-N HSQC-NOESY-HSQC experiment were analyzed to determine the extent of continuous helical structure. Since only the linker region chemical shifts are perturbed upon phosphorylation, NOE cross-peaks for only 30 residues centered on Y39 were included in the analysis. The rest of the micelle-binding region is expected to show the same pattern of sequential NOEs as the unphosphorylated protein [71]. Sequential NOE cross-peaks were detected for all residues in the region analyzed, although the intensity of NOE peaks between residue pairs 41/42 and 42/43, was quite weak (Figure 4.8C). While this suggests that the helix is continuous throughout the linker region, these NOE peaks can also arise from the compact and rigid turn structure that the linker adopts in the broken-helix state. In fact, weak

NOE cross-peaks have been detected for unphosphorylated wild-type alpha-synuclein under similar conditions as well (see below, Figure 4.11C).

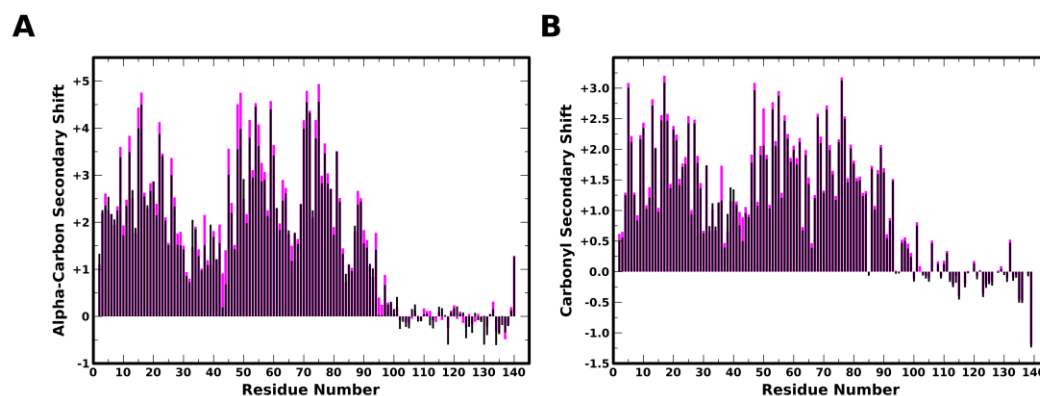


**Figure 4.10: Alpha-carbon and carbonyl secondary shifts for wild-type and Y39E alpha-synuclein in the presence of SDS micelles.**

Plot of alpha-carbon (A) and carbonyl (B) secondary shifts *versus* residue number for wild-type (black) and Y39E (purple) alpha-synuclein in 40 mM SDS.

Due to the difficulty of obtaining sufficient quantities of pure phosphorylated protein, a parallel set of experiments were carried out with the Y39E mutant of alpha-synuclein, which served as a phosphorylation mimic, although a glutamic acid side-chain differs from a phosphorylated tyrosine side-chain in length, chemical composition, flexibility, and number of charges at neutral pH. The  $^1\text{H}, ^{15}\text{N}$ -HSQC spectrum of alpha-synuclein Y39E in the presence of 40 mM SDS showed significant differences from that of the wild-type protein in the same region as, though to a lesser extent than, the phosphorylated protein (Figure 4.9). Alpha-carbon and carbonyl secondary shifts, averaged over the entire linker region, were more

positive for alpha-synuclein Y39E than wild-type protein (0.27 ppm greater for alpha-carbon, 0.02 ppm greater for carbonyl) (Figure 4.10); however, the extent of secondary shift increase was much lower than for the authentically phosphorylated protein (compare Figure 4.7). These data suggest that the linker region of the mutant protein also exhibits increased helicity, although less so than in the phosphorylated protein.

The extended or broken nature of the helices in the SDS-bound state of alpha-synuclein Y39E was also queried by intramolecular PRE and HSQC-NOESY-HSQC experiments in 40 mM SDS. The PRE effect from a spin-label covalently attached at position 9 was seen on the C-terminal end of helix-2 (residues 90-105), much as in wild-type protein (Figure 4.11A,B). In addition,  $i,i+1$  amide proton NOE cross-peaks were present between residue pairs 41/42 and 42/43, although at a low intensity; in fact, NOE cross-peaks were present for all pairs of residues in the linker region that could be resolved from the dominant diagonal peaks (Figure 4.11C). Notably, a parallel matched experiment on wild-type protein revealed a similar pattern of  $i, i+1$  NOE cross-peaks in the linker region at this SDS concentration (Figure 4.11C). Thus, the mutant protein does not differ significantly from the wild-type in secondary structure at the linker region.

As the wild-type protein has definitively been shown to adopt a non-helical conformation in the linker region [74], the continuous  $i,i+1$  NOE peaks may result from the relatively structured turn that the linker adopts, bringing residues close together. In fact, helix-1 was determined to end at residue 37, while strong  $i,i+1$  NOEs continue at

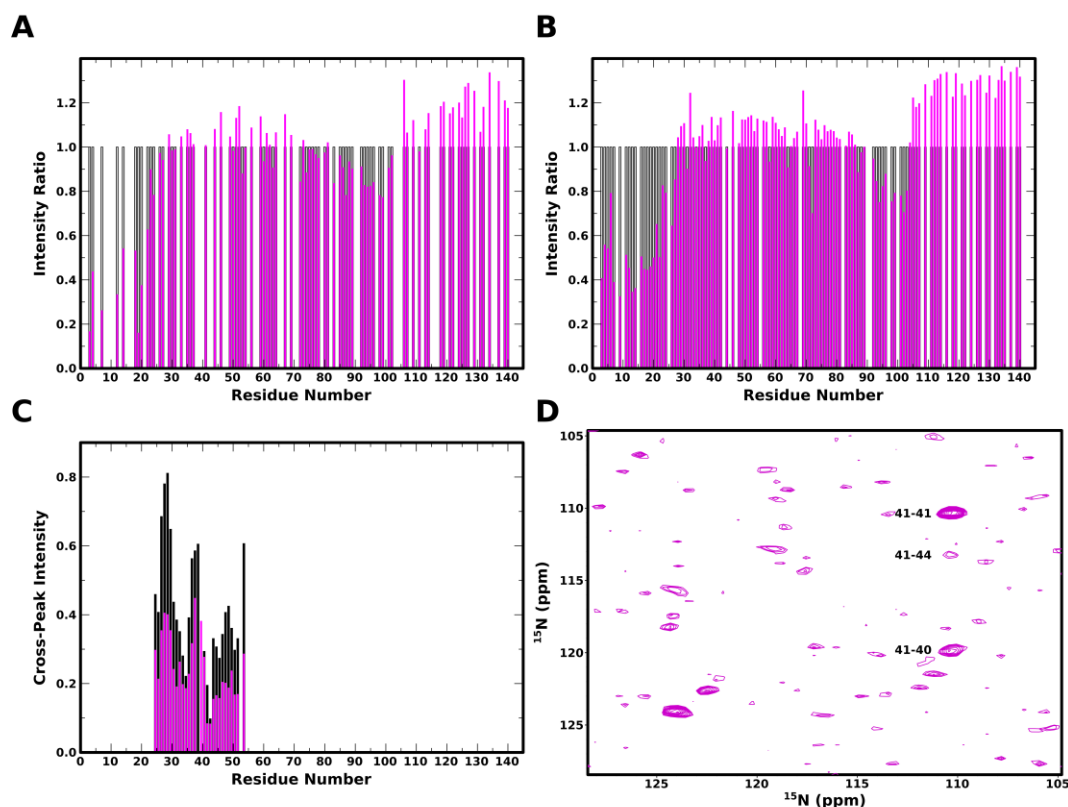


**Figure 4.11: Intramolecular PRE and partial sequential amide-amide NOE cross-peaks for wild-type and Y39E alpha-synuclein in the presence of SDS micelles.** Plot of the ratio of peak intensity for samples paramagnetically labeled at S9C to peak intensity in unlabeled samples *versus* residue number for wild-type (A) and Y39E (B) alpha-synuclein in 40 mM SDS. The gray bars indicate which peaks were included in the analysis. (C) Plot of average intensity of the sequential amide NOE cross-peaks between each pair of residues between 24 and 53 in 40 mM SDS *versus* residue number for wild-type (black) and Y39E (purple) alpha-synuclein. (D) Plane of HSQC-NOESY-HSQC spectrum showing strong  $i,i-1$  NOE peak for residues 40/41 and weak  $i,i+3$  NOE peak for residues 41/44.

least until position 40, suggesting that these NOEs do arise from the compact conformation of the linker, and not from helical structure. One interesting spectral difference between the wild-type and Y39E

alpha-synuclein is the presence of a weak  $i,i+3$  NOE cross-peak between residue 41 and 44 in the mutant protein in the presence of SDS micelles (Figure 4.11D). This cross-peak may be indicative of more compact structure in the linker region, although it was not detected for pY39 alpha-synuclein.

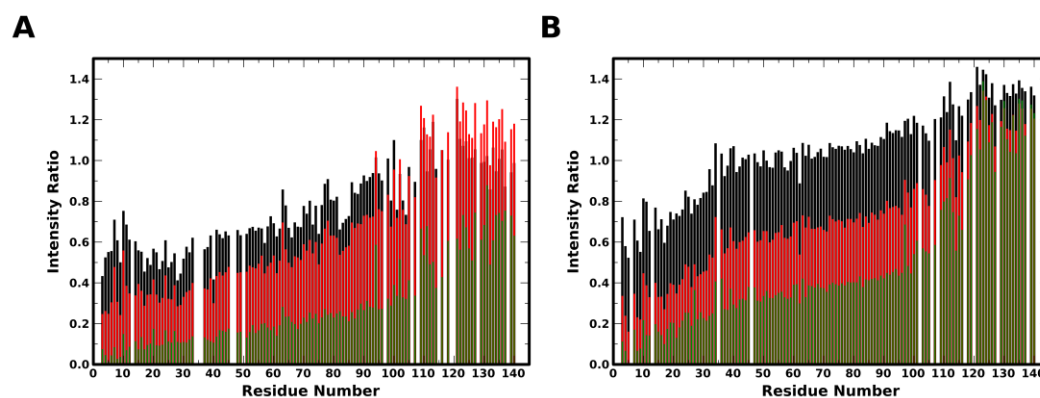


**Figure 4.12: Binding profiles of unphosphorylated and pY39 alpha-synuclein to low negative charge SUVs.** Plot of the ratio of peak intensity in the presence of 3 (black), 6 (red), and 12 (green) mM 15% PS SUVs to peak intensity in the absence of vesicles *versus* residue number for unphosphorylated wild-type alpha-synuclein (A) and pY39 alpha-synuclein Y125F Y133F (B).

*Binding of helix-2 to lipid vesicles is lost in pY39 and Y39E alpha-synuclein* – The addition of a negatively-charged phosphate group in the middle of the membrane-binding domain of alpha-synuclein might be expected to perturb alpha-synuclein binding to negatively-charged lipid vesicles. Parallel titrations using matched samples made from the same lipid vesicle stock of 15% DOPS, 60% DOPC, 25% DOPE SUVs with unphosphorylated wild-type and pY39 Y125F Y133F alpha-synuclein showed an interesting binding profile for the phosphorylated protein (Figure 4.12). The extent of binding at the N-terminus (until

residue ~40) is very similar for both wild-type and mutant protein; however, C-terminal to position 30, the mutant displays greatly reduced binding at all lipid concentrations.

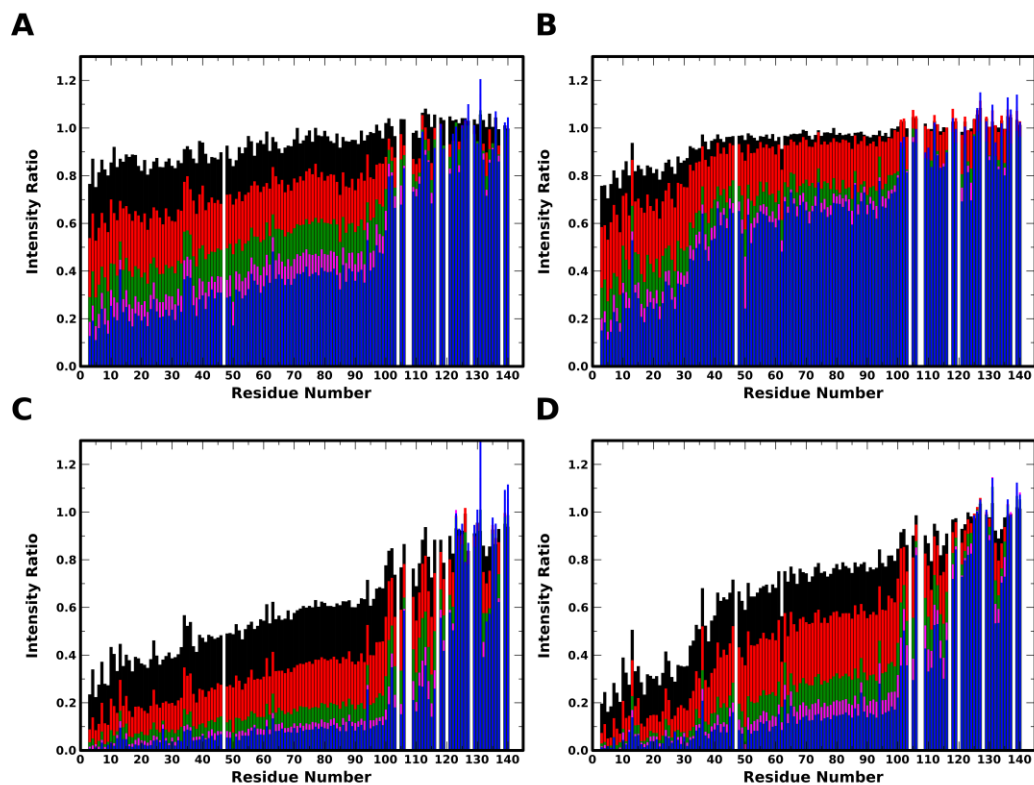


**Figure 4.13: Binding profiles of wild-type and Y39E alpha-synuclein to low and high negative charge SUVs.** Plot of the ratio of peak intensity in the presence of 1.5 (black), 3 (red), 6 (green), 9 (purple), and 12 (blue) mM 15% (A,B) and 50% (C,D) PS SUVs to peak intensity in the absence of vesicles *versus* residue number for wild-type (A,C) and Y39E (B,D) alpha-synuclein. Bound fractions of total binding and fully-helical binding were calculated and fit to equation 2, with the  $K_{D,app}$  values shown in Table 4.1.

Due to phosphorylated sample limitations, the Y39E mutant of alpha-synuclein was also used as a phosphomimic for lipid vesicle titration experiments, allowing for a more thorough and quantitative

comparison. Parallel titrations using matched samples of 15% DOPS, 60% DOPC, 25% DOPE SUVs with wild-type and Y39E alpha-synuclein showed that the mutant protein binds in a similar manner to the authentically phosphorylated protein (Figure 4.13A,B). Bound fractions for total binding and fully-helical binding were calculated and fit to equation 2 to extract apparent dissociation constants for both binding modes. The calculated  $K_{D,app}$  values are shown in Table 4.1 and are very similar for total binding of wild-type and mutant alpha-synuclein ( $3.8 \pm 0.5$  versus  $3.4 \pm 0.4$  mM), but differ by nearly a factor of 3 for the fully-helical binding mode ( $9.9 \pm 1.0$  versus  $26.0 \pm 1.1$  mM). The wild-type binding affinities are also similar to that measured for the “unmodified alpha-synuclein” in section III.c.

**Table 4.1: Computed apparent  $K_D$  values and other parameters for wild-type and Y39E alpha-synuclein with low and high negative charge SUVs.** Apparent  $K_D$  values were calculated from fitting titrations to equation 2 (see Figure 4.13) using total lipid concentration. “Full Helix Fraction” was calculated using equation 5 (see section II.).

Protein and Lipid	Total Binding $K_{D,app}$ (mM)	Fully-Helical Binding $K_{D,app}$ (mM)	Full Helix Fraction
15% DOPS			
WT	$3.8 \pm 0.5$	$9.9 \pm 1.0$	0.38
Y39E	$3.4 \pm 0.4$	$26.0 \pm 1.1$	0.13
50% DOPS			
WT	$0.6 \pm 0.1$	$2.1 \pm 0.3$	0.29
Y39E	$0.4 \pm 0.1$	$3.4 \pm 0.4$	0.13

The “helix extension” parameter (see section II.d), which also estimates the percent of fully-helical binding, was computed from the apparent dissociation constants (Table 4.1). This parameter illustrates the striking difference in binding between the wild-type and mutant

protein, with 38% of the bound wild-type alpha-synuclein in the fully-helical state, compared to only 13% for alpha-synuclein Y39E. These data show that binding in the fully-helical state is strongly disfavored by the tyrosine-to-glutamate mutation and that helix-2 binding is lost while helix-1 remains bound. Based on the similar shape of the binding profiles for pY39 and Y39E alpha-synuclein, a similar effect likely occurs in the authentically phosphorylated protein.

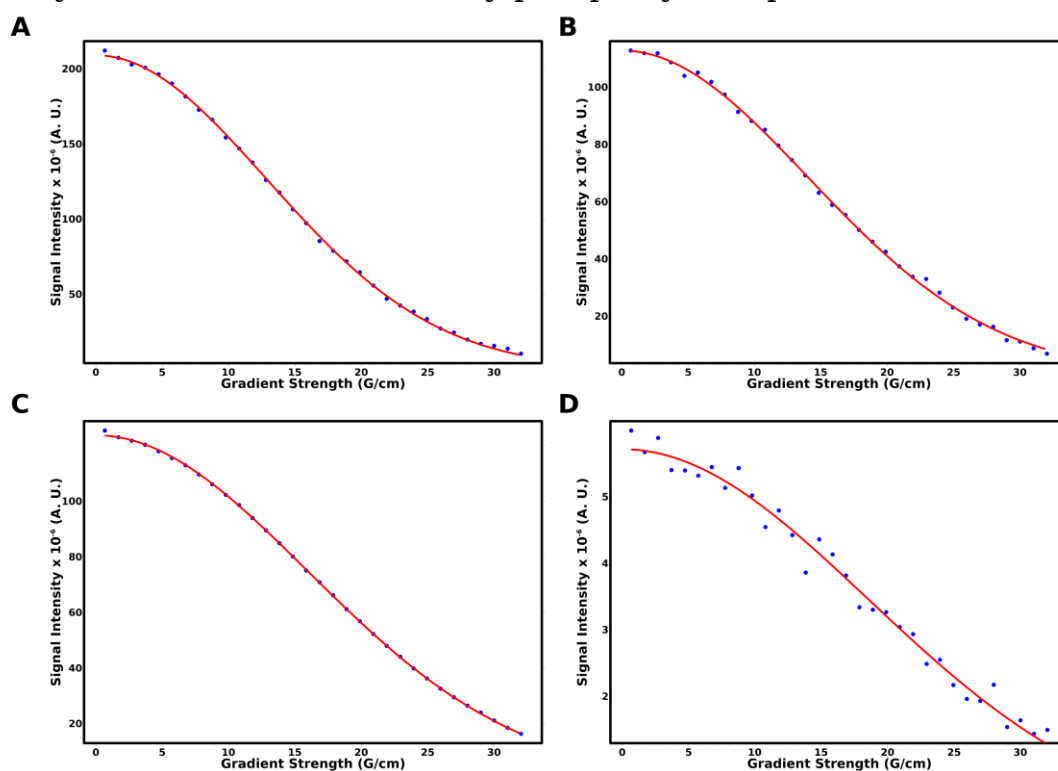


**Figure 4.14: PFG LED diffusion fits for alpha-synuclein in low and high SDS.** Representative plots of the intensity for SDS (A,C) and alpha-synuclein (B,D) signal with increasing gradient strength in 40 (A,B) and 450 (C,D) mM  $^2\text{H}$  SDS. The points are fit to equation 7 and the diffusion coefficients shown in Table 4.2.

A binding titration was also carried out with SUVs composed of 50% DOPS, 15% DOPE, 35% DOPC to determine if higher negative

charge content ameliorates the loss of helix-2 binding due to the Y39E mutation. The binding profiles in the presence of higher negative charge vesicles are qualitatively similar to those in the presence of lower negative charge vesicles (Figure 4.13C,D). Apparent dissociation constants were computed for different binding modes, and although binding affinity was greater across the board, alpha-synuclein Y39E still showed decreased fully-helical binding (Table 4.1). The “helix extension” parameter illustrates that, while the percent of bound alpha-synuclein in the fully-helical state is slightly lower than in the presence of lower negative charge SUVs for the wild-type protein (29% *versus* 38%), the percentage is very similar for the mutant protein (12% *versus* 13%) (Table 4.1). Thus, increased negative charge does not overcome the inhibitory effect of the Y39E mutant on helix-2 binding.

**Table 4.2: Hydrodynamic radii and diffusion coefficients for alpha-synuclein-micelle complex at low and high SDS.** Diffusion coefficients were extracted by fitting PFG experiments to equation 7, and hydrodynamic radii calculated relative to the known radius of dioxane.

	40 mM SDS		450 mM SDS		
Signal	D (cm <sup>2</sup> /sec)	R <sub>H</sub> (Å)	D (cm <sup>2</sup> /sec)	R <sub>H</sub> (Å)	R <sub>H,450</sub> / R <sub>H,40</sub>
Dioxane	8.97 x 10 <sup>-10</sup>	2.12	6.67 x 10 <sup>-10</sup>	2.12	
SDS	8.66 x 10 <sup>-11</sup>	22.0	5.17 x 10 <sup>-11</sup>	27.4	1.25
alpha-synuclein	7.40 x 10 <sup>-11</sup>	25.7	3.58 x 10 <sup>-11</sup>	39.5	1.54

*High SDS concentrations slightly favor extended state of alpha-synuclein* – At higher concentrations of SDS (> 400 mM), detergent micelles are expected to take on an elongated shape [84]. This geometry could favor the formation of the extended-helix conformation

of alpha-synuclein [84]. The size of the protein-micelle complex at different concentrations of SDS was measured by determining the diffusion coefficient using SDS and protein signals in a PFG diffusion experiment, then converting to the hydrodynamic radius using a known standard (dioxane, 2.12 Å). Representative PFG diffusion plots derived from the protein and detergent signals are shown in Figure 4.14 and hydrodynamic radii summarized in Table 4.2. The increased hydrodynamic radius of the detergent micelle at 450 mM SDS (1.25 times greater than at 40 mM SDS) confirms the presence of elongated micelles. In addition, the protein signals, which ostensibly report on the subset of micelles which also have protein bound, show an even greater hydrodynamic radius increase (1.54 times greater than at 40 mM SDS), suggesting the presence of the extended-helix state of alpha-synuclein on these elongated micelles. However, intramolecular PRE experiments show that contact between helix-1 and helix-2 is not fully lost at the high detergent concentration (Figure 4.15).

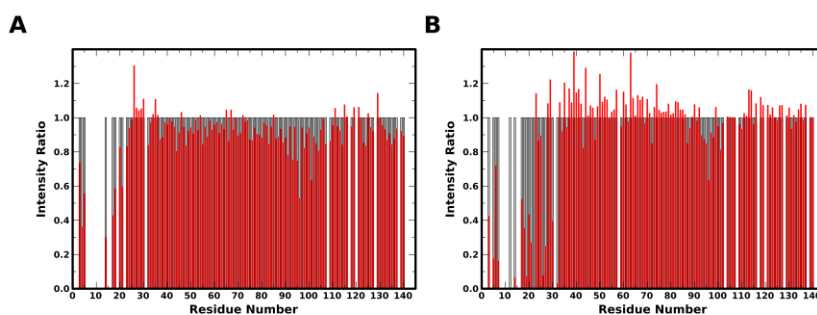


**Figure 4.15: Intramolecular PRE for alpha-synuclein at low and high SDS.** Plot of the ratio of peak intensity for samples paramagnetically labeled at S9C to peak intensity in unlabeled samples *versus* residue number for alpha-synuclein in 40 (A) and 450 (B) mM SDS. The gray bars indicate which peaks were included in the analysis.

*Results summary* – The effect of tyrosine phosphorylation on the structure of alpha-synuclein and its interactions with membranes and detergents strongly depends on the location of the modified residue in the polypeptide chain of alpha-synuclein. Phosphorylation of Y125, located in the extended C-terminal tail that does not interact with membrane surfaces, does not have a major effect on the conformations of alpha-synuclein both in dilute aqueous buffer and in the presence of membrane-mimetic detergent micelles. The addition of a phosphate group does result in locally more expanded conformations in the C-terminal tail; while the effect on transient C- to N-terminal contacts was not able to be determined directly via PRE measurements, the overall hydrodynamic radius of the protein is not significantly altered.

Phosphorylation of Y39 by c-Abl tyrosine kinase was followed in real-time by collecting successive HSQC spectra. Peaks arising from the unphosphorylated protein decreased in intensity while those arising from the phosphorylated species increased in intensity. The affected peaks seemed to localize to the vicinity of the modification site. Backbone assignments confirmed that only the ~10 residues around Y39 were affected in amide chemical shift. However, in the presence of spheroidal SDS micelles, the area of effect was expanded to ~20 residues and secondary shifts of both alpha- and carbonyl carbon nuclei increased, suggesting higher helicity in the non-helical linker region. These effects on the chemical shifts were recapitulated by the phosphomimic Y39E mutation, although to a lesser extent. In both cases (pY39 and Y39E), the secondary shifts of the linker region did not reach the high levels of the stable helix-1 and helix-2.

The effects on chemical shifts suggested that phosphorylation of Y39 may be promoting the existence of the extended-helix state, in which the linker region becomes helical, fusing the two antiparallel helices into one long helix. Inter-helix PRE effects are characteristic of the broken-helix state and thus were used to test this hypothesis. For both pY39 and Y39E in the presence of spheroidal SDS micelles, the PRE effect remained, indicating that there was still a population containing an antiparallel helix arrangement. Additionally, the intensity of sequential NOE cross-peaks throughout the linker region was not very different from that of unphosphorylated wild-type alpha-synuclein for both mutant and phosphorylated alpha-synuclein, and none of the experiments recapitulated the clear break around residue 42 observed for the wild-type protein previously [71]. This could be due to slightly different micelle geometry/concentration or the fact that partially deuterated protein was used in previous work, minimizing spin diffusion effects. In addition,  $i, i+1$  NOE cross-peaks past position 37 may not result from helical structure, as the linker has been shown to adopt a non-helical conformation on the micelle surface [74]. These follow-up experiments argue strongly against the phosphorylated or phosphomimic protein adopting an extended-helix conformation.

The phosphorylation of Y39 also has a clear effect on alpha-synuclein binding to lipid vesicles. Upon the addition of the phosphate group or mutation to glutamate, alpha-synuclein binding to 15% PS SUVs is severely decreased C-terminal to the modification site. While the N-terminal ~40 residues of both modified and unmodified alpha-synuclein bind to a similar extent, the C-terminal half of the lipid

binding domain, corresponding roughly to helix-2, binds much less, suggesting that phosphorylation at Y39 can uncouple helix-1 and helix-2 binding to membranes. The same binding profile is seen for Y39E alpha-synuclein in the presence of 50% PS SUVs, arguing that increased attraction to the vesicle surface due to increased negative charge does not suffice for helix-2 binding.

#### **IV.d. General structural effects of phosphotyrosine**

There have been relatively few studies of the direct effects of phosphorylation on the inherent structural properties of polypeptide chains. The addition of two negative charges via the phosphate group can be expected to repel other negative charges or form salt bridges with positively-charged side-chains. Thus, phosphorylation can destroy existing or form new secondary structure elements through tertiary contacts, or promote or inhibit intermolecular interactions with binding partners. However, in the case of a disordered protein like alpha-synuclein, the effects of phosphorylation are harder to predict. In addition, among phosphorylated amino acids, tyrosine is the least studied structurally. One important difference between phosphotyrosine and phosphoserine/threonine is the length of the side-chain. The tyrosine side-chain is significantly longer, allowing the phosphate group to interact with somewhat distant atoms. For this reason, the common phosphomimics glutamate and aspartate are not ideal for emulating the effects of phosphotyrosine (Figure 4.16).

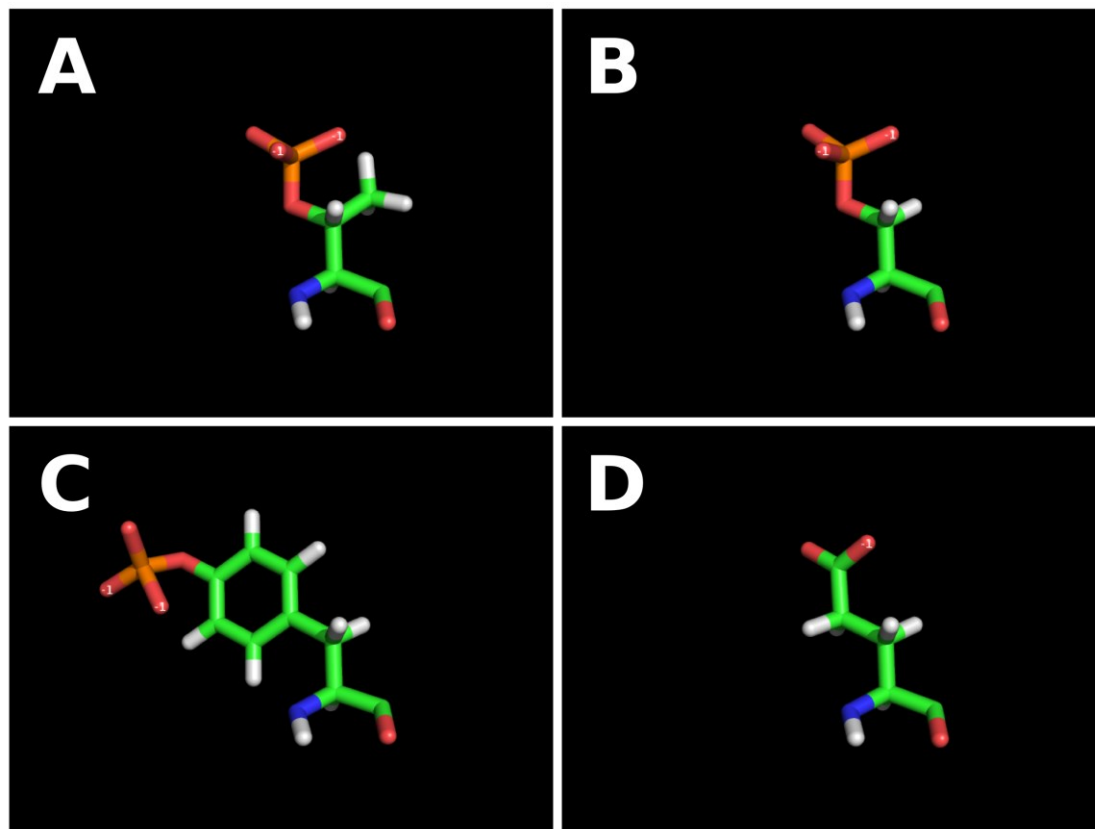


**Figure 4.16: Model of phosphorylated and phosphomimic amino acids.** Phospho-threonine (A), phospho-serine (B), phospho-tyrosine (C) and glutamate (D) were modeled in PyMol.

One effect of the addition of the phosphate group is the formation of hydrogen bonds between the phosphate and backbone amide protons nearby. This sort of hydrogen bonding occurs for glutamate side-chains with amide protons belonging to the glutamate or a nearby residue [265]. Possibly acting through a similar hydrogen bonding mechanism, phosphoserine and phosphothreonine were found to change the preferred backbone structures of short disordered peptides, as measured by coupling constants [247]. However, the same study found no such effects for phosphotyrosine, except in the

presence of flanking charges (arising from the unblocked N- and C-termini of the short peptides). This difference suggests that the length and rotational range of the tyrosine side-chain precludes interactions with nearby backbone atoms, but allows for longer-range interactions.

Chemical shift values reflect the entire electrochemical environment of a nucleus; as such, this one parameter combines myriad inputs, from nearby chemical groups, transient contacts, hydrogen bonds, secondary structure, backbone angle preferences, etc. It is often difficult to extract the structural cause of a chemical shift change. While carbonyl and alpha-carbon shifts are more sensitive to secondary structure, and thus used to delineate secondary structure elements, they still reflect many contributions from different sources. Thus, the effects of phosphorylation of alpha-synuclein on chemical shifts (proton, nitrogen, and carbon) in the disordered state is likely a combination of the effects of introduction of a highly-negatively-charged moiety, altered transient contacts with other charged regions of the polypeptide chain, and newly preferred backbone conformations. In the presence of detergent micelles, all of these contributing factors remain, and thus it is difficult to use chemical shift changes alone to determine the effect of phosphorylation on interaction with the micelle.

#### **IV.e. Functional implications for pY125 alpha-synuclein**

The evidence of implicating pY125 in alpha-synuclein function and dysfunction is scant: the levels of pY125 alpha-synuclein were

found to decrease with age (especially in PD brains) and to correlate with decreased alpha-synuclein oligomers in fly models [165]. These few findings suggest that pY125 alpha-synuclein may play a neuroprotective role; however, the structural findings here do not suggest any obvious mechanism for the modification to affect alpha-synuclein function. It is likely that phosphorylation at Y125 affects transient contacts between the N- and C-terminal regions of alpha-synuclein, as these are mediated by electrostatics. In addition, pY125 has been shown to modulate the preferred binding sites for various metal ions in alpha-synuclein [266]. Furthermore, the C-terminal tail of alpha-synuclein is known to be a protein-protein interaction motif [90], and phosphorylation of residues in this region may regulate protein-protein interactions of alpha-synuclein. It is likely that if phosphorylation of Y125 plays some role in alpha-synuclein biology, it is through these mechanisms.

#### **IV.f. Does pY39 alpha-synuclein form an extended-helix?**

While most of the phosphorylation sites in alpha-synuclein are in the C-terminal tail that remains disordered even in the presence of membranes, the location of Y39 suggests that pY39 would have a significant effect on the membrane-bound form. In fact, the amide proton and nitrogen, as well as alpha- and carbonyl carbon, chemical shifts in the entire linker region are strongly affected by phosphorylation at Y39. The region showing chemical shift

perturbations is almost exactly coincident with the non-helical region that links the two helices in the broken-helix state. That coincidence, along with the increased carbon secondary shifts indicative of greater helicity upon phosphorylation, suggested that the linker region may be becoming helical, leading to alpha-synuclein adopting an extended-helix conformation.

Would phosphorylation of tyrosine be expected to increase intrinsic helicity of peptide? In early studies of context-independent amino acid helical propensity, tyrosine was found to be a helix-breaking residue in both model peptides and model protein helices [267,268]. This helix-destabilizing effect is usually attributed to the conformational restriction of tyrosine side-chains (along with other  $\beta$ -substituted and  $\beta$ -branched amino acids) in the helical state compared to the conformational freedom these side-chains experience in the random coil state.

Addition of a charged phosphate group to the tyrosine side-chain can be expected to complicate matters. Charged amino acids in model peptides can form hydrogen bonds with the peptide backbone in unfolded states, but these potential hydrogen bonds are lost in the rigid helical conformation; thus, charged amino acids are not likely to promote helix formation [267]. However, this helix-destabilization seems to decrease with side-chain length due to the lower likelihood of forming hydrogen bonds in the random coil state [268]. In addition, charged side-chains such as glutamate have been shown to form electrostatic interactions with nearby oppositely charged residues, specifically in  $i,i+3$  and  $i,i+4$  patterns [268–270]. As alpha-synuclein

contains many lysine residues (present in the KTKEGV repeat core sequence), and specifically one at position 43, the potential electrostatic interaction with the very long negatively-charged side-chain of phosphotyrosine can be expected to promote helical structure. The presence of the membrane-mimicking detergent micelle factors in as well, since a conformation in which the negatively-charged phosphotyrosine side-chain is facing away from the negatively-charged micelle surface will be favored as well. These theoretical considerations support the conclusion that pY39 increase helicity in the linker region, drawn from increased carbon secondary shifts.

However, as mentioned above, chemical shifts report on many disparate structural and electrochemical properties, and the perturbations could simply be a result of inserting a highly negative moiety into a region of the protein that is closely associated with the (negative) SDS micelle. Therefore, further examination is required to determine whether pY39 alpha-synuclein adopts the extended-helix conformation. The existence of an inter-helical PRE effect in the pY39 and phosphomimic Y39E proteins argues quite strongly against an extended-helix conformation. The PRE effect scales with the distance between the nuclei to the power of -6, so it can be observed between two nuclei that that not more than  $\sim 25$  Å apart. The distance between the two alpha-synuclein helices in the broken-helix state on spheroidal SDS micelles is  $\sim 23$  Å [74]; thus, the PRE effect is expected to be lost if the helices splay apart even slightly more. The NOE data is more difficult to interpret, with weak sequential NOEs observed throughout the linker region for pY39 and Y39E alpha-synuclein. While this would

argue for continuous helical structure throughout that region of the polypeptide chain, similar weak NOEs are also observed for wild-type alpha-synuclein with similar SDS concentrations. Thus, the NOEs could arise from the compact turn-like structure of the linker region, without requiring helical structure, or by spin diffusion through aliphatic protein protons, given the long NOE mixing time employed (300 msec). The chemical shift changes would then be attributed to the presence of the phosphate group and potential dissociation of the linker region from the negatively-charged micelle. It is possible that in pY39 alpha-synuclein, the helical structure of helix-2 is stabilized in the N-terminal direction, but without complete fusion with helix-1.

Alternatively, pY39 and Y39E alpha-synuclein could be adopting a flexible-yet-fully-helical conformation, such as that proposed for a shuffled alpha-synuclein variant on larger SLAS micelles [229]. Such flexibility or possibly an interconversion that allows the molecules to transiently sample the broken-helix state could be enough to explain the PRE effect, which is very sensitive to even short-lived contacts [192]. In fact, even at concentrations of SDS that result in larger micelles (Table 4.2) and longer interhelical distances as measured by ESR [79], an interhelical PRE effect is still visible (Figure 4.15).

#### **IV.g. Functional implications for pY39 alpha-synuclein**

It seems likely that the *in vivo* functional effect of phosphorylation of alpha-synuclein at Y39 involves the binding of the

protein to lipid vesicles rather than the conformation it adopts in the presence of detergent micelles. In the presence of negatively-charged lipid vesicles, pY39 and Y39E alpha-synuclein show significantly decreased binding of the entire helix-2 region, which is C-terminal to the site of the modification. The interaction is likely perturbed due to electrostatic repulsion between the phosphate group and the membrane surface, and the affinity of helix-2 for the membrane is not sufficient to overcome the loss of helix folding propagation from the N-terminal helix-1. One can envision the phosphorylation at Y39 as a spatial and temporal cue for helix-2 to detach from the membrane alpha-synuclein is bound to (possibly synaptic vesicle membrane), allowing it to interact with protein binding partners or other cellular membranes (such as the synaptic plasma membrane) (Figure 4.17). In addition, this detachment of the helix-2 region may play a role in facilitating alpha-synuclein aggregation, as it contains the highly hydrophobic region that forms the core of the alpha-synuclein amyloid fibrils [271,272].

In the published structure of the SDS-micelle-associated alpha-synuclein, the side-chain of Y39 is pointing toward the micelle surface, possibly inserted into the hydrophobic core [74]. This is expected due to the hydrophobic nature of the ring in the tyrosine side-chain (although tyrosine also contains a polar hydroxide). However, addition of a highly charged phosphate to the end of the side-chain most likely abrogates any insertion into and interaction with the micelle. The strong repulsion could potentially be mitigated by adoption of the extended-helix state, in which the tyrosine side-chain is expected to be

on the hydrophilic face of the helix [71], as well as detachment of the linker region from the micelle surface. If the linker region is detached, the more C-terminal helix-2 region remains helical and likely bound to the micelle surface.

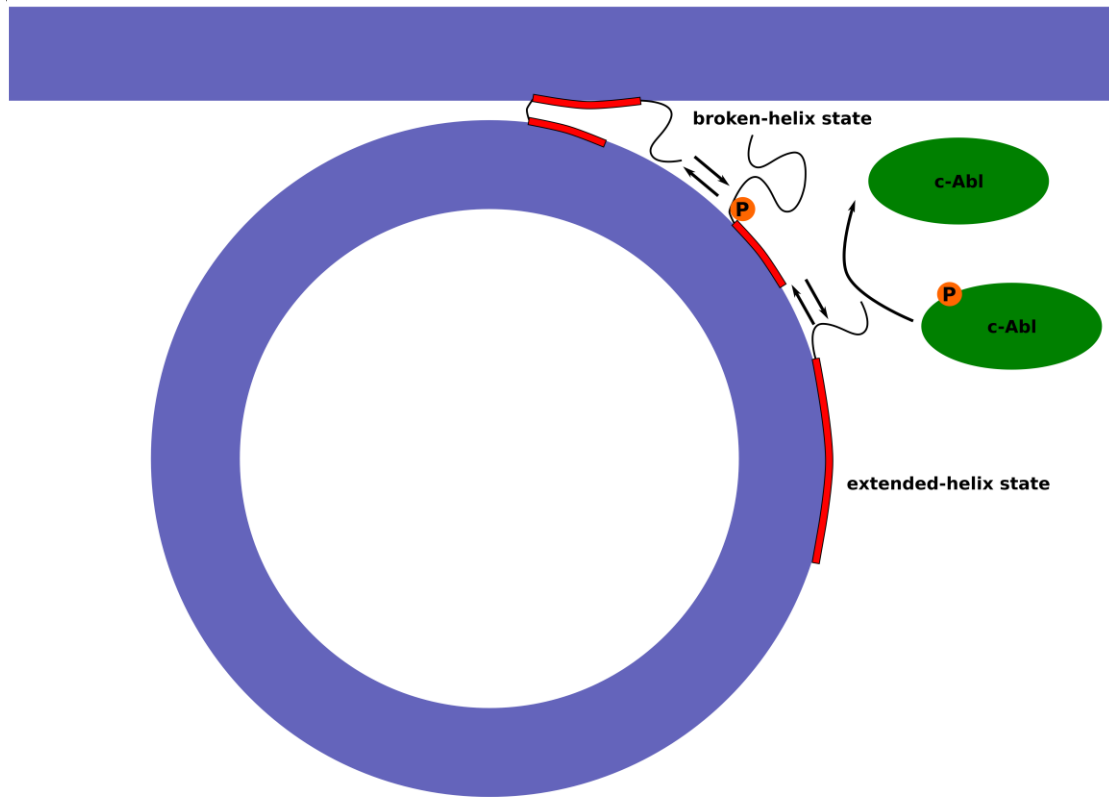


**Figure 4.17: Model of pY39 alpha-synuclein modulating the interconversion between lipid-bound states.** Phosphorylation (orange) of alpha-synuclein at tyrosine 39 by c-Abl (green) is envisioned to detach the helix-2 region from the synaptic vesicle surface and potentially allow it to bind to other membrane surfaces, such as the plasma membrane. Compare Figure 1.3.

In the presence of negatively-charged SUVs, however, the linker region and helix-2 both seem to detach from the vesicle surface. This difference suggests that the affinity of helix-2 for spherical SDS

micelles and SUVs is very different. It remains to be determined what property is responsible for this difference in affinity. SDS micelles are both more negative and more highly curved than the SUVs studied here. The increased negative charge is unlikely to be responsible, since the fractional binding of helix-2 was not increased on SUVs with higher negative charge (Table 4.1). Increased curvature may be responsible for increased helix-2 affinity (see section III.f). Regardless, it is likely that some membrane composition exists that helix-2 has a high affinity for, and binding to such a membrane may be facilitated by phosphorylation of alpha-synuclein at Y39 by c-Abl.

## **V. PD-linked H50Q and G51D mutations have disparate effects on alpha-synuclein structure and interactions**

### **V.a. Introduction**

Throughout the study of alpha-synuclein, PD-linked point mutations have been discovered and used to propose and test potential mechanisms of alpha-synuclein pathology. However, unifying mechanisms among all PD-linked point mutations have been hard to come by, leading some to conclude that the mutants cause PD via diverse pathways (Table 5.1). The first two mutations discovered were A53T [11] and A30P [10]. From the beginning, the effects of these two mutations on alpha-synuclein were found to be different: the A30P mutation decreased the rate of mature amyloid fibril formation while A53T increased this rate. More relevant to the work described here, A30P decreased alpha-synuclein binding to crudely purified synaptic vesicles in a co-floitation assay while A53T did not [39]. This finding ruled out impairment of membrane binding as a common mechanism of alpha-synuclein pathology in PD, although altered membrane interactions remain as a hypothesis for alpha-synuclein dysfunction.

**Table 5.1: Summary of biophysical effects of alpha-synuclein mutations A30P, E46K, and A53T.**

Mutation	Lipid Binding	Helicity	Transient Contacts	Fibril Formation	Partly-Bound State Proportion
A53T	No effect	Decrease	No effect	Increase	Increase
A30P	Decrease	Decrease	No effect	Decrease	Increase
E46K	Increase	Increase	Increase	Increase	No effect

After the disordered state of alpha-synuclein was shown to have helical propensity, the effect of PD point mutations on this latent secondary structure was posited to mediate alpha-synuclein pathogenicity, since the A30P and (to a lesser degree) A53T mutations were shown to decrease this helical propensity [43]. The discovery of the E46K mutation [13] afforded an opportunity to test the early hypotheses. Unlike A30P, the E46K mutation was shown to increase alpha-synuclein binding to lipid membranes [50], and unlike both A30P and A53T, E46K alpha-synuclein displays slightly increased local helical propensity [228]. Thus, the effects of the three PD-linked mutations on both alpha-synuclein lipid binding and helical propensity are variable.

Another hypothesized common property of alpha-synuclein mutants was impaired transient long-range intramolecular contacts. Originally, these contacts were thought to be lost in A30P and A53T alpha-synuclein [48,49] and were thus proposed to be protective against aggregation. However, the E46K mutation was shown to enhance these contacts [44]. Additionally, the effect of A30P and A53T on the intramolecular contacts was not able to be replicated. As a result, another potential commonality of the PD-linked mutants was discarded. As mentioned above, the PD-linked mutations do not even affect alpha-synuclein fibrillization rate in the same way. The A53T and E46K mutations were shown to increase the rate of fibril formation while A30P decreases it [50,51].

A more recently proposed common mechanism involves the relative populations of different conformations of alpha-synuclein on

lipid vesicles. The population of N-terminal partially-bound states was found to be higher for the A30P and A53T mutants, relative to fully-bound states, while the absolute population of the partially-bound states was increased by the E46K mutation [92]. These findings suggest that a more subtle perturbation of alpha-synuclein binding to lipids may be the common thread among the PD-linked mutations. The effects of these three mutations on different structural properties of alpha-synuclein are summarized in Table 5.1.

Recently, two newly-discovered mutations in alpha-synuclein have come to the forefront: H50Q, identified in patients with late-onset PD [12,166], and G51D, identified in patients with early-onset PD and multiple system atrophy [9,167]. Interestingly, both of these mutations localize near to two of the previously characterized PD-associated mutations, E46K and A53T, potentially implicating this region in the pathogenic role of alpha-synuclein [273]. The discovery of these two mutations allows previously proposed hypotheses regarding the roles of disease-linked mutations in alpha-synuclein dysfunction to be tested.

## **V.b. Methods**

*Protein Samples* – The mutant alpha-synuclein proteins were produced as described in section II.a.

*Basic NMR Experiments* – Backbone assignments were transferred from those previously determined for the wild-type [42,71]

by using high-resolution HNCA experiments, which also provided alpha-carbon chemical shifts for secondary structure analysis (see section II.f). Amide chemical shift deviations derived from  $^1\text{H},^{15}\text{N}$ -HSQC experiments were used to monitor the effects of mutations (see section II.c). The effect of H50Q and G51D on the broken-helix state of alpha-synuclein was assessed at 40 mM SDS, a concentration at which the detergent is expected to form spheroidal micelles [225,226]. Again, secondary structure information was derived from HNCA experiments. Intramolecular contacts in the free state of H50Q alpha-synuclein were assessed using PRE experiments. Paramagnetic spin-labels were covalently linked to cysteine residues introduced by mutagenesis at position 20. For more details on the preparation of samples and execution of PRE experiments, see section II.h. Binding to lipid vesicles was measured by decrease of amide cross-peak intensity in  $^1\text{H},^{15}\text{N}$ -HSQC spectra in the presence of lipid vesicles as detailed in section II.d. Protein concentration was  $\sim 140 \mu\text{M}$ , as determined by SDS-PAGE comparison with BSA stocks, and lipid concentration was 3 mM.

*Metal Binding Experiments* – Binding of  $\text{Cu}^{2+}$  and of  $\text{Fe}^{3+}$  and  $\text{Zn}^{2+}$  were assessed in two different ways. Since paramagnetic copper(II) ions lead to loss of NMR signal from nuclei in their vicinity, binding to  $\text{Cu}^{2+}$  was measured by decrease of amide cross-peak intensity in  $^1\text{H},^{15}\text{N}$ -HSQC spectra of  $\sim 140 \mu\text{M}$  H50Q alpha-synuclein in the presence of 280  $\mu\text{M}$   $\text{CuCl}_2$  and compared to wild-type data previously collected in the lab [274]. Binding to the diamagnetic iron(III) and zinc(II) was assessed by amide chemical shift deviations derived from  $^1\text{H},^{15}\text{N}$ -

HSQC experiments on ~140  $\mu\text{M}$  wild-type and H50Q alpha-synuclein in the absence and presence of 1 mM  $\text{FeCl}_3$  and 1 mM  $\text{ZnSO}_4$ .

### **V.c. Results Overview**

*H50Q mutation does not perturb free or lipid-bound state of alpha-synuclein* – The effect of the H50Q mutation on the disordered state of alpha-synuclein in aqueous buffer is quite small, with amide chemical shift perturbations limited to the immediate vicinity ( $\pm 5$  residues) of the mutation site (Figure 5.1A). The mutation also does not significantly affect either the secondary structure or the transient intramolecular contacts within alpha-synuclein in aqueous buffer (Figure 5.1B,C). Due to the location of the mutation site in the middle of the lipid-binding domain, the mutation might be expected to affect binding to membranes and membrane mimics. Substitution of a glutamine for the histidine at position 50 results in significant amide chemical shift differences extending up to 10 residues N- and C-terminal to the site of mutation in the micelle-bound state, suggesting potential effects on secondary structure (Figure 5.2A). However, the secondary structure, as measured by alpha-carbon secondary shifts, is nearly unperturbed by the mutation (Figure 5.2B), suggesting that the extent of amide chemical shift changes is mostly due to the compact nature of the micelle-bound state. Additionally, the wild-type and mutant protein bind to the same extent to SUVs composed of 15%

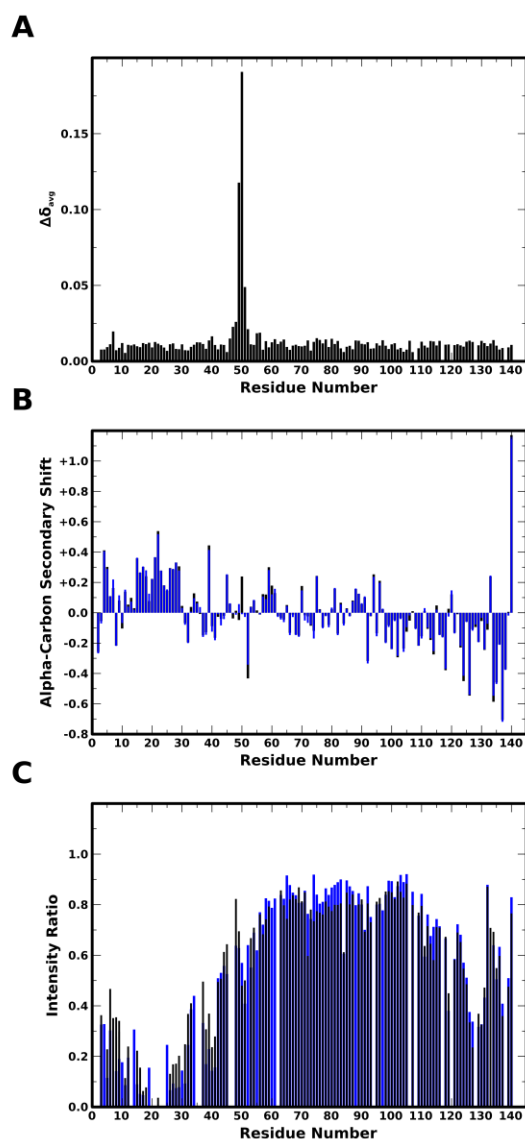


**Figure 5.1: Amide chemical shift difference, alpha-carbon secondary shifts, and intramolecular contacts for wild-type and H50Q alpha-synuclein in aqueous buffer.** (A) Plot of amide chemical shift differences (equation 1) between wild-type and H50Q alpha-synuclein in aqueous buffer *versus* residue number. (B) Plot of alpha-carbon secondary shifts *versus* residue number for wild-type (black) and H50Q alpha-synuclein (blue) in aqueous buffer. (C) Plot of the ratio of peak intensity for samples paramagnetically labeled at E20C to peak intensity in unlabeled samples *versus* residue number for wild-type (black) and H50Q alpha-synuclein (blue) in aqueous buffer.

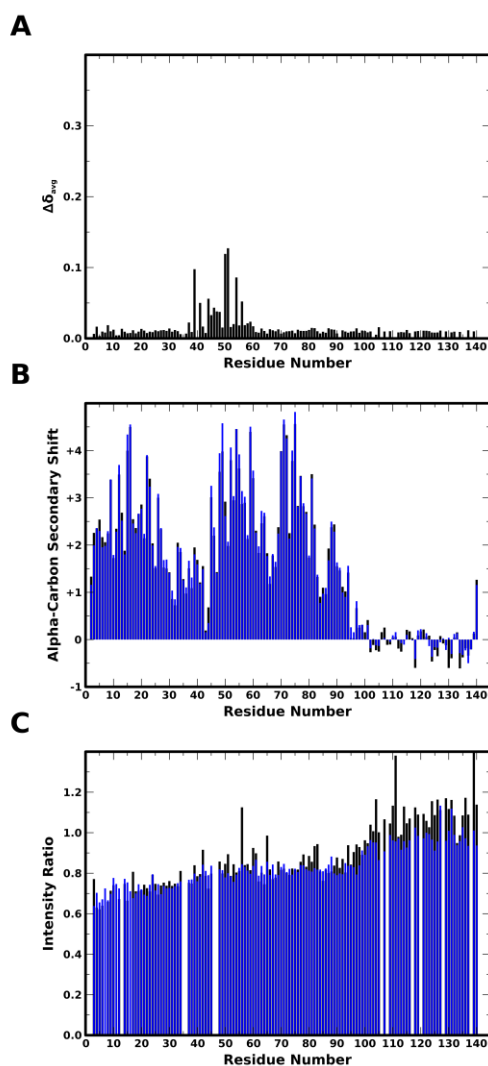


**Figure 5.2: Amide chemical shift difference and alpha-carbon secondary shifts in the presence of SDS micelles, and binding to low negative charge SUVs, for wild-type and H50Q alpha-synuclein.**

(A) Plot of amide chemical shift differences (equation 1) between wild-type and H50Q alpha-synuclein in 40 mM SDS *versus* residue number. (B) Plot of alpha-carbon secondary shifts *versus* residue number for wild-type (black) and H50Q alpha-synuclein (blue) in 40 mM SDS. (C) Plot of the ratio of peak intensity in the presence of 3 mM 15% PS SUVs to peak intensity in the absence of vesicles *versus* residue number for wild-type (black) and H50Q alpha-synuclein (blue). Bound fractions of total binding, fully-helical binding, and partly-helical binding are shown in Table 5.2.

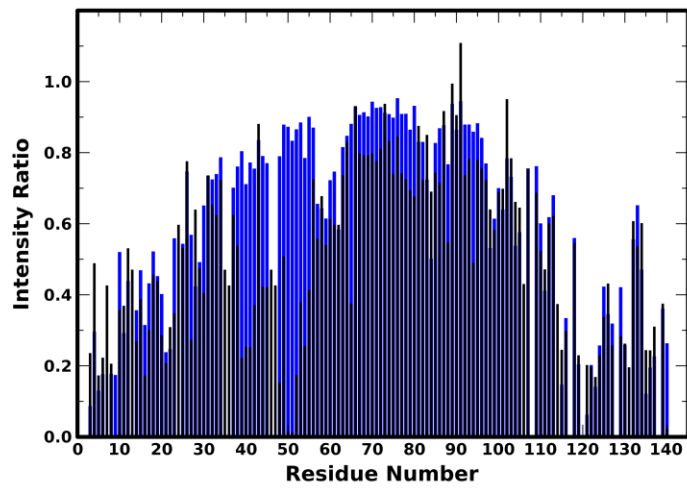
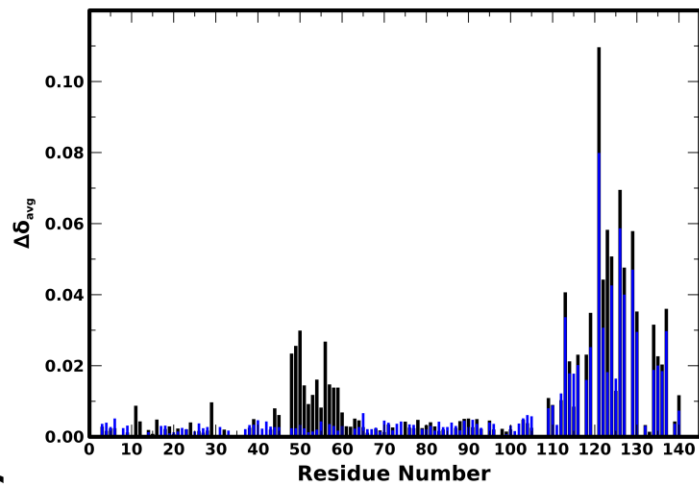
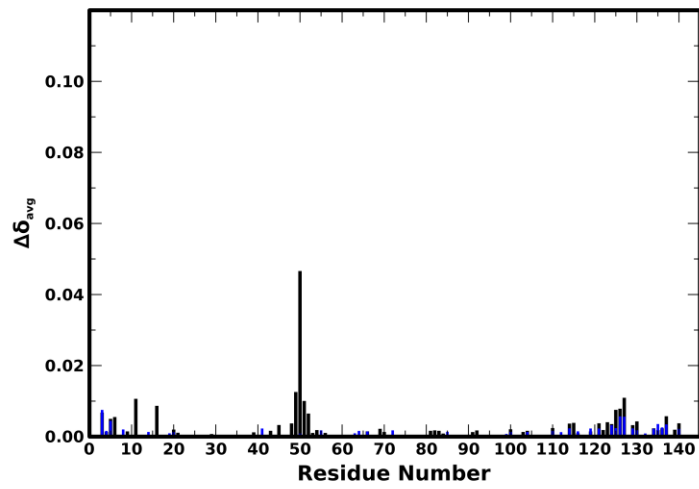
DOPS, 60% DOPC, 25% DOPE (Figure 5.2C; Table 5.2), although the H50Q alpha-synuclein displays slightly less fully-bound protein and slightly more partly-bound protein. These data strongly suggest that the H50Q mutation does not significantly perturb membrane- and micelle-binding of alpha-synuclein.

**Table 5.2: Bound fractions of different populations of wild-type and PD-mutant alpha-synuclein in the presence of low negative charge SUVs.** Bound populations were calculated according to Bodner, et. al., which also provided starred data for wild-type, A30P, E46K, and A53T [92].

Protein	Total Bound Population	Partly-Bound Population	Fully-Bound Population	Partly- to Fully-Bound Ratio
WT	0.378 ± 0.065	0.122 ± 0.115	0.256 ± 0.050	0.48
H50Q	0.313 ± 0.050	0.142 ± 0.104	0.171 ± 0.054	0.83
G51D	0.383 ± 0.068	0.279 ± 0.126	0.103 ± 0.058	2.70
WT*	0.63	0.21	0.43	0.49
A30P*	0.54	0.30	0.25	1.20
E46K*	0.81	0.26	0.53	0.49
A53T*	0.58	0.24	0.33	0.73

*H50Q mutation alters metal binding only at position 50* – The histidine at position 50 is a coordination site for various metal ions, such as copper (II) [274]. Thus, loss of the histidine side-chain would be expected to locally abrogate alpha-synuclein binding to metal ions. Binding of alpha-synuclein to copper (II) was assayed by incubating alpha-synuclein with varying concentrations of CuCl<sub>2</sub> and measuring amide-cross peak intensity loss due to the presence of the paramagnetic copper ions. Wild-type and mutant alpha-synuclein bound copper to the same extent and at the same binding sites, except for the expected loss of the binding site at position 50 (Figure 5.3A).

**Figure 5.3: Binding of wild-type and H50Q alpha-synuclein to copper(II), zinc(II), and iron(III).** (A) Plot of the ratio of peak intensity in the presence of 2:1  $\text{CuCl}_2$  to peak intensity in the absence of vesicles *versus* residue number for wild-type (black, [274]) and H50Q (blue) alpha-synuclein. (B,C) Plot of amide chemical shift differences (equation 1) in the presence of 1 mM  $\text{ZnSO}_4$  (B) and  $\text{FeCl}_3$  (C) *versus* residue number for wild-type (black) and H50Q (blue) alpha-synuclein.

**A****B****C**

While there was also loss of the partial binding at two sites near residues 40 and 80, other major binding sites in the C- and N-terminal regions were unaffected, confirming a general lack of cooperativity in copper (II) binding by alpha-synuclein. Binding to zinc (II) and iron (III) was assayed by the amide chemical shift changes in the presence of metal ions due to their diamagnetic nature. Again, the binding site at position 50 was lost in the mutant but binding sites in the C-terminus were unaffected (Figure 5.3B,C). Thus, the H50Q mutation mostly affects alpha-synuclein coordination of metal ions at the mutation site.

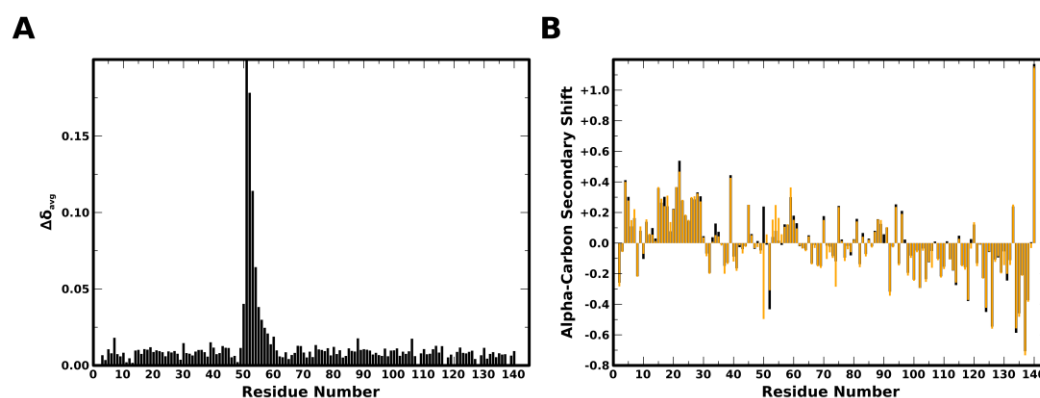


**Figure 5.4: Amide chemical shift difference and alpha-carbon secondary shifts for wild-type and G51D alpha-synuclein in aqueous buffer.** (A) Plot of amide chemical shift differences (equation 1) between wild-type and G51D alpha-synuclein in aqueous buffer *versus* residue number. (B) Plot of alpha-carbon secondary shifts *versus* residue number for wild-type (black) and G51D alpha-synuclein (orange) in aqueous buffer.

*G51D mutation does not alter free state but disrupts lipid binding*

– Like the H50Q mutation, the effect of this mutation on the disordered state of alpha-synuclein in aqueous buffer is limited to the immediate vicinity ( $\pm 5$  residues) of the mutation site (Figure 5.4A).

While the mutation does perturb the alpha-carbon chemical shifts in the same small region, there is no concerted loss or gain of secondary structure, and the conformation remains disordered (Figure 5.4B).

Unlike the H50Q mutation, which is somewhat conservative, the introduction of a negatively-charged aspartate side-chain into the N-terminal domain is likely to disrupt its interaction with negatively-charged phospholipids and detergent micelles, similar to introduction of a phosphate group at Y39 (see section IV.c). A comparison of the  $^1\text{H}$ ,  $^{15}\text{N}$ -HSQC spectra of wild-type and G51D alpha-synuclein in the presence of spheroidal SDS micelles does reveal a large effect of the amino acid substitution, resulting in amide chemical shift changes that extend from approximately residue 40 to residue 60 (Figure 5.5A). While the extent of the effects throughout the peptide chain is comparable to that seen for H50Q, the magnitude of the peak shifts is about 2 times greater, even when disregarding the necessarily large peak shift upon mutation from glycine to aspartate. Unlike the situation for H50Q, the amide chemical shift changes for alpha-synuclein G51D in the presence of micelles are accompanied by significant alpha-carbon secondary shift changes indicating a decrease in helicity from residue 45 to 55, as well as slightly increased helicity at residues 30-40 and 60-65 (Figure 5.5B). While the loss of helical structure near the mutation site is expected due to the likely electrostatic repulsion between the aspartate and micelle surface, the other, long-range effects on secondary structure are not expected. Although the magnitude of the differences is small, the continuous stretches of increased helicity in the mutant strongly suggest a real

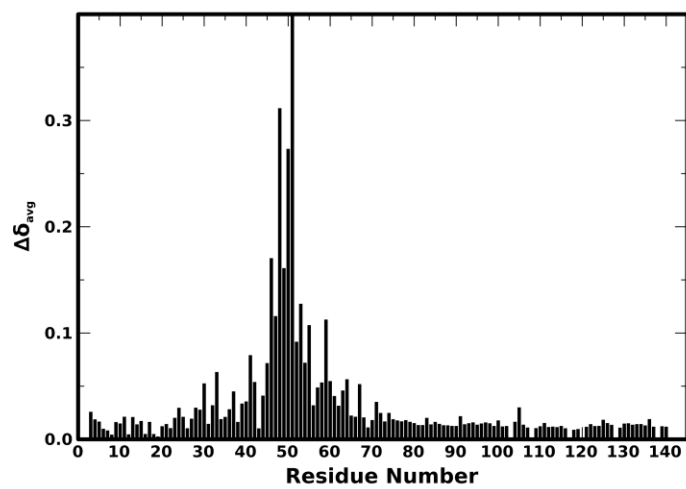
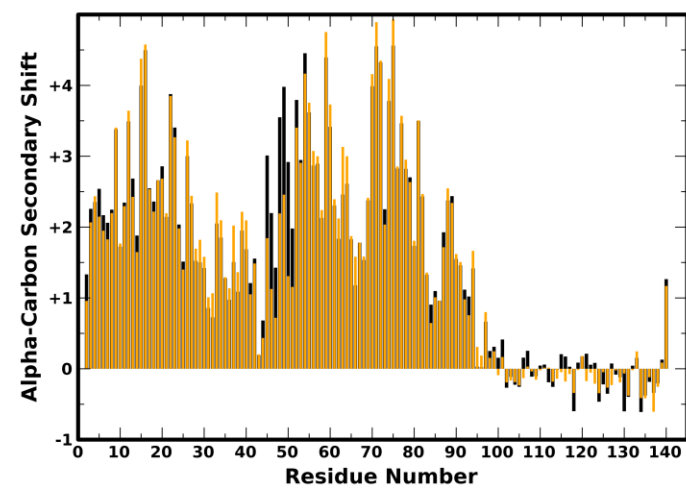
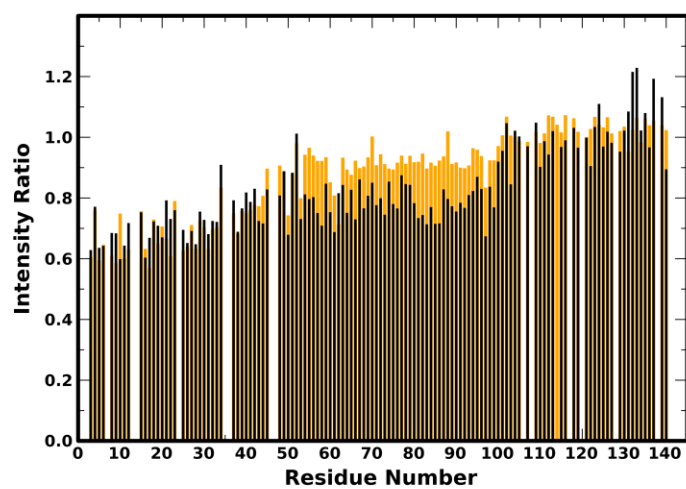
**Figure 5.5: Amide chemical shift difference and alpha-carbon secondary shifts in the presence of SDS micelles, and binding to low negative charge SUVs, for wild-type and G51D alpha-synuclein.**

(A) Plot of amide chemical shift differences (equation 1) between wild-type and G51D alpha-synuclein in 40 mM SDS *versus* residue number.

(B) Plot of alpha-carbon secondary shifts *versus* residue number for wild-type (black) and G51D alpha-synuclein (orange) in 40 mM SDS.

(C) Plot of the ratio of peak intensity in the presence of 3 mM 15% PS SUVs to peak intensity in the absence of vesicles *versus* residue number for wild-type (black) and G51D alpha-synuclein (orange).

Bound fractions of total binding, fully-helical binding, and partly-helical binding are shown in Table 5.2.

**A****B****C**

effect. Possibly, the structure of alpha-synuclein on the micelle is rearranged slightly to compensate for the loss of binding at the mutation site.

The G51D mutation also greatly perturbs alpha-synuclein binding to negatively-charged lipid vesicles. In the presence of SUVs composed of 15% DOPS, 60% DOPC, 25% DOPE, binding at the mutation site is abrogated in the mutant, as well as in the lipid-binding domain C-terminal to the mutation site (Figure 5.5C). This binding profile is qualitatively similar to that seen for pY39 and Y39E alpha-synuclein (Figures 4.12 and 4.13), suggesting that insertion of a negative charge stops helix binding and propagation at the insertion site and illustrating that different regions of the lipid-binding domain can bind as separate modules. In fact, while the total amount of vesicle-bound alpha-synuclein is quite similar to the wild-type protein, the relative partly-bound population is greatly increased and fully-bound population greatly decreased, resulting in a very high ratio of partly- to fully-bound populations of alpha-synuclein (2.70 *versus* 0.49 for wild-type) (Table 5.2).

*PD-linked mutations do not affect compactness of alpha-synuclein*  
– The effect of four of the five currently identified PD-linked mutations (A30P, E46K, H50Q, A53T) on alpha-synuclein compactness in aqueous buffer was determined by measuring the diffusion coefficient of the protein in D<sub>2</sub>O and calculating the radius of hydration (see section II.j). The calculated radius of hydration did not vary significantly between the mutant and wild-type proteins (~24-25 Å) (Table 5.3).

**Table 5.3: Hydrodynamic radii and diffusion coefficients for wild-type alpha-synuclein and PD-linked mutants in D<sub>2</sub>O.** Diffusion coefficients were extracted by fitting PFG experiments to equation 7, and hydrodynamic radii calculated relative to the known radius of dioxane.

Protein	D <sub>dioxane</sub> (cm <sup>2</sup> /sec)	D <sub>prot</sub> (cm <sup>2</sup> /sec)	R <sub>H,prot</sub> (Å)
WT	7.97 x 10 <sup>-10</sup>	6.69 x 10 <sup>-11</sup>	25.3
A30P	7.76 x 10 <sup>-10</sup>	6.78 x 10 <sup>-11</sup>	24.3
E46K	8.02 x 10 <sup>-10</sup>	6.92 x 10 <sup>-11</sup>	24.6
H50Q	7.98 x 10 <sup>-10</sup>	6.65 x 10 <sup>-11</sup>	25.4
A53T	7.83 x 10 <sup>-10</sup>	6.65 x 10 <sup>-11</sup>	25.0

#### V.d. Potential role of H50Q mutation

The H50Q mutation, which was identified in late-onset PD patients [12,166], does not have a major impact on the structural properties of alpha-synuclein. The disordered conformation alpha-synuclein adopts in dilute aqueous buffer is not significantly perturbed by the presence of the H50Q mutation, nor is the helical conformation of alpha-synuclein when bound to SDS micelles. As histidine 50 is a major metal ion-chelating site, the mutation of histidine to glutamine results in loss of metal binding [Cu(II), Zn(II) and Fe(III)] at that site, and potentially perturbs Cu(II) binding at nearby sites. However, major metal ion chelation sites near the N- and C-termini are unaffected by the H50Q mutation. Additionally, alpha-synuclein binding to 15% PS SUVs is largely the same in the presence and absence of the H50Q mutation; however, there is a small effect on the ratio of partly- to fully-bound alpha-synuclein states that could

play a role in PD pathology. Overall, the H50Q mutation seems fairly conservative in terms of its structural consequences, which may be related to the later onset of the disease it is associated with.

### **V.e. Effect of G51D mutation on lipid vesicle binding**

In contrast, the G51D mutation has a larger effect on alpha-synuclein interactions with membrane surfaces. While the mutation does not significantly perturb the disordered conformation of alpha-synuclein in dilute aqueous buffer, the SDS-bound conformation is altered. The substitution of a negatively-charged aspartate for a glycine residue results in loss of helical structure around the site of the mutation, likely due to repulsion of the N-terminal ~5 residues of helix-2 from the negatively-charged micelle surface. In addition, regions N- and C-terminal to the area of decreased helicity show slightly increased alpha-carbon secondary shifts, suggesting that the secondary structure is affected as the protein (and potentially micelle) rearranges to accommodate the disruption in the structure of helix-2. In the presence of 15% PS SUVs, the effect of the G51D mutation is even more pronounced, with disruption of binding occurring at the site of mutation but persisting throughout the helix-2 region. The binding profile (Figure 5.5C) clearly demonstrates that helix-2 can bind or release as a module, with a relatively constant intensity decrease or increase, corresponding to fraction of protein molecules that are

bound, throughout. Meanwhile, binding N-terminal to the mutation site is not affected.

While the N-terminus of alpha-synuclein G51D binds normally to the vesicle surface and helix propagation continues through the linker region, the presence of the negatively-charged aspartate residue at the beginning of helix-2 brings the extension of the helix to a premature end. Interestingly, the more C-terminal parts of helix-2 do not bind to membrane surface, suggesting that the entire helix-2 binds or does not bind in a concerted fashion. The binding profile is very similar to that seen for phosphorylation at Y39 and the Y39E mutation (section IV.c), although the point of perturbation (position 51) is at the beginning of helix-2 rather than at the beginning of the linker region (position 39). Nevertheless, these two binding perturbations (both caused by insertion of negative charge) both decouple helix-1 and helix-2 binding to lipid vesicles.

#### **V.f. Comparison of G51D effects to other mutations and modifications**

In its effect on alpha-synuclein-membrane interactions, the G51D mutation is qualitatively similar to the A30P mutation. The A30P alpha-synuclein shows a similar binding profile to SUVs, although the break in binding occurs at a different position (due to the different mutation site). In both cases, the mutations severely abrogate membrane binding and increase the proportion of partly-helical

conformations of alpha-synuclein on the vesicle surface (Table 5.2). In the study by Bodner, et. al., the A30P and A53T mutations were found to increase this proportion despite having different effects on overall vesicle binding, leading to the hypothesis that promoting the existence of the partly-helical states is a common thread among PD-linked mutants ([92] and Table 5.2). While the E46K mutation did not change the ratio of partly-helical to fully-helical states, the overall increased binding results in a higher absolute population of partly-helical states. The two mutants examined here, H50Q and G51D, both increase the ratio of partly- to fully-helical states on lipid vesicles, though the effect of G51D is much more pronounced. In this way, G51D acts very similarly to A30P, while H50Q is more similar to A53T in having a moderate effect on the relative population of partly-helical states. In cells, G51D alpha-synuclein shows decreased membrane association, suggesting that the *in vitro* findings of impaired vesicle binding also apply in cells [275]). Due to the mild effects on alpha-synuclein structure, the pathogenic effects of H50Q are thus more likely to be mediated by its altered metal-binding, enhanced secretion, or extracellular toxicity [276].

One interesting structural observation is the flatness of the binding profile C-terminal to perturbations by G51D, pY39/Y39E, and A30P (Figure 5.5C, Figure 4.12B, Figure 4.13B,[92]). Despite the different nature of the binding perturbations, in all cases the helix propagation/binding is stopped before the entire helical domain (~100 residues) is bound. In the case of wild-type alpha-synuclein, the binding profile for this domain shows either monotonic or stepped

increase in signal intensity (decrease in binding) in the C-terminal direction. This can be interpreted as a superposition of signals from alpha-synuclein molecules with successively longer helices bound, with a greater number of shorter helices and fewer longer helices. This reflects a distribution of alpha-synuclein molecules with different lengths of folded/bound helix; for example, there are many molecules in which residues 1-9 form a helix, fewer in which residues 1-12 form a helix, etc. This suggests that folding of the alpha-synuclein helices and the concomitant binding to the membrane surface proceeds by propagation towards the C-terminus from a nucleation or anchor site at the N-terminus, with increasingly longer helical conformations more scarce. However, after loss of binding at any point in the middle of this region (residue 30, 39, or 51), the profile is quite flat, likely resulting from a superposition of two populations: one in which the entire C-terminal part is free and one in which it is bound. Since the peptide chain does not resume folding/binding C-terminal to the perturbation site, it appears that propagation from the anchoring N-terminus is necessary for the binding of the rest of the helical region.

## **VI. Conclusions and future directions**

While many post-translational modifications and point mutations result in small changes of chemical groups and local physicochemical properties on a protein molecule, their effects on protein function can be great. This is the case for alpha-synuclein, specifically for two of the modifications studied here, N-terminal acetylation and phosphorylation on residue tyrosine 39. Both modifications have their most pronounced effects on the binding of alpha-synuclein to lipid membranes, which is considered to be an essential part of its as of yet poorly-defined native function. As a result, these modifications are likely to play an important role in the normal function as well as possibly in the dysfunction of alpha-synuclein in the brain.

### **VI.a. Effects of N-terminal acetylation and tyrosine phosphorylation**

The major effect of N-terminal acetylation is to promote or stabilize helical states at the N-terminus of alpha-synuclein, likely via N-terminal helix capping. This stabilization results in tighter binding to more curved, less negatively-charged vesicles in *in vitro* assays when compared with the unmodified recombinant protein. This result constitutes an important contribution to a more complete understanding of alpha-synuclein function since physiological alpha-

synuclein protein is N-terminally acetylated, and its putative binding target, synaptic vesicles, are small, highly-curved vesicles with a comparable proportion of negatively-charged phospholipids. Furthermore, for N-terminally acetylated alpha-synuclein, it appears that electrostatic attraction may not play as large a role in lipid membrane binding in the cell as previously thought on the basis of work with the unmodified protein. Additionally, the increased affinity of acetylated alpha-synuclein for less charged surfaces allowed for the identification and direct observation of a never-before-seen partly-helical state of alpha-synuclein in the presence of BOG micelles, which may mimic partly-helical states that are thought to exist on vesicles *in vivo* and be involved in aggregation.

The effects of phosphorylation at Y39 are more complex, with apparently divergent results in the presence of SDS micelles, a common NMR-friendly model for membranes, compared with those obtained in the presence of more physiologically-relevant synthetic lipid vesicles. On SDS micelles, Y39 phosphorylation potentially increases local helical character in the linker between the two helices of the broken-helix state, yet without driving the protein into a fully stable extended-helix state. On lipid vesicles, the addition of a phosphate group leads to decreased binding of the entire helix-2 domain to the vesicle surface, which may allow alpha-synuclein to bind two different membrane surfaces and bridge two apposed membranes. The PD-linked G51D mutation has a similar phenotype in the presence of negatively-charged lipid vesicles, suggesting that these two modifications may also promote the existence of potentially

pathogenic partly-helical states. In addition, these two modifications demonstrate that membrane binding by helix-1 and helix-2 can be decoupled.

### **VI.b. Insights into the normal function of alpha-synuclein**

What is the native function of alpha-synuclein (and other synucleins)? Why have vertebrates evolved this small, soluble protein that binds lipid membranes reversibly in their nervous systems? Many organisms, including *C. elegans* and *D. melanogaster*, have perfectly well-functioning nervous systems without any synucleins at all. It is thus difficult to implicate synuclein as a core member of the synaptic transmission machinery. However, it is reasonable to assume that some unique aspect of the vertebrate nervous system needs synucleins for optimal function. Alternatively, alpha-synuclein may be an accessory protein that makes some aspect of synaptic transmission more efficient, making it useful in a system with much greater burden on the synapses.

What sort of function could this be? From the current literature on alpha-synuclein, it appears likely that its main function involves vesicle transport, and its localization at the synapse implicates synaptic vesicles as the target. Removal or overexpression of alpha-synuclein perturbs pools of vesicles that are docked or about to be released. These data, coupled with the unique antiparallel arrangement adopted by the amphipathic helices of alpha-synuclein

(at least when binding to detergent micelles), tantalizingly suggest that alpha-synuclein can serve to stabilize or sense the unique geometry of docked vesicles at the synapse [107]. This binding could also serve to localize alpha-synuclein to the vicinity of docked vesicles, where it can interact with another protein via its free C-terminal tail. There is no shortage of potential protein partners for alpha-synuclein in the literature. One proposed binding partner for alpha-synuclein is the v-SNARE synaptobrevin (see Appendix 2). Recent data from Südhof and coworkers suggest that alpha-synuclein binds to this protein through its C-terminal tail and somehow acts as a chaperone for the SNARE complex, preventing activity-dependent degradation [133,234]. Alternatively, alpha-synuclein could be altering the properties of the membranes it binds to and influencing exocytosis in that way.

While alpha-synuclein is heavily implicated in a neuronal function, not least because of its role in a neurodegenerative disorder, the protein is highly expressed in other cell types. For example, red blood cells have been shown to express significant amounts of alpha-synuclein [115,116]. This is a perplexing finding, as red blood cells are not likely to need a regulator or effector of membrane trafficking or fusion. One potentially interesting recent finding is that alpha-synuclein N-terminal methionine residues are readily oxidized by lipid hydroperoxides found in the membranes alpha-synuclein is bound to and just as readily reduced by methionine sulfoxide reductase [277]. This suggests a mechanism for alpha-synuclein to act as a “membrane reductase” that relieves potentially dangerous oxidative damage to membrane lipids as it cycles on and off the membrane. The dopamine

biosynthesis pathway active in the dopaminergic neurons of the *substantia nigra* results in a high burden of oxidative species [278] and elevated levels of lipid hydroperoxides have been found in PD brains [279]. Interestingly, red blood cells also contain an abundance of oxidative species that can oxidize the membrane lipids, as well as lack *de novo* lipid synthesis to replace damaged lipid molecules [280,281]. Thus, these cells could also benefit from a “membrane reductase” activity.

### **VI.c. Future directions**

These are but two of the possible functions of alpha-synuclein. Determining what alpha-synuclein does *in vivo* and which aspect of that function is disrupted in PD will take time and more research. Some of the findings presented here open up new avenues of research. For example, the detachment of helix-2 from the synaptic-vesicle-like SUVs examined here by pY39 and G51D leaves open the question of whether helix-2 can then bind to another lipid membrane with different properties. Thus, it would be beneficial to determine what type of membrane helix-2 can bind to with tight affinity, as well as to test more realistic synaptic-vesicle-like and plasma-membrane-like lipid compositions for alpha-synuclein binding preferences. For example, the effect of cholesterol and acyl chain length and saturation has been largely ignored in this work and has high relevance to synaptic lipid compositions. Additionally, the identification of Y39E as

a potential mimic of pY39 alpha-synuclein function allows for it to be studied in cells using standard molecular biology techniques. If the glutamate side-chain does not fully mimic the double negative charge of pY39, an L38D Y39E double-mutant may be employed. These alpha-synuclein mutants could be used to examine the effects of phosphorylation on alpha-synuclein localization in cells, as well as whether increasing the population of partly-helical states contributes to aggregation and toxicity in cells.

In addition, the effect of the PD-linked mutations on the structure and folding of the partly-helical state can now be examined at high resolution due to the discovery of the BOG-bound state. While many of the questions addressed herein are targeted toward understanding more about the murky native function of alpha-synuclein, the insights gained can be applied to studies of both function and dysfunction in disease. The study of alpha-synuclein can never truly focus on only one side of this equation. Discoveries in PD patients are constantly informing basic science research about synaptic vesicle exocytosis, and findings about the native function of alpha-synuclein can lead to ideas for novel therapeutic strategies for Parkinson's disease.

## APPENDICES

### **A1. Appendix 1: StARD4**

#### **1a. Introduction**

Different membrane compartments within the cell contain different and tightly controlled levels of sterols. For instance, the plasma membrane and endocytic recycling compartments contain ~30% cholesterol [282,283]. By contrast, the ER contains 5% cholesterol, although it is the site of cholesterol synthesis [284,285]. The cholesterol level in the ER is strictly maintained since the cell relies on sensing this level to regulate cholesterol synthesis through the SREBP pathway [284]. Thus, cholesterol transport between the ER and other organelles is crucial for myriad cell processes. This transport can take place through vesicular or non-vesicular means. There are many sterol-binding proteins, such as the OSBPs (oxysterol-binding proteins) [286] and START (StAR-related lipid transfer) domain proteins [287,288], which contribute to non-vesicular cholesterol transport.

The founding member of the START domain family is the steroidogenic acute regulatory protein (StAR), which was discovered in mouse Leydig cells and delivers cholesterol to the P450 side-chain cleavage enzyme localized to the inner membrane of mitochondria [289–291]. This delivery of cholesterol facilitates its conversion to

pregnenolone as a step in hormone biosynthesis. The StAR protein (also designated StARD1) contains a mitochondrial localization sequence prepended to a ~210 residue START domain, which is responsible for the cholesterol binding and transfer [291]. There are 15 START domain-containing proteins in mammalian genomes, grouped into nine families, depending on ligand-specificity (sterol, phospholipid, sphingolipid) and the identity of other fused domains [287]. As there are many START domain proteins, there is also an abundance of crystal structures of START domains available, although the majority of them are in an apo, ligand-free form [292–294]. The ligand-bound structures that do exist are all of proteins that bind phospho- or sphingolipids [295–297]; thus, no sterol-bound START domains structure exists. The structures that have been solved all show a compact  $\alpha/\beta$  helix/grip fold with a large (900–2000 Å<sup>3</sup>) hydrophobic cavity in which the various ligands bind. The size of the cavity is thought to correspond to the size of the native ligand of the protein [292].

StARD4, together with StARD5 and StARD6, is part of a subfamily of proteins that consist solely of a START domain. StARD4 was originally identified as a protein downregulated in the livers of mice fed a high-cholesterol diet, and later to be directly activated by SREBP-2 in response to lack of cholesterol [298,299]. StARD4 was shown, indirectly, to transport cholesterol within mammalian cells in a steroidogenesis assay [299]. Sterol transport between different lipid membranes by StARD4 was more directly observed in cells and *in vitro* using the fluorescent sterol DHE, suggesting that StARD4 functions as

a general cholesterol transfer protein whose activity is required for proper processing of cholesterol, specifically acetylation in the ER [300]. It seems likely that the cholesterol transport function of StARD4 can be compensated for, at least to some extent, by other cholesterol transport proteins, as StARD4 knockout in mice has only a mild phenotype, including slight weight decrease [301].

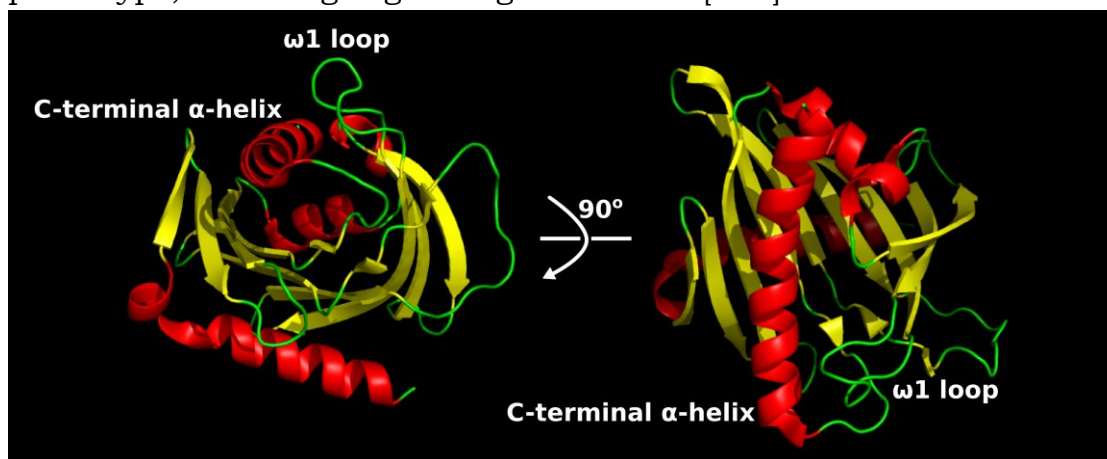


**Figure A1.1: Crystal structure of mouse StARD4.** Structure is visualized in PyMol from PDB entry 1JSS [293], with helices in red, sheets in yellow, and loops in green. The right view is looking down the putative ligand cavity from the C-terminal helix face.

These data suggest that StARD4 may play an important, though not essential, role in cholesterol homeostasis in cells and in whole organisms and may be a target in disease therapies. However, mechanistic data on the process of sterol uptake, binding, and transfer by StARD4 (or other START domain proteins) is limited. Early NMR studies on StAR showed some promise [302], but have not yielded any insights into sterol binding, although StARD5, which is highly related to StARD4, has been suggested to bind bile acids rather than sterols [303]. Additionally, a computational study of cholesterol-docking into

structures of apo-START-domain proteins delineated a potential mechanism of cholesterol entry/exit into the binding cavity, involving motion of the C-terminal  $\alpha$ -helix and  $\omega$ 1 loop [304] (Figure A1.1). With the thought that StARD4 may serve as a positive control for cholesterol-binding studies of alpha-synuclein, the mechanism of cholesterol binding and transfer by StARD4 was investigated by NMR spectroscopy.

## **1b. Methods**

*Protein Expression and Purification* – The cDNA for mouse StARD4 (Dr. Jan Breslow, Rockefeller University) was cloned into the pET-SUMO vector (Invitrogen/Life Technologies), and the L124D mutant was generated using a QuikChange Site-Directed Mutagenesis Kit (Agilent). The L124D mutation greatly improved the stability of the protein and the quality of three-dimensional NMR spectra, presumably by reducing intermolecular interactions or aggregation of the wild-type protein. The pET-SUMO vector contains an N-terminally-fused 6xHis-tagged yeast Smt3 SUMO protein that facilitates solubility, expression, and purification [305]. After purification using nickel affinity chromatography, the SUMO tag is efficiently cleaved using Ulp1 SUMO protease, which recognizes the SUMO fold rather than a specific cut site, eliminating unnecessary left-over linking residues. The SUMO tag and SUMO protease can then be removed by another round of nickel affinity chromatography.

To produce isotopically-labeled protein, transformed *E. coli* cells were grown in LB broth (4 L) until an OD of 0.6-1.0 was reached, then centrifuged at 6,000 rpm (6,900 x g) for 15 minutes at 24 °C and the pellet resuspended in 1 L “wash medium,” consisting of M9 minimal medium without carbon or nitrogen sources and containing appropriate antibiotics. The cell culture was then centrifuged again at 6,000 rpm (6,900 x g) for 15 minutes at 24 °C and the pellet resuspended in M9 minimal medium, supplemented with BME vitamins, the appropriate antibiotics, and either 1 g uniformly labeled <sup>15</sup>N ammonium chloride and 4 g natural abundance dextrose or 1 g <sup>15</sup>N ammonium chloride and 2 g <sup>13</sup>C glucose for <sup>15</sup>N-labeled protein or <sup>15</sup>N,<sup>13</sup>C-labeled protein, respectively. After recovery at 37 °C in minimal medium for 0.5-1 hr, protein expression was induced using ~1 mM IPTG and continued for 3-3.5 hr. A 1 mL sample was taken every 1 hr to check OD and saved to estimate protein expression using SDS-PAGE. Cells were harvested by centrifugation at 6,000 rpm (6,900 x g) for 15 minutes and the pellet stored at -20 °C.

Protein-containing cell pellets were resuspended in lysis buffer (350 mM NaCl, 20 mM tris pH 8, 20 mM imidazole, 1 mM PMSF, 0.2 mM EDTA, 2 mM DTT, 1.5 mM BME) and was subjected to sonication by a tip sonifier (Branson) for 2 x 6 minutes at a power setting of 6 with a duty cycle of 50%. The sample was stirred between the two applications of the sonifier. The lysed cell suspension was then subjected to ultracentrifugation at 40,000 rpm (145,000 x g) for 1 hr at 4 °C. A Ni-NTA column was equilibrated with 100 mL equilibration buffer (350 mM NaCl, 20 mM tris pH 8, 20 mM imidazole, 2 mM DTT,

1.5 mM BME), and the ultracentrifugation supernatant loaded onto the column. Equilibration buffer (50 mL) was applied to the column as a wash step, with 5 fractions collected, followed by elution with ~100 mL elution buffer (350 mM NaCl, 20 mM tris pH 8, 250 mM imidazole, 2 mM DTT, 1.5 mM BME). Approximately 75 mL of the eluate were collected, then dialyzed overnight against ~1 L cleavage buffer (150 mM NaCl, 20 mM tris pH 8, 1 mM DTT). The fusion protein was then incubated with 6xHis-tagged SUMO protease (~1:50 protease:protein) for 2 hr at 4 °C. The cleavage reaction mixture was passed over a Ni-NTA column pre-equilibrated with 100 mL equilibration buffer, with the StARD4-containing flowthrough being collected. The column was washed with 50 mL equilibration buffer and the 6xHis-tagged SUMO tag and SUMO protease eluted with ~100 mL elution buffer. The StARD4 protein was run on a Superose6 gel filtration column (GE Healthcare) as a final cleanup and buffer exchange step, using 20 mM NaCl, 20 mM tris, 5 mM DTT, pH 6.4 buffer (“StARD4 NMR buffer”). The low salt and low pH of the StARD4 NMR buffer increased the number of observable peaks in triple-resonance spectra. NMR experiments were usually carried out immediately after purification, else the protein was stored at 4 °C for no more than 1 week.

*Sample Preparation* – Large unilamellar lipid vesicles composed of 31% POPC, 23% POPE, 23% POPS, and 23% cholesterol were prepared for measuring membrane binding of StARD4 and to produce StARD4-sterol complexes. Cholesterol was sometimes replaced with DHE or a paramagnetic cholesterol analogue (3 $\beta$ -doxyl-5 $\alpha$ -cholestane) at the same molar ratio. All phospholipids and cholesterol were

purchased from Avanti Polar Lipids as chloroform solutions, while DHE was purchased from Sigma-Aldrich and spin-labeled cholestane was kindly provided by Dr. Boris Dzikovski (ACERT), as powder which was dissolved in 2:1 methanol:chloroform prior to use. LUVs were prepared by mixing the lipid solutions in the appropriate ratios, drying under nitrogen at 50 °C, followed by drying under vacuum for 2 hr. The dried lipid film was resuspended by pipetting up and down and vortexing in StARD4 NMR buffer. The suspension was frozen (in liquid nitrogen) and thawed (in room temperature water) 10 times, then passed 21 times through a 400 nm membrane and 21 times through a 100 nm membrane using an Avanti mini-extruder.

Final StARD4 samples for triple-resonance NMR experiments consisted of protein concentrated to between 0.5 to 1 mM protein, estimated by the absorbance at 280 nm (using an extinction coefficient of 51910 M<sup>-1</sup>\*cm<sup>-1</sup>). Lipid binding or sterol loading experiments were usually performed on samples containing ~50-100 μM StARD4 and the requisite lipid vesicles or cholesterol solubilized using 20 mM methyl-β-cyclodextrin or 5% v/v ethanol. Sterol or sterol analogue loading from liposomes was measured in the presence of non-excess amounts of liposomes or after removing liposomes by either ultracentrifugation or passage through a Superose6 gel filtration column, as indicated. All NMR samples were supplemented with 10% D<sub>2</sub>O. All NMR experiments were performed at 23 °C.

Backbone assignments for mouse StARD4 L124D were determined using the following experiments, all collected at 600 MHz with spectral widths of 20 and 30 ppm in the proton and nitrogen

dimensions: HNCO, with 68 points and 10 ppm in the carbon dimension; HNCA and HN(CO)CA, with 136 points and 25 ppm in the carbon dimension; and HBHA(CO)NH, with 128 points and 10.8 ppm in the indirect proton dimension. Additionally, two experiments were collected at 800 MHz with spectral widths of 12 and 30 ppm in the proton and nitrogen dimensions: HNCACB, with 76 points and 65 ppm in the carbon dimension, and HN(CO)CACB, with 64 points and 65 ppm in the carbon dimension. The amide proton and nitrogen, as well as alpha-carbon, assignments were transferred to wild-type StARD4 using an HNCA experiment with spectral widths of 16 and 30 ppm in the proton and nitrogen dimensions and 68 points and 25 ppm in the carbon dimension. Transverse relaxation ( $R_2$ ) rates were measured using a standard HSQC-based  $T_2$  pulse sequence with time delays of 0.01, 0.03, 0.05 (x3), 0.07, 0.09, and 0.11 sec for L124D and 0.01, 0.03 (x2), and 0.07 sec for wild-type StARD4.

### **1c. Results**

Of the 224 (213 non-proline) residues in mouse StARD4 L124D, backbone assignments were determined for 200 amide proton and nitrogen resonances, 217 alpha- and beta-carbon resonances, 200 carbonyl carbon resonances, and 194 alpha-proton resonances. This results in 90-95% coverage of the backbone, with many (10) of the unassigned residues, due to no or fragmentary observed resonance peaks, residing in the N-terminal 23 residues of the protein, which are

not resolved in the X-ray crystal structure [293], likely due to a highly labile conformation, and most of which are absent in the human homologue of the protein. Secondary structure elements were predicted by submitting the chemical shifts of all assigned resonances to TALOS+ [306] and agreed fairly well with those in the published crystal structure [293].

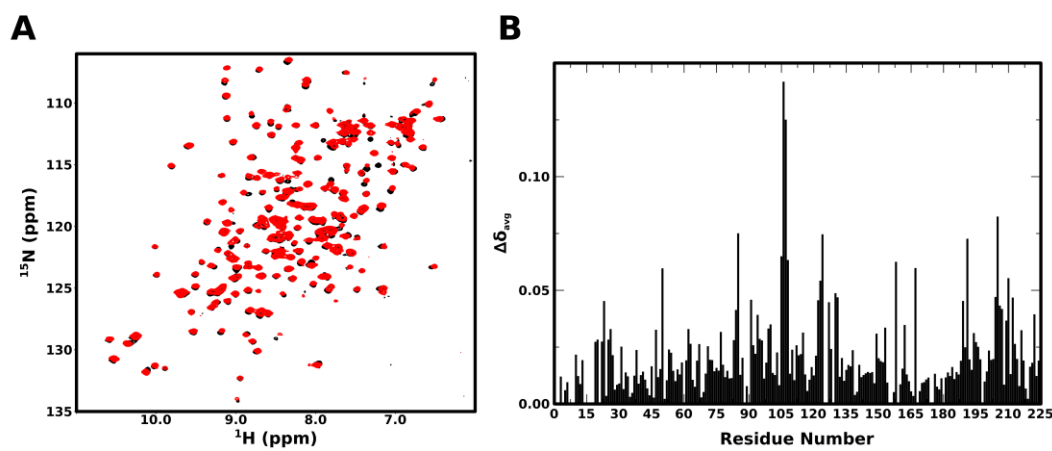


**Figure A1.2: HSQC spectra and amide chemical shift differences for wild-type and L124D StARD4.** (A)  $^1\text{H}$ ,  $^{15}\text{N}$ -HSQC spectra of wild-type (black) and L124D (red) StARD4 in aqueous buffer. (B) Plot of amide chemical shift differences (equation 1) between wild-type and L124D StARD4 *versus* residue number.

Amide proton and nitrogen, and alpha-carbon assignments were transferred to the wild-type protein using an HNCA experiment. The chemical shift differences between wild-type and L124D StARD4 localized regions around residues 80, 105, 120-130 (site of mutation), and 190-210 (Figure A1.2). These residues are all roughly found near the end of the ligand cavity capped by the C-terminal helix and  $\omega$ 1 loop, except for leucine 105, which is located on a different surface of the molecule. It is possible that Leu-105 is participating in the

intermolecular interactions mediated by Leu-124 and lost in the L124D mutant, since Leu-105 is a surface-accessible residue and flanked by aspartate and glutamate residues, which would be repulsed by the aspartate at position 124 in the mutant. Peak intensity for  $\omega 1$  loop residues and residues 205-210 were greatly decreased.

In addition to backbone chemical shift assignments, the relative motions of wild-type and mutant StARD4 on the picosecond-nanosecond time-scale were analyzed by measuring the  $R_2$  transverse relaxation rates of each protein on a per-residue basis, in the absence of ligand or liposomes. Consistent with the crystal structure of StARD4, which suggests a rigid molecule with no specific regions of high flexibility, the transverse relaxation rate was relatively constant throughout the protein, both wild-type and L124D. Somewhat surprisingly, the regions predicted to move to allow ligand uptake and transfer did not display increased mobility on this time-scale (Figure A1.3A). Instead, part of the  $\omega 1$  loop displayed increased rigidity in the wild-type protein, but not the L124D mutant (residues 110-125). In addition, residues 185-195 and 205-215 displayed increased rigidity in both protein variants. These regions (colored red in Figure A1.3B,C) form part of the ligand-binding cavity, and thus may contribute to its stability in the presence or absence of ligand. The region that did display slightly increased mobility in both proteins was around residues 100-110, which forms a  $\beta$ -strand that is on the surface of the protein. Additionally, the L124D protein shows increased flexibility around residues 90-100, which share the same surface of the protein molecule with the mutated  $\omega 1$  loop (Figure A1.3C, blue).

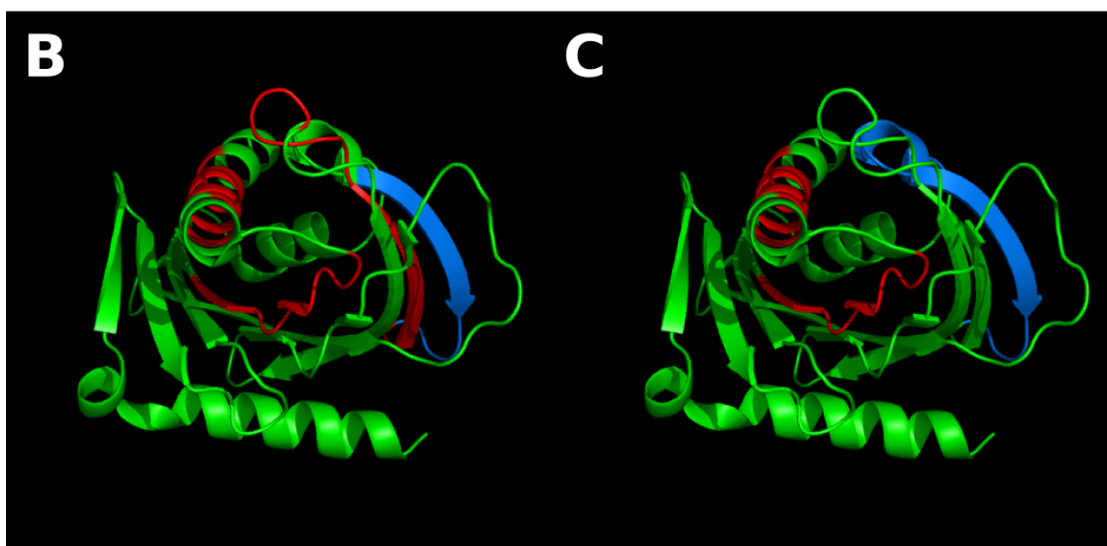
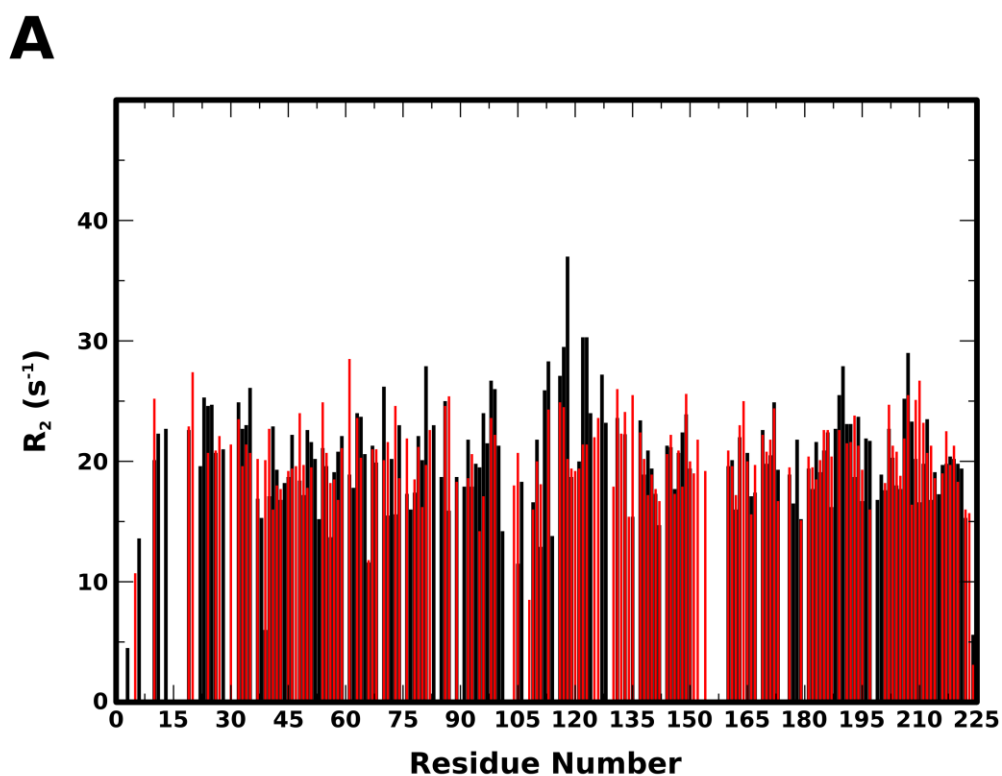


**Figure A1.3: Amide nitrogen  $R_2$  relaxation rates for apo wild-type and L124D StARD4.** (A) Plot of transverse relaxation rate  $R_2$  for wild-type (black) and L124D (red) StARD4 versus residue number. Crystal structure of StARD4 (1JSS) with approximate regions of rigidity (red) and flexibility (blue) for wild-type (B) and L124D (C) StARD4.

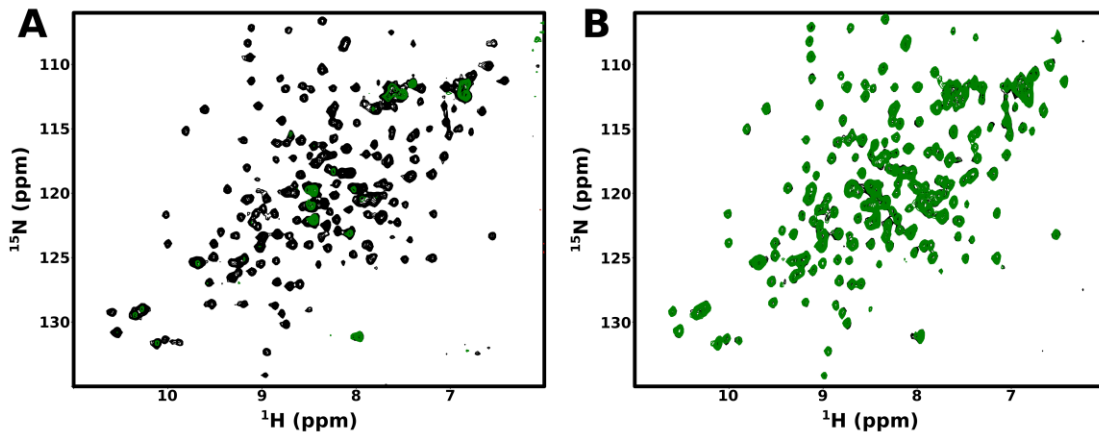


**Figure A1.4: HSQC spectra for wild-type and L124D StARD4 in the absence and presence of lipid vesicles.**  $^1\text{H},^{15}\text{N}$ -HSQC spectra of wild-type (A) and L124D (B) StARD4 in the absence (black) and presence (green) of 15 mM lipid vesicles composed of 31% POPC, 23% POPE, 23% POPS, and 23% cholesterol.

As a putative cholesterol transporter, StARD4 is expected to interact with lipid membranes within the cell at least transiently during ligand uptake and deposit. Both wild-type and L124D StARD4 were incubated with an excess of synthetic LUVs meant to mimic a cholesterol-rich donor membrane (31% POPC, 23% POPE, 23% POPS, and 23% cholesterol) [300]. The wild-type protein displayed drastically reduced amide cross-peak intensity in the presence of liposomes, likely due to the formation of slow-tumbling protein-liposome complexes (Figure A1.4A). Unlike the binding regime of alpha-synuclein, in which different regions of the protein display different intensity decreases due to nonuniform binding, the loss of peak intensity is relatively uniform throughout the StARD4 spectrum. This uniformity illustrates that StARD4 molecules bind to lipid vesicles as a whole, unlike alpha-synuclein, in which regions of the molecule that are not directly bound

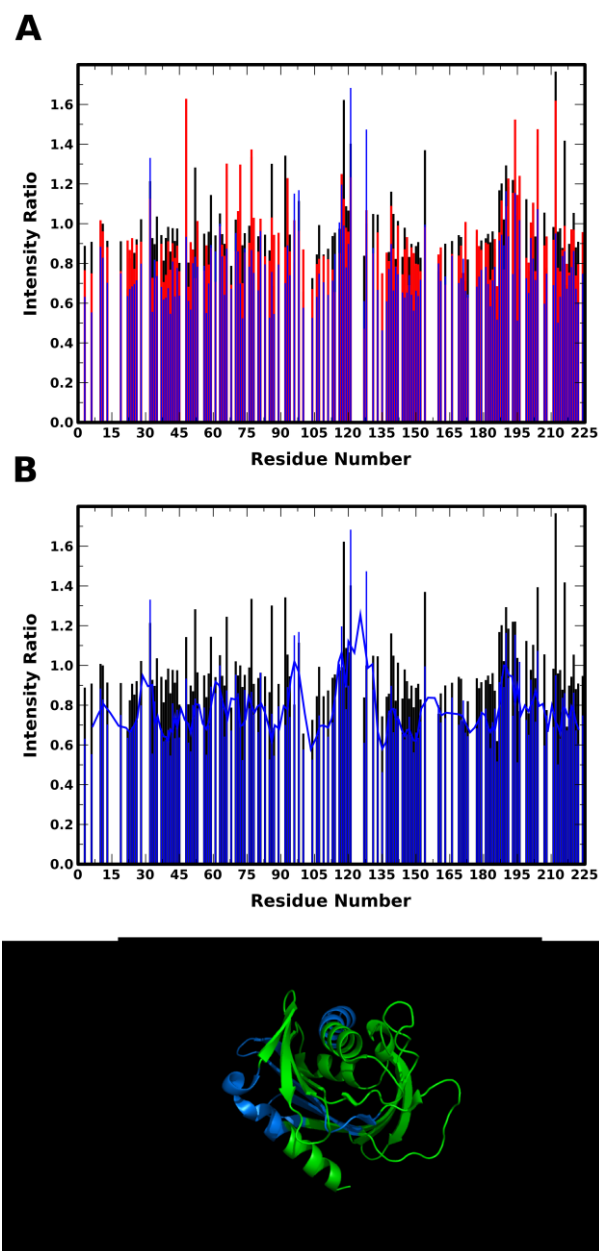


**Figure A1.5: PRE effect for wild-type StARD4 in the presence of increasing concentrations of doped lipid vesicles.** (A) Plot of the ratio of peak intensity in the presence of 0.5:1 (black), 1:1 (red), and 2:1 (blue) lipid vesicles doped with 5% 5-doxyI-stearate to peak intensity in the absence of vesicles for wild-type StARD4 *versus* residue number. (B) The 0.5:1 (black) and 2:1 (blue, with 3-residue average line) intensity ratios from panel A. (C) Crystal structure of StARD4 (1JSS) with approximate regions of PRE effect (blue).

retain their disordered character. Thus, no specific membrane-binding regions could be delineated by this approach. By contrast, the presence of lipid vesicles had no effect on the cross-peak intensity of L124D StARD4 spectra, showing that the mutant protein does not appreciably bind these liposomes (Figure A1.4B).

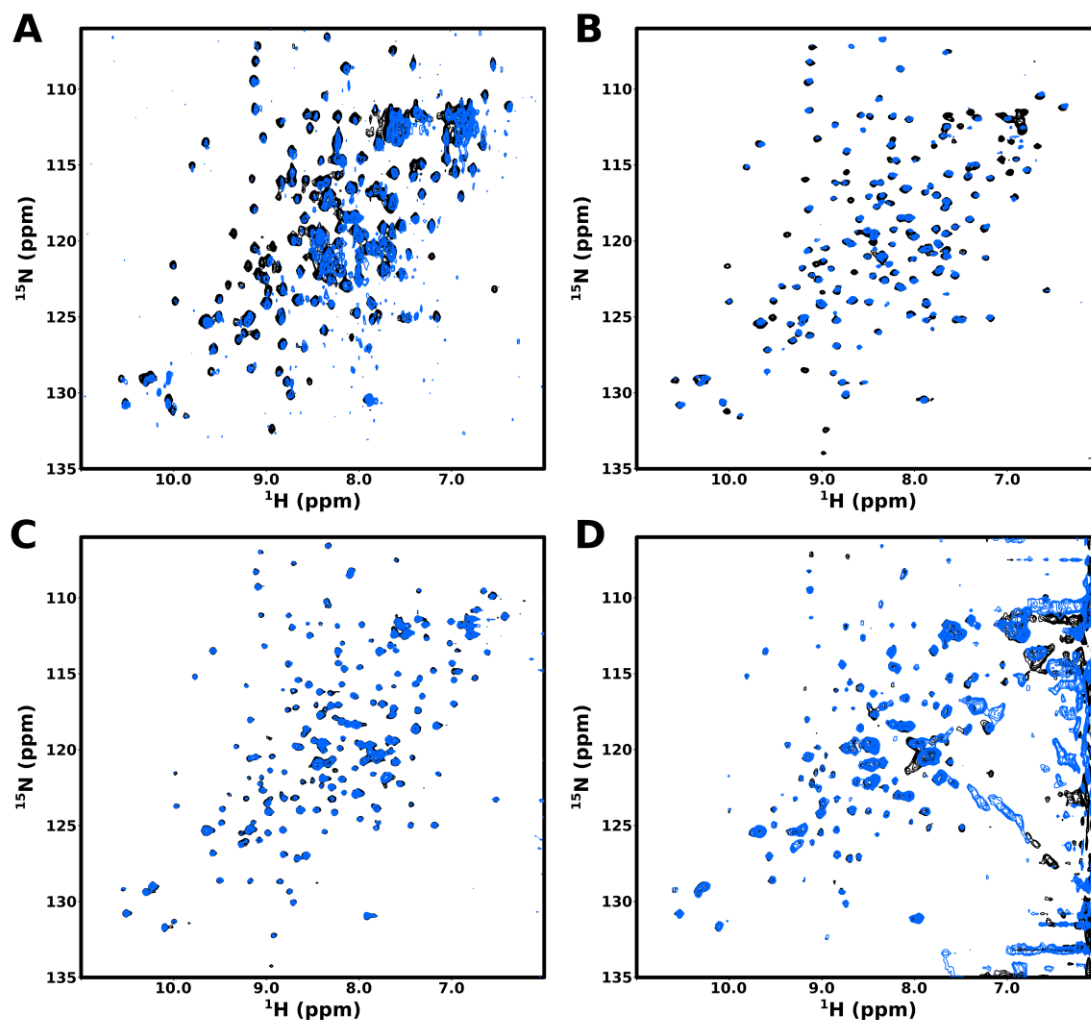


**Figure A1.6: HSQC spectra for wild-type StARD4 in the absence and presence of sterols presented by different means.**  $^1\text{H}$ ,  $^{15}\text{N}$ -HSQC spectra of wild-type StARD4 in the absence (black) and presence (blue) of cholesterol presented in lipid vesicles (A), lipid vesicles removed by gel filtration (B), 5% v/v ethanol (C), and 20 mM methyl- $\beta$ -cyclodextrin (D).

In order to delineate regions that specifically bind to or insert into the membrane, HSQC spectra were collected on StARD4 protein with increasing concentrations, at close to stoichiometric ratios, of liposomes doped with 5% 5-doxyl-stearic acid, a fatty acid with a paramagnetic moiety. In addition to the intensity loss due to formation of protein-liposome complexes, regions that come in proximity to the paramagnetic label can be expected to experience greater intensity loss due to PRE. Regions that display increased intensity loss are around residues 35-45, 140-150, 165-185, and 210-225 (Figure A1.5). Several of these regions are near a basic patch proposed to interact with negatively-charged lipid membranes [300] (Figure A1.5C). The other regions are found on the opposite side of the ligand-binding cavity, suggesting the possibility that some StARD4 molecules may take up the hydrophobic paramagnetic fatty acid, leading to PRE effects in that region.

Since StARD4 is proposed to bind and transport cholesterol [293,300], binding of cholesterol should result in observable chemical shift changes of the residues near the binding site. Unfortunately, cholesterol is highly hydrophobic and not very soluble in aqueous buffer; thus, delivery of the ligand to the protein is quite difficult. Cholesterol can be presented to the protein in cholesterol-rich vesicles, mimicking the situation inside the cell, or solubilized with small molecules such as MBCD or cosolvents such as ethanol. All of these methods were attempted in order to obtain stable StARD4-cholesterol complexes that could be analyzed via heteronuclear NMR and yield information about the cholesterol binding site. While small chemical

shift changes were occasionally observed, no reproducible and significant spectral changes were seen by any of these methods (Figure A1.6). It is unclear whether the cholesterol-bound state does not result in significant chemical shift changes to the amide nuclei, or whether binding was simply never achieved.

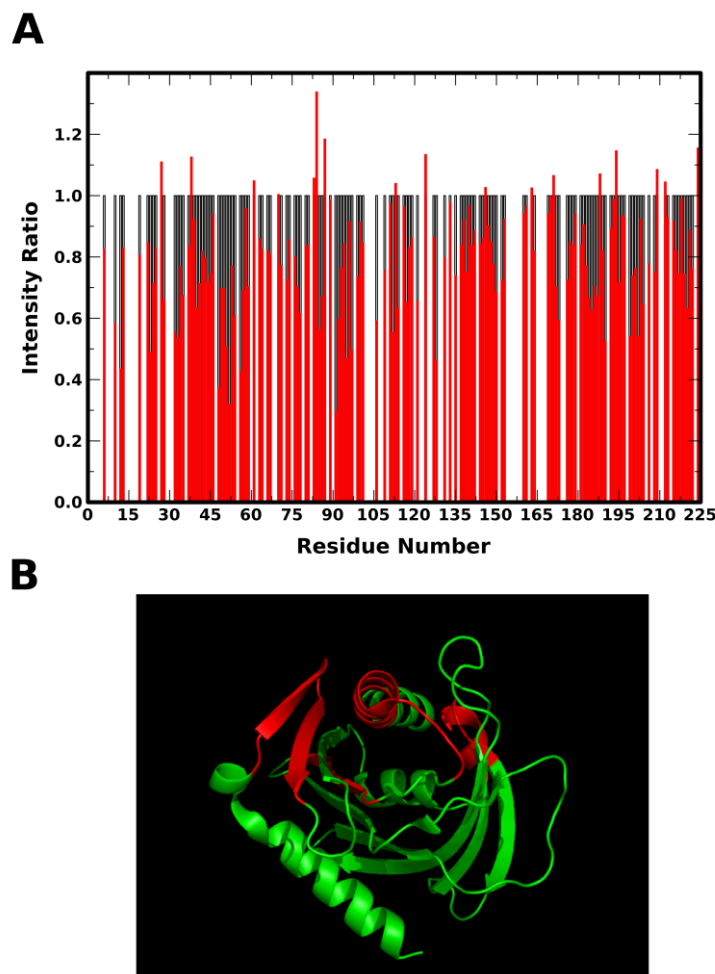


**Figure A1.7: PRE effect for wild-type StARD4 in the presence of lipid vesicles containing spin-labeled cholestane.** (A) Plot of the ratio of peak intensity in the presence of lipid vesicles (31% POPC, 23% POPE, 23% POPS, and 23% spin-labeled cholestane) to peak intensity in the absence of vesicles for wild-type StARD4 *versus* residue number. (C) Crystal structure of StARD4 (1JSS) with approximate regions of PRE effect (red).

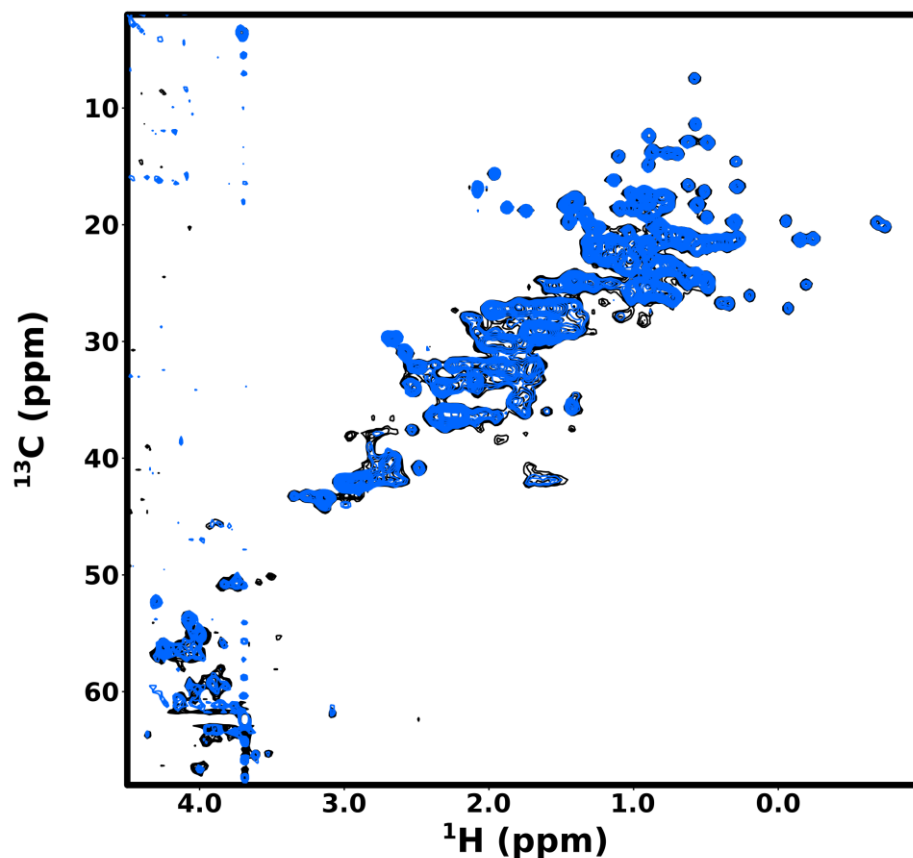


**Figure A1.8: Carbon HSQC spectra for wild-type StARD4 in the absence and presence of lipid vesicles containing spin-labeled cholestane.**  $^1\text{H}$ ,  $^{13}\text{C}$ -HSQC spectra of wild-type StARD4 in the absence (black) and presence (blue) of lipid vesicles (31% POPC, 23% POPE, 23% POPS, and 23% spin-labeled cholestane).

Binding of sterol analogues was also queried by using spin-labeled cholestane in place of cholesterol, delivered in liposomes. Both  $^1\text{H}$ ,  $^{15}\text{N}$ - and  $^1\text{H}$ ,  $^{13}\text{C}$ -HSQC spectra were collected on the apo and ostensibly loaded protein. If the interactions with ligand do not involve backbone amide groups, the  $^1\text{H}$ ,  $^{13}\text{C}$ -HSQC spectra can report on PRE effects on the side-chain nuclei, which may be more sensitive. The amide data showed several regions that may interact preferentially

with the spin-labeled moiety, such as residues 45-60, 90-100, 180-190, and 195-210 (Figure A1.7A). These regions are near in primary sequence to but distinct from those modulated by the (presumably membrane-retained) 5-doxyl-stearate (Figure A1.5) and mostly localize to the C-terminal end of the ligand-binding cavity (Figure A1.7B). The  $^1\text{H}$ ,  $^{13}\text{C}$ -HSQC spectra showed potentially localized signal ablation by the spin-labeled ligand, but the lack of resonance assignments precludes any real conclusions from being drawn (Figure A1.8).

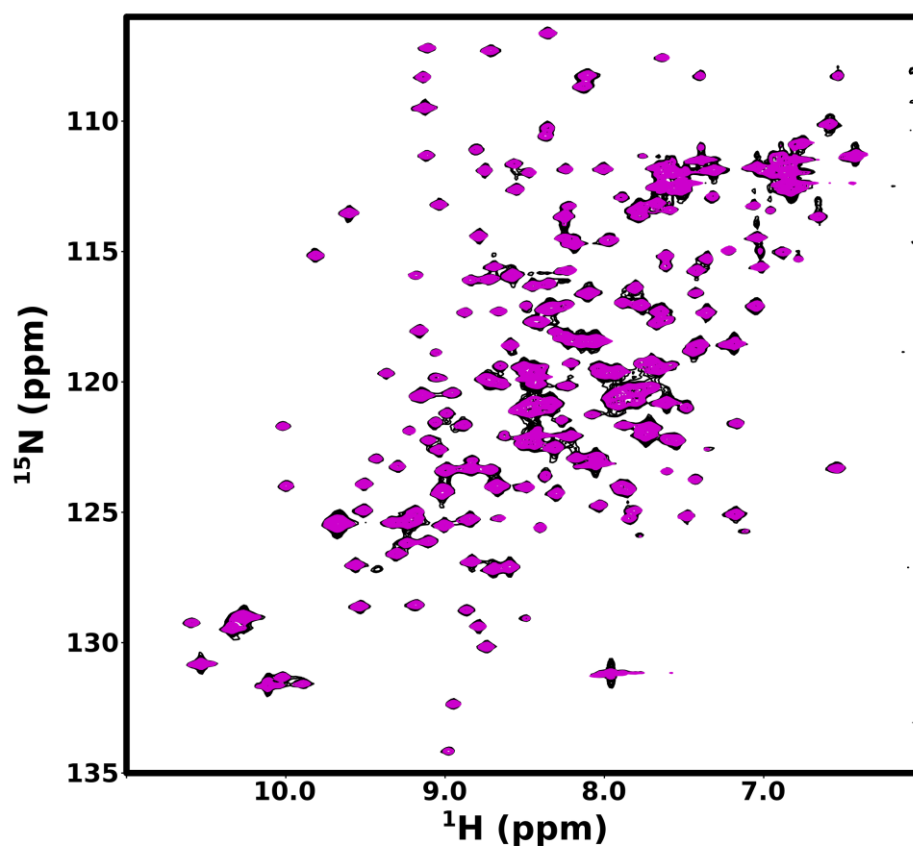


**Figure A1.9: HSQC spectra for wild-type StARD4 in the absence and presence of IP<sub>2</sub>(4,5).**  $^1\text{H}$ ,  $^{15}\text{N}$ -HSQC spectra of wild-type StARD4 in the absence (black) and presence (purple) of 2:1 IP<sub>2</sub>(4,5).

Early evidence suggests that StARD4 cholesterol transfer activity is stimulated by PI(4,5)P<sub>2</sub> lipids (Iaea and Maxfield, unpublished). Therefore, StARD4 was incubated with two times excess concentration of the soluble headgroup IP<sub>2</sub>(4,5). No large spectral changes were seen in the backbone amide cross-peaks, although this could be a low affinity interaction that requires a large excess of IP<sub>2</sub>(4,5) to see (Figure A1.9).

### **1d. Conclusions**

In conclusion, more work is required to obtain reproducible sterol-loaded StARD4 complexes. In this case, the fluorescent cholesterol analogue DHE may be beneficial as its presence can be confirmed via fluorescence. Once these are in hand, the assignment data provides a good base for further structural studies using the backbone amide or side-chain nuclei as probes. In addition, the lipid membrane interactions can be studied further using techniques such as hydrogen-deuterium exchange NMR.

## **A2. Appendix 2: Alpha-synuclein and synaptobrevin**

### **2a. Introduction**

One recently proposed function for alpha-synuclein in the synaptic vesicle cycle is a chaperone-like promotion of SNARE complex formation [133,234,307,308]. The SNARE complex consists of proteins attached to the vesicle membrane (v-SNAREs) and the target membrane (t-SNAREs), which recognize each other and zipper up to mediate membrane fusion [131]. At the synapse, these functions are fulfilled by the v-SNARE synaptobrevin-2 (Syb, VAMP) and the t-SNAREs syntaxin-1 and SNAP-25 [309]. The interaction between alpha-synuclein and the SNARE complex is thought to be mediated by the C-terminal tail of alpha-synuclein and the N-terminal 28 residues of Syb [133]. However, the existence and functional relevance of this protein-protein interaction remains controversial [130,310]. Thus, the interaction of full-length synaptobrevin-2 and alpha-synuclein was investigated using NMR spectroscopy in membrane and detergent systems.

### **2b. Methods**

*Protein Expression and Purification* – The cDNA for a cysteine-free version of rat synaptobrevin-2 (C103A) was obtained as a GST-fusion

vector, kindly donated by Dr. Yeon-kyun Shin (Iowa State University). The cDNA was cloned into the pET-SUMO vector (Invitrogen/Life Technologies). The pET-SUMO vector contains an N-terminally-fused 6xHis-tagged yeast Smt3 SUMO protein that facilitates solubility, expression, and purification [305]. After purification using nickel affinity chromatography, the SUMO tag is efficiently cleaved using Ulp1 SUMO protease, which recognizes the SUMO fold rather than a specific cut site, eliminating unnecessary left-over linking residues. The SUMO tag and SUMO protease can then be removed by another round of nickel affinity chromatography.

To produce isotopically-labeled protein, transformed *E. coli* cells were grown in LB broth (4 L) until an OD of 0.6-1.0 was reached, then centrifuged at 6,000 rpm (6,900 x g) for 15 minutes at 24 °C and the pellet resuspended in 1 L “wash medium,” consisting of M9 minimal medium without carbon or nitrogen sources and containing appropriate antibiotics. The cell culture was then centrifuged again at 6,000 rpm (6,900 x g) for 15 minutes at 24 °C and the pellet resuspended in M9 minimal medium, supplemented with BME vitamins, the appropriate antibiotics, and either 1 g uniformly labeled <sup>15</sup>N ammonium chloride and 4 g natural abundance dextrose for <sup>15</sup>N-labeled protein. After recovery at 37 °C in minimal medium for 0.5-1 hr, protein expression was induced using ~1 mM IPTG and continued for 3-3.5 hr. A 1 mL sample was taken every 1 hr to check OD and saved to estimate protein expression using SDS-PAGE. Cells were harvested by centrifugation at 6,000 rpm (6,900 x g) for 15 minutes and the pellet stored at -20 °C.

Since the Syb construct contains the transmembrane helix portion of the protein, all purification buffers contained 2% w/v sodium cholate (Amresco) to help solubilize the protein. Protein-containing cell pellets were resuspended in lysis buffer (350 mM NaCl, 20 mM tris pH 8, 20 mM imidazole, 1 mM PMSF, 0.2 mM EDTA, 2 mM DTT, 1.5 mM BME, 2% sodium cholate) and was subjected to sonication by a tip sonifier (Branson) for 2 x 6 minutes at a power setting of 6 with a duty cycle of 50%. The sample was stirred between the two applications of the sonifier. The lysed cell suspension was then subjected to ultracentrifugation at 40,000 rpm (145,000 x g) for 1 hr at 4 °C. A Ni-NTA column was equilibrated with 100 mL equilibration buffer (350 mM NaCl, 20 mM tris pH 8, 20 mM imidazole, 2 mM DTT, 1.5 mM BME, 2% sodium cholate), and the ultracentrifugation supernatant loaded onto the column. Equilibration buffer (50 mL) was applied to the column as a wash step, with 5 fractions collected, followed by elution with ~100 mL elution buffer (350 mM NaCl, 20 mM tris pH 8, 250 mM imidazole, 2 mM DTT, 1.5 mM BME, 2% sodium cholate).

Approximately 75 mL of the eluate were collected, then dialyzed overnight against ~1 L cleavage buffer (150 mM NaCl, 20 mM tris pH 8, 1 mM DTT, 2% sodium cholate). Sodium cholate, SDS, and Triton X-100 were tested for their effect on the cleavage reaction and sodium cholate had the least deleterious effect. The fusion protein was then incubated with 6xHis-tagged SUMO protease (~1:50 protease:protein) for 2 hr at 4 °C. The cleavage reaction mixture was passed over a Ni-NTA column pre-equilibrated with 100 mL equilibration buffer, with

the StARD4-containing flowthrough being collected. The column was washed with 50 mL equilibration buffer and the 6xHis-tagged SUMO tag and SUMO protease eluted with ~100 mL elution buffer. The Syb protein was run on a Superose6 gel filtration column (GE Healthcare) as a final cleanup and buffer exchange step, using 100 mM NaCl, 10 mM NaH<sub>2</sub>PO<sub>4</sub>, 25 mM sodium cholate, pH 6.8 buffer. NMR experiments were usually carried out immediately after purification, else the protein was stored at 4 °C for no more than 1 week.

*Sample Preparation* – NMR samples consisted of natural abundance or isotopically-labeled Syb protein reconstituted in SDS micelles or 15% DOPS, 60% DOPC, 25% DOPE SUVs with or without isotopically-labeled or natural abundance alpha-synuclein. In order to reconstitute Syb in SDS, protein solubilized in sodium cholate was dialyzed against 40x volume of SDS solution (100 mM) at room temperature overnight, usually involving 1 or 2 changes of dialysis buffer. It is important to keep the temperature above ~18 °C, the Krafft point of SDS. However, the formation of protein-detergent complexes made it difficult to obtain expected concentrations of SDS and sodium cholate, so experiments can be affected by inaccurate or un-matched detergent concentrations. The solubilized Syb was then mixed with alpha-synuclein dissolved in 100 mM SDS and supplemented with 10% D<sub>2</sub>O to make NMR samples.

In order to reconstitute Syb in SUVs, the appropriate lipids, dissolved in chloroform (Avanti Polar Lipids), were mixed and dried under nitrogen at 50 °C, followed by drying under vacuum. The dried lipid film was resuspended in NMR buffer by pipetting up and down,

then vortexing. SUVs were prepared by sonicating the multilamellar vesicle suspension in a bath sonicator 4 times for 3 min. During sonication, sodium cholate powder was added to a final concentration of 25 mM (slightly above the CMC). The detergent is meant to disrupt the vesicles. After sonication, the SUV and detergent mixture was mixed with Syb dissolved in NMR buffer with 25 mM sodium cholate. The detergent was removed by diluting the sample in 3x detergent-free buffer, then dialysis overnight. The suspension was finally centrifuged at 60,000 rpm (160,000 x g) at 4 °C for 2 hr to remove larger vesicles. The Syb-containing SUVs were used as NMR samples, or mixed with alpha-synuclein dissolved in NMR buffer.

For <sup>15</sup>N-labeled Syb reconstitution, the final concentrations were about 15 mM SUVs and 100 μM Syb. This ratio results in ~75 Syb molecules per vesicle, with half facing the vesicle lumen and half facing outwards. In order to test alpha-synuclein binding to Syb-containing SUVs, two samples of SUVs composed of 15% DOPS, 60% DOPC, 25% DOPE were produced via the abovementioned reconstitution protocol in parallel. One batch was mixed with natural-abundance Syb dissolved in sodium cholate, while the other with the same detergent buffer without protein. To allow for significant populations of bound and free alpha-synuclein after mixing with SUVs, a lower concentration (3 mM) of SUVs was used, while the Syb concentration was kept relatively high (75 μM) to promote potential protein-protein interactions. This resulted in higher concentration of Syb molecules on the vesicles (~250 per vesicle). As for alpha-

synuclein, NMR experiments were performed at 40 °C on SDS-containing samples, and at 10 °C on SUV-containing samples.

## 2c. Results

Isotopically-labeled Syb was solubilized in 100 mM SDS and examined via a  $^1\text{H},^{15}\text{N}$ -HSQC experiment. The resulting spectrum was consistent with a protein containing both helical and disordered character (Figure A2.1A, black). Approximately 100 amide cross-peaks could be resolved, suggesting that most of the 116-residue peptide chain gives rise to signals in SDS. Additionally, two peaks could be observed at higher proton and nitrogen field, likely corresponding to the indole amides of two tryptophan residues. However, the addition of natural-abundance alpha-synuclein (~180  $\mu\text{M}$  Syb, ~90  $\mu\text{M}$  alpha-synuclein) did not result in any significant spectral changes (Figure A2.1A, red). The reverse experiment, consisting of ~60  $\mu\text{M}$   $^{15}\text{N}$ -labeled alpha-synuclein in 100 mM SDS with and without ~180  $\mu\text{M}$  Syb also showed no significant spectral changes (Figure A2.1B). These results argue against a robust interaction between alpha-synuclein and Syb, although potentially, higher concentrations of the proteins may be required to see evidence of an interaction. While the SDS-bound state of alpha-synuclein is thought to resemble at least one of the membrane-bound states of the protein that exist *in vivo*, it is possible

that the interaction between the two proteins requires a more realistic membrane environment.

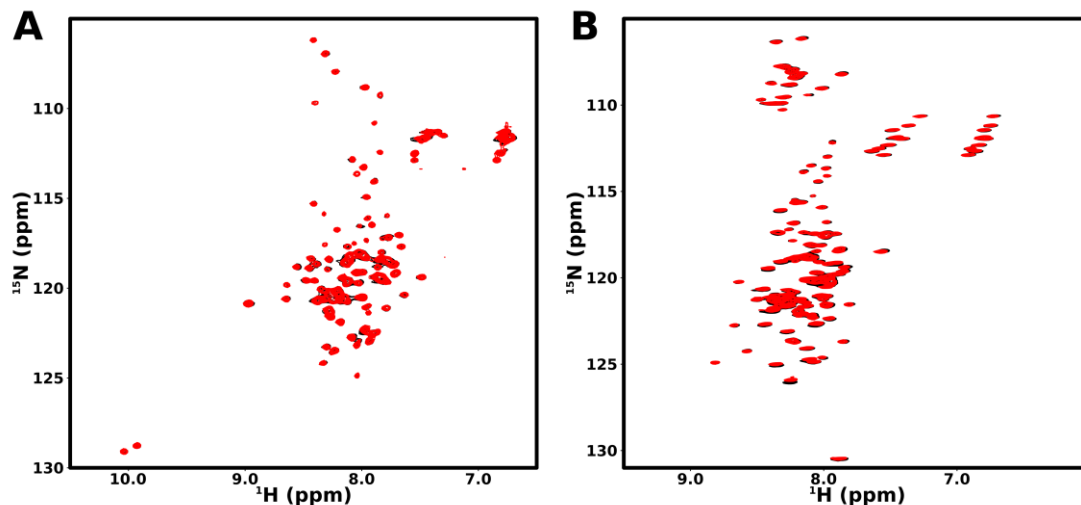


**Figure A2.1: HSQC spectra of alpha-synuclein and synaptobrevin-2 in the presence of SDS micelles.** (A)  $^1\text{H},^{15}\text{N}$ -HSQC spectra of isotopically-labeled synaptobrevin-2 in the absence (black) and presence (red) of unlabeled alpha-synuclein in 100 mM SDS. (B)  $^1\text{H},^{15}\text{N}$ -HSQC spectra of isotopically-labeled alpha-synuclein in the absence (black) and presence (red) of unlabeled synaptobrevin-2 in 100 mM SDS.

To this end, Syb was reconstituted in synthetic SUVs composed of 15% DOPS, 60% DOPC, 25% DOPE, meant to mimic the composition of synaptic vesicles that normally house synaptobrevin. The  $^1\text{H},^{15}\text{N}$ -HSQC spectrum was different from that observed in the presence of SDS micelles, although this difference could be partially due to the different temperature. The spectrum of SUV-reconstituted Syb contained fewer peaks (~80) and displayed less dispersion along the proton axis, suggesting that the helical residues of the transmembrane segment (including the tryptophan residues) do not

give rise to observable resonances (Figure A2.2). This finding, and in fact the entire spectrum, is similar to that for Syb reconstituted in phospholipid-containing nanodiscs, in which case the transmembrane helix and a few residues proximal to it did not give rise to cross-peaks due to their tumbling at the overall rate of the large nanodisc [311].

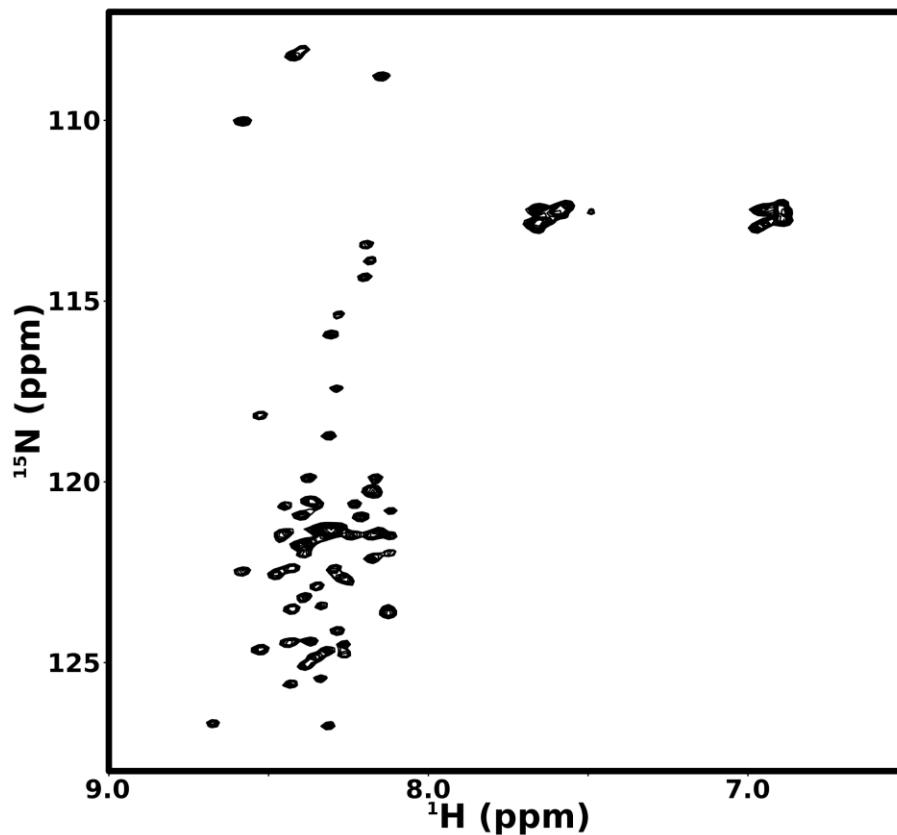


**Figure A2.2: HSQC spectrum of synaptobrevin reconstituted in SUVs.**  $^1\text{H}$ ,  $^{15}\text{N}$ -HSQC spectrum of synaptobrevin-2 reconstituted in 15 mM 15% DOPS, 60% DOPC, 25% DOPE SUVs.

In order to test Syb binding to alpha-synuclein, isotopically-labeled acetylated alpha-synuclein was incubated with SUVs that contained natural-abundance Syb and protein-free SUVs, made in

parallel, and the extent of alpha-synuclein binding to SUVs quantified. While acetylated alpha-synuclein in the presence of protein-free SUVs gave rise to a binding profile similar to those observed previously (Figure A2.3, black) (compare to Chapter III; [91]), the binding of acetylated alpha-synuclein to Syb-containing liposomes was significantly reduced in the N-terminal domain while the C-terminal tail residues showed decreased peak intensity (Figure A2.3, red).

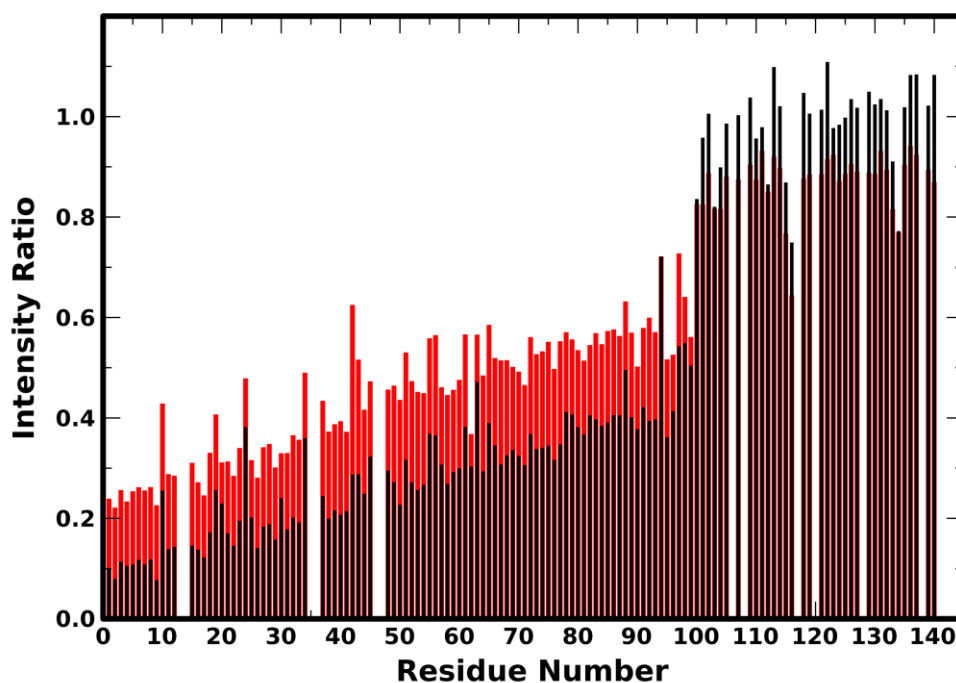


**Figure A2.3: Binding profile of acetylated alpha-synuclein to SUVs with and without synaptobrevin.** Plot of the ratio of peak intensity in the presence of 3 mM 15% PS SUVs with (red) and without (black) synaptobrevin to peak intensity in the absence of vesicles *versus* residue number for acetylated alpha-synuclein.

There are two possible explanations for the difference in C-terminal intensities: the samples were not well-matched in concentration, or there is an interaction between the C-terminal tail and the Syb embedded in the liposomes. The bound populations of different alpha-synuclein states can be estimated using both interpretations. In the first, acetylated alpha-synuclein shows significantly decreased binding to Syb-containing liposomes and an increased relative population of N-terminal partly-helical states (0.717 total bound fraction and 44.2% partly-helical states *versus* 0.893 and 27.2%). In the second interpretation, if the C-terminal resonance intensities from the protein-free SUV experiment are used to normalize the intensities in the experiment with Syb-containing vesicles, the fraction of C-terminal tail interacting with Syb is approximately 0.115. The normalized bound fractions of different states still show decreased total binding and increased proportion of partly-helical states compared to the protein-free liposomes (0.750 total bound fraction and 37.4% partly-helical states *versus* 0.893 and 27.2%).

## **2d. Conclusions**

The liposome data show that acetylated alpha-synuclein binding to 15% PS SUVs is reduced overall when those vesicles contain Syb. This could be due to repulsion between the alpha-synuclein and Syb molecules, or simply due to crowding, with the large number of Syb molecules per vesicle (~250) taking up the surface required for alpha-

synuclein binding. These results are consistent with a previously published short report finding that alpha-synuclein has reduced affinity for v-SNARE-containing 50% PS SUVs by a factor of 2 [310]. The data in the presence of SDS micelles also does not indicate any stable interaction between the alpha-synuclein and Syb molecules. On the other hand, the decrease in C-terminal tail resonance intensities in the presence of Syb-containing SUVs may suggest binding of the C-terminal tail to Syb, which would be consistent with the model proposed by Burré, et. al. [133,234].

### **A3. Appendix 3: Alpha-synuclein and Hsc70**

#### **3a. Introduction**

Soon after its categorization as an intrinsically disordered protein, alpha-synuclein was proposed to interact with cytoplasmic chaperone proteins to mitigate its aggregation potential [312]. Since expression of Hsp70, a chaperone that refolds misfolded proteins [313] can reduce the toxicity of other aggregation-prone proteins [314], it was posited that Hsp70, or its constitutively-expressed homologue Hsc70, could do the same for alpha-synuclein. The positive effects of Hsp70 on alpha-synuclein-mediated toxicity were shown in several cellular and animal models [312,315–318]. However, the exact mechanism by which Hsp70 alleviates cytotoxicity induced by alpha-synuclein is unclear. Since alpha-synuclein overexpression results in massive protein aggregation and misfolding, it is reasonable that adding more protein refolding activity would ameliorate the negative effects. But is there a direct interaction between Hsp70 and alpha-synuclein, in which alpha-synuclein acts as an unfolded client for Hsp70 chaperone activity?

Hsp70 was shown to inhibit alpha-synuclein fibril formation *in vitro* and to interact preferentially with pre-fibrillar alpha-synuclein oligomers (by gel filtration) [319,320]. The inhibition of fibrillation was additionally shown to require only the substrate-binding C-terminal domain (CTD) of Hsp70 [320]. The highly hydrophobic NAC region of

alpha-synuclein was shown to be necessary for this inhibition of fibril formation by Hsp70 [321]. These results suggest, though do not demonstrate, a model in which Hsc/p70 (via its substrate-binding CTD) binds to the hydrophobic and amyloidogenic NAC region of alpha-synuclein, likely in oligomeric states, to prevent further oligomerization. In a contrasting model, chemical crosslinking studies indicate that Hsc70 CTD binds alpha-synuclein in two regions: residues 10-45 and residues 97-102 [322]. These two regions flank the NAC region (residues 61-95). Yet another model of alpha-synuclein interaction with Hsp70 is based on in-cell fluorescence lifetime measurements that indicate that Hsp70 reduces intramolecular N- to C-terminal contacts in alpha-synuclein molecules [323]. In addition, interactions between monomeric alpha-synuclein and full-length Hsp70 were ruled out on the basis of lack of chemical shift perturbations or resonance intensity decreases [319]. These findings do not lead to a consistent and clean understanding of how alpha-synuclein interacts with Hsp70.

### **3b. Methods**

The CTD of Hsc70 from rat was exchanged into NMR buffer (100 mM NaCl, 10 mM Na<sub>2</sub>HPO<sub>4</sub>, 10% D<sub>2</sub>O, pH 6.8) and mixed with <sup>15</sup>N-labeled alpha-synuclein, both N-terminally acetylated and unmodified, at different stoichiometries. Due to scarcity of Hsc70 CTD protein, relatively low concentrations were used (30 μM alpha-synuclein, 0-60

$\mu\text{M}$  Hsc70 CTD), requiring long acquisition times for the  $^1\text{H},^{15}\text{N}$ -HSQC spectra. Chemical shifts and intensities of amide cross-peaks arising from alpha-synuclein in the absence and presence of Hsc70 CTD were compared to find evidence of a direct interaction between the two proteins.

### 3c. Results

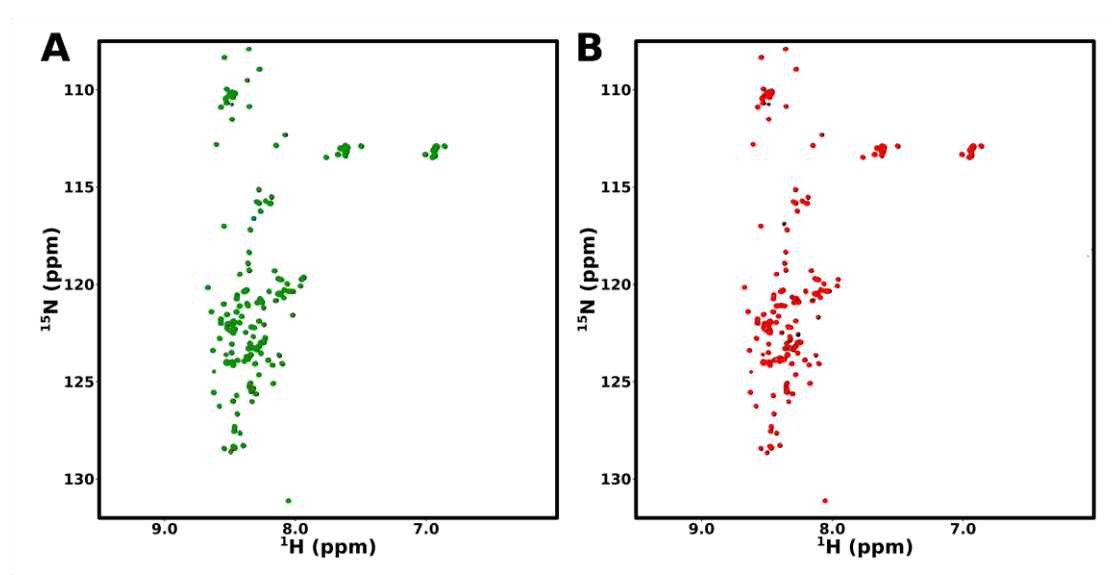


**Figure A3.1: HSQC spectra of acetylated and unmodified alpha-synuclein in the presence of Hsc70 CTD.**  $^1\text{H},^{15}\text{N}$ -HSQC spectra of acetylated (A) and unmodified (B) alpha-synuclein in the absence (black) and presence of 0.5:1 (blue), 1:1 (red), and 2:1 (green) unlabeled Hsc70 CTD.

The addition of 1:1 and 2:1 Hsc70 CTD to both unmodified and acetylated alpha-synuclein did not result in any significant chemical shift changes in the backbone amide peaks as seen in the  $^1\text{H},^{15}\text{N}$ -HSQC spectra (Figure A3.1). However, certain peak intensities were

decreased. When the intensity ratio to Hsc70-free spectra was plotted *versus* residue number, the majority of intensity decreases for both unmodified and acetylated alpha-synuclein were localized to the N-terminal ~100 residues, with the greatest intensity decrease occurring in the very N-terminal 10 or 25 residues (Figure A3.2). These results are in contrast to previous NMR studies of unmodified alpha-synuclein with Hsp70 [319]. Since the Hsc70 CTD is ~30 kDa in size, the combined protein-protein complex should be ~45 kDa, which is not as large and slowly-tumbling as a protein-vesicle complex, but comparable to a protein-micelle complex. Therefore, the relaxation rate would be expected to increase due to somewhat slower tumbling of the larger complex, and/or due to loss of the flexible, disordered character of the N-terminal region by immobilization on Hsc70 CTD.

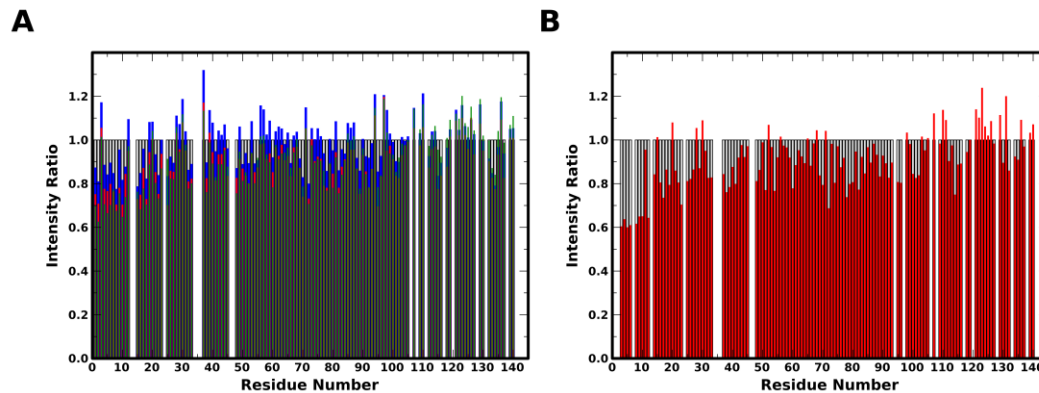


**Figure A3.2: Binding profiles of acetylated and unmodified alpha-synuclein to Hsc70 CTD.** Plots of the ratio of peak intensity in the presence of 0.5:1 (blue), 1:1 (red), and 2:1 (green) Hsc70 CTD to peak intensity in the absence of Hsc70 CTD *versus* residue number for acetylated (A) and unmodified (B) alpha-synuclein.

The potential interaction of alpha-synuclein with Hsp104, another molecular chaperone that works together with Hsp/c70 to disassemble protein aggregates was also assayed by NMR. Isotopically-labeled unmodified alpha-synuclein was incubated with and without natural abundance Hsp104 in buffer containing 50 mM HEPES pH 7.5, 10 mM MgCl<sub>2</sub>, and 5 mM ATP and <sup>1</sup>H,<sup>15</sup>N-HSQC spectra were collected as previously described. The spectra of alpha-synuclein in the absence and presence of Hsp104 were virtually identical, suggesting that the two proteins did not interact under these conditions.

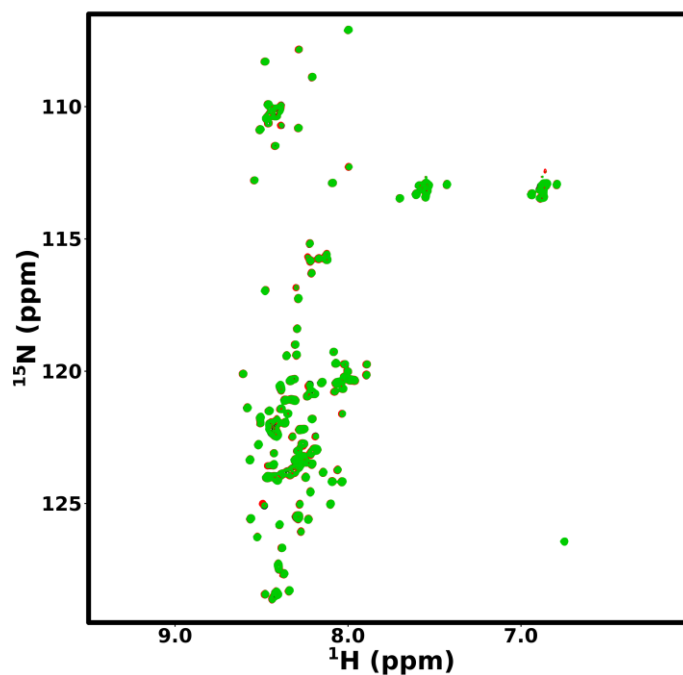


**Figure A3.3: HSQC spectra of unmodified alpha-synuclein in the presence of Hsp104.** <sup>1</sup>H,<sup>15</sup>N-HSQC spectra of unmodified alpha-synuclein in the absence (black) and presence of 1:1 (red) and 5:1 (green) unlabeled Hsp104 in aqueous buffer.

### **3d. Conclusions**

This interaction can be studied in greater detail by using isotopically-labeled Hsc70 to determine the binding site for alpha-synuclein using reverse titrations. In addition, the alpha-synuclein intensity ratio data can be repeated at higher protein concentrations to achieve saturation of binding, and the contribution of different types of relaxation can be determined using relaxation experiments. Additionally, the effects of a full-length Hsc70 protein and the addition of ATP on alpha-synuclein binding can be investigated, as well as whether transient intramolecular interactions within alpha-synuclein are affected.

## **A4. Appendix 4: Alpha-synuclein and TAT fusions**

### **4a. Introduction**

The Tat protein from HIV was one of the first proteins discovered to be transduced into cells [324,325]. This ability was eventually harnessed in the form of fusions of the minimal 11-residue TAT peptide (YGRKKRRQRRR) in order to transduce any protein of interest into desired mammalian cells [326,327]. To that end, N-terminal and C-terminal fusions of the TAT peptide to alpha-synuclein, with different linkers, were prepared: TAT-aSyn (MRGSYGRKKRRQRRRGGGCGH – [alpha-synuclein 1-140]), aSyn-TAT ([alpha-synuclein 1-140] – LECRKKRRQRRR), and aSyn-N-TAT ([alpha-synuclein 1-140] – LEGGGCGHSYGRKKRRQRRR). The latter fusion construct made use of the same linker used for the N-terminal TAT fusion. Due to the highly positively-charged character of the TAT peptide, it may be expected to affect the structure or biophysical properties of the fused alpha-synuclein protein, potentially through electrostatic interactions.

While the TAT fusions had no major effect on neither the overall disordered conformation of the fusion protein in aqueous buffer nor binding to lipid vesicles, the fusion proteins were shown to aggregate more readily than the wild-type protein (C. Desobry and H. Lashuel, unpublished results). In addition, the TAT-aSyn protein elutes later on a size exclusion column, suggesting a more compact structure, while

also being more efficiently internalized than the unfused alpha-synuclein and the aSyn-TAT fusion. The aSyn-N-TAT fusion also elutes slightly later than unmodified alpha-synuclein, showing some level of compaction as well (C. Desobry and H. Lashuel, unpublished results).

#### **4b. Methods**

The alpha-synuclein TAT fusion proteins were produced recombinantly in *E. coli* as previously described. The proteins were lyophilized for storage. The three constructs each contained a cysteine residue in the linker between the TAT peptide and alpha-synuclein sequence to facilitate labeling. This allowed paramagnetic spin-label (MTSL) to be conjugated near to the TAT peptide to investigate the intramolecular contacts that the peptide may make to the rest of the protein. Lyophilized protein was dissolved in NMR buffer and PRE samples prepared and analyzed as described in section II.h.

#### **4c. Results**

The overall structural characteristics of the different alpha-synuclein TAT fusion constructs were assessed using NMR spectroscopy. In particular, PRE NMR was used to examine the extent of potential intramolecular contacts between the highly positively charged TAT peptide and different regions along the polypeptide chain.

The diamagnetic spectra for all constructs served as a control and were very similar to those previously obtained for wild-type alpha-synuclein (Figure A4.1). Additional cross-peaks arising from the linker residues and TAT peptide were seen, as well some peak shifts near the N- or C-terminus of the alpha-synuclein sequence. However, the majority of the peaks arising from alpha-synuclein were unchanged in any of the three fusion proteins, suggesting that no secondary or tertiary structure is induced by the addition of the TAT peptide. Comparison of the peak intensities in the paramagnetic and diamagnetic spectra showed several regions of decreased intensity, indicating paramagnetic relaxation enhancement resulting from proximity to the spin-label.

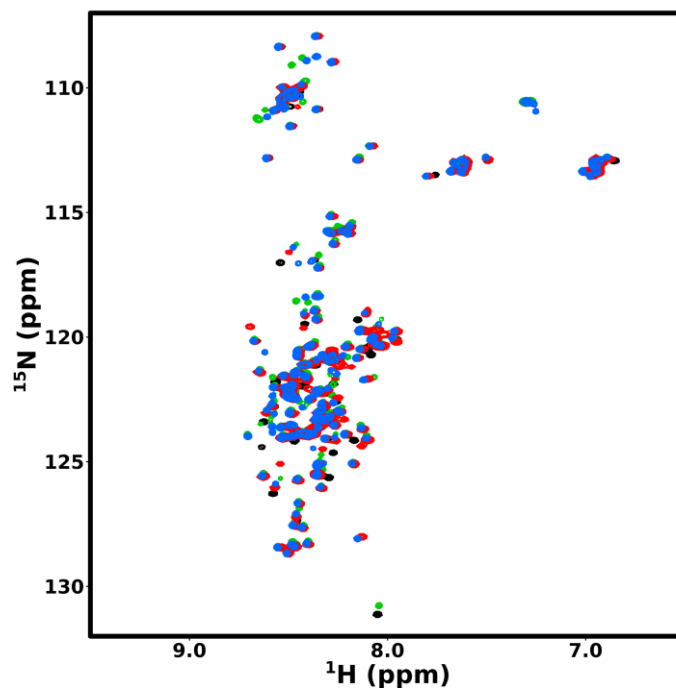


**Figure A4.1: HSQC spectra of unmodified alpha-synuclein and TAT fusion proteins in aqueous buffer.**  $^1\text{H}$ ,  $^{15}\text{N}$ -HSQC spectra of unmodified alpha-synuclein (black), TAT-aSyn (green), aSyn-TAT (red), and aSyn-N-TAT (blue) in aqueous buffer.

The N-terminally-linked TAT construct (TAT-aSyn) shows significant PRE effects that are strongest at the N-terminal (centered around residue 7) and C-terminal (centered around residue 125) regions (Figure A4.2A). These data indicate that the paramagnetic spin-label (located at position -3) interacts favorably with both the N- and C-terminal regions of the alpha-synuclein polypeptide. The latter interaction is most likely mediated by electrostatic attraction between the highly positive TAT peptide and negatively-charged C-terminus of alpha-synuclein. Notably, the C- and N-terminal regions of wild-type alpha-synuclein have previously been shown to interact with each other as well [44]. The current PRE data cannot distinguish between direct interactions of the TAT peptide with the N- and C-terminal regions of alpha-synuclein and indirect interactions mediated by pre-existing intrinsic intramolecular interactions of unmodified alpha-synuclein. Nevertheless, the data clearly show that the conformation of the TAT-aSyn peptide is likely to be quite compact (Figure A4.3A).

The C-terminally linked TAT constructs were made with two different linkers: a shorter one, aSyn-TAT; and a longer one identical to the N-terminal linker, aSyn-N-TAT. The aSyn-TAT fusion protein shows a strong PRE effect at the C-terminus (centered on residue 125), as well as a weaker effect on the N-terminus (Figure A4.2B). The C-terminal PRE could be a local effect due to the proximity of the spin-labeled cysteine residue (position 143), but also likely reflects some interactions between the positively-charged TAT peptide and negatively-charged C-terminal tail of alpha-synuclein. The PRE effect on the N-terminal region, on the other hand, is unlikely due to direct

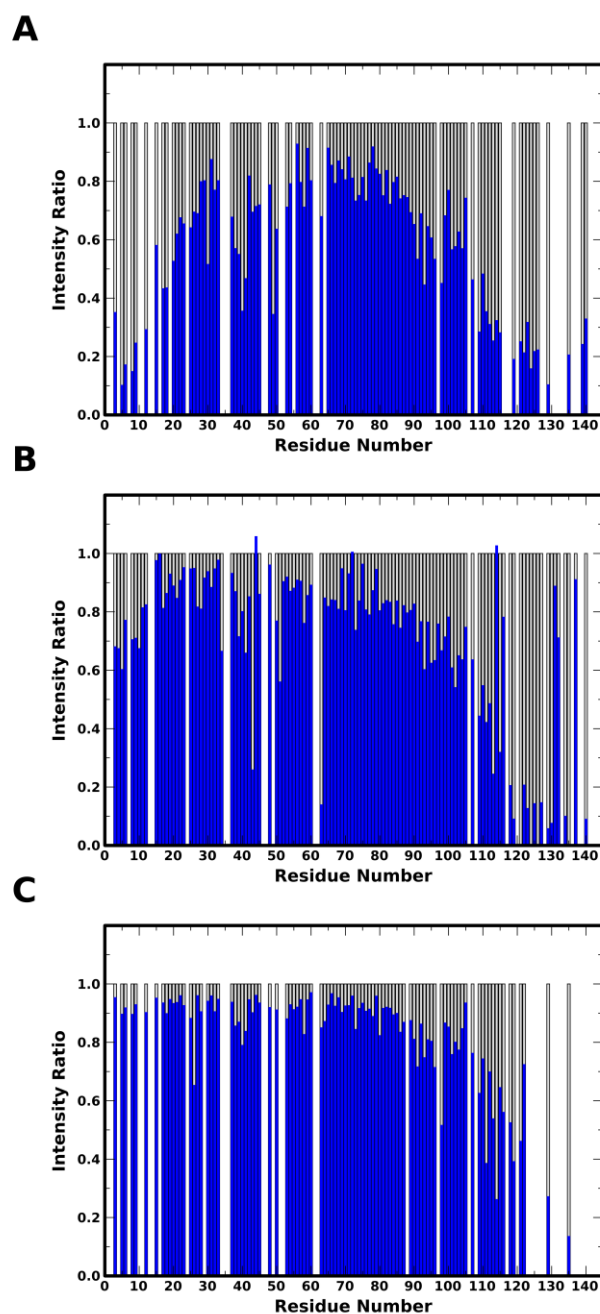


**Figure A4.2: Intramolecular PRE effect for alpha-synuclein TAT fusion proteins from a spin-labeled linker.** Plots of the ratio of peak intensity for samples paramagnetically labeled in the linker to peak intensity in unlabeled samples *versus* residue number for TAT-aSyn (labeled at position -3) (A), aSyn-TAT (labeled at position 143), and aSyn-N-TAT (labeled at position 147) (C) in aqueous buffer.

interactions between the TAT peptide and the N-terminal region, as both are overall positively-charged, and instead reflects these two regions indirectly coming into proximity, mediated by the well-known N- to C-terminal contacts of unmodified alpha-synuclein (Figure A4.3B).

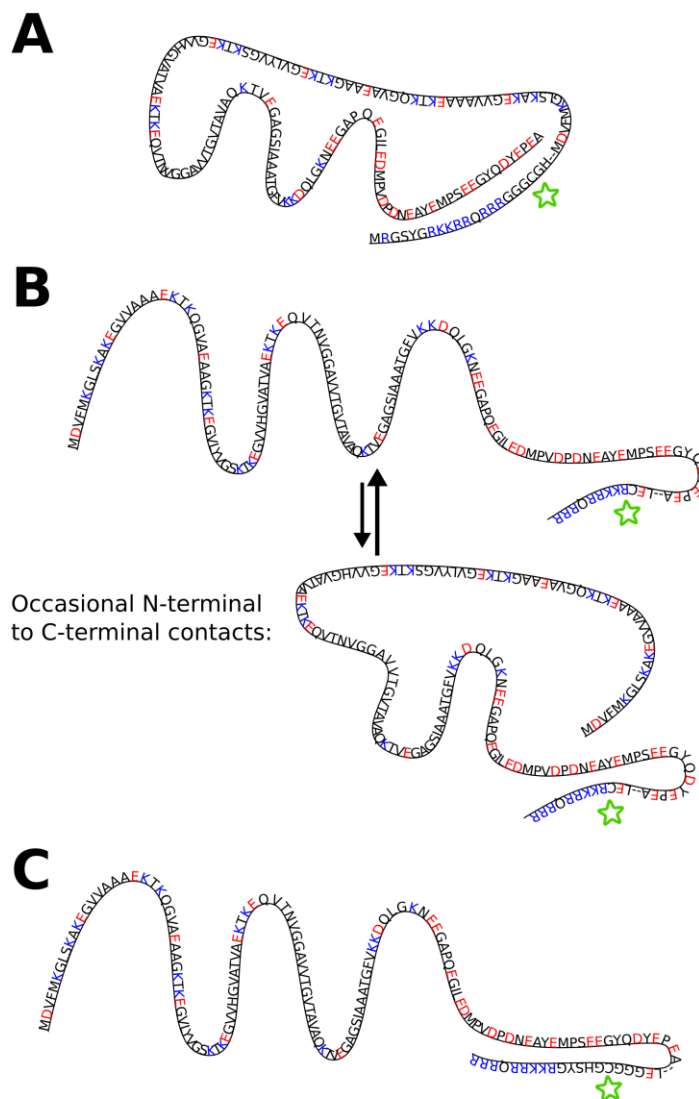


**Figure A4.3: Diagrams of likely intramolecular contacts for alpha-synuclein TAT fusion proteins.** (A) TAT-aSyn, (B) aSyn-TAT, (C) aSyn-N-TAT. Positively- (blue) and negatively-charged (red) side-chains are highlighted. The green star represents the spin-label position.

The aSyn-N-TAT fusion protein was constructed to be more comparable to the TAT-aSyn protein, which is more efficiently internalized into cells. This fusion construct shows a significantly weaker PRE effect than TAT-aSyn, localized to the C-terminal region (centered on residue 130) (Figure A4.2C). It is likely that the highly positive TAT peptide again interacts with the negatively-charged C-terminal tail of alpha-synuclein, but this interaction is now more local since these two regions are adjacent. There is no evidence of longer-range intramolecular contacts of the spin-labeled region as with the other constructs, suggesting that this peptide is more extended in character than TAT-aSyn and aSyn-TAT (Figure A4.3C).

#### **4d. Conclusions**

The TAT-fused alpha-synuclein proteins are quite similar to the unmodified protein in adopting a set of disordered conformations with transient intramolecular contacts in aqueous solution. While the N-terminally fused TAT-aSyn construct appears the most compact by SEC-MALS and displays the most intense PRE effects at the N- and C-termini, indicative of significant contacts between the spin-label near the TAT peptide and the rest of the polypeptide chain, these contacts seem to be very similar or mediated through those that unmodified alpha-synuclein exhibits. This fusion protein also shows the greatest cell internalization efficiency (C. Desobry and H. Lashuel, unpublished results), suggesting that the contacts made by the TAT peptide to the

rest of the protein are not inhibitory. In the case of aSyn-TAT, which shows decreased internalization efficiency, the contacts are again similar to those seen in unmodified alpha-synuclein, although less strong than those seen for TAT-aSyn. When the linker between the alpha-synuclein sequence and TAT peptide is extended, in aSyn-N-TAT, the intramolecular contacts appear the least intense, suggesting that this fusion protein occupies the most extended conformations (Figure A4.3).

## BIBLIOGRAPHY

- [1] Nussbaum RL, Ellis CE. Alzheimer's disease and Parkinson's disease. *N Engl J Med* 2003;348:1356–64. doi:10.1056/NEJM2003ra020003.
- [2] Braak H, Braak E. Pathoanatomy of Parkinson's disease. *J Neurol* 2000;247:II3–10. doi:10.1007/PL00007758.
- [3] Tolleson CM, Fang JY. Advances in the mechanisms of Parkinson's disease. *Discov Med* 2013;15:61–6.
- [4] Spillantini MG, Crowther RA, Jakes R, Hasegawa M, Goedert M. alpha-Synuclein in filamentous inclusions of Lewy bodies from Parkinson's disease and dementia with lewy bodies. *Proc Natl Acad Sci USA* 1998;95:6469–73.
- [5] Wakabayashi K, Matsumoto K, Takayama K, Yoshimoto M, Takahashi H. NACP, a presynaptic protein, immunoreactivity in Lewy bodies in Parkinson's disease. *Neurosci Lett* 1997;239:45–8.
- [6] Hashimoto M, Hsu LJ, Sisk A, Xia Y, Takeda A, Sundsmo M, et al. Human recombinant NACP/alpha-synuclein is aggregated and fibrillated in vitro: Relevance for Lewy body disease. *Brain Research* 1998;799:301–6. doi:10.1016/S0006-8993(98)00514-9.
- [7] Conway KA, Harper JD, Lansbury PT. Accelerated in vitro fibril formation by a mutant alpha-synuclein linked to early-onset Parkinson disease. *Nat Med* 1998;4:1318–20. doi:10.1038/3311.
- [8] Takeda A, Mallory M, Sundsmo M, Honer W, Hansen L, Masliah E. Abnormal accumulation of NACP/alpha-synuclein in neurodegenerative disorders. *Am J Pathol* 1998;152:367–72.
- [9] Kiely AP, Asi YT, Kara E, Limousin P, Ling H, Lewis P, et al. alpha-Synucleinopathy associated with G51D SNCA mutation: a link between Parkinson's disease and multiple system atrophy? *Acta Neuropathol* 2013;125:753–69. doi:10.1007/s00401-013-1096-7.

- [10] Krüger R, Kuhn W, Müller T, Voitalla D, Graeber M, Kösel S, et al. Ala30Pro mutation in the gene encoding  $\alpha$ -synuclein in Parkinson's disease. *Nat Genet* 1998;18:106–8. doi:10.1038/ng0298-106.
- [11] Polymeropoulos MH, Lavedan C, Leroy E, Ide SE, Dehejia A, Dutra A, et al. Mutation in the  $\alpha$ -Synuclein Gene Identified in Families with Parkinson's Disease. *Science* 1997;276:2045–7. doi:10.1126/science.276.5321.2045.
- [12] Proukakis C, Dudzik CG, Brier T, MacKay DS, Cooper JM, Millhauser GL, et al. A novel  $\alpha$ -synuclein missense mutation in Parkinson disease. *Neurology* 2013;80:1062–4. doi:10.1212/WNL.0b013e31828727ba.
- [13] Zarranz JJ, Alegre J, Gómez-Esteban JC, Lezcano E, Ros R, Ampuero I, et al. The new mutation, E46K, of alpha-synuclein causes Parkinson and Lewy body dementia. *Ann Neurol* 2004;55:164–73. doi:10.1002/ana.10795.
- [14] Chartier-Harlin M-C, Kachergus J, Roumier C, Mouroux V, Douay X, Lincoln S, et al. Alpha-synuclein locus duplication as a cause of familial Parkinson's disease. *Lancet* 2004;364:1167–9. doi:10.1016/S0140-6736(04)17103-1.
- [15] Singleton AB, Farrer M, Johnson J, Singleton A, Hague S, Kachergus J, et al. alpha-Synuclein locus triplication causes Parkinson's disease. *Science* 2003;302:841. doi:10.1126/science.1090278.
- [16] Liu J, Xiao Q, Wang Y, Xu Z-M, Wang Y, Yang Q, et al. Analysis of genome-wide association study-linked loci in Parkinson's disease of Mainland China. *Mov Disord* 2013;28:1892–5. doi:10.1002/mds.25599.
- [17] Simón-Sánchez J, Schulte C, Bras JM, Sharma M, Gibbs JR, Berg D, et al. Genome-wide association study reveals genetic risk underlying Parkinson's disease. *Nature Genetics* 2009;41:1308–12. doi:10.1038/ng.487.

- [18] Lansbury PT. Evolution of amyloid: What normal protein folding may tell us about fibrillogenesis and disease. PNAS 1999;96:3342–4. doi:10.1073/pnas.96.7.3342.
- [19] Volles MJ, Lansbury PT Jr. Zeroing in on the pathogenic form of alpha-synuclein and its mechanism of neurotoxicity in Parkinson's disease. Biochemistry 2003;42:7871–8. doi:10.1021/bi030086j.
- [20] Maroteaux L, Scheller RH. The rat brain synucleins; family of proteins transiently associated with neuronal membrane. Molecular Brain Research 1991;11:335–43. doi:10.1016/0169-328X(91)90043-W.
- [21] Maroteaux L, Campanelli JT, Scheller RH. Synuclein: a neuron-specific protein localized to the nucleus and presynaptic nerve terminal. J Neurosci 1988;8:2804–15.
- [22] Nakajo S, Omata K, Aiuchi T, Shibayama T, Okahashi I, Ochiai H, et al. Purification and Characterization of a Novel Brain-Specific 14-kDa Protein. Journal of Neurochemistry 1990;55:2031–8. doi:10.1111/j.1471-4159.1990.tb05792.x.
- [23] Shibayama-Imazu T, Okahashi I, Omata K, Nakajo S, Ochiai H, Nakai Y, et al. Cell and tissue distribution and developmental change of neuron specific 14 kDa protein (phosphoneuroprotein 14). Brain Res 1993;622:17–25.
- [24] Jakes R, Spillantini MG, Goedert M. Identification of two distinct synucleins from human brain. FEBS Letters 1994;345:27–32. doi:10.1016/0014-5793(94)00395-5.
- [25] Uéda K, Fukushima H, Masliah E, Xia Y, Iwai A, Yoshimoto M, et al. Molecular cloning of cDNA encoding an unrecognized component of amyloid in Alzheimer disease. PNAS 1993;90:11282–6.
- [26] George JM, Jin H, Woods WS, Clayton DF. Characterization of a novel protein regulated during the critical period for song learning in the zebra finch. Neuron 1995;15:361–72. doi:10.1016/0896-6273(95)90040-3.

- [27] Hashimoto M, Rockenstein E, Mante M, Mallory M, Masliah E. beta-Synuclein inhibits alpha-synuclein aggregation: a possible role as an anti-parkinsonian factor. *Neuron* 2001;32:213–23.
- [28] Sung Y-H, Eliezer D. Residual structure, backbone dynamics, and interactions within the synuclein family. *Journal of Molecular Biology* 2007;372:689–707.
- [29] George J. The synucleins. *Genome Biology* 2001;3. doi:10.1186/gb-2001-3-1-reviews3002.
- [30] Lavedan C, Leroy E, Dehejia A, Buchholtz S, Dutra A, Nussbaum RL, et al. Identification, localization and characterization of the human gamma-synuclein gene. *Hum Genet* 1998;103:106–12.
- [31] Goedert M. Alpha-synuclein and neurodegenerative diseases. *Nat Rev Neurosci* 2001;2:492–501. doi:10.1038/35081564.
- [32] Uversky VN, Li J, Souillac P, Millett IS, Doniach S, Jakes R, et al. Biophysical properties of the synucleins and their propensities to fibrillate: inhibition of alpha-synuclein assembly by beta- and gamma-synucleins. *J Biol Chem* 2002;277:11970–8. doi:10.1074/jbc.M109541200.
- [33] Ahmad M, Attoub S, Singh MN, Martin FL, El-Agnaf OMA. Gamma-synuclein and the progression of cancer. *FASEB J* 2007;21:3419–30. doi:10.1096/fj.07-8379rev.
- [34] Segrest JP, Jackson RL, Morrisett JD, Gotto AM. A molecular theory of lipid-protein interactions in the plasma lipoproteins. *FEBS Lett* 1974;38:247–58.
- [35] Segrest JP, De Loof H, Dohlman JG, Brouillette CG, Anantharamaiah GM. Amphipathic helix motif: classes and properties. *Proteins* 1990;8:103–17. doi:10.1002/prot.340080202.
- [36] Segrest JP, Jones MK, Loof HD, Brouillette CG, Venkatachalapathi YV, Anantharamaiah GM. The amphipathic helix in the exchangeable apolipoproteins: a review of secondary structure and function. *J Lipid Res* 1992;33:141–66.

- [37] Irizarry MC, Kim TW, McNamara M, Tanzi RE, George JM, Clayton DF, et al. Characterization of the precursor protein of the non-A beta component of senile plaques (NACP) in the human central nervous system. *J Neuropathol Exp Neurol* 1996;55:889–95.
- [38] Kahle PJ, Neumann M, Ozmen L, Müller V, Jacobsen H, Schindzielorz A, et al. Subcellular Localization of Wild-Type and Parkinson's Disease-Associated Mutant  $\alpha$ -Synuclein in Human and Transgenic Mouse Brain. *J Neurosci* 2000;20:6365–73.
- [39] Jensen PH, Nielsen MS, Jakes R, Dotti CG, Goedert M. Binding of alpha-synuclein to brain vesicles is abolished by familial Parkinson's disease mutation. *J Biol Chem* 1998;273:26292–4.
- [40] Weinreb PH, Zhen W, Poon AW, Conway KA, Lansbury PT Jr. NACP, a protein implicated in Alzheimer's disease and learning, is natively unfolded. *Biochemistry* 1996;35:13709–15. doi:10.1021/bi961799n.
- [41] Kim J. Evidence that the Precursor Protein of Non-A $\beta$  Component of Alzheimer's Disease Amyloid (NACP) Has an Extended Structure Primarily Composed of Random-coil. *The Korean Society for Molecular and Cellular Biology* 1997:78–83.
- [42] Eliezer D, Kutluay E, Bussell R, Browne G. Conformational properties of  $\alpha$ -synuclein in its free and lipid-associated states. *Journal of Molecular Biology* 2001;307:1061–73. doi:10.1006/jmbi.2001.4538.
- [43] Bussell R, Eliezer D. Residual structure and dynamics in Parkinson's disease-associated mutants of alpha-synuclein. *J Biol Chem* 2001;276:45996–6003. doi:10.1074/jbc.M106777200.
- [44] Rospigliosi CC, McClendon S, Schmid AW, Ramlall TF, Barré P, Lashuel HA, et al. E46K Parkinson's-Linked Mutation Enhances C-Terminal-to-N-Terminal Contacts in  $\alpha$ -Synuclein. *Journal of Molecular Biology* 2009;388:1022–32. doi:10.1016/j.jmb.2009.03.065.

- [45] Wu K-P, Kim S, Fela DA, Baum J. Characterization of conformational and dynamic properties of natively unfolded human and mouse alpha-synuclein ensembles by NMR: implication for aggregation. *J Mol Biol* 2008;378:1104–15. doi:10.1016/j.jmb.2008.03.017.
- [46] Kang L, Janowska MK, Moriarty GM, Baum J. Mechanistic insight into the relationship between N-terminal acetylation of  $\alpha$ -synuclein and fibril formation rates by NMR and fluorescence. *PLoS ONE* 2013;8:e75018. doi:10.1371/journal.pone.0075018.
- [47] Dedmon MM, Lindorff-Larsen K, Christodoulou J, Vendruscolo M, Dobson CM. Mapping long-range interactions in alpha-synuclein using spin-label NMR and ensemble molecular dynamics simulations. *J Am Chem Soc* 2005;127:476–7. doi:10.1021/ja044834j.
- [48] Bertocini CW, Jung Y-S, Fernandez CO, Hoyer W, Griesinger C, Jovin TM, et al. Release of long-range tertiary interactions potentiates aggregation of natively unstructured alpha-synuclein. *Proc Natl Acad Sci USA* 2005;102:1430–5. doi:10.1073/pnas.0407146102.
- [49] Bertocini CW, Fernandez CO, Griesinger C, Jovin TM, Zweckstetter M. Familial mutants of alpha-synuclein with increased neurotoxicity have a destabilized conformation. *J Biol Chem* 2005;280:30649–52. doi:10.1074/jbc.C500288200.
- [50] Choi W, Zibae S, Jakes R, Serpell LC, Davletov B, Anthony Crowther R, et al. Mutation E46K increases phospholipid binding and assembly into filaments of human  $\alpha$ -synuclein. *FEBS Letters* 2004;576:363–8. doi:10.1016/j.febslet.2004.09.038.
- [51] Conway KA, Lee SJ, Rochet JC, Ding TT, Williamson RE, Lansbury PT. Acceleration of oligomerization, not fibrillization, is a shared property of both alpha-synuclein mutations linked to early-onset Parkinson's disease: implications for pathogenesis and therapy. *Proc Natl Acad Sci USA* 2000;97:571–6.
- [52] Der-Sarkissian A, Jao CC, Chen J, Langen R. Structural Organization of  $\alpha$ -Synuclein Fibrils Studied by Site-directed Spin

Labeling. *J Biol Chem* 2003;278:37530–5.  
doi:10.1074/jbc.M305266200.

- [53] Vilar M, Chou H-T, Lührs T, Maji S, Riek-Loher D, Verel R, et al. The fold of alpha-synuclein fibrils. *Proceedings of the National Academy of Sciences of the United States of America* 2008;105:8637–42. doi:10.1073/pnas.0712179105.
- [54] McNulty BC, Young GB, Pielak GJ. Macromolecular Crowding in the *Escherichia coli* Periplasm Maintains  $\alpha$ -Synuclein Disorder. *Journal of Molecular Biology* 2006;355:893–7. doi:10.1016/j.jmb.2005.11.033.
- [55] Davidson WS, Jonas A, Clayton DF, George JM. Stabilization of alpha-synuclein secondary structure upon binding to synthetic membranes. *J Biol Chem* 1998;273:9443–9.
- [56] Perrin RJ, Woods WS, Clayton DF, George JM. Interaction of human alpha-Synuclein and Parkinson's disease variants with phospholipids. Structural analysis using site-directed mutagenesis. *J Biol Chem* 2000;275:34393–8. doi:10.1074/jbc.M004851200.
- [57] Jo E, McLaurin J, Yip CM, George-Hyslop PS, Fraser PE.  $\alpha$ -Synuclein Membrane Interactions and Lipid Specificity. *J Biol Chem* 2000;275:34328–34. doi:10.1074/jbc.M004345200.
- [58] Bussell R Jr, Eliezer D. Effects of Parkinson's disease-linked mutations on the structure of lipid-associated alpha-synuclein. *Biochemistry* 2004;43:4810–8. doi:10.1021/bi036135+.
- [59] Nuscher B, Kamp F, Mehnert T, Odoy S, Haass C, Kahle P, et al. Alpha-synuclein has a high affinity for packing defects in a bilayer membrane: a thermodynamics study. *The Journal of Biological Chemistry* 2004;279:21966–75. doi:10.1074/jbc.M401076200.
- [60] Rhoades E, Ramlall T, Webb W, Eliezer D. Quantification of alpha-synuclein binding to lipid vesicles using fluorescence correlation spectroscopy. *Biophysical Journal* 2006;90:4692–700. doi:10.1529/biophysj.105.079251.

- [61] Middleton ER, Rhoades E. Effects of curvature and composition on  $\alpha$ -synuclein binding to lipid vesicles. *Biophys J* 2010;99:2279–88. doi:10.1016/j.bpj.2010.07.056.
- [62] Pranke I, Morello V, Bigay J, Gibson K, Verbavatz J-M, Antonny B, et al.  $\alpha$ -Synuclein and ALPS motifs are membrane curvature sensors whose contrasting chemistry mediates selective vesicle binding. *The Journal of Cell Biology* 2011;194:89–103. doi:10.1083/jcb.201011118.
- [63] Kamp F, Beyer K. Binding of alpha-synuclein affects the lipid packing in bilayers of small vesicles. *J Biol Chem* 2006;281:9251–9. doi:10.1074/jbc.M512292200.
- [64] Bigay J, Antonny B. Curvature, lipid packing, and electrostatics of membrane organelles: defining cellular territories in determining specificity. *Dev Cell* 2012;23:886–95. doi:10.1016/j.devcel.2012.10.009.
- [65] Lee H-J, Choi C, Lee S-J. Membrane-bound alpha-synuclein has a high aggregation propensity and the ability to seed the aggregation of the cytosolic form. *J Biol Chem* 2002;277:671–8. doi:10.1074/jbc.M107045200.
- [66] Cole NB, Murphy DD, Grider T, Rueter S, Brasaemle D, Nussbaum RL. Lipid droplet binding and oligomerization properties of the Parkinson's disease protein alpha-synuclein. *J Biol Chem* 2002;277:6344–52. doi:10.1074/jbc.M108414200.
- [67] Outeiro TF, Lindquist S. Yeast Cells Provide Insight into Alpha-Synuclein Biology and Pathobiology. *Science* 2003;302:1772–5. doi:10.1126/science.1090439.
- [68] Cooper AA, Gitler AD, Cashikar A, Haynes CM, Hill KJ, Bhullar B, et al. Alpha-synuclein blocks ER-Golgi traffic and Rab1 rescues neuron loss in Parkinson's models. *Science* 2006;313:324–8. doi:10.1126/science.1129462.
- [69] Nemani VM, Lu W, Berge V, Nakamura K, Onoa B, Lee MK, et al. Increased expression of alpha-synuclein reduces neurotransmitter release by inhibiting synaptic vesicle

reclustering after endocytosis. *Neuron* 2010;65:66–79.  
doi:10.1016/j.neuron.2009.12.023.

- [70] Rozek A, Sparrow JT, Weisgraber KH, Cushley RJ. Conformation of human apolipoprotein C-I in a lipid-mimetic environment determined by CD and NMR spectroscopy. *Biochemistry* 1999;38:14475–84.
- [71] Bussell R, Eliezer D. A Structural and Functional Role for 11-mer Repeats in  $\alpha$ -Synuclein and Other Exchangeable Lipid Binding Proteins. *Journal of Molecular Biology* 2003;329:763–78. doi:10.1016/S0022-2836(03)00520-5.
- [72] Chandra S, Chen X, Rizo J, Jahn R, Südhof TC. A broken alpha-helix in folded alpha-Synuclein. *J Biol Chem* 2003;278:15313–8. doi:10.1074/jbc.M213128200.
- [73] Bisaglia M, Tessari I, Pinato L, Bellanda M, Giraudo S, Fasano M, et al. A topological model of the interaction between alpha-synuclein and sodium dodecyl sulfate micelles. *Biochemistry* 2005;44:329–39. doi:10.1021/bi048448q.
- [74] Ulmer T, Bax A, Cole N, Nussbaum R. Structure and Dynamics of Micelle-bound Human  $\alpha$ -Synuclein. *Journal of Biological Chemistry* 2005;280:9595–603. doi:10.1074/jbc.M411805200.
- [75] Bussell R, Ramlall TF, Eliezer D. Helix periodicity, topology, and dynamics of membrane-associated alpha-synuclein. *Protein Science* 2005;14:862–72. doi:10.1110/ps.041255905.
- [76] Jao CC, Der-Sarkissian A, Chen J, Langen R. Structure of membrane-bound  $\alpha$ -synuclein studied by site-directed spin labeling. *PNAS* 2004;101:8331–6. doi:10.1073/pnas.0400553101.
- [77] Jao CC, Hegde BG, Chen J, Haworth IS, Langen R. Structure of membrane-bound alpha-synuclein from site-directed spin labeling and computational refinement. *Proc Natl Acad Sci USA* 2008;105:19666–71. doi:10.1073/pnas.0807826105.
- [78] Borbat P, Ramlall TF, Freed JH, Eliezer D. Inter-helix distances in lysophospholipid micelle-bound alpha-synuclein from pulsed

ESR measurements. *J Am Chem Soc* 2006;128:10004–5.  
doi:10.1021/ja063122l.

- [79] Georgieva E, Ramlall T, Borbat P, Freed J, Eliezer D. Membrane-Bound  $\alpha$ -Synuclein Forms an Extended Helix: Long-Distance Pulsed ESR Measurements Using Vesicles, Bicelles, and Rodlike Micelles. *Journal of the American Chemical Society* 2008;130:12856–7. doi:10.1021/ja804517m.
- [80] Ferreon ACM, Gambin Y, Lemke EA, Deniz AA. Interplay of alpha-synuclein binding and conformational switching probed by single-molecule fluorescence. *Proc Natl Acad Sci USA* 2009;106:5645–50. doi:10.1073/pnas.0809232106.
- [81] Trexler A, Rhoades E.  $\alpha$ -Synuclein Binds Large Unilamellar Vesicles as an Extended Helix. *Biochemistry* 2009;48:2304–6. doi:10.1021/bi900114z.
- [82] Bortolus M, Tombolato F, Tessari I, Bisaglia M, Mammi S, Bubacco L, et al. Broken Helix in Vesicle and Micelle-Bound  $\alpha$ -Synuclein: Insights from Site-Directed Spin Labeling-EPR Experiments and MD Simulations. *J Am Chem Soc* 2008;130:6690–1. doi:10.1021/ja8010429.
- [83] Drescher M, Godschalk F, Veldhuis G, van Rooijen BD, Subramaniam V, Huber M. Spin-Label EPR on  $\alpha$ -Synuclein Reveals Differences in the Membrane Binding Affinity of the Two Antiparallel Helices. *ChemBioChem* 2008;9:2411–6. doi:10.1002/cbic.200800238.
- [84] Georgieva E, Ramlall T, Borbat P, Freed J, Eliezer D. The lipid-binding domain of wild type and mutant alpha-synuclein: compactness and interconversion between the broken and extended helix forms. *The Journal of Biological Chemistry* 2010;285:28261–74. doi:10.1074/jbc.M110.157214.
- [85] Necula M, Chirita CN, Kuret J. Rapid anionic micelle-mediated alpha-synuclein fibrillization in vitro. *J Biol Chem* 2003;278:46674–80. doi:10.1074/jbc.M308231200.

- [86] Mizuno N, Varkey J, Kegulian N, Hegde B, Cheng N, Langen R, et al. Remodeling of Lipid Vesicles into Cylindrical Micelles by  $\alpha$ -Synuclein in an Extended  $\alpha$ -Helical Conformation. *J Biol Chem* 2012;287:29301–11. doi:10.1074/jbc.M112.365817.
- [87] Varkey J, Mizuno N, Hegde BG, Cheng N, Steven AC, Langen R.  $\alpha$ -Synuclein Oligomers with Broken Helical Conformation Form Lipoprotein Nanoparticles. *J Biol Chem* 2013;288:17620–30. doi:10.1074/jbc.M113.476697.
- [88] Ouberai MM, Wang J, Swann MJ, Galvagnion C, Guilliams T, Dobson CM, et al.  $\alpha$ -Synuclein Senses Lipid Packing Defects and Induces Lateral Expansion of Lipids Leading to Membrane Remodeling. *J Biol Chem* 2013;288:20883–95. doi:10.1074/jbc.M113.478297.
- [89] Varkey J, Isas JM, Mizuno N, Jensen MB, Bhatia VK, Jao CC, et al. Membrane curvature induction and tubulation are common features of synucleins and apolipoproteins. *J Biol Chem* 2010;285:32486–93. doi:10.1074/jbc.M110.139576.
- [90] Eliezer D. Protein folding and aggregation in in vitro models of Parkinson's Disease: Structure and function of alpha-synuclein. In: Nass R, Przedborski S, editors. *Parkinson's Disease: molecular and therapeutic insights from model systems*. 1st ed., Academic Press; 2008, p. 575–95.
- [91] Bodner C, Dobson C, Bax A. Multiple tight phospholipid-binding modes of alpha-synuclein revealed by solution NMR spectroscopy. *Journal of Molecular Biology* 2009;390:775–90. doi:10.1016/j.jmb.2009.05.066.
- [92] Bodner C, Maltsev A, Dobson C, Bax A. Differential phospholipid binding of alpha-synuclein variants implicated in Parkinson's disease revealed by solution NMR spectroscopy. *Biochemistry* 2010;49:862–71. doi:10.1021/bi901723p.
- [93] Lokappa SB, Ulmer TS. Alpha-synuclein populates both elongated and broken helix states on small unilamellar vesicles. *J Biol Chem* 2011;286:21450–7. doi:10.1074/jbc.M111.224055.

- [94] Munishkina LA, Phelan C, Uversky VN, Fink AL. Conformational Behavior and Aggregation of  $\alpha$ -Synuclein in Organic Solvents: Modeling the Effects of Membranes†. *Biochemistry* 2003;42:2720–30. doi:10.1021/bi027166s.
- [95] Anderson V, Ramlall T, Rospigliosi C, Webb W, Eliezer D. Identification of a helical intermediate in trifluoroethanol-induced alpha-synuclein aggregation. *Proceedings of the National Academy of Sciences of the United States of America* 2010;107:18850–5. doi:10.1073/pnas.1012336107.
- [96] Fusco G, De Simone A, Gopinath T, Vostrikov V, Vendruscolo M, Dobson CM, et al. Direct observation of the three regions in  $\alpha$ -synuclein that determine its membrane-bound behaviour. *Nat Commun* 2014;5:3827. doi:10.1038/ncomms4827.
- [97] Uversky VN, Li J, Fink AL. Evidence for a partially folded intermediate in alpha-synuclein fibril formation. *J Biol Chem* 2001;276:10737–44. doi:10.1074/jbc.M010907200.
- [98] Uversky VN, Li J, Fink AL. Pesticides directly accelerate the rate of  $\alpha$ -synuclein fibril formation: a possible factor in Parkinson's disease. *FEBS Letters* 2001;500:105–8. doi:10.1016/S0014-5793(01)02597-2.
- [99] Uversky VN, Li J, Fink AL. Metal-triggered Structural Transformations, Aggregation, and Fibrillation of Human  $\alpha$ -Synuclein A POSSIBLE MOLECULAR LINK BETWEEN PARKINSON'S DISEASE AND HEAVY METAL EXPOSURE. *J Biol Chem* 2001;276:44284–96. doi:10.1074/jbc.M105343200.
- [100] Uversky VN, Lee HJ, Li J, Fink AL, Lee SJ. Stabilization of partially folded conformation during alpha-synuclein oligomerization in both purified and cytosolic preparations. *J Biol Chem* 2001;276:43495–8. doi:10.1074/jbc.C100551200.
- [101] Ptitsyn OB, Bychkova VE, Uversky VN. Kinetic and Equilibrium Folding Intermediates. *Phil Trans R Soc Lond B* 1995;348:35–41. doi:10.1098/rstb.1995.0043.

- [102] Bychkova VE, Dujsekina AE, Klenin SI, Tiktopulo EI, Uversky VN, Ptitsyn OB. Molten Globule-Like State of Cytochrome c under Conditions Simulating Those Near the Membrane Surface†. *Biochemistry* 1996;35:6058–63. doi:10.1021/bi9522460.
- [103] Perrin RJ, Woods WS, Clayton DF, George JM. Exposure to Long Chain Polyunsaturated Fatty Acids Triggers Rapid Multimerization of Synucleins. *J Biol Chem* 2001;276:41958–62. doi:10.1074/jbc.M105022200.
- [104] Jo E, Darabie AA, Han K, Tandon A, Fraser PE, McLaurin J. alpha-Synuclein-synaptosomal membrane interactions: implications for fibrillogenesis. *Eur J Biochem* 2004;271:3180–9. doi:10.1111/j.1432-1033.2004.04250.x.
- [105] Narayanan V, Scarlata S. Membrane Binding and Self-Association of  $\alpha$ -Synucleins. *Biochemistry* 2001;40:9927–34. doi:10.1021/bi002952n.
- [106] Zhu M, Fink AL. Lipid binding inhibits alpha-synuclein fibril formation. *J Biol Chem* 2003;278:16873–7. doi:10.1074/jbc.M210136200.
- [107] Dikiy I, Eliezer D. Folding and misfolding of alpha-synuclein on membranes. *Biochim Biophys Acta* 2012;1818:1013–8. doi:10.1016/j.bbamem.2011.09.008.
- [108] Aisenbrey C, Borowik T, Byström R, Bokvist M, Lindström F, Misiak H, et al. How is protein aggregation in amyloidogenic diseases modulated by biological membranes? *Eur Biophys J* 2008;37:247–55. doi:10.1007/s00249-007-0237-0.
- [109] Giehm L, Oliveira CLP, Christiansen G, Pedersen JS, Otzen DE. SDS-Induced Fibrillation of  $\alpha$ -Synuclein: An Alternative Fibrillation Pathway. *Journal of Molecular Biology* 2010;401:115–33. doi:10.1016/j.jmb.2010.05.060.
- [110] Rivers R, Kumita J, Tartaglia GG, Dedmon M, Pawar A, Vendruscolo M, et al. Molecular determinants of the aggregation behavior of alpha- and beta-synuclein. *Protein Science : A*

Publication of the Protein Society 2008;17:887–98.  
doi:10.1110/ps.073181508.

- [111] Ahmad MF, Ramakrishna T, Raman B, Rao CM. Fibrillogenic and non-fibrillogenic ensembles of SDS-bound human alpha-synuclein. *J Mol Biol* 2006;364:1061–72.  
doi:10.1016/j.jmb.2006.09.085.
- [112] Bartels T, Ahlstrom LS, Leftin A, Kamp F, Haass C, Brown MF, et al. The N-Terminus of the Intrinsically Disordered Protein  $\alpha$ -Synuclein Triggers Membrane Binding and Helix Folding. *Biophysical Journal* 2010;99:2116–24.  
doi:10.1016/j.bpj.2010.06.035.
- [113] Gruschus JM, Yap TL, Pistolesi S, Maltsev AS, Lee JC. NMR structure of calmodulin complexed to an N-terminally acetylated  $\alpha$ -synuclein peptide. *Biochemistry* 2013;52:3436–45.  
doi:10.1021/bi400199p.
- [114] Bartels T, Choi J, Selkoe D.  $\alpha$ -Synuclein occurs physiologically as a helically folded tetramer that resists aggregation. *Nature* 2011;477:107–10. doi:10.1038/nature10324.
- [115] Barbour R, Kling K, Anderson JP, Banducci K, Cole T, Diep L, et al. Red Blood Cells Are the Major Source of Alpha-Synuclein in Blood. *Neurodegenerative Diseases* 2008;5:55–9.  
doi:10.1159/000112832.
- [116] Scherzer C, Grass J, Liao Z, Pepivani I, Zheng B, Eklund A, et al. GATA transcription factors directly regulate the Parkinson's disease-linked gene  $\alpha$ -synuclein. *Proceedings of the National Academy of Sciences of the United States of America* 2008;105:10907–12. doi:10.1073/pnas.0802437105.
- [117] Wang W, Perovic I, Chittuluru J, Kaganovich A, Nguyen L, Liao J, et al. A soluble  $\alpha$ -synuclein construct forms a dynamic tetramer. *Proceedings of the National Academy of Sciences of the United States of America* 2011;108:17797–802.  
doi:10.1073/pnas.1113260108.

- [118] Trexler A, Rhoades E. N-Terminal acetylation is critical for forming  $\alpha$ -helical oligomer of  $\alpha$ -synuclein. *Protein Science* 2012;21:601–5. doi:10.1002/pro.2056.
- [119] Fauvet B, Mbefo M, Fares M-B, Desobry C, Michael S, Ardah M, et al.  $\alpha$ -Synuclein in Central Nervous System and from Erythrocytes, Mammalian Cells, and Escherichia coli Exists Predominantly as Disordered Monomer. *Journal of Biological Chemistry* 2012;287:15345–64. doi:10.1074/jbc.M111.318949.
- [120] Binolfi A, Theillet F-X, Selenko P. Bacterial in-cell NMR of human  $\alpha$ -synuclein: a disordered monomer by nature? *Biochem Soc Trans* 2012;40:950–4. doi:10.1042/BST20120096.
- [121] Burré J, Vivona S, Diao J, Sharma M, Brunger AT, Südhof TC. Properties of native brain  $\alpha$ -synuclein. *Nature* 2013;498:E4–6. doi:10.1038/nature12125.
- [122] Selkoe D, Dettmer U, Luth E, Kim N, Newman A, Bartels T. Defining the native state of  $\alpha$ -synuclein. *Neurodegener Dis* 2014;13:114–7. doi:10.1159/000355516.
- [123] Abeliovich A, Schmitz Y, Fariñas I, Choi-Lundberg D, Ho WH, Castillo PE, et al. Mice lacking alpha-synuclein display functional deficits in the nigrostriatal dopamine system. *Neuron* 2000;25:239–52.
- [124] Yavich L, Tanila H, Vepsäläinen S, Jäkälä P. Role of  $\alpha$ -Synuclein in Presynaptic Dopamine Recruitment. *J Neurosci* 2004;24:11165–70. doi:10.1523/JNEUROSCI.2559-04.2004.
- [125] Cabin DE, Shimazu K, Murphy D, Cole NB, Gottschalk W, McIlwain KL, et al. Synaptic Vesicle Depletion Correlates with Attenuated Synaptic Responses to Prolonged Repetitive Stimulation in Mice Lacking  $\alpha$ -Synuclein. *J Neurosci* 2002;22:8797–807.
- [126] Withers GS, George JM, Banker GA, Clayton DF. Delayed localization of synelfin (synuclein, NACP) to presynaptic terminals in cultured rat hippocampal neurons. *Developmental Brain Research* 1997;99:87–94. doi:10.1016/S0165-3806(96)00210-6.

- [127] Murphy DD, Rueter SM, Trojanowski JQ, Lee VM. Synucleins are developmentally expressed, and alpha-synuclein regulates the size of the presynaptic vesicular pool in primary hippocampal neurons. *J Neurosci* 2000;20:3214–20.
- [128] Liu S, Ninan I, Antonova I, Battaglia F, Trinchese F, Narasanna A, et al. alpha-Synuclein produces a long-lasting increase in neurotransmitter release. *EMBO J* 2004;23:4506–16. doi:10.1038/sj.emboj.7600451.
- [129] Chandra S, Fornai F, Kwon H-B, Yazdani U, Atasoy D, Liu X, et al. Double-knockout mice for  $\alpha$ - and  $\beta$ -synucleins: Effect on synaptic functions. *PNAS* 2004;101:14966–71. doi:10.1073/pnas.0406283101.
- [130] Chandra S, Gallardo G, Fernández-Chacón R, Schlüter O, Südhof T.  $\alpha$ -Synuclein Cooperates with CSP $\alpha$  in Preventing Neurodegeneration. *Cell* 2005;123:383–96. doi:10.1016/j.cell.2005.09.028.
- [131] Südhof TC. Neurotransmitter release: the last millisecond in the life of a synaptic vesicle. *Neuron* 2013;80:675–90. doi:10.1016/j.neuron.2013.10.022.
- [132] Greten-Harrison B, Polydoro M, Morimoto-Tomita M, Diao L, Williams AM, Nie EH, et al.  $\alpha\beta\gamma$ -Synuclein triple knockout mice reveal age-dependent neuronal dysfunction. *PNAS* 2010;107:19573–8. doi:10.1073/pnas.1005005107.
- [133] Burré J, Sharma M, Tsetsenis T, Buchman V, Etherton M, Südhof T.  $\alpha$ -Synuclein Promotes SNARE-Complex Assembly in Vivo and in Vitro. *Science (New York, NY)* 2010;329:1663–7. doi:10.1126/science.1195227.
- [134] Garcia-Reitböck P, Anichtchik O, Bellucci A, Iovino M, Ballini C, Fineberg E, et al. SNARE protein redistribution and synaptic failure in a transgenic mouse model of Parkinson's disease. *Brain* 2010;133:2032–44. doi:10.1093/brain/awq132.

- [135] Narita K. Isolation of acetylpeptide from enzymic digests of TMV-protein. *Biochimica et Biophysica Acta* 1958;28:184–91.  
doi:10.1016/0006-3002(58)90445-1.
- [136] Brown JL, Roberts WK. Evidence that approximately eighty per cent of the soluble proteins from Ehrlich ascites cells are Nalpha-acetylated. *J Biol Chem* 1976;251:1009–14.
- [137] Arnesen T, Van Damme P, Polevoda B, Helsen K, Evjenth R, Colaert N, et al. Proteomics analyses reveal the evolutionary conservation and divergence of N-terminal acetyltransferases from yeast and humans. *Proc Natl Acad Sci USA* 2009;106:8157–62. doi:10.1073/pnas.0901931106.
- [138] Arnesen T. Towards a Functional Understanding of Protein N-Terminal Acetylation. *PLoS Biol* 2011;9:e1001074.  
doi:10.1371/journal.pbio.1001074.
- [139] Pestana A, Pitot HC. Acetylation of nascent polypeptide chains on rat liver polyribosomes in vivo and in vitro. *Biochemistry* 1975;14:1404–12.
- [140] Polevoda B, Brown S, Cardillo TS, Rigby S, Sherman F. Yeast N(alpha)-terminal acetyltransferases are associated with ribosomes. *J Cell Biochem* 2008;103:492–508.  
doi:10.1002/jcb.21418.
- [141] Boissel JP, Kasper TJ, Bunn HF. Cotranslational amino-terminal processing of cytosolic proteins. Cell-free expression of site-directed mutants of human hemoglobin. *J Biol Chem* 1988;263:8443–9.
- [142] Polevoda B, Sherman F. Nα-terminal Acetylation of Eukaryotic Proteins. *J Biol Chem* 2000;275:36479–82.  
doi:10.1074/jbc.R000023200.
- [143] Polevoda B, Sherman F. N-terminal acetyltransferases and sequence requirements for N-terminal acetylation of eukaryotic proteins. *J Mol Biol* 2003;325:595–622.

- [144] Starheim KK, Gevaert K, Arnesen T. Protein N-terminal acetyltransferases: when the start matters. *Trends Biochem Sci* 2012;37:152–61. doi:10.1016/j.tibs.2012.02.003.
- [145] Jones JD, O'Connor CD. Protein acetylation in prokaryotes. *Proteomics* 2011;11:3012–22. doi:10.1002/pmic.201000812.
- [146] Anderson JP, Walker DE, Goldstein JM, de Laat R, Banducci K, Caccavello RJ, et al. Phosphorylation of Ser-129 is the dominant pathological modification of alpha-synuclein in familial and sporadic Lewy body disease. *J Biol Chem* 2006;281:29739–52. doi:10.1074/jbc.M600933200.
- [147] Zabrocki P, Bastiaens I, Delay C, Bammens T, Ghillebert R, Pellens K, et al. Phosphorylation, lipid raft interaction and traffic of alpha-synuclein in a yeast model for Parkinson. *Biochimica et Biophysica Acta* 2008;1783:1767–80. doi:10.1016/j.bbamcr.2008.06.010.
- [148] Fischer EH, Krebs EG. CONVERSION OF PHOSPHORYLASE b TO PHOSPHORYLASE a IN MUSCLE EXTRACTS. *J Biol Chem* 1955;216:121–32.
- [149] Olsen JV, Blagoev B, Gnäd F, Macek B, Kumar C, Mortensen P, et al. Global, In Vivo, and Site-Specific Phosphorylation Dynamics in Signaling Networks. *Cell* 2006;127:635–48. doi:10.1016/j.cell.2006.09.026.
- [150] Hunter T. Why nature chose phosphate to modify proteins. *Phil Trans R Soc B* 2012;367:2513–6. doi:10.1098/rstb.2012.0013.
- [151] Nussinov R, Tsai C-J, Xin F, Radivojac P. Allosteric post-translational modification codes. *Trends Biochem Sci* 2012;37:447–55. doi:10.1016/j.tibs.2012.07.001.
- [152] Hejjaoui M, Butterfield S, Fauvet B, Vercruyse F, Cui J, Dikiy I, et al. Elucidating the Role of C-Terminal Post-Translational Modifications Using Protein Semisynthesis Strategies:  $\alpha$ -Synuclein Phosphorylation at Tyrosine 125. *Journal of the American Chemical Society* 2012;134:5196–210.

- [153] Mbefo MK, Paleologou KE, Boucharaba A, Oueslati A, Schell H, Fournier M, et al. Phosphorylation of synucleins by members of the Polo-like kinase family. *J Biol Chem* 2010;285:2807–22. doi:10.1074/jbc.M109.081950.
- [154] Paleologou K, Oueslati A, Shakked G, Rospigliosi C, Kim H-Y, Lamberto G, et al. Phosphorylation at S87 is enhanced in synucleinopathies, inhibits alpha-synuclein oligomerization, and influences synuclein-membrane interactions. *The Journal of Neuroscience* 2010;30:3184–98. doi:10.1523/JNEUROSCI.5922-09.2010.
- [155] Paleologou K, Schmid A, Rospigliosi C, Kim H-Y, Lamberto G, Fredenburg R, et al. Phosphorylation at Ser-129 but Not the Phosphomimics S129E/D Inhibits the Fibrillation of  $\alpha$ -Synuclein. *Journal of Biological Chemistry* 2008;283:16895–905. doi:10.1074/jbc.M800747200.
- [156] Basso E, Antas P, Marijanovic Z, Gonçalves S, Tenreiro S, Outeiro TF. PLK2 modulates  $\alpha$ -synuclein aggregation in yeast and mammalian cells. *Mol Neurobiol* 2013;48:854–62. doi:10.1007/s12035-013-8473-z.
- [157] Muntané G, Ferrer I, Martinez-Vicente M.  $\alpha$ -synuclein phosphorylation and truncation are normal events in the adult human brain. *Neuroscience* 2012;200:106–19. doi:10.1016/j.neuroscience.2011.10.042.
- [158] Fujiwara H, Hasegawa M, Dohmae N, Kawashima A, Masliah E, Goldberg MS, et al.  $\alpha$ -Synuclein is phosphorylated in synucleinopathy lesions. *Nat Cell Biol* 2002;4:160–4. doi:10.1038/ncb748.
- [159] Okochi M, Walter J, Koyama A, Nakajo S, Baba M, Iwatsubo T, et al. Constitutive Phosphorylation of the Parkinson's Disease Associated  $\alpha$ -Synuclein. *J Biol Chem* 2000;275:390–7. doi:10.1074/jbc.275.1.390.
- [160] Smith WW, Margolis RL, Li X, Troncoso JC, Lee MK, Dawson VL, et al.  $\alpha$ -Synuclein Phosphorylation Enhances Eosinophilic

Cytoplasmic Inclusion Formation in SH-SY5Y Cells. *J Neurosci* 2005;25:5544–52. doi:10.1523/JNEUROSCI.0482-05.2005.

- [161] Kim EJ, Sung JY, Lee HJ, Rhim H, Hasegawa M, Iwatsubo T, et al. Dyrk1A phosphorylates alpha-synuclein and enhances intracellular inclusion formation. *J Biol Chem* 2006;281:33250–7. doi:10.1074/jbc.M606147200.
- [162] Nakamura T, Yamashita H, Takahashi T, Nakamura S. Activated Fyn Phosphorylates  $\alpha$ -Synuclein at Tyrosine Residue 125. *Biochemical and Biophysical Research Communications* 2001;280:1085–92. doi:10.1006/bbrc.2000.4253.
- [163] Ellis CE, Schwartzberg PL, Grider TL, Fink DW, Nussbaum RL.  $\alpha$ -Synuclein Is Phosphorylated by Members of the Src Family of Protein-tyrosine Kinases. *J Biol Chem* 2001;276:3879–84. doi:10.1074/jbc.M010316200.
- [164] Negro A, Brunati AM, Donella-Deana A, Massimino ML, Pinna LA. Multiple phosphorylation of alpha-synuclein by protein tyrosine kinase Syk prevents eosin-induced aggregation. *FASEB J* 2002;16:210–2. doi:10.1096/fj.01-0517fje.
- [165] Chen L, Periquet M, Wang X, Negro A, McLean PJ, Hyman BT, et al. Tyrosine and serine phosphorylation of  $\alpha$ -synuclein have opposing effects on neurotoxicity and soluble oligomer formation. *Journal of Clinical Investigation* 2009. doi:10.1172/JCI39088.
- [166] Appel-Cresswell S, Vilarino-Guell C, Encarnacion M, Sherman H, Yu I, Shah B, et al. Alpha-synuclein p.H50Q, a novel pathogenic mutation for Parkinson's disease. *Mov Disord* 2013;28:811–3. doi:10.1002/mds.25421.
- [167] Lesage S, Anheim M, Letournel F, Bousset L, Honoré A, Rozas N, et al. G51D  $\alpha$ -synuclein mutation causes a novel parkinsonian-pyramidal syndrome. *Ann Neurol* 2013;73:459–71. doi:10.1002/ana.23894.
- [168] Johnson M, Coulton A, Geeves M, Mulvihill D. Targeted Amino-Terminal Acetylation of Recombinant Proteins in *E. coli*. *PLoS ONE* 2010;5:e15801. doi:10.1371/journal.pone.0015801.

- [169] Johnson M, Geeves MA, Mulvihill DP. Production of amino-terminally acetylated recombinant proteins in *E. coli*. *Methods Mol Biol* 2013;981:193–200. doi:10.1007/978-1-62703-305-3\_15.
- [170] Marley J, Lu M, Bracken C. A method for efficient isotopic labeling of recombinant proteins. *J Biomol NMR* 2001;20:71–5.
- [171] Schindelin J, Arganda-Carreras I, Frise E, Kaynig V, Longair M, Pietzsch T, et al. Fiji: an open-source platform for biological-image analysis. *Nat Meth* 2012;9:676–82. doi:10.1038/nmeth.2019.
- [172] McClendon S, Rospigliosi CC, Eliezer D. Charge neutralization and collapse of the C-terminal tail of alpha-synuclein at low pH. *Protein Sci* 2009;18:1531–40. doi:10.1002/pro.149.
- [173] Bax A, Ikura M, Kay LE, Torchia DA, Tschudin R. Comparison of different modes of two-dimensional reverse-correlation NMR for the study of proteins. *Journal of Magnetic Resonance (1969)* 1990;86:304–18. doi:10.1016/0022-2364(90)90262-8.
- [174] Delaglio F, Grzesiek S, Vuister GW, Zhu G, Pfeifer J, Bax A. NMRPipe: a multidimensional spectral processing system based on UNIX pipes. *J Biomol NMR* 1995;6:277–93.
- [175] Johnson BA, Blevins RA. NMR View: A computer program for the visualization and analysis of NMR data. *J Biomol NMR* 1994;4:603–14. doi:10.1007/BF00404272.
- [176] Snead D, Wragg RT, Dittman JS, Eliezer D. Membrane curvature sensing by the C-terminal domain of complexin. *Nat Commun* 2014;5:4955. doi:10.1038/ncomms5955.
- [177] Pfefferkorn CM, Lee JC. Tryptophan probes at the alpha-synuclein and membrane interface. *J Phys Chem B* 2010;114:4615–22. doi:10.1021/jp908092e.
- [178] Barnes C, Monteith W, Pielak G. Internal and global protein motion assessed with a fusion construct and in-cell NMR spectroscopy. *Chembiochem : A European Journal of Chemical Biology* 2011;12:390–1. doi:10.1002/cbic.201000610.

- [179] Bax A, Ikura M. An efficient 3D NMR technique for correlating the proton and <sup>15</sup>N backbone amide resonances with the alpha-carbon of the preceding residue in uniformly <sup>15</sup>N/<sup>13</sup>C enriched proteins. *J Biomol NMR* 1991;1:99–104.
- [180] Kay LE, Ikura M, Tschudin R, Bax A. Three-dimensional triple-resonance NMR spectroscopy of isotopically enriched proteins. *Journal of Magnetic Resonance (1969)* 1990;89:496–514. doi:10.1016/0022-2364(90)90333-5.
- [181] Clubb RT, Thanabal V, Wagner G. A constant-time three-dimensional triple-resonance pulse scheme to correlate intraresidue <sup>1</sup>HN, <sup>15</sup>N, and <sup>13</sup>C' chemical shifts in <sup>15</sup>N,<sup>13</sup>C-labelled proteins. *J Magn Res* 1992;97:213–7. doi:10.1016/0022-2364(92)90252-3.
- [182] Grzesiek S, Bax A. Correlating backbone amide and side chain resonances in larger proteins by multiple relayed triple resonance NMR. *J Am Chem Soc* 1992;114:6291–3. doi:10.1021/ja00042a003.
- [183] Hoffman RC, Moy FJ, Price V, Richardson J, Kaubisch D, Frieden EA, et al. Resonance assignments for Oncostatin M, a 24-kDa alpha-helical protein. *J Biomol NMR* 1996;7:273–82.
- [184] Kjaergaard M, Poulsen FM. Sequence correction of random coil chemical shifts: correlation between neighbor correction factors and changes in the Ramachandran distribution. *J Biomol NMR* 2011;50:157–65. doi:10.1007/s10858-011-9508-2.
- [185] Kjaergaard M, Brander S, Poulsen FM. Random coil chemical shift for intrinsically disordered proteins: effects of temperature and pH. *J Biomol NMR* 2011;49:139–49. doi:10.1007/s10858-011-9472-x.
- [186] Wishart DS, Sykes BD, Richards FM. Relationship between nuclear magnetic resonance chemical shift and protein secondary structure. *Journal of Molecular Biology* 1991;222:311–33. doi:10.1016/0022-2836(91)90214-Q.

- [187] Wüthrich K. *NMR of Proteins and Nucleic Acids*. 1 edition. New York: Wiley-Interscience; 1986.
- [188] Zhang O, Forman-Kay JD, Shortle D, Kay LE. Triple-resonance NOESY-based experiments with improved spectral resolution: applications to structural characterization of unfolded, partially folded and folded proteins. *J Biomol NMR* 1997;9:181–200.
- [189] Grzesiek S, Wingfield P, Stahl S, Kaufman JD, Bax A. Four-Dimensional <sup>15</sup>N-Separated NOESY of Slowly Tumbling Perdeuterated <sup>15</sup>N-Enriched Proteins. Application to HIV-1 Nef. *J Am Chem Soc* 1995;117:9594–5. doi:10.1021/ja00142a040.
- [190] Eliezer D, Chung J, Dyson HJ, Wright PE. Native and Non-native Secondary Structure and Dynamics in the pH 4 Intermediate of Apomyoglobin†. *Biochemistry* 2000;39:2894–901. doi:10.1021/bi992545f.
- [191] Palmer AG, Skelton NJ, Chazin WJ, Wright PE, Rance M. Suppression of the effects of cross-correlation between dipolar and anisotropic chemical shift relaxation mechanisms in the measurement of spin-spin relaxation rates. *Molecular Physics* 1992;75:699–711. doi:10.1080/00268979200100511.
- [192] Clore GM, Tang C, Iwahara J. Elucidating transient macromolecular interactions using paramagnetic relaxation enhancement. *Curr Opin Struct Biol* 2007;17:603–16. doi:10.1016/j.sbi.2007.08.013.
- [193] Donaldson LW, Skrynnikov NR, Choy WY, Muhandiram DR, Sarkar B, Forman-Kay JD, et al. Structural characterization of proteins with an attached ATCUN motif by paramagnetic relaxation enhancement NMR spectroscopy. *J Am Chem Soc* 2001;123:9843–7.
- [194] Eliezer D. Distance information for disordered proteins from NMR and ESR measurements using paramagnetic spin labels. *Methods Mol Biol* 2012;895:127–38. doi:10.1007/978-1-61779-927-3\_10.

- [195] Chou JJ, Baber JL, Bax A. Characterization of phospholipid mixed micelles by translational diffusion. *J Biomol NMR* 2004;29:299–308. doi:10.1023/B:JNMR.0000032560.43738.6a.
- [196] Wu DH, Chen AD, Johnson CS. An Improved Diffusion-Ordered Spectroscopy Experiment Incorporating Bipolar-Gradient Pulses. *Journal of Magnetic Resonance, Series A* 1995;115:260–4. doi:10.1006/jmra.1995.1176.
- [197] Ferrage F, Zoonens M, Warschawski DE, Popot J-L, Bodenhausen G. Slow diffusion of macromolecular assemblies by a new pulsed field gradient NMR method. *J Am Chem Soc* 2003;125:2541–5. doi:10.1021/ja0211407.
- [198] Wilkins DK, Grimshaw SB, Receveur V, Dobson CM, Jones JA, Smith LJ. Hydrodynamic Radii of Native and Denatured Proteins Measured by Pulse Field Gradient NMR Techniques†. *Biochemistry* 1999;38:16424–31. doi:10.1021/bi991765q.
- [199] Holz M, Weingartner H. Calibration in accurate spin-echo self-diffusion measurements using <sup>1</sup>H and less-common nuclei. *Journal of Magnetic Resonance (1969)* 1991;92:115–25. doi:10.1016/0022-2364(91)90252-O.
- [200] Sreerama N, Woody RW. Computation and analysis of protein circular dichroism spectra. *Meth Enzymol* 2004;383:318–51. doi:10.1016/S0076-6879(04)83013-1.
- [201] Greenfield NJ. Using circular dichroism spectra to estimate protein secondary structure. *Nat Protoc* 2006;1:2876–90. doi:10.1038/nprot.2006.202.
- [202] Whitmore L, Wallace BA. Protein secondary structure analyses from circular dichroism spectroscopy: methods and reference databases. *Biopolymers* 2008;89:392–400. doi:10.1002/bip.20853.
- [203] Lees JG, Smith BR, Wien F, Miles AJ, Wallace BA. CDtool—an integrated software package for circular dichroism spectroscopic data processing, analysis, and archiving. *Anal Biochem* 2004;332:285–9. doi:10.1016/j.ab.2004.06.002.

- [204] Venyaminov SY, Baikalov IA, Shen ZM, Wu CS, Yang JT. Circular dichroic analysis of denatured proteins: inclusion of denatured proteins in the reference set. *Anal Biochem* 1993;214:17–24.
- [205] Holzwarth G, Doty P. The Ultraviolet Circular Dichroism of Polypeptides1. *J Am Chem Soc* 1965;87:218–28. doi:10.1021/ja01080a015.
- [206] Greenfield N, Fasman GD. Computed circular dichroism spectra for the evaluation of protein conformation. *Biochemistry* 1969;8:4108–16.
- [207] Xiao S, Raleigh DP. A Critical Assessment of Putative Gatekeeper Interactions in the Villin Headpiece Helical Subdomain. *Journal of Molecular Biology* 2010;401:274–85. doi:10.1016/j.jmb.2010.05.070.
- [208] Ferreon ACM, Deniz AA.  $\alpha$ -Synuclein Multistate Folding Thermodynamics: Implications for Protein Misfolding and Aggregation†. *Biochemistry* 2007;46:4499–509. doi:10.1021/bi602461y.
- [209] Luo P, Baldwin RL. Mechanism of helix induction by trifluoroethanol: a framework for extrapolating the helix-forming properties of peptides from trifluoroethanol/water mixtures back to water. *Biochemistry* 1997;36:8413–21. doi:10.1021/bi9707133.
- [210] Rohl CA, Baldwin RL. Comparison of NH Exchange and Circular Dichroism as Techniques for Measuring the Parameters of the Helix–Coil Transition in Peptides. *Biochemistry* 1997;36:8435–42. doi:10.1021/bi9706677.
- [211] Hwang C-S, Shemorry A, Varshavsky A. N-terminal acetylation of cellular proteins creates specific degradation signals. *Science* 2010;327:973–7. doi:10.1126/science.1183147.
- [212] Shemorry A, Hwang C-S, Varshavsky A. Control of protein quality and stoichiometries by N-terminal acetylation and the N-

end rule pathway. *Mol Cell* 2013;50:540–51.  
doi:10.1016/j.molcel.2013.03.018.

- [213] Caesar R, Blomberg A. The stress-induced Tfs1p requires NatB-mediated acetylation to inhibit carboxypeptidase Y and to regulate the protein kinase A pathway. *J Biol Chem* 2004;279:38532–43. doi:10.1074/jbc.M402939200.
- [214] Coulton AT, East DA, Galinska-Rakoczy A, Lehman W, Mulvihill DP. The recruitment of acetylated and unacetylated tropomyosin to distinct actin polymers permits the discrete regulation of specific myosins in fission yeast. *J Cell Sci* 2010;123:3235–43. doi:10.1242/jcs.069971.
- [215] Scott DC, Monda JK, Bennett EJ, Harper JW, Schulman BA. N-terminal acetylation acts as an avidity enhancer within an interconnected multiprotein complex. *Science* 2011;334:674–8. doi:10.1126/science.1209307.
- [216] Arnaudo N, Fernández IS, McLaughlin SH, Peak-Chew SY, Rhodes D, Martino F. The N-terminal acetylation of Sir3 stabilizes its binding to the nucleosome core particle. *Nat Struct Mol Biol* 2013;20:1119–21. doi:10.1038/nsmb.2641.
- [217] Jarvis JA, Ryan MT, Hoogenraad NJ, Craik DJ, Høj PB. Solution structure of the acetylated and noncleavable mitochondrial targeting signal of rat chaperonin 10. *J Biol Chem* 1995;270:1323–31.
- [218] Venkatachalapathi YV, Phillips MC, Eband RM, Eband RF, Tytler EM, Segrest JP, et al. Effect of end group blockage on the properties of a class A amphipathic helical peptide. *Proteins* 1993;15:349–59. doi:10.1002/prot.340150403.
- [219] Chakrabartty A, Doig AJ, Baldwin RL. Helix capping propensities in peptides parallel those in proteins. *Proc Natl Acad Sci USA* 1993;90:11332–6.
- [220] Murthi A, Hopper AK. Genome-Wide Screen for Inner Nuclear Membrane Protein Targeting in *Saccharomyces cerevisiae* Roles

for N-Acetylation and an Integral Membrane Protein. *Genetics* 2005;170:1553–60. doi:10.1534/genetics.105.043620.

- [221] Behnia R, Panic B, Whyte JRC, Munro S. Targeting of the Arf-like GTPase Arl3p to the Golgi requires N-terminal acetylation and the membrane protein Sys1p. *Nat Cell Biol* 2004;6:405–13. doi:10.1038/ncb1120.
- [222] Setty SRG, Strohlic TI, Tong AHY, Boone C, Burd CG. Golgi targeting of ARF-like GTPase Arl3p requires its Na-acetylation and the integral membrane protein Sys1p. *Nat Cell Biol* 2004;6:414–9. doi:10.1038/ncb1121.
- [223] Behnia R, Barr FA, Flanagan JJ, Barlowe C, Munro S. The yeast orthologue of GRASP65 forms a complex with a coiled-coil protein that contributes to ER to Golgi traffic. *J Cell Biol* 2007;176:255–61. doi:10.1083/jcb.200607151.
- [224] Tercero JC, Dinman JD, Wickner RB. Yeast MAK3 N-acetyltransferase recognizes the N-terminal four amino acids of the major coat protein (gag) of the L-A double-stranded RNA virus. *J Bacteriol* 1993;175:3192–4.
- [225] Otzen DE. Protein unfolding in detergents: effect of micelle structure, ionic strength, pH, and temperature. *Biophys J* 2002;83:2219–30. doi:10.1016/S0006-3495(02)73982-9.
- [226] Holmberg K, Jönsson B, Kronberg B, Lindman B. Phase Behaviour of Concentrated Surfactant Systems. *Surfactants and Polymers in Aqueous Solution*, John Wiley & Sons, Ltd; 2002, p. 67–96.
- [227] Emsley L, Bodenhausen G. Optimization of shaped selective pulses for NMR using a quaternion description of their overall propagators. *Journal of Magnetic Resonance* (1969) 1992;97:135–48. doi:10.1016/0022-2364(92)90242-Y.
- [228] Fredenburg RA, Rospigliosi C, Meray RK, Kessler JC, Lashuel HA, Eliezer D, et al. The impact of the E46K mutation on the properties of alpha-synuclein in its monomeric and oligomeric states. *Biochemistry* 2007;46:7107–18. doi:10.1021/bi7000246.

- [229] Rao JN, Kim YE, Park LS, Ulmer TS. Effect of Pseudorepeat Rearrangement on  $\alpha$ -Synuclein Misfolding, Vesicle Binding, and Micelle Binding. *Journal of Molecular Biology* 2009;390:516–29. doi:10.1016/j.jmb.2009.05.058.
- [230] Fauvet B, Fares M-B, Samuel F, Dikiy I, Tandon A, Eliezer D, et al. Characterization of semisynthetic and naturally N<sub>α</sub>-acetylated  $\alpha$ -synuclein in vitro and in intact cells: implications for aggregation and cellular properties of  $\alpha$ -synuclein. *J Biol Chem* 2012;287:28243–62. doi:10.1074/jbc.M112.383711.
- [231] Maltsev AS, Ying J, Bax A. Impact of N-Terminal Acetylation of  $\alpha$ -Synuclein on Its Random Coil and Lipid Binding Properties. *Biochemistry* 2012;51:5004–13. doi:10.1021/bi300642h.
- [232] Aurora R, Rosee GD. Helix capping. *Protein Science* 1998;7:21–38. doi:10.1002/pro.5560070103.
- [233] Richardson JS, Richardson DC. Amino acid preferences for specific locations at the ends of alpha helices. *Science* 1988;240:1648–52.
- [234] Burré J, Sharma M, Südhof TC.  $\alpha$ -Synuclein assembles into higher-order multimers upon membrane binding to promote SNARE complex formation. *Proc Natl Acad Sci USA* 2014. doi:10.1073/pnas.1416598111.
- [235] Takamori S, Holt M, Stenius K, Lemke E, Grønborg M, Riedel D, et al. Molecular Anatomy of a Trafficking Organelle. *Cell* 2006;127:831–46. doi:10.1016/j.cell.2006.10.030.
- [236] Vance JE, Steenbergen R. Metabolism and functions of phosphatidylserine. *Progress in Lipid Research* 2005;44:207–34. doi:10.1016/j.plipres.2005.05.001.
- [237] Lemmon MA, Schlessinger J. Cell Signaling by Receptor Tyrosine Kinases. *Cell* 2010;141:1117–34. doi:10.1016/j.cell.2010.06.011.
- [238] Zoncu R, Efeyan A, Sabatini DM. mTOR: from growth signal integration to cancer, diabetes and ageing. *Nat Rev Mol Cell Biol* 2011;12:21–35. doi:10.1038/nrm3025.

- [239] Kyriakis JM, Avruch J. Mammalian MAPK Signal Transduction Pathways Activated by Stress and Inflammation: A 10-Year Update. *Physiological Reviews* 2012;92:689–737. doi:10.1152/physrev.00028.2011.
- [240] Nishi H, Hashimoto K, Panchenko AR. Phosphorylation in Protein-Protein Binding: Effect on Stability and Function. *Structure* 2011;19:1807–15. doi:10.1016/j.str.2011.09.021.
- [241] Querfurth C, Diernfellner ACR, Gin E, Malzahn E, Höfer T, Brunner M. Circadian Conformational Change of the Neurospora Clock Protein FREQUENCY Triggered by Clustered Hyperphosphorylation of a Basic Domain. *Molecular Cell* 2011;43:713–22. doi:10.1016/j.molcel.2011.06.033.
- [242] Iakoucheva LM, Radivojac P, Brown CJ, O'Connor TR, Sikes JG, Obradovic Z, et al. The importance of intrinsic disorder for protein phosphorylation. *Nucl Acids Res* 2004;32:1037–49. doi:10.1093/nar/gkh253.
- [243] Gsponer J, Futschik ME, Teichmann SA, Babu MM. Tight Regulation of Unstructured Proteins: From Transcript Synthesis to Protein Degradation. *Science* 2008;322:1365–8. doi:10.1126/science.1163581.
- [244] Johnson LN, Lewis RJ. Structural Basis for Control by Phosphorylation. *Chem Rev* 2001;101:2209–42. doi:10.1021/cr000225s.
- [245] Xin F, Radivojac P. Post-translational modifications induce significant yet not extreme changes to protein structure. *Bioinformatics* 2012;28:2905–13. doi:10.1093/bioinformatics/bts541.
- [246] Shan Y, Eastwood MP, Zhang X, Kim ET, Arkhipov A, Dror RO, et al. Oncogenic mutations counteract intrinsic disorder in the EGFR kinase and promote receptor dimerization. *Cell* 2012;149:860–70. doi:10.1016/j.cell.2012.02.063.
- [247] Tholey A, Lindemann A, Kinzel V, Reed J. Direct effects of phosphorylation on the preferred backbone conformation of

peptides: a nuclear magnetic resonance study. *Biophys J* 1999;76:76–87. doi:10.1016/S0006-3495(99)77179-1.

- [248] Deshmukh L, Meller N, Alder N, Byzova T, Vinogradova O. Tyrosine Phosphorylation as a Conformational Switch A CASE STUDY OF INTEGRIN  $\beta$ 3 CYTOPLASMIC TAIL. *J Biol Chem* 2011;286:40943–53. doi:10.1074/jbc.M111.231951.
- [249] Inglis KJ, Chereau D, Brigham EF, Chiou S-S, Schöbel S, Frigon NL, et al. Polo-like Kinase 2 (PLK2) Phosphorylates  $\alpha$ -Synuclein at Serine 129 in Central Nervous System. *J Biol Chem* 2009;284:2598–602. doi:10.1074/jbc.C800206200.
- [250] Oueslati A, Schneider BL, Aebischer P, Lashuel HA. Polo-like kinase 2 regulates selective autophagic  $\alpha$ -synuclein clearance and suppresses its toxicity in vivo. *Proc Natl Acad Sci USA* 2013;110:E3945–54. doi:10.1073/pnas.1309991110.
- [251] Visanji N, Wislet-Gendebien S, Oschipok L, Zhang G, Aubert I, Fraser P, et al. Effect of Ser-129 phosphorylation on interaction of  $\alpha$ -synuclein with synaptic and cellular membranes. *The Journal of Biological Chemistry* 2011;286:35863–73. doi:10.1074/jbc.M111.253450.
- [252] Giasson BI, Duda JE, Murray IVJ, Chen Q, Souza JM, Hurtig HI, et al. Oxidative Damage Linked to Neurodegeneration by Selective  $\alpha$ -Synuclein Nitration in Synucleinopathy Lesions. *Science* 2000;290:985–9. doi:10.1126/science.290.5493.985.
- [253] Perry TL, Godin DV, Hansen S. Parkinson's disease: a disorder due to nigral glutathione deficiency? *Neurosci Lett* 1982;33:305–10.
- [254] Zuo L, Motherwell MS. The impact of reactive oxygen species and genetic mitochondrial mutations in Parkinson's disease. *Gene* 2013;532:18–23. doi:10.1016/j.gene.2013.07.085.
- [255] Good PF, Hsu A, Werner P, Perl DP, Olanow CW. Protein nitration in Parkinson's disease. *J Neuropathol Exp Neurol* 1998;57:338–42.

- [256] Danielson SR, Held JM, Schilling B, Oo M, Gibson BW, Andersen JK. Preferentially increased nitration of alpha-synuclein at tyrosine-39 in a cellular oxidative model of Parkinson's disease. *Anal Chem* 2009;81:7823–8. doi:10.1021/ac901176t.
- [257] Hodara R, Norris EH, Giasson BI, Mishizen-Eberz AJ, Lynch DR, Lee VM-Y, et al. Functional consequences of alpha-synuclein tyrosine nitration: diminished binding to lipid vesicles and increased fibril formation. *J Biol Chem* 2004;279:47746–53. doi:10.1074/jbc.M408906200.
- [258] Sevcsik E, Trexler A, Dunn J, Rhoades E. Allostery in a Disordered Protein: Oxidative Modifications to  $\alpha$ -Synuclein Act Distally To Regulate Membrane Binding. *Journal of the American Chemical Society* 2011. doi:10.1021/ja2009554.
- [259] Wu K-P, Baum J. Detection of Transient Interchain Interactions in the Intrinsically Disordered Protein  $\alpha$ -Synuclein by NMR Paramagnetic Relaxation Enhancement. *Journal of the American Chemical Society* 2010;132:5546–7. doi:10.1021/ja9105495.
- [260] Souza JM, Giasson BI, Chen Q, Lee VM-Y, Ischiropoulos H. Dityrosine Cross-linking Promotes Formation of Stable  $\alpha$ -Synuclein Polymers IMPLICATION OF NITRATIVE AND OXIDATIVE STRESS IN THE PATHOGENESIS OF NEURODEGENERATIVE SYNUCLEINOPATHIES. *J Biol Chem* 2000;275:18344–9. doi:10.1074/jbc.M000206200.
- [261] Shavali S, Combs CK, Ebadi M. Reactive macrophages increase oxidative stress and alpha-synuclein nitration during death of dopaminergic neuronal cells in co-culture: relevance to Parkinson's disease. *Neurochem Res* 2006;31:85–94. doi:10.1007/s11064-005-9233-x.
- [262] McCormack AL, Mak SK, Shenasa M, Langston WJ, Forno LS, Di Monte DA. Pathologic modifications of alpha-synuclein in 1-methyl-4-phenyl-1,2,3,6-tetrahydropyridine (MPTP)-treated squirrel monkeys. *J Neuropathol Exp Neurol* 2008;67:793–802. doi:10.1097/NEN.0b013e318180f0bd.

- [263] Yu Z, Xu X, Xiang Z, Zhou J, Zhang Z, Hu C, et al. Nitrated  $\alpha$ -Synuclein Induces the Loss of Dopaminergic Neurons in the Substantia Nigra of Rats. *PLoS ONE* 2010;5:e9956. doi:10.1371/journal.pone.0009956.
- [264] Mahul-Mellier A-L, Fauvet B, Gysbers A, Dikiy I, Oueslati A, Georgeon S, et al. c-Abl phosphorylates  $\alpha$ -syn and regulates its degradation, implication for  $\alpha$ -syn clearance and contribution to the pathogenesis of Parkinson's Disease. *Hum Mol Genet* 2014;23:674. doi:10.1093/hmg/ddt674.
- [265] Ebina S, Wüthrich K. Amide proton titration shifts in bull seminal inhibitor IIA by two-dimensional correlated  $^1\text{H}$  nuclear magnetic resonance (COSY): Manifestation of conformational equilibria involving carboxylate groups. *Journal of Molecular Biology* 1984;179:283–8. doi:10.1016/0022-2836(84)90469-8.
- [266] Lu Y, Prudent M, Fauvet B, Lashuel HA, Girault HH. Phosphorylation of  $\alpha$ -Synuclein at Y125 and S129 Alters Its Metal Binding Properties: Implications for Understanding the Role of  $\alpha$ -Synuclein in the Pathogenesis of Parkinson's Disease and Related Disorders. *ACS Chem Neurosci* 2011;2:667–75. doi:10.1021/cn200074d.
- [267] Chakrabartty A, Kortemme T, Baldwin RL. Helix propensities of the amino acids measured in alanine-based peptides without helix-stabilizing side-chain interactions. *Protein Sci* 1994;3:843–52. doi:10.1002/pro.5560030514.
- [268] Horovitz A, Matthews JM, Fersht AR. Alpha-helix stability in proteins. II. Factors that influence stability at an internal position. *J Mol Biol* 1992;227:560–8.
- [269] Donald JE, Kulp DW, DeGrado WF. Salt bridges: Geometrically specific, designable interactions. *Proteins* 2011;79:898–915. doi:10.1002/prot.22927.
- [270] Marqusee S, Baldwin RL. Helix stabilization by Glu-...Lys+ salt bridges in short peptides of de novo design. *Proc Natl Acad Sci USA* 1987;84:8898–902.

- [271] Iwai A, Yoshimoto M, Masliah E, Saitoh T. Non-A $\beta$ . Component of Alzheimer's Disease Amyloid (NAC) is Amyloidogenic. *Biochemistry* 1995;34:10139–45. doi:10.1021/bi00032a006.
- [272] Giasson BI, Murray IV, Trojanowski JQ, Lee VM. A hydrophobic stretch of 12 amino acid residues in the middle of alpha-synuclein is essential for filament assembly. *J Biol Chem* 2001;276:2380–6. doi:10.1074/jbc.M008919200.
- [273] Kara E, Lewis PA, Ling H, Proukakis C, Houlden H, Hardy J.  $\alpha$ -Synuclein mutations cluster around a putative protein loop. *Neurosci Lett* 2013;546:67–70. doi:10.1016/j.neulet.2013.04.058.
- [274] Sung Y-H, Rospigliosi C, Eliezer D. NMR mapping of copper binding sites in alpha-synuclein. *Biochim Biophys Acta* 2006;1764:5–12. doi:10.1016/j.bbapap.2005.11.003.
- [275] Fares M-B, Ait-Bouziad N, Dikiy I, Mbefo MK, Jovičić A, Kiely A, et al. The novel Parkinson's disease linked mutation G51D attenuates in vitro aggregation and membrane binding of  $\alpha$ -synuclein, and enhances its secretion and nuclear localization in cells. *Hum Mol Genet* 2014;23:4491–509. doi:10.1093/hmg/ddu165.
- [276] Khalaf O, Fauvet B, Oueslati A, Dikiy I, Mahul-Mellier A-L, Ruggeri FS, et al. The H50Q Mutation Enhances  $\alpha$ -Synuclein Aggregation, Secretion, and Toxicity. *J Biol Chem* 2014;289:21856–76. doi:10.1074/jbc.M114.553297.
- [277] Maltsev AS, Chen J, Levine RL, Bax A. Site-Specific Interaction between  $\alpha$ -Synuclein and Membranes Probed by NMR-Observed Methionine Oxidation Rates. *J Am Chem Soc* 2013;135:2943–6. doi:10.1021/ja312415q.
- [278] Sulzer D, Zecca L. Intraneuronal dopamine-quinone synthesis: a review. *Neurotox Res* 2000;1:181–95.
- [279] Barnham KJ, Masters CL, Bush AI. Neurodegenerative diseases and oxidative stress. *Nat Rev Drug Discov* 2004;3:205–14. doi:10.1038/nrd1330.

- [280] Rifkind JM, Nagababu E. Hemoglobin redox reactions and red blood cell aging. *Antioxid Redox Signal* 2013;18:2274–83. doi:10.1089/ars.2012.4867.
- [281] Renella R, Schlehe JS, Selkoe DJ, Williams DA, LaVoie MJ. Genetic deletion of the GATA1-regulated protein  $\alpha$ -synuclein reduces oxidative stress and nitric oxide synthase levels in mature erythrocytes. *Am J Hematol* 2014;89:974–7. doi:10.1002/ajh.23796.
- [282] Ikonen E. Cellular cholesterol trafficking and compartmentalization. *Nat Rev Mol Cell Biol* 2008;9:125–38. doi:10.1038/nrm2336.
- [283] Hao M, Lin SX, Karylowski OJ, Wüstner D, McGraw TE, Maxfield FR. Vesicular and Non-vesicular Sterol Transport in Living Cells THE ENDOCYTIC RECYCLING COMPARTMENT IS A MAJOR STEROL STORAGE ORGANELLE. *J Biol Chem* 2002;277:609–17. doi:10.1074/jbc.M108861200.
- [284] Radhakrishnan A, Goldstein JL, McDonald JG, Brown MS. Switch-like Control of SREBP-2 Transport Triggered by Small Changes in ER Cholesterol: A Delicate Balance. *Cell Metabolism* 2008;8:512–21. doi:10.1016/j.cmet.2008.10.008.
- [285] Mesmin B, Maxfield FR. Intracellular sterol dynamics. *Biochimica et Biophysica Acta (BBA) - Molecular and Cell Biology of Lipids* 2009;1791:636–45. doi:10.1016/j.bbalip.2009.03.002.
- [286] Lehto M, Olkkonen VM. The OSBP-related proteins: a novel protein family involved in vesicle transport, cellular lipid metabolism, and cell signalling. *Biochimica et Biophysica Acta (BBA) - Molecular and Cell Biology of Lipids* 2003;1631:1–11. doi:10.1016/S1388-1981(02)00364-5.
- [287] Clark BJ. The mammalian START domain protein family in lipid transport in health and disease. *J Endocrinol* 2012;212:257–75. doi:10.1530/JOE-11-0313.
- [288] Iaea DB, Mao S, Maxfield FR. Steroidogenic Acute Regulatory Protein-related Lipid Transfer (START) Proteins in Non-vesicular

Cholesterol Transport. In: Clark BJ, Stocco DM, editors. Cholesterol Transporters of the START Domain Protein Family in Health and Disease, Springer New York; 2014, p. 173–88.

- [289] Krueger RJ, Orme-Johnson NR. Acute adrenocorticotrophic hormone stimulation of adrenal corticosteroidogenesis. Discovery of a rapidly induced protein. *J Biol Chem* 1983;258:10159–67.
- [290] Clark BJ, Wells J, King SR, Stocco DM. The purification, cloning, and expression of a novel luteinizing hormone-induced mitochondrial protein in MA-10 mouse Leydig tumor cells. Characterization of the steroidogenic acute regulatory protein (StAR). *J Biol Chem* 1994;269:28314–22.
- [291] Kallen CB, Billheimer JT, Summers SA, Stayrook SE, Lewis M, Strauss JF. Steroidogenic Acute Regulatory Protein (StAR) Is A Sterol Transfer Protein. *J Biol Chem* 1998;273:26285–8. doi:10.1074/jbc.273.41.26285.
- [292] Thorsell A-G, Lee WH, Persson C, Siponen MI, Nilsson M, Busam RD, et al. Comparative Structural Analysis of Lipid Binding START Domains. *PLoS ONE* 2011;6:e19521. doi:10.1371/journal.pone.0019521.
- [293] Romanowski M, Soccio R, Breslow J, Burley S. Crystal structure of the *Mus musculus* cholesterol-regulated START protein 4 (StarD4) containing a StAR-related lipid transfer domain. *Proceedings of the National Academy of Sciences of the United States of America* 2002;99:6949–54.
- [294] Tsujishita Y, Hurley JH. Structure and lipid transport mechanism of a StAR-related domain. *Nat Struct Biol* 2000;7:408–14. doi:10.1038/75192.
- [295] Roderick S, Chan W, Agate D, Olsen L, Vetting M, Rajashankar K, et al. Structure of human phosphatidylcholine transfer protein in complex with its ligand. *Nature Structural Biology* 2002;9:507–11. doi:10.1038/nsb812.
- [296] Kudo N, Kumagai K, Tomishige N, Yamaji T, Wakatsuki S, Nishijima M, et al. Structural basis for specific lipid recognition

by CERT responsible for nonvesicular trafficking of ceramide. Proc Natl Acad Sci USA 2008;105:488–93. doi:10.1073/pnas.0709191105.

- [297] Kudo N, Kumagai K, Matsubara R, Kobayashi S, Hanada K, Wakatsuki S, et al. Crystal structures of the CERT START domain with inhibitors provide insights into the mechanism of ceramide transfer. J Mol Biol 2010;396:245–51. doi:10.1016/j.jmb.2009.12.029.
- [298] Soccio RE, Adams RM, Romanowski MJ, Sehayek E, Burley SK, Breslow JL. The cholesterol-regulated StarD4 gene encodes a StAR-related lipid transfer protein with two closely related homologues, StarD5 and StarD6. Proc Natl Acad Sci USA 2002;99:6943–8. doi:10.1073/pnas.052143799.
- [299] Soccio RE, Adams RM, Maxwell KN, Breslow JL. Differential gene regulation of StarD4 and StarD5 cholesterol transfer proteins. Activation of StarD4 by sterol regulatory element-binding protein-2 and StarD5 by endoplasmic reticulum stress. J Biol Chem 2005;280:19410–8. doi:10.1074/jbc.M501778200.
- [300] Mesmin B, Pipalia N, Lund F, Ramlall T, Sokolov A, Eliezer D, et al. STARD4 abundance regulates sterol transport and sensing. Molecular Biology of the Cell 2011;22:4004–15.
- [301] Riegelhaupt JJ, Waase MP, Garbarino J, Cruz DE, Breslow JL. Targeted disruption of steroidogenic acute regulatory protein D4 leads to modest weight reduction and minor alterations in lipid metabolism. J Lipid Res 2010;51:1134–43. doi:10.1194/jlr.M003095.
- [302] Barbar E, Lehoux J-G, Lavigne P. Toward the NMR structure of StAR. Molecular and Cellular Endocrinology 2009;300:89–93.
- [303] Létourneau D, Lorin A, Lefebvre A, Frappier V, Gaudreault F, Najmanovich R, et al. StAR-related lipid transfer domain protein 5 binds primary bile acids. J Lipid Res 2012;53:2677–89. doi:10.1194/jlr.M031245.

- [304] Murcia M, Faráldo-Gómez J, Maxfield F, Roux B. Modeling the structure of the StART domains of MLN64 and StAR proteins in complex with cholesterol. *Journal of Lipid Research* 2006;47:2614–30.
- [305] Malakhov MP, Mattern MR, Malakhova OA, Drinker M, Weeks SD, Butt TR. SUMO fusions and SUMO-specific protease for efficient expression and purification of proteins. *J Struct Func Genom* 2004;5:75–86. doi:10.1023/B:JSFG.0000029237.70316.52.
- [306] Shen Y, Delaglio F, Cornilescu G, Bax A. TALOS+: a hybrid method for predicting protein backbone torsion angles from NMR chemical shifts. *J Biomol NMR* 2009;44:213–23. doi:10.1007/s10858-009-9333-z.
- [307] Burré J, Sharma M, Südhof TC. Systematic mutagenesis of  $\alpha$ -synuclein reveals distinct sequence requirements for physiological and pathological activities. *J Neurosci* 2012;32:15227–42. doi:10.1523/JNEUROSCI.3545-12.2012.
- [308] Diao J, Burré J, Vivona S, Cipriano DJ, Sharma M, Kyoung M, et al. Native  $\alpha$ -synuclein induces clustering of synaptic-vesicle mimics via binding to phospholipids and synaptobrevin-2/VAMP2. *Elife* 2013;2:e00592. doi:10.7554/eLife.00592.
- [309] Fasshauer D, Eliason WK, Brünger AT, Jahn R. Identification of a minimal core of the synaptic SNARE complex sufficient for reversible assembly and disassembly. *Biochemistry* 1998;37:10354–62. doi:10.1021/bi980542h.
- [310] DeWitt DC, Rhoades E.  $\alpha$ -Synuclein can inhibit SNARE-mediated vesicle fusion through direct interactions with lipid bilayers. *Biochemistry* 2013;52:2385–7. doi:10.1021/bi4002369.
- [311] Brewer K, Li W, Horne BE, Rizo J. Reluctance to membrane binding enables accessibility of the synaptobrevin SNARE motif for SNARE complex formation. *Proceedings of the National Academy of Sciences of the United States of America* 2011;108:12723–8. doi:10.1073/pnas.1105128108.

- [312] Auluck PK, Chan HYE, Trojanowski JQ, Lee VMY, Bonini NM. Chaperone suppression of alpha-synuclein toxicity in a *Drosophila* model for Parkinson's disease. *Science* 2002;295:865–8. doi:10.1126/science.1067389.
- [313] Taldone T, Ochiana SO, Patel PD, Chiosis G. Selective targeting of the stress chaperome as a therapeutic strategy. *Trends Pharmacol Sci* 2014. doi:10.1016/j.tips.2014.09.001.
- [314] Warrick JM, Chan HY, Gray-Board GL, Chai Y, Paulson HL, Bonini NM. Suppression of polyglutamine-mediated neurodegeneration in *Drosophila* by the molecular chaperone HSP70. *Nat Genet* 1999;23:425–8. doi:10.1038/70532.
- [315] McLean PJ, Kawamata H, Shariff S, Hewett J, Sharma N, Ueda K, et al. TorsinA and heat shock proteins act as molecular chaperones: suppression of  $\alpha$ -synuclein aggregation. *Journal of Neurochemistry* 2002;83:846–54. doi:10.1046/j.1471-4159.2002.01190.x.
- [316] Klucken J, Shin Y, Masliah E, Hyman BT, McLean PJ. Hsp70 Reduces alpha-Synuclein Aggregation and Toxicity. *J Biol Chem* 2004;279:25497–502. doi:10.1074/jbc.M400255200.
- [317] Kilpatrick K, Novoa JA, Hancock T, Guerriero CJ, Wipf P, Brodsky JL, et al. Chemical induction of Hsp70 reduces  $\alpha$ -synuclein aggregation in neuroglioma cells. *ACS Chem Biol* 2013;8:1460–8. doi:10.1021/cb400017h.
- [318] Moloney TC, Hyland R, O'Toole D, Paucard A, Kirik D, O'Doherty A, et al. Heat shock protein 70 reduces  $\alpha$ -synuclein-induced predegenerative neuronal dystrophy in the  $\alpha$ -synuclein viral gene transfer rat model of Parkinson's disease. *CNS Neurosci Ther* 2014;20:50–8. doi:10.1111/cns.12200.
- [319] Dedmon MM, Christodoulou J, Wilson MR, Dobson CM. Heat shock protein 70 inhibits alpha-synuclein fibril formation via preferential binding to prefibrillar species. *J Biol Chem* 2005;280:14733–40. doi:10.1074/jbc.M413024200.

- [320] Huang C, Cheng H, Hao S, Zhou H, Zhang X, Gao J, et al. Heat shock protein 70 inhibits alpha-synuclein fibril formation via interactions with diverse intermediates. *J Mol Biol* 2006;364:323–36. doi:10.1016/j.jmb.2006.08.062.
- [321] Luk KC, Mills IP, Trojanowski JQ, Lee VM-Y. Interactions between Hsp70 and the hydrophobic core of alpha-synuclein inhibit fibril assembly. *Biochemistry* 2008;47:12614–25. doi:10.1021/bi801475r.
- [322] Redeker V, Pemberton S, Bienvenut W, Bousset L, Melki R. Identification of protein interfaces between  $\alpha$ -synuclein, the principal component of Lewy bodies in Parkinson disease, and the molecular chaperones human Hsc70 and the yeast Ssa1p. *J Biol Chem* 2012;287:32630–9. doi:10.1074/jbc.M112.387530.
- [323] Klucken J, Outeiro TF, Nguyen P, McLean PJ, Hyman BT. Detection of novel intracellular alpha-synuclein oligomeric species by fluorescence lifetime imaging. *FASEB J* 2006;20:2050–7. doi:10.1096/fj.05-5422com.
- [324] Frankel AD, Pabo CO. Cellular uptake of the tat protein from human immunodeficiency virus. *Cell* 1988;55:1189–93.
- [325] Green M, Loewenstein PM. Autonomous functional domains of chemically synthesized human immunodeficiency virus tat transactivator protein. *Cell* 1988;55:1179–88.
- [326] Becker-Hapak M, McAllister SS, Dowdy SF. TAT-Mediated Protein Transduction into Mammalian Cells. *Methods* 2001;24:247–56. doi:10.1006/meth.2001.1186.
- [327] Nagahara H, Vocero-Akbani AM, Snyder EL, Ho A, Latham DG, Lissy NA, et al. Transduction of full-length TAT fusion proteins into mammalian cells: TAT-p27Kip1 induces cell migration. *Nat Med* 1998;4:1449–52. doi:10.1038/4042.